Polarization in diffractive optics and metasurfaces

Noah A. Rubin,[1,*] Zhujun Shi,[2,3] and Federico Capasso[1]

[1]*Harvard John A. Paulson School of Engineering and Applied Sciences, Harvard University, Cambridge, Massachusetts 02138, USA*
[2]*Department of Physics, Harvard University, Cambridge, Massachusetts 02138, USA*
[3]*Apple Inc., Cupertino, California 95014, USA*
Corresponding author: noahrubin@seas.harvard.edu

Polarization, the path traced by light's electric field vector, appears in all areas of optics. In recent decades, various technologies have enabled the precise control of light's polarization state, even on a subwavelength scale, at optical frequencies. In this review, we provide a thorough, high-level review of the fundamentals of polarization optics and detail how the Jones calculus, alongside Fourier optics, can be used to analyze, classify, and compare these optical elements. We provide a review of work in this area across multiple technologies and research areas, including recent developments in optical metasurfaces. This review unifies a large body of work on spatially varying polarization optics and may be of interest to both researchers in optics and designers of optical systems more generally.   © 2022 Optical Society of America

Polarization in diffractive optics and metasurfaces

NOAH A. RUBIN, ZHUJUN SHI, AND FEDERICO CAPASSO

1. MOTIVATION

1.1. Why This Review Paper Exists and Who It Is For

Polarization is the path along which light's electric field oscillates and follows naturally from the plane wave solution of Maxwell's equations. It is an essential concept that touches nearly every area of the physical sciences, from light scattering in atmospheres to the fundamental quantum mechanics of atomic transitions. Today, polarization plays a key part in a variety of technologies, too, from liquid crystal (LC) displays, the fiber optic backbone of modern telecommunications, and even glare-reducing sunglasses.

It is indeed possible, however, to imagine optical fields in which polarization is *not* at all uniform, in which the polarization state of light changes—possibly rapidly— from point-to-point in space. This is an especially relevant consideration in light of recent work, roughly over the last half-century, that has enabled the creation of optical elements whose polarization transfer characteristics may be precisely and adeptly engineered across a surface. This is an exciting frontier of optical design that enables optical elements with interesting new functions.

Work of this nature now possesses an extensive literature, with perhaps thousands of published papers. But, as is common in science, similar ideas have emerged among different groups of people at different times. Often, work in this field—even at the level of article and book titles—is labeled by a particular enabling technology. Among these terms are polarization holograms, polarization gratings, LCs, and most recently, metasurfaces. These names can reflect real, substantive technological differences. At the same time, though, this multitude of names can serve as an obstacle: researchers in any one of these fields may work without awareness of the others despite common goals and theoretical underpinnings, hampering clarity, risking unintended redundancy, and, ultimately, undermining efforts to put these new components to practical use.

In this review, we attempt to remedy this state of affairs by, first, presenting a consistent treatment of the subject that could well apply to any thin (paraxial) polarization-sensitive diffractive optical element. This permits a high-level understanding of the subject and allows for comparisons between different platforms and approaches with a consistent formalism. We hope that what follows can, given polarization's fundamental nature, be of use to anyone with an interest in optics, both researchers and technologists. Recently, however, this area has seen intense interest in nanophotonics (metasurfaces in particular). This review, then, may be of particular interest to researchers in that area.

1.2. How to Read This Paper

We hope that the length of this article will not discourage potential readers. Though the sections flow from one another as a cohesive whole, they need not be read in succession. Different audiences may be interested in only one section or another. Here, we give a summary of each.

Section 2 **:** Given that all light has a polarization state, polarization is covered to some degree in almost every optics book and course, usually at the beginning. This ubiquity, however, can mean that polarization is often trivialized. Polarization is a mathematically deep subject, deeper than many optics researchers may at first realize. To that end, in Section 2 we present a self-contained summary of polarization optics at a high level with concepts that may be new to many readers. We describe several abstractions that are useful in reasoning through polarization problems. The concepts and notation from Section 2 are employed throughout the review. Section 2 is a reference and can be read in parts, as necessary, wherever concepts are unfamiliar. The concepts of the matrix polar decomposition (Subsection 2.3) and retardance and diattenuation spaces (Subsection 2.6a) are, however, used throughout the rest of the review.

Section 3 **:** In our view, part of the problem is an inconsistency in mathematical treatment and language. At different times, polarization-sensitive diffractive optics has been treated with different approaches and language. Building on Section 2, in Section 3 we show how these optics can be analyzed by a combination of Fourier optics and the Jones calculus, enabling description without regard to the polarization state of incident light. This treatment generalizes several past approaches to the description and design of these optical elements.

Section 4 **:** Using this formalism, in Section 4 we review different research areas and technologies in which diffractive elements with spatially varying polarization properties have been investigated, with a particular focus on metasurfaces. We facilitate cross-comparison by using the language of Section 2 to categorize and classify (in mathematical terms) the extent of polarization control possible by each. The individual subsections of Section 4 do not rely on one another and can be read according to the reader's interest.

Finally, in Section 5, we offer some very brief concluding notes and predictions for the future.

Throughout the review, certain topical subheadings appear **in bold**. This is meant as a visual aide to break larger sections of text into visually digestible units.

2. INTRODUCTION

In this section, we provide a self-contained, concise review of polarization optics. This is a subject with coverage, to some degree, in any optics book. Indeed, there are many excellent texts dedicated solely to polarization optics [1–6], in addition to introductory texts that treat it with some sophistication [7,8]. For consistency, Table 1 defines the mathematical notation used throughout this section and the review when dealing with polarization.

Here, we endeavor to highlight some aspects of polarization theory that are either subtle or overlooked that have particular relevance to spatially varying polarization optics. We begin with some brief historical context.

2.1. Historical Note

The electromagnetic field of light is characterized by a number of properties. Some of these, like frequency and intensity, are familiar in human experience through their sensory manifestations as color and brightness, while others, such as the temporal and spatial coherence of optical fields, are more abstract and of relatively recent discovery in physics. As a degree-of-freedom of light, polarization stands somewhere in-between the two: (mostly) imperceptible to the human eye, but readily rendered

so in possession of the correct optics. Throughout its nearly 400-year history in science, polarization has been viewed on many levels of abstraction. We provide some highlights below, without attempting to retell that history here (instead, the reader is referred to the account of Brosseau [9] from which much of this discussion is derived).

Polarization's entrance into western science is owed to a rock quarry in the fjords of eastern Iceland, near Reyðarfjörður [10]. At some point in the 17th century, exceptionally transparent, rhombohedral crystals of calcite ($CaCO_3$)—which accordingly earned the name "Iceland spar"—were discovered there (Fig. 1). It is well-known today that calcite is strongly birefringent, playing host to the phenomenon of doubly refracted images of objects viewed through it due to the difference in refractive index of light polarized along its fast and slow crystalline axes (which are equally present in unpolarized natural light). These crystals gradually became distributed throughout continental Europe, and this double refraction was first formally reported by Bartholinus in Denmark in 1670. Despite a current lack of archaeological evidence, there is some speculation that calcite and its birefringence were perhaps used by the Vikings (who occupied Iceland) for the purpose of navigation under overcast conditions by using the polarization of the sky. This is an active subject of debate in the historical and scientific communities [11–14].

Early work on this Iceland spar was phenomenological in nature. Nonetheless, much was understood by the mid-19th century, with significant progress in the first decades of that century. Malus noted that light reflected from a dielectric interface could form just *one* image when passed through an Iceland spar, coining the term polarization and observing the cosine-squared power trend now known as Malus' law in 1808. In 1815, Brewster then explained that this angle depended on the refractive index of the underlying dielectric medium. A breakthrough came with the work of Fresnel, who, on the basis of an assumption that light takes the form of a transverse elastic wave, derived the reflection and transmission laws now known as the Fresnel equations in 1821. Fresnel's work established the role of phase in the description of polarization and the notions of linear, circular, and elliptical polarization, as well as the concept of orthogonal polarizations, emerged from his work.

In Fresnel's work can be found all the essential elements of coherent polarization optics (polarization ellipse, orthogonality, etc.) and even some elements of an

Table 1. Definition of Notation Used Throughout Section 2 and This Review

Symbol	Description	Value
	Notation Used Throughout Section 2	
$\tilde{a}$	Complex number	$a + ib$
$\lvert E \rangle$	Jones vector	$\begin{pmatrix} \tilde{E}_x \\ \tilde{E}_y \end{pmatrix}$
$\langle E \rvert$	Jones vector	$(\lvert E \rangle)^\dagger = \begin{pmatrix} \tilde{E}_x^* & \tilde{E}_y^* \end{pmatrix}$
$\langle E_1 \vert E_2 \rangle$	Inner product, projection	$\tilde{E}_{x,1}^* \tilde{E}_{x,2} + \tilde{E}_{y,1}^* \tilde{E}_{y,2}$
$\lvert j \rangle$ and $\lvert j^\perp \rangle$	Orthogonal polarization states	$\langle j \vert j^\perp \rangle = 0$
J	Jones matrix	$\begin{pmatrix} \tilde{J}_{11} & \tilde{J}_{12} \\ \tilde{J}_{21} & \tilde{J}_{22} \end{pmatrix}$
$\vec{S}$	Stokes vector	$\begin{pmatrix} S_0 & S_1 & S_2 & S_3 \end{pmatrix}^T$
$\vec{S}'$	Abbreviated Stokes vector	$\begin{pmatrix} S_1 & S_2 & S_3 \end{pmatrix}^T$
DoP	Degree-of-polarization (DOP)	$\sqrt{S_1^2 + S_2^2 + S_3^2}/S_0$
$\hat{s}$	Stokes state-of-polarization (SOP)	$\begin{pmatrix} s_1 & s_2 & s_3 \end{pmatrix}^T$ with $s_1^2 + s_2^2 + s_3^2 = 1$
$\mathbb{I}$	Identity matrix	$\begin{pmatrix} 1 & 0 \\ 0 & 1 \end{pmatrix}$
$\sigma_0, \sigma_1, \sigma_2,$ and σ_3	Pauli matrices	$\mathbb{I}, \begin{pmatrix} 1 & 0 \\ 0 & -1 \end{pmatrix}, \begin{pmatrix} 0 & 1 \\ 1 & 0 \end{pmatrix},$ and $\begin{pmatrix} 0 & -i \\ i & 0 \end{pmatrix}$
$\vec{\sigma}$	Pauli vector	$\begin{pmatrix} \sigma_0 & \sigma_1 & \sigma_2 & \sigma_3 \end{pmatrix}^T$
$\vec{\sigma}'$	Abbreviated Pauli vector	$\begin{pmatrix} \sigma_1 & \sigma_2 & \sigma_3 \end{pmatrix}^T$
$\vec{a} \cdot \vec{\sigma}$	Dot product with Pauli vector	$a_0 \sigma_0 + a_1 \sigma_1 + a_2 \sigma_2 + a_3 \sigma_3$

incoherent theory: Fresnel and Arago both noted that two beams, even in identical polarization states, could not form interference fringes if derived from independent sources. In 1852, Stokes posited the alternative description of light's polarization in terms of experimental observables—in units of intensity, rather than electric field—that now bears his name (discussed in Subsection 2.4), which extended this observation with the ability to describe un- and partially polarized light. It is notable that all of this occurred prior to 1864, when Maxwell's equations put the ideas of light as a transverse electromagnetic wave on rigorous footing.

More recently, the history of polarization optics has been characterized by new polarization optics, as well as more substantive and deeper mathematical descriptions of polarized light. We describe that history where relevant to our review of the physics of polarization below.

2.2. Jones Formalism

2.2a. Scalar Wave Equation and Plane Wave Solution

Maxwell's equations, the basis of all of modern optics, can be combined in a linear, isotropic, nondispersive, and homogeneous medium [7,15] to yield the scalar wave equation,

$$\nabla^2 \vec{E}(\vec{r}, t) = \mu\epsilon \frac{\partial^2}{\partial t^2} \vec{E}(\vec{r}, t), \tag{1}$$

where the electric field $\vec{E} = E_x\hat{x} + E_y\hat{y} + E_z\hat{z}$ with $\{x, y, z\}$ being the normal Cartesian coordinates, $\{\hat{x}, \hat{y}, \hat{z}\}$ being unit vectors along them, $\vec{r}$ being a spatial coordinate, and μ and ϵ being the permeability and permittivity, respectively, of the homogeneous medium. An identical relation exists for the magnetic field. In media meeting the above constraints, the Cartesian components of the electric field obey independent and identical wave equations, and each can be treated as independent scalar fields with no coupling. Equation (1) is, thus, known as the scalar wave equation.

A simple solution of Eq. (1), obtained by separation of space and time variables, is the monochromatic plane wave, whose electric field is given by

Figure 1
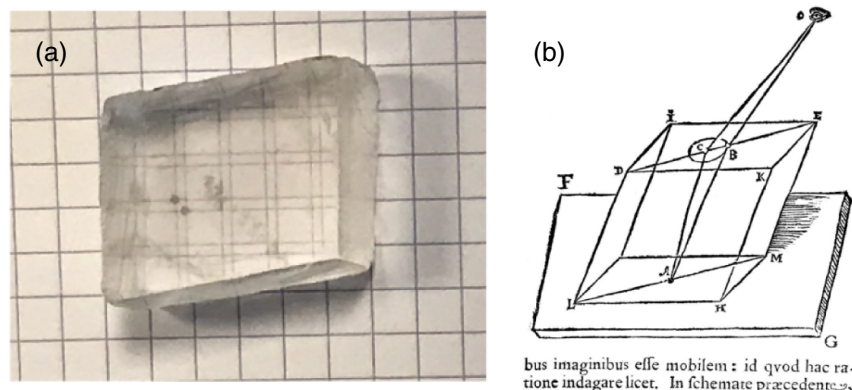
(a) Well-formed rhombohedral crystal of "Iceland spar" (i.e., calcite, $CaCO_3$) is strongly birefringent and exhibits doubly refracted images in transmission, in this case of a square lattice and a single dot. (b) This effect was first formally reported (in Latin) by the Dane Bartholinus in 1670, as exhibited by his own sketch of this effect [10].

$$\vec{E}(\vec{r}, t) = \vec{E}_0 \cos(\vec{k} \cdot \vec{r} - \omega t) = \vec{E}_0 \text{Re}\{e^{i(\vec{k}\cdot\vec{r}-\omega t)}\}. \tag{2}$$

Here ω is the usual angular frequency, and $\vec{k} = (k_x, k_y, k_z)$, with purely real entries, is the wave vector with $|\vec{k}| = \omega\sqrt{\mu\epsilon}$. This last relation gives the dispersion for a medium characterized by (ϵ, μ), where neither property varies with ω—that is, a *nondispersive* medium. At a given time t, Eq. (2) defines planes of constant phase given by $\vec{r}$ with constant values of $\vec{k} \cdot \vec{r}$. Equation (2) additionally stipulates that we are permitted to treat plane waves in complex exponential form, significantly easing mathematical analysis so long as we recall to take its real part when computing any observables in the end. The linearity of Eq. (1) means that any superposition of fields of the form of Eq. (2)—along arbitrary $\vec{k}$ and with arbitrary frequencies ω—is also a solution of Maxwell's equations.

Substitution of Eq. (2) into Maxwell's equations results in the time-harmonic, plane wave form of Maxwell's equations. These stipulate that in a uniform, isotropic medium, $\vec{k} \cdot \vec{E}_0 = 0$, i.e., that a plane wave is transverse, with its electric field confined to a plane perpendicular to its wave vector. The same holds for the magnetic field, and the so-called Poynting vector, the direction along which energy flows, is parallel to the wave vector $\vec{k}$.

If our coordinate system is oriented along the z axis such that $\vec{k} = k\hat{z}$, then the plane wave's electric field is constrained to lie in the $x - y$ plane, and we have, in general, that

$$\vec{E}(z, t) = (E_x e^{i\phi_x}\hat{x} + E_y e^{i\phi_y}\hat{y})e^{i(\omega t - kz)}, \tag{3}$$

neatly packaged in vector notation as

$$\vec{E}(z, t) = \begin{pmatrix} E_x e^{i\phi_x} \\ E_y e^{i\phi_y} \end{pmatrix} e^{i(\omega t - kz)}. \tag{4}$$

Removal of an overall phase and normalization of the vector's amplitude yields

$$\vec{E}(z, t) = E_0 e^{i\phi_x} \begin{pmatrix} \cos\chi \\ \sin\chi\, e^{i\phi} \end{pmatrix} e^{i(\omega t - kz)}, \tag{5}$$

where E_0 is a real-valued amplitude with $E_0^2 = E_x^2 + E_y^2$ and $\phi = \phi_y - \phi_x$.

2.2b. Jones Vectors

Neglecting the frequency and k-vector dependence, we focus on the central part of Eq. (5), which dictates the "shape" of the electric field vector, given by

$$|j\rangle = \begin{pmatrix} \cos\chi \\ \sin\chi\, e^{i\phi} \end{pmatrix}. \tag{6}$$

Both the x and y components oscillate at a frequency ω and differ only in amplitude and phase. Equation (6), thus, describes a shape that is in general an ellipse. The two angles χ and ϕ are a common parameterization of $|j\rangle$, which is commonly referred to as a "Jones vector." Cases in which $\phi = 0$ describe oscillation of the field along a line, *linear* polarization. When $\chi = \pm\frac{\pi}{4}$ and $\phi = \pm\frac{\pi}{2}$, the ellipse traces out a circle whose rotation is right- or left-handed (depending on the sign of ϕ), *circular* polarization. All other cases describe *elliptical* polarization (Fig. 2).

We note that in Eq. (6) we have adopted the bra–ket (or Dirac) notation for Jones vectors, which is commonly used in quantum mechanics but rather seldomly in

polarization optics. Advanced by authors such as Damask [4] and others, we find it to be a convenient and, occasionally, illuminating notation (especially in Subsection 2.5, where the Jones and Stokes formalisms are connected, and throughout Section 3).

We briefly review this notation here. A ket denotes a Jones vector, a polarization state. While $|j\rangle$ denotes the most generic normalized Jones vector, a Jones vector is in general given by

$$|E\rangle = \begin{pmatrix} \tilde{E}_x \\ \tilde{E}_y \end{pmatrix}. \tag{7}$$

Corresponding to this ket is a bra, which is the Hermitian conjugate, denoted by the † symbol, which entails a transposition of dimensions and a complex conjugation. That is,

$$\langle E| = (|E\rangle)^\dagger = \begin{pmatrix} \tilde{E}_x^* & \tilde{E}_y^* \end{pmatrix}. \tag{8}$$

Any closed bra–ket set is a scalar quantity denoting an inner product between two Jones vectors, a projection of one onto another. For two generic Jones vectors $|E_1\rangle = (\tilde{E}_{x,1} \ \tilde{E}_{y,1})^T$ and $|E_2\rangle = (\tilde{E}_{x,2} \ \tilde{E}_{y,2})^T$,

$$\langle E_1|E_2\rangle = \tilde{E}_{x,1}^* \tilde{E}_{x,2} + \tilde{E}_{y,1}^* \tilde{E}_{y,2}. \tag{9}$$

A normalized Jones vector such as $|j\rangle$ in Eq. (6) has a normalized inner product with itself, i.e., $\langle j|\lambda\rangle = 1$. For a generic Jones vector $|E\rangle$, $\langle E|E\rangle$ evaluates to the intensity of the corresponding plane wave, its square-amplitude.

Jones vectors are said to be orthogonal to one another if their inner product evaluates to zero. The orthogonal counterpart to the normalized Jones vector $|j\rangle$ [Eq. (6)], which is also normalized, is given by

$$|\lambda^\perp\rangle = \begin{pmatrix} -\sin\chi \\ \cos\chi \, e^{i\phi} \end{pmatrix}, \tag{10}$$

Figure 2
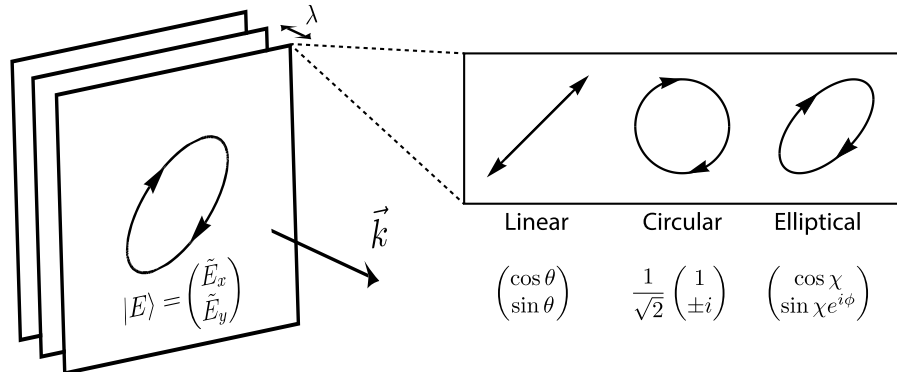
Polarization ellipse and the Jones vector. The plane wave solution of the wave equation [Eq. (1)] gives an electric field that, in general, traces out an ellipse with time when observed in a fixed plane. Planes of constant phase are perpendicular to the electric field and are separated by the wavelength λ along the $\vec{k} = 2\pi/\lambda$ vector. The shape of the electric field is described by the two-element Jones vector, examples of which are shown at the right.

which is chosen to ensure $\langle \lambda^\perp | \lambda \rangle = 0$. Any choice of two orthogonal Jones vectors is a sufficient basis to span the space of all Jones vectors.

2.2c. Jones Matrices

As plane waves transform—by passing through optical elements, or perhaps after undergoing reflection or refraction at material interfaces—the polarization state as described by the Jones vector can change in a way that depends on what the original polarization state was. If this occurs under the guise of linear optics, then knowledge of how the polarization is transformed for any given orthogonal set of Jones vectors is sufficient knowledge to say how *any* Jones vector should be transformed.

In this case, the linear transformation mapping one Jones vector $|E\rangle$ into another $|E'\rangle$ is given by

$$|E'\rangle = \mathbf{J}|E\rangle, \tag{11}$$

where $\mathbf{J}$ is a 2×2 operator known as a Jones matrix. A generic Jones matrix $\mathbf{J}$ has four complex entries (eight degrees-of-freedom in all) and is given by

$$\mathbf{J} = \begin{pmatrix} \tilde{J}_{11} & \tilde{J}_{12} \\ \tilde{J}_{21} & \tilde{J}_{22} \end{pmatrix}. \tag{12}$$

Again, as dictated by linearity, the action of $\mathbf{J}$ on any chosen orthogonal basis of Jones vectors $|j\rangle$ and $|j^\perp\rangle$ mathematically constrains all of its entries. We suppose

$$|j'\rangle = \mathbf{J}|j\rangle \tag{13}$$

and

$$|j^{\perp,'}\rangle = \mathbf{J}|j^\perp\rangle. \tag{14}$$

Writing the input Jones vectors as the columns of a 2×2 matrix $\mathbf{A}$,

$$\mathbf{A} = \begin{pmatrix} | & | \\ |j\rangle & |j^\perp\rangle \\ | & | \end{pmatrix}, \tag{15}$$

and similarly the output set of Jones vectors as the columns of a second 2×2 matrix $\mathbf{B}$,

$$\mathbf{B} = \begin{pmatrix} | & | \\ |j'\rangle & |j^{\perp,'}\rangle \\ | & | \end{pmatrix}, \tag{16}$$

enables us to recast Eqs. (13) and (14) as a single matrix equation given by

$$\mathbf{J}\mathbf{A} = \mathbf{B}, \tag{17}$$

with each of the two original equations residing in the two columns of the matrix equation. Since $\mathbf{A}$ has orthogonal, normalized columns, its inverse is given by $\mathbf{A}^{-1} = \mathbf{A}^\dagger$ ($\mathbf{A}$ is unitary—more on that in Subsection 2.3), and we have straightforwardly that

$$\mathbf{J} = \mathbf{B}\mathbf{A}^\dagger \tag{18}$$

for any choice of orthonormal Jones vector basis contained in **A** with † the Hermitian conjugate. Knowledge of the response of **J** to any orthogonal set of Jones vectors is sufficient to fully constrain it. Practically speaking, this requires the ability to measure output Jones vectors including *phase*. This is readily achieved in much of the radio-frequency (RF) domain, but at optical frequencies, polarization and polarization-sensitive samples must be characterized using intensity measurements. See Subsections 2.4 and 2.7.

A given Jones matrix **J** may amplify or attenuate a given incident polarization, and it may advance or retard it in phase, or perform these operations selectively on orthogonal components of the polarization; one matrix **J** may do all of these things to a given Jones vector but something entirely different to another provided that linearity, and thus superposition, hold. This is described more systematically in the next section.

Finally, we note that in the bra–ket notation a combination of a ket and a bra signifies an outer product and results in a 2×2 matrix quantity, a Jones matrix. For two generic Jones vectors $|E_1\rangle = (\tilde{E}_{x,1} \ \tilde{E}_{y,1})^T$ and $|E_2\rangle = (\tilde{E}_{x,2} \ \tilde{E}_{y,2})^T$,

$$|E_2\rangle\langle E_1| = \begin{pmatrix} \tilde{E}_{x,1}^* \tilde{E}_{x,2} & \tilde{E}_{y,1}^* \tilde{E}_{x,2} \\ \tilde{E}_{x,1}^* \tilde{E}_{y,2} & \tilde{E}_{y,1}^* \tilde{E}_{y,2} \end{pmatrix}. \qquad (19)$$

A combination of a Jones bra and ket in the opposite order yields an inner product, a projection of one polarization state onto another:

$$\langle E_1|E_2\rangle = \tilde{E}_{x,1}^* \tilde{E}_{x,2} + \tilde{E}_{y,1}^* \tilde{E}_{y,2}. \qquad (20)$$

By inspection of Eqs. (19) and (20), the two can be related by the matrix trace operation as

$$\langle E_2|E_1\rangle = \mathrm{Tr}(|E_2\rangle\langle E_1|). \qquad (21)$$

2.2d. Origins of the Jones Calculus

This way of treating polarization, in terms of two-dimensional (2D) state vectors, and the optical transformations that transform between them in the form of 2×2 matrices, is known broadly as the *Jones calculus*. The Jones calculus deals directly with the electric field of plane waves and, thus, follows naturally from the wave equation. Despite this close kinship between the two, the use of a matrix formalism to handle polarized light was first proposed by Robert Clark Jones, a graduate student at Harvard University and namesake of this Jones calculus, in a series of eight papers [16–23] beginning only in 1941—some 76 years after Maxwell's work.

It helps to consider the context in which Jones' work occurred. Early works in polarization generally employed crystals, like Iceland spar, but also Nicols and Wollaston prisms, in which multiple output beams are produced. Starting in the 1920s as an undergraduate at Harvard, and later as founder of the Polaroid Corporation, Edwin Land developed several technologies for polarizing sheet in which long molecules are coaxed into alignment in an imitation of a wire-grid polarizer [9]. Notably, these allowed for mass-produced polarizers yielding only one on-axis output beam. The presence of a single output beam, and the complex, difficult-to-visualize transformations that can occur as a polarization ellipse transforms through a series of polarization optics, necessitated the Jones calculus. Shurcliff's book, written with mentorship from Land and Jones, addresses this [1].

Jones' work extended well beyond merely introducing a matrix formalism (including the so-called "N-matrices," which we address indirectly in Subsection 2.5). In the words of Jones, "this purely formal step of introducing matrix notation turned out to be fruitful ... because of the large bag of tricks which may be used in the manipulation of matrices" [20]. We explore some of these in the next section.

2.3. Matrix Polar Decomposition

2.3a. Hermitian and Unitary Jones Matrices

In analogy with quantum mechanics, unitary and Hermitian operators take on a special importance in polarization optics.

A Jones matrix $\mathbf{U}$ is unitary if

$$\mathbf{U}^{\dagger}\mathbf{U} = \mathbb{I} = \begin{pmatrix} 1 & 0 \\ 0 & 1 \end{pmatrix}. \tag{22}$$

Throughout this review, $\mathbb{I}$ refers to the 2×2 identity matrix. In mathematics, unitary matrices preserve inner product, and in polarization optics, unitary Jones matrices preserve the amplitude of Jones vectors and inner products between them [a direct consequence of Eq. (22)].

In this way, it can be said that unitary matrices are phase-only. A unitary matrix can apply an overall polarization-independent phase shift and a relative phase shift between two orthogonal polarization states. In general, this basis of polarization states can be elliptical and requires two angles [e.g., χ and ϕ in Eq. (6)] to fully define. Counted along with the aforementioned overall and relative phase shifts, a unitary Jones matrix $\mathbf{U}$ is defined by four independent angles.

Physically speaking, a unitary matrix projects an incident polarization onto an orthogonal basis of polarizations, retards one of these components in phase relative to the other, and applies an overall phase shift to both. This can be written compactly in bra–ket notation as

$$\mathbf{U} = e^{i\phi}(e^{i\frac{\Delta}{2}}|j\rangle\langle j| + e^{-i\frac{\Delta}{2}}|j^{\perp}\rangle\langle j^{\perp}|). \tag{23}$$

In Eq. (23), ϕ is an overall phase shift, Δ is known as the *retardance*, and $|j\rangle$ and $|\lambda^{\perp}\rangle$ are an arbitrary, orthonormal basis of polarization states defined by two angles (χ and ϕ) as in Eqs. (6) and (10). The notation of Eq. (23) defines its action. Each term of Eq. (23) is the Jones matrix of a polarizer. In the first term, for instance, the bra $\langle\lambda|$ extracts the part of the incident polarization lying along $|j\rangle$, while the ket $e^{i\frac{\Delta}{2}}|j\rangle$ stipulates that this light is phase-shifted with its polarization preserved. The eigenvectors of $\mathbf{U}$, then, are $|j\rangle$ and $|\lambda^{\perp}\rangle$.

In a laboratory setting, wave plates—uniaxial or biaxial crystals cut so light can propagate along a crystalline axis, precisely ground to a desired thickness—implement unitary Jones matrices but almost always with a basis that consists of linear polarizations. A quarter-wave plate ("$\lambda/4$") implements Eq. (23) with a retardance $\Delta = \pi/2$, an unspecified value of ϕ, and a basis corresponding to orthogonal linear polarizations oriented at the angle of the fast-axis of the wave plate (that is, the axis along which light propagates faster sees a lower refractive index and, consequently, accrues less phase).

A Jones matrix $\mathbf{H}$ is Hermitian if

$$\mathbf{H}^{\dagger} = \mathbf{H}, \tag{24}$$

i.e., the matrix equals its own Hermitian conjugate (with $A^\dagger = (A^T)^*$). Hermitian matrices describe amplitude changes—polarization-dependent loss (or gain)—with no phase shifts. A Hermitian matrix is defined by an overall polarization-independent loss, a differential loss between two polarizations, and an orthogonal basis containing those two polarization states. In other words, **H** is defined by two scalars (common mode and differential loss) and two angles (e.g., χ and ϕ) to define an orthogonal Jones vector basis, four parameters overall.

In the bra–ket notation,

$$\mathbf{H} = e^{-\frac{\alpha_0}{2}} (e^{\frac{\alpha}{2}} |j\rangle\langle j| + e^{-\frac{\alpha}{2}} |j^\perp\rangle\langle j^\perp|), \tag{25}$$

where α_0 is a common loss (or gain, if $\alpha_0 < 0$), α is a differential loss, and $|j\rangle$ and $|\lambda^\perp\rangle$ are again an orthogonal eigenbasis of polarization states. In laboratory experience, Hermitian Jones matrices correspond to polarizers. A linear polarizer, for instance, has an eigenbasis of linear polarization states and is often treated as perfect—one polarization is passed without attenuation, while the orthogonal polarization is completely extinguished. This mandates $\alpha_0 = \alpha = \infty$ if $|j\rangle$ is the Jones vector with maximum transmission. In reality, no polarizer or polarizing effect is perfect, and both losses are finite. In that case, we define the quantity

$$\mathcal{D} = \frac{I_{|j\rangle} - I_{|j^\perp\rangle}}{I_{|j\rangle} + I_{|j^\perp\rangle}} = \frac{e^\alpha - e^{-\alpha}}{e^\alpha + e^{-\alpha}} = \tanh \alpha. \tag{26}$$

$\mathcal{D}$ is known as the diattenuation and is the contrast in intensity transmitted by **H** when $|j\rangle$ and $|j^\perp\rangle$—the polarization states of maximum and minimum transmission, respectively—are incident. For a perfect polarizer, $\mathcal{D} = 1$; for $\mathbf{H} = \mathbb{I}$ (which is both unitary and Hermitian), no contrast exists in transmitted power with incident polarization and $\mathcal{D} = 0$. Cases in-between represent a partial polarizer, often referred to as a diattenuator.

Any Jones matrix contains both Hermitian and unitary parts. Hermitian and unitary matrices taken together form the building blocks of all Jones matrices and, consequently, all linear polarization elements. This follows from the singular value decomposition (SVD), which exists for all matrices of arbitrary dimension. A general square Jones matrix **J** has an SVD given by

$$\mathbf{J} = \mathbf{A}\mathbf{D}\mathbf{V}^\dagger, \tag{27}$$

where **A** and **V** are 2×2 unitary matrices and **D** is a diagonal, positive, and real 2×2 matrix. By definition, $\mathbf{V}^\dagger\mathbf{V}$ and $\mathbf{A}^\dagger\mathbf{A}$ both equal $\mathbb{I}$, so we can insert either anywhere in Eq. (27). We first write

$$\mathbf{J} = (\mathbf{A}\mathbf{V}^\dagger)(\mathbf{V}\mathbf{D}\mathbf{V}^\dagger). \tag{28}$$

By inspection, the first parenthesized matrix $\mathbf{U} = \mathbf{A}\mathbf{V}^\dagger$ is unitary with $\mathbf{U}^\dagger\mathbf{U} = \mathbf{V}\mathbf{A}^\dagger\mathbf{A}\mathbf{V}^\dagger = \mathbb{I}$, while the second $\mathbf{H} = \mathbf{V}\mathbf{D}\mathbf{V}^\dagger$ is Hermitian with $\mathbf{H}^\dagger = \mathbf{H}$. We can then write any Jones matrix **J** as a product of a unitary matrix **U** and a Hermitian matrix **H**,

$$\mathbf{J} = \mathbf{U}\mathbf{H}. \tag{29}$$

By an analogous argument, we can also reverse order and write

$$\mathbf{J} = \mathbf{H}'\mathbf{U}' \tag{30}$$

for a Hermitian $\mathbf{H}' = \mathbf{ADA}^\dagger$ and a unitary $\mathbf{U}' = \mathbf{AV}^\dagger$. This is known as the matrix polar decomposition. Mathematically equivalent to the SVD, it is a matrix analog to the scalar polar decomposition wherein a complex number $\tilde{q}$ can be written in amplitude-phase form as $\tilde{q} = Ae^{i\theta}$ with a real-valued amplitude A and a phase angle θ.

A key difference is that matrix multiplication is not in general commutative and Eqs. (29) and (30) in general represent different decompositions (the "right" and "left" polar decompositions, respectively). For special $\mathbf{J}$, often referred to as "homogeneous Jones matrices" [2,24], the right and left polar decompositions are identical; the Hermitian and unitary components share a common eigenbasis and can commute.

Since unitary and Hermitian Jones matrices each have four free parameters, the polar decomposition reflects the fact that an arbitrary Jones matrix has eight degrees-of-freedom.

In polarization optics, the matrix polar decomposition is physically significant. A given optical element or process that affects light's polarization and can be written as a Jones matrix $\mathbf{J}$ can be thought of as comprising a diattenuator (partial polarizer) followed by a wave plate, or vice versa (though not the same partial polarizer and wave plate). This can be used as an intuitive aid: The possibly complex polarization-dependent effect of any linear polarization transformation can be thought of as a cascade of two optical elements analogous to real laboratory optics, whose parameters (diattenuation, common mode loss, overall phase, retardance, and the polarization eigenbases of each) are governed by the polar decomposition. This is shown in Fig. 3. The polar decomposition (and SVD) can be found by a variety of numerical schemes.

2.3b. Power Transfer Characteristic of a Jones Matrix

The matrix $\mathbf{J}$ produces the state $\mathbf{J}|j\rangle$ for a generic input, with a power given by $\langle j|\mathbf{J}^\dagger\mathbf{J}|j\rangle$. Averaged over all possible normalized input polarizations $\{|j\rangle\}$, the expected power output is $\frac{1}{2}\mathrm{Tr}(\mathbf{J}^\dagger\mathbf{J})$, where Tr denotes the matrix trace operation. If we take the right polar decomposition of Eq. (29), $\mathbf{J} = \mathbf{UH}$. Then, the unitarity of

Figure 3
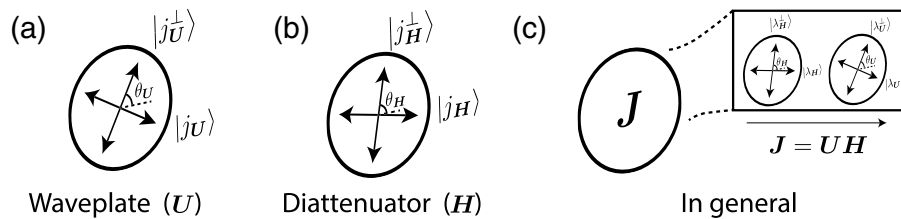
Jones matrix polar decomposition. Two broad classes of polarization transformations exist. (a) A unitary transformation (described by a Jones matrix $\boldsymbol{U}$ for which $\boldsymbol{U}^\dagger\boldsymbol{U} = \mathbb{I}$) is a lossless transformation in which the components of an incident plane wave along orthogonal eigenvectors are retarded in phase. Physically, wave plates can enact a unitary Jones matrix. (b) A Hermitian transformation is described by a Jones matrix $\boldsymbol{H}$ for which $\boldsymbol{H}^\dagger = \boldsymbol{H}$. These attenuate (or, less commonly, amplify) an orthogonal eigenbasis of polarizations. Devices implementing Hermitian Jones matrices are known as diattenuators, of which a polarizer is a limiting case. (c) Any *linear* polarization transformation given by a 2×2 Jones matrix $\boldsymbol{J}$ can be written as a cascade of a Hermitian device—a diattenuator—followed by a unitary device—a wave plate. Note that this is true for any $\boldsymbol{J}$ (which may not itself have an orthogonal eigenbasis).

U gives $\mathbf{J}^{\dagger}\mathbf{J} = \mathbf{H}^{\dagger}\mathbf{H}$, and the power transfer of the Jones matrix is given solely by its Hermitian part and its common loss $e^{-\alpha_0}$ (the factor of 1/2 is removed due to the squaring in going from field to intensity). A similar argument holds if the left polar decomposition is used owing to the invariance of the trace to the order of matrix multiplication.

2.4. Stokes/Mueller Formalism

2.4a. Stokes Vector

The Jones formalism, while convenient, makes explicit reference to the electric field. It is a coherent description in which phase matters. This can be convenient in the RF (e.g., in radar) domain where direct phase measurements are possible, but detectors cannot follow the electric field at optical frequencies. Instead, the intensity—proportional to the square of the electric field—is measured by a linear detector.

Through its manifestation as a power modulation when passed through an analyzer, polarization is readily observed. In 1852, Sir George G. Stokes recast Fresnel's description of polarized light as an ellipse in terms of series of these measurements. The experiments involve measuring the intensity of a beam passed through analyzers for $|x\rangle$, $|y\rangle$, $|45°\rangle$, $|135°\rangle$, $|R\rangle$, and $|L\rangle$—four equally spaced linear polarizations, as well as both chiralities of circular polarization. These comprise three orthogonal polarization bases. Practically speaking, all six analyzers can be constructed from a rotatable linear polarizer and quarter-wave plate (for the circular measurements). These measured intensities are labeled $I_{|q\rangle}$, where $|q\rangle$ is the preferred polarization of the polarizer.

These six measurements are transformed into four quantities and represented as a column vector, appropriately dubbed the Stokes vector, given by

$$\vec{S} = \begin{pmatrix} S_0 \\ S_1 \\ S_2 \\ S_3 \end{pmatrix} = \begin{pmatrix} I_{|x\rangle} + I_{|y\rangle} \\ I_{|x\rangle} - I_{|y\rangle} \\ I_{|45°\rangle} - I_{|135°\rangle} \\ I_{|R\rangle} - I_{|L\rangle} \end{pmatrix}. \tag{31}$$

In the remote sensing and astronomy, the Stokes vector is often labeled as $\vec{S} = (I\ Q\ U\ V)^T$, though we use the convention of Eq. (31) here. The first Stokes vector S_0 quantifies the power of the beam and could be given by the sum of the powers measured in any orthogonal basis (i.e., $S_0 = I_{|45°\rangle} + I_{|135°\rangle} = I_{|R\rangle} + I_{|L\rangle}$ as well). It constrains the overall size of the polarization ellipse. The next three Stokes parameters define the shape of the polarization ellipse. Each is a differential measurement of the beam's preference for different polarizations—$|x\rangle$ over $|y\rangle$ (S_1), $|45°\rangle$ over $|135°\rangle$ (S_2), and $|R\rangle$ over $|L\rangle$ (S_3). Some examples of polarization states represented using the Stokes formalism (and their analog in the Jones representation) are provided in Table 2.

It is sometimes remarked that the Stokes vector does not comprise a true vector space because not all Stokes vectors are physical (so that some prefer the term "Stokes parameters"). A Stokes vector must satisfy

$$\sqrt{S_1^2 + S_2^2 + S_3^2} \leq S_0. \tag{32}$$

Equation (32) is a physicality requirement and states that the polarized power in a beam must be equal (in the case of fully polarized light) or less than (in the case of partially polarized light) the overall beam's power. In other words, the act of passing

a beam through an analyzer cannot impart energy on it. In geometrical terms, Eq. (32) constrains the set of all possible Stokes vectors to lie inside a cone in four-dimensional space [25].

Often, the last three Stokes parameters are normalized by the first to yield the *state-of-polarization* (SOP) as

$$\vec{s} = \begin{pmatrix} S_1/S_0 \\ S_2/S_0 \\ S_3/S_0 \end{pmatrix} = \begin{pmatrix} s_1 \\ s_2 \\ s_3 \end{pmatrix}. \tag{33}$$

In the case of fully polarized light, Eq. (32) becomes

$$s_1^2 + s_2^2 + s_3^2 = 1. \tag{34}$$

The SOP $\vec{s}$ is an alternate (but equivalent) description of the polarization ellipse. Its parameters s_1, s_2, and s_3 as normalized differential powers are all strictly real. In light of the physicality requirement Eq. (34), though, the SOP has only two free parameters. These correspond in number to the two free parameters of the normalized Jones vector, the angles χ and ϕ in Eq. (6). All information on the linear nature of the polarization ellipse is contained in s_1 and s_2, which constrain its azimuthal orientation. Its ellipticity—how eccentric the ellipse is—is governed solely by s_3.

A polarization ellipse is defined by its size, azimuthal orientation, and this ellipticity. The Stokes vector Eq. (31), however, contains four parameters. The last degree-of-freedom of polarization is the degree-of-polarization (DoP), the statistical certainty with which the polarization ellipse can be known, discussed in Subsection 2.4c.

Stokes' description of polarized light was itself largely forgotten for a century after publication, only to be revived in a study of radiative transfer by the astrophysicist Chandrasekhar in the 1950s [26].

2.4b. Poincaré Sphere

By inspection, Eq. (34) defines the surface of a sphere if the normalized Stokes parameters (s_1, s_2, s_3) are taken as Cartesian coordinates. In the Poincaré sphere representation (named for the prolific French mathematician to whom this insight belongs), all polarization ellipses—all SOPs—can be thought of as residing on the surface of a sphere. The equator of this sphere where $s_3 = 0$ contains all linear polarization states whose azimuthal orientations vary with longitude. The poles of the sphere where $s_1, s_2 = 0$ and $s_3 = \pm 1$ correspond to circular polarization states of opposite handedness. In-between the equator and the poles stand all elliptical SOPs, with lines of constant latitude (constant s_3) defining a fixed ellipticity and lines of constant

Table 2.   Various Stokes Vectors and Their Corresponding Jones Vectors

Polarization State	Stokes	Jones
$|x\rangle$	$\begin{pmatrix} 1 & 1 & 0 & 0 \end{pmatrix}^T$	$\begin{pmatrix} 1 \\ 0 \end{pmatrix}$
$|y\rangle$	$\begin{pmatrix} 1 & -1 & 0 & 0 \end{pmatrix}^T$	$\begin{pmatrix} 0 \\ 1 \end{pmatrix}$
General linear polarization	$\begin{pmatrix} 1 & \cos 2\theta & \sin 2\theta & 0 \end{pmatrix}^T$	$\begin{pmatrix} \cos\theta \\ \sin\theta \end{pmatrix}$
$|R\rangle$	$\begin{pmatrix} 1 & 0 & 0 & 1 \end{pmatrix}^T$	$\frac{1}{\sqrt{2}}\begin{pmatrix} 1 \\ i \end{pmatrix}$
Unpolarized light	$\begin{pmatrix} 1 & 0 & 0 & 0 \end{pmatrix}^T$	No direct analog. Can be written as $\begin{pmatrix} 1 \\ 0 \end{pmatrix} + e^{i\tilde{\phi}}\begin{pmatrix} 0 \\ 1 \end{pmatrix}$ for $\tilde{\phi}$ random in time.

longitude (constant s_2/s_1) defining fixed azimuthal orientations of the polarization ellipse. The interior of the Poincaré sphere can be thought of as containing partially polarized states of light, with the origin corresponding to completely unpolarized light (Subsection 2.7). The Poincaré sphere is depicted in Fig. 4.

Orthogonal polarizations on the Poincaré sphere are given by polarization states whose Stokes vectors are diametrically opposite, that is, inverted about the origin. A given Stokes vector is orthogonal to another if each of S_1, S_2, and S_3 are equal in magnitude but inverted in sign. This is a geometric subtlety of the Poincaré sphere and the Stokes formalism more generally—orthogonality means a separation of 180° rather than the conventional notion of perpendicularity at 90°. All physical angles of the polarization ellipse are doubled in converting to the Stokes representation. This is shown in Fig. 4(b).

The Poincaré sphere, an example of the more general notion of a Bloch sphere in physics, is an intuitive aid that will be used extensively in this review. In addition to representing polarization states, the Poincaré sphere is also of use in visualizing polarization transformations and polarization-transforming optical elements (Subsections 2.5 and 2.6).

2.4c. Partially and Unpolarized Light

Coherent and incoherent addition. The fact that orthogonal polarizations lie on opposite sides of the Poincaré sphere has consequences that, at first brush, can be confusing. Consider, for instance, the interference of light linearly polarized along x with light linearly polarized along y both with intensities of $1/2$ (in some arbitrary units):

$$\vec{S} = \vec{X} + \vec{Y}$$

$$= \frac{1}{2}\begin{pmatrix} 1 \\ 1 \\ 0 \\ 0 \end{pmatrix} + \frac{1}{2}\begin{pmatrix} 1 \\ -1 \\ 0 \\ 0 \end{pmatrix} = \begin{pmatrix} 1 \\ 0 \\ 0 \\ 0 \end{pmatrix}. \tag{35}$$

Figure 4

(a)   (b)
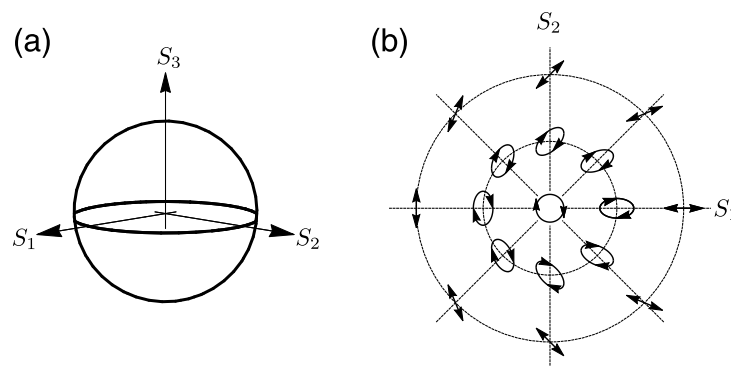
All plane wave polarization states can be imagined to lie on the surface of a sphere known as the Poincaré sphere [(a), with a view of the northern hemisphere given in (b)]. All linear polarization states lie along its equator and circular polarization states of opposite handedness occupy its poles; everywhere in-between is elliptical. All angles are doubled with respect to the physical polarization ellipse so that orthogonal polarizations lie at diametrically opposite points. The origin corresponds to unpolarized light, while the interior corresponds to partially polarized states (Subsection 2.4c).

Intuitively, we might first hazard that the interference of the two should yield light linearly polarized at 45° so that the result of the addition should have an SOP of $\vec{s} = (0, 1, 0)^T$. Instead, the SOP seems to be $\vec{s} = (0, 0, 0)^T$. This begs another question. The interference of x- and y-polarized light only yields 45° if the two are in phase; if the phase shift, for instance, is $\pi/2$, we have circular polarization. A general phase shift between the two yields an infinite number of elliptical polarization states. In the addition of Stokes vectors, which of these relative phases is meant?

Being based on intensity measurements, the Stokes formalism can make no reference to phase. This underlies the result of Eq. (35), which actually describes completely *unpolarized* light. In the Stokes calculus, all addition is incoherent. This means that a completely random phase relation must be assumed. In adding the Stokes vectors for x- and y-polarized light, all possible relative phases are included simultaneously, so the result can be seen as a superposition of all of these at once. At any one instant in time, the phase between x and y could take on any value between 0 and 2π randomly so that the polarization ellipse itself has a random shape. Stated differently, the path of the electric field vector is completely uncorrelated with that an instant in time later.

Degree-of-polarization. This correlation between the polarization ellipse at one instant of time with that a short time later—a notion of how *pure* the polarization itself is—is quantified by the DoP, given for a Stokes vector $\vec{S}$ in Eq. (31) as

$$\text{DoP}(\vec{S}) = p = \frac{\sqrt{S_1^2 + S_2^2 + S_3^2}}{S_0}. \tag{36}$$

DoP $= 1$ signifies complete certainty over the polarization ellipse, while DoP $= 0$ signifies complete *un*certainty. Values in-between signify some, but not perfect, correlation: partial polarization. Values below 0 or above 1 are not physical. A consequence of this definition is that, geometrically, partially polarized states of polarization can be understood to occupy the interior of the Poincaré sphere, with completely unpolarized light sitting at the origin.

The DoP is a measure of how strongly a beam can be suppressed in intensity by a polarization analyzer (a polarizer). Any perfectly constant polarization ellipse can be fully suppressed given possession of a polarizer whose pass-axis corresponds to its orthogonal counterpart (this is, in general, an elliptical polarizer). When light is partially polarized, it has a preferred polarization ellipse, a sort of "average" path taken by the electric field vector. A polarizer whose pass polarization is orthogonal to this state will maximally extinguish the beam, but no polarizer can fully extinguish a partially polarized beam. The DoP is the "contrast"—the normalized difference—between the intensity of the beam itself and this minimum analyzed intensity. In the limit of completely unpolarized light, there is no contrast obtained by passing a beam through polarizers at different orientations and with different characteristic polarizations.

In other words, any Stokes vector can be thought of as part fully polarized (with a specific SOP) and part unpolarized. The DoP value p dictates the distribution between the two as

$$\vec{S} = \begin{pmatrix} S_0 \\ S_1 \\ S_2 \\ S_3 \end{pmatrix} = S_0 \left[(1-p) \begin{pmatrix} 1 \\ 0 \\ 0 \\ 0 \end{pmatrix} + p \begin{pmatrix} 1 \\ \frac{S_1}{S_1^2 + S_2^2 + S_3^2} \\ \frac{S_2}{S_1^2 + S_2^2 + S_3^2} \\ \frac{S_3}{S_1^2 + S_2^2 + S_3^2} \end{pmatrix} \right]. \tag{37}$$

The first term of Eq. (37) is completely unpolarized while the second term is fully polarized with the same SOP as the original beam.

Inherent in the definition of the DoP is a notion of time-averaging, which follows from the definition of the Stokes parameters in terms of intensity measurements, which necessarily involve integration of some signal (usually electrical). That means that a plane wave that appears to have a fixed polarization (DoP = 1) on one time scale may appear completely unpolarized if intensity integration is carried out over longer times, allowing the polarization ellipse to vary. The limit of this line of thought is the tracing of the electric field vector at the time scale of the light's frequency itself, which is possible at lower frequencies (RF) but not in optics.

Examples of partially polarized light. The DoP represents a manifestation of partial coherence in polarization optics and forms the basis of the modern view of the polarization of light as a statistical phenomenon alongside other statistical properties of light, such as temporal and spatial coherence [7,27–29]. We do not dwell much on this here. We note, however, that, while Eq. (36) defines the DoP, it does not provide a physical explanation for what partial polarization *is*, or how to prepare it. Any effect in which multiple polarization ellipses are averaged will produce the requisite uncertainty to drive the DoP down from unity. This could be due to several factors, however, including time-varying sources and even sources whose polarization ellipse varies over the spatial aperture of the detector. We provide two simple examples of signals with DoP < 1, also depicted in Fig. 5:

- Consider a beam in a superposition of x and y linearly polarized light (dictated by an orientation angle θ, constant in time) with a phase shift $\phi(t)$ between the two that depends on time. Its instantaneous Jones vector is given by

$$|E(t)\rangle = \begin{pmatrix} \cos\theta \\ \sin\theta\, e^{i\phi(t)} \end{pmatrix}.$$

(38)

The instantaneous Stokes vector (a bit of a misnomer, since this cannot be measured) corresponding to $|E(t)\rangle$ is given by

$$\vec{S}(t) = \begin{pmatrix} 1 \\ \cos 2\theta \\ \sin 2\theta \cos\phi(t) \\ \sin 2\theta \sin\phi(t) \end{pmatrix}.$$

(39)

We suppose that after some characteristic *coherence* time τ, $\phi(t)$ is uncorrelated with itself. That is, $\langle\cos\phi(t)\rangle_T = \langle\sin\phi(t)\rangle_T = 0$, where $T \gg \tau$ and $\langle x(t)\rangle_T$ denotes a time average of $x(t)$ over a time period $t = T$, i.e., $\langle x(t)\rangle_T = \frac{1}{T}\int_0^T x(t)\mathrm{d}t$. Assuming a suitably long averaging period, the "average Stokes vector" (which corresponds to the one actually measured) is given by

$$\langle\vec{S}(t)\rangle_T = \begin{pmatrix} 1 \\ \cos 2\theta \\ 0 \\ 0 \end{pmatrix},$$

(40)

which describes partially polarized light with DoP $= \cos 2\theta$. This example falls under what is sometimes referred to as "naturally" depolarized light—the origin of this depolarization rests with the physics of the source itself, some aspect of which [encapsulated in the phase function $\phi(t)$ and its coherence time τ] causes randomness in the polarization ellipse. In a laboratory, light can be depolarized in

this way using two polarization beam splitters constructed into a Mach–Zehnder interferometer with a path length difference that is much longer than, e.g., the coherence length of the laser source or lamp being used. This is shown in Fig. 5(a).

- A second example concerns a source that is composed of two plane waves of different frequency with time-invariant polarization states:

$$|E(t)\rangle = |E_1(t)\rangle + |E_2(t)\rangle = e^{i\omega_1 t}\begin{pmatrix} \cos\chi_1 \\ \sin\chi_1 e^{i\phi_1} \end{pmatrix} + e^{i\omega_2 t}\begin{pmatrix} \cos\chi_2 \\ \sin\chi_2 e^{i\phi_2} \end{pmatrix}. \quad \textbf{(41)}$$

We can compute the first component of the Stokes vector as

$$S_1(t) = (E_1^{(x)}(t))^* E_1^{(x)}(t) - (E_1^{(y)}(t))^* E_1^{(y)}(t)$$

$$= (e^{-i\omega_1 t}\cos\chi_1 + e^{-i\omega_2 t}\cos\chi_1)(e^{i\omega_1 t}\cos\chi_1 + e^{i\omega_2 t}\cos\chi_1)$$

$$\quad - (e^{-i\omega_1 t}e^{-i\phi_1}\sin\chi_1 + e^{-i\omega_2 t}e^{-i\phi_2}\sin\chi_1)(e^{i\omega_1 t}e^{i\phi_1}\sin\chi_1 + e^{i\omega_2 t}e^{i\phi_2}\sin\chi_1)$$

$$= (\cos^2\chi_1 + \cos^2\chi_2 + 2\cos((\omega_1 - \omega_2)t)\cos\chi_1\cos\chi_2)$$

$$\quad - (\sin^2\chi_1 + \sin^2\chi_2 + 2\cos((\omega_1 - \omega_2)t + (\phi_1 - \phi_2))\sin\chi_1\sin\chi_2).$$

$$\textbf{(42)}$$

Averaged over a period of time much greater than the "beat" period $T = 2\pi/(\omega_1 - \omega_2)$, the time-dependent cosines average to zero, and we have

$$\langle S_1(t)\rangle = (\cos^2\chi_1 - \sin^2\chi_1) + (\cos^2\chi_2 - \sin^2\chi_2) = S_1^{(1)} + S_1^{(2)}, \quad \textbf{(43)}$$

that is, just the sum of the Stokes components for $|E_1(t)\rangle$ and $|E_2(t)\rangle$ individually. The same is true of the other three entries of the Stokes vector. Then,

$$\text{DoP} = \frac{(S_1^{(1)} + S_1^{(2)}) + (S_2^{(1)} + S_2^{(2)}) + (S_3^{(1)} + S_3^{(2)})}{S_0^{(1)} + S_0^{(2)}} \le 1. \quad \textbf{(44)}$$

Given control over the two polarization states, the DoP can take any physical value. If the two are identical, the light is fully polarized; if the two are orthogonal (such as x and y), the numerator sums to zero, and the light is fully unpolarized.

This is an example of what is sometimes referred to as "pseudo" depolarized light because it is composed of fully coherent, polarized components. It is only the polychromaticity of the signal (paired with a suitably long averaging time) that renders the light depolarized. This is shown in Fig. 5(b).

As a final note, the DoP and partially polarized light can be equivalently treated in terms of Jones vectors if the coherency matrix (a polarization analog of the quantum mechanical density matrix, which involves time-averaging) is formed. This is amply described in many other references (e.g., [7,28]), and we do not take it up here.

2.4d. Mueller Calculus

A change in the polarization state of a beam can be modeled using Stokes vectors. A linear transformation that maps an input Stokes vector into an output Stokes vector is known as a Mueller matrix (named for Hans Mueller, an instructor at the Massachusetts Institute of Technology in the 1940s [9]). It is a 4×4 matrix with strictly real entries:

$$\mathbf{M} = \begin{pmatrix} m_{00} & m_{01} & m_{02} & m_{03} \\ m_{10} & m_{11} & m_{12} & m_{13} \\ m_{20} & m_{21} & m_{22} & m_{23} \\ m_{30} & m_{31} & m_{32} & m_{33} \end{pmatrix}. \tag{45}$$

An output beam passing through a system described by $\mathbf{M}$ is given by a simple matrix multiplication as

$$\vec{S}^{\text{out}} = \mathbf{M}\vec{S}^{\text{in}}, \tag{46}$$

and the Mueller matrix of a composite system can be described by multiplication of its constituent Mueller matrices.

Transformations that do not *depolarize* light can be described equally well with Jones or Mueller matrices—that is, up to an overall phase shift (as an incoherent description, absolute phase does not exist in the Stokes/Mueller formalism). We discuss the transformation between the two formalisms in Subsection 2.5b.

The additional information content of a Mueller matrix, above the eight parameters that compose a Jones matrix, is to model transformations that change the degree to which light is polarized. Not all real 4×4 matrices, however, can be called Mueller matrices. In analogy with Eq. (32), there are physicality requirements that constrain some of its entries. The first row and the first column of the Mueller matrix are of particular importance. The first row dictates the power transfer characteristics of a Mueller matrix $\mathbf{M}$ with incident polarization because S_0^{out}, the power of the output

Figure 5
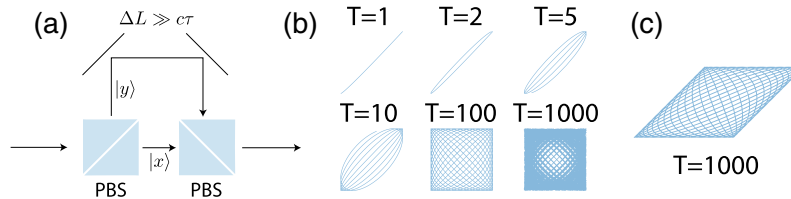
Partially polarized light. Illustrations of the two examples given in Subsection 2.4c of how light may be partially (or un-) polarized. (a) The coherence properties of a light source can be used to deterministically produce partially polarized light. Light can be split (and then recombined) using polarization beam splitters, projecting the incident polarization into orthogonal components. These are then delayed by a path length ΔL that is much longer than the source's coherence length, $c\tau$. If the initial polarization is such that equal intensity goes along each path, the resultant light is completely unpolarized. (b) Partially polarized light can also be prepared by combining two (or more) frequencies of completely coherent light in different polarization states. Here the path of the electric field of two slightly different frequencies in x and y linear polarization states is shown after several multiples of the characteristic "beat" time between the two frequencies, $2\pi/(\omega_1 - \omega_2)$. The electric field traces out a Lissajous figure. At short times, a preferred direction is evident; over these time scales, the light is partially polarized. Over longer times, the electric field fills out a full square. All polarization ellipses are equally represented, and the light is unpolarized. (c) If, on the other hand, the two frequencies have polarization states that are *not* orthogonal, partially polarized light is produced. Here, x and $45°$ linearly polarized states of slightly different frequencies are allowed to interfere for $T = 100$ beat periods. There is now a preferred direction of the electric field.

beam, is only dictated by this row. In other words, this first row dictates the diattenuation of the Mueller matrix and the orthogonal polarization basis for which there is maximum and minimum transmission. This first row can itself be treated as a Stokes vector,

$$\vec{\mathcal{D}} = \begin{pmatrix} m_{00} & m_{01} & m_{02} & m_{03} \end{pmatrix}^T, \tag{47}$$

which is called the diattenuation vector. The SOP of the polarization that experiences maximum transmission is given by $\vec{s}_{\max} = \frac{1}{m_{00}} \begin{pmatrix} m_{01} & m_{02} & m_{03} \end{pmatrix}^T$, while $\vec{s}_{\min} = \frac{1}{m_{00}} \begin{pmatrix} -m_{01} & -m_{02} & -m_{03} \end{pmatrix}^T$ experiences minimum transmission. The contrast in intensity between the two, the diattenuation [cf. Eq. (26)] of **M**, is given by

$$\mathcal{D} = \frac{\sqrt{m_{01}^2 + m_{02}^2 + m_{03}^2}}{m_{00}}. \tag{48}$$

The top left element of the Mueller matrix, m_{00}, gives the mean power transmitted averaged over all possible input polarization states and is the average of the transmitted power when $\vec{s}_{\max}$ and $\vec{s}_{\min}$ are incident.

The first column of the Mueller matrix is also significant, being the output Stokes vector when **M** acts on completely unpolarized light (whose definition we provide below). For a more complete discussion of different parts of the Mueller matrix and their physical interpretation, see Chipman et al. [2].

Mueller matrices corresponding to unitary and Hermitian Jones matrix transformations take on a special form [2,4]. The Mueller matrix of a Hermitian transformation has a matching first row and first column

$$\mathbf{M}_H = \begin{pmatrix} m_{00} & m_{01} & m_{02} & m_{03} \\ m_{01} & \cdot & \cdot & \cdot \\ m_{02} & \cdot & \cdot & \cdot \\ m_{03} & \cdot & \cdot & \cdot \end{pmatrix}, \tag{49}$$

reflecting the fact that the polarization analyzed is the polarization created when unpolarized light is incident.

Mueller matrices corresponding to strictly unitary transformations have a form given by

$$\mathbf{M}_U = \begin{pmatrix} 1 & 0 & 0 & 0 \\ 0 & \cdot & \cdot & \cdot \\ 0 & \cdot & \cdot & \cdot \\ 0 & \cdot & \cdot & \cdot \end{pmatrix}. \tag{50}$$

This reflects the fact that all polarizations are passed without attenuation and that only the SOP can be modified. This is enacted by the lower right 3×3 submatrix of $\mathbf{M}_U$, which, as we discuss in Subsection 2.6, is given by a rotation matrix.

The polar decomposition applied to Jones matrices in Subsection 2.3 has an analog in the Mueller formalism, first shown by Lu and Chipman. Any Mueller matrix can be written as

$$\mathbf{M} = \mathbf{M}_\Delta \mathbf{M}_U \mathbf{M}_H, \tag{51}$$

where $\mathbf{M}_U$ and $\mathbf{M}_H$ are Hermitian and unitary transforms—diattenuators and retarders, in other words—and $\mathbf{M}_\Delta$ has a purely depolarizing effect [it should be noted that

the order given in Eq. (51) is not unique]. If **M** directly corresponds to a Jones matrix, there is no depolarization (i.e., $\mathbf{M}_\Delta$ is an identity matrix) and the Lu–Chipman decomposition reduces to the Jones matrix polar decomposition up to an overall phase [30].

2.5. Pauli Matrices in Polarization Optics

2.5a. Motivation: The Stokes Vector from the Jones Vector

The definition of the Stokes vector in Eq. (31) was motivated by a physical experiment. Here we show that it has a mathematical basis as well.

Suppose the unknown polarization whose Stokes vector $\vec{S}$ is to be determined has a Jones vector given by $|s\rangle$. A polarizer that passes $|q\rangle$ completely has a Jones matrix given by $\mathbf{A}_{|q\rangle} = |q\rangle\langle q|$, where $|q\rangle$ is the normalized Jones vector of the polarization state passed by the analyzer. When the unknown polarization $|s\rangle$ encounters the analyzer $\mathbf{A}_{|q\rangle}$, $\mathbf{A}_{|q\rangle}|s\rangle$ results with an intensity given by

$$I_{|q\rangle} = |\mathbf{A}_{|q\rangle}|s\rangle|^2 = \langle s|\mathbf{A}_{|q\rangle}^\dagger \mathbf{A}_{|q\rangle}\rangle s. \tag{52}$$

Note, however, that as an analyzer $\mathbf{A}_{|q\rangle}$ is Hermitian and $\mathbf{A}_{|q\rangle}^\dagger = \mathbf{A}_{|q\rangle}$ so that $\mathbf{A}_{|q\rangle}^\dagger \mathbf{A}_{|q\rangle} = \mathbf{A}_{|q\rangle} = |q\rangle\langle q|$.

In general, then

$$I_{|q\rangle} = \langle s|q\rangle\langle q|s\rangle = |\langle s|q\rangle|^2, \tag{53}$$

which is a statement of the intuitive result that a polarizer projects the electric field of incident light onto its preferred polarization.

The first Stokes parameter S_0 can be then expressed as

$$S_0 = I_{|x\rangle} + I_{|y\rangle} = \langle s|x\rangle\langle x|s\rangle + \langle s|y\rangle\langle y|s\rangle = \langle s|\begin{pmatrix}1 & 0\\0 & 0\end{pmatrix}|s\rangle + \langle s|\begin{pmatrix}0 & 0\\0 & 1\end{pmatrix}|s\rangle = \langle s|s\rangle. \tag{54}$$

This is the expected result: As a complete basis, the outer products $|x\rangle\langle x|$ and $|y\rangle\langle y|$ sum to the identity operator $\mathbb{I}$. Equation (54) simply states that S_0 is the overall beam power.

We can repeat this analysis for the next three Stokes parameters, which are instead differential measurements:

$$S_1 = I_{|x\rangle} - I_{|y\rangle} = \langle s|x\rangle\langle x|s\rangle - \langle s|y\rangle\langle y|s\rangle = \langle s|\begin{pmatrix}1 & 0\\0 & 0\end{pmatrix}|s\rangle - \langle s|\begin{pmatrix}0 & 0\\0 & 1\end{pmatrix}|s\rangle, \tag{55}$$

$$S_2 = I_{|45°\rangle} - I_{|135°\rangle} = \frac{1}{2}\langle s|\begin{pmatrix}1 & 1\\1 & 1\end{pmatrix}|s\rangle - \frac{1}{2}\langle s|\begin{pmatrix}1 & -1\\-1 & 1\end{pmatrix}|s\rangle, \tag{56}$$

$$S_3 = I_{|R\rangle} - I_{|L\rangle} = \frac{1}{2}\langle s|\begin{pmatrix}1 & -i\\i & 1\end{pmatrix}|s\rangle - \frac{1}{2}\langle s|\begin{pmatrix}1 & i\\-i & 1\end{pmatrix}|s\rangle. \tag{57}$$

Equations (54)–(57) can be expressed very succinctly as

$$\vec{S} = \langle s|\vec{\sigma}|s\rangle, \tag{58}$$

where $\vec{\sigma}$ is the Pauli vector, a vector containing the set of four Pauli matrices. That is,

$$\vec{\sigma} = \begin{pmatrix} \sigma_0 & \sigma_1 & \sigma_2 & \sigma_3 \end{pmatrix}^T, \tag{59}$$

where

$$\sigma_0 = \mathbb{I} = \begin{pmatrix} 1 & 0 \\ 0 & 1 \end{pmatrix} \tag{60}$$

is the 2×2 identity matrix and

$$\sigma_1 = \begin{pmatrix} 1 & 0 \\ 0 & -1 \end{pmatrix}, \quad \sigma_2 = \begin{pmatrix} 0 & 1 \\ 1 & 0 \end{pmatrix}, \quad \sigma_3 = \begin{pmatrix} 0 & -i \\ i & 0 \end{pmatrix}. \tag{61}$$

The Pauli matrices also appear in the quantum mechanics of two-level spin systems; as suggested by the analogy between the Poincaré and Bloch spheres, the mathematics of polarization and electron spin dynamics are closely associated, though in quantum mechanical convention the Pauli matrices take on a different order in which σ_2 (by our definition) comes first, σ_3 second, and σ_1 third. While Stokes was not aware of the Pauli matrices, their appearance here shows that Stokes' proposed experiment involving six power measurements—which at first glance may have seemed somewhat improvised or even arbitrary—has fundamental significance. The Pauli matrices are built into the linear algebra of polarization optics.

Equation (58) is the most succinct formula for mapping a given Jones vector $|s\rangle$ to its corresponding Stokes vector $\vec{S}$. The overall phase of $|s\rangle$ is lost in this process. Consequently, then, if we wish to reverse the process, a Stokes vector $\vec{S}$ can be converted to a corresponding Jones vector $|s\rangle$ only up to an arbitrary, overall phase. Moreover, only purely polarized Stokes vectors (with $S_0^2 = S_1^2 + S_2^2 + S_3^2$) have corresponding Jones vectors. In this way, only the last three elements of the Stokes vector, the SOP, are relevant in computing the corresponding Jones vector; the first element S_0, the intensity, simply dictates the Jones vector's amplitude, the overall size of the polarization ellipse.

The Pauli matrices also form a complete basis for Jones matrices, and four, complex-valued coefficients [one for each Pauli matrix in Eqs. (60) and (64)] are enough to uniquely specify the eight degrees-of-freedom of a Jones matrix. A general Jones operator J can be written as

$$J = \vec{\alpha} \cdot \vec{\sigma} = a_0 \sigma_0 + a_1 \sigma_1 + a_2 \sigma_2 + a_3 \sigma_3, \tag{62}$$

where $\vec{\alpha}$ is a complex-valued four vector containing the coefficient for each Pauli matrix. Given a Jones operator J, this Pauli matrix decomposition $\vec{\alpha}$ is given by

$$\alpha_i = \frac{1}{2} \mathrm{Tr}(J \sigma_i), \tag{63}$$

where i ranges from 0 to 3. Equation (63) is readily derived from the fact that all Pauli matrices have zero trace, except for the identity matrix σ_0.

The normalized Jones vector can be found from the SOP $\vec{s}$ (the normalized triplet of the last three components of the Stokes vector) up to an arbitrary overall phase by constructing the matrix [4]

$$\vec{s} \cdot \vec{\sigma}' = s_1 \sigma_1 + s_2 \sigma_2 + s_3 \sigma_3 \tag{64}$$

(the notation σ' signifies the last three matrices of the Pauli vector, i.e., excluding the identity matrix $\mathbb{I}$).

It can be shown [4,31] that the Jones vector $|s\rangle$ corresponding to the SOP $\vec{s}$ is given by the solution to

$$(\hat{s} \cdot \vec{\sigma}')|s\rangle = |s\rangle. \tag{65}$$

The Jones matrix $\hat{s} \cdot \vec{\sigma}'$ has two eigenvectors. The one corresponding to a $+1$ eigenvalue is the desired Jones vector. Its amplitude can be scaled up (or down) by a factor of $\sqrt{S_0}$.

When switching between the Jones and Stokes formalisms, it is important to recall that, in the Stokes formalism, orthogonal polarization states lie on diametrically opposite points on the Poincaré sphere. Projections of one polarization state onto another, then, are not simply given by the dot product of their Stokes vectors. The power given by a projection of one normalized Jones vector $|q\rangle$ onto a second Jones vector normalized $|p\rangle$ is given by

$$|\langle p|q\rangle|^2 = \frac{1}{2}(1 + \hat{p} \cdot \hat{q}), \tag{66}$$

where $\hat{q}$ and $\hat{p}$ are their corresponding SOPs, or coordinates on the Poincaré sphere. From Eq. (66), it is clear that orthogonality ($\langle p|q\rangle = 0$) necessitates $\hat{p} \cdot \hat{q} = -1$, i.e., antiparallelism.

2.5b. Connection between Jones and Mueller Matrices

The Jones calculus cannot handle partially polarized light, and the Stokes/Mueller calculus cannot keep track of overall phase. Every Jones matrix has a corresponding Mueller matrix, but since overall phase is necessarily lost in the conversion, all Jones matrices up to an overall, polarization-independent phase have the same Mueller matrix. Moreover, only some Mueller matrices have a corresponding Jones matrix. In particular, Mueller matrices that can *decrease* the DoP of an incident Stokes vector have no equivalent in the Jones formalism. Mueller matrices that do have an equivalent Jones matrix, the so-called Jones-Mueller or non-depolarizing Mueller matrices, can only be converted to a Jones matrix up to an overall phase.

What is the Mueller matrix $\boldsymbol{M}$ corresponding to $\boldsymbol{J}$? To answer this, consider a transformation in which a Jones vector $|s\rangle$ is transformed to $|t\rangle$ by $\boldsymbol{J}$ as

$$|t\rangle = \boldsymbol{J}|s\rangle, \tag{67}$$

which has a corresponding Mueller matrix $\boldsymbol{M}$:

$$\vec{T} = \boldsymbol{M}\vec{S}. \tag{68}$$

The ith element of the output Stokes vector $\vec{T}$ corresponding to $|t\rangle$ is given by [Eq. (58)]

$$T_i = \langle t|\boldsymbol{\sigma}_i|t\rangle = \langle s|\boldsymbol{J}^\dagger \boldsymbol{\sigma}_j \boldsymbol{J}|s\rangle. \tag{69}$$

Using Eq. (21) to exchange the inner and outer products, we can write

$$T_i = \mathrm{Tr}(|s\rangle\langle s|\boldsymbol{J}^\dagger \boldsymbol{\sigma}_i \boldsymbol{J}). \tag{70}$$

Expansion of the outer product $|s\rangle\langle s|$ in the Pauli basis [as in Eq. (62)] can be verified to give

$$|s\rangle\langle s| = \frac{1}{2}\langle s|s\rangle \mathrm{Tr}(\mathbb{I} + \hat{s} \cdot \vec{\sigma}'), \tag{71}$$

so that we may write

$$T_i = \mathrm{Tr}(|s\rangle\langle s| \boldsymbol{J}^\dagger \boldsymbol{\sigma}_i \boldsymbol{J})$$

$$= \frac{1}{2}\langle s|s\rangle \mathrm{Tr}(\boldsymbol{J}^\dagger(\mathbb{I} + \hat{s}\cdot\vec{\sigma}')\boldsymbol{\sigma}_i \boldsymbol{J})$$

$$= \frac{1}{2}\mathrm{Tr}(\boldsymbol{J}^\dagger(\vec{S}\cdot\vec{\sigma})\boldsymbol{\sigma}_i \boldsymbol{J})$$

$$T_i = \frac{1}{2}\sum_{j=0}^{3} \mathrm{Tr}(\boldsymbol{J}\boldsymbol{\sigma}_j \boldsymbol{J}^\dagger \boldsymbol{\sigma}_i)S_j, \tag{72}$$

where we have used the fact that the trace of a product of matrices is invariant under commutation and that the trace of a sum is the sum of the traces. The last line of Eq. (72) is the long form of a matrix multiplication, mapping the ith element of the Stokes vector $\vec{T}$ to the input Stokes vector $\vec{S}$. We can define the Mueller matrix $\boldsymbol{M}$ corresponding to the Jones matrix $\boldsymbol{J}$ as

$$m_{ij} = \frac{1}{2}\mathrm{Tr}(\boldsymbol{J}\boldsymbol{\sigma}_j \boldsymbol{J}^\dagger \boldsymbol{\sigma}_i), \tag{73}$$

where m_{ij} is the element of $\boldsymbol{M}$ in the ith row and j^{th} column. Equation (73) is the most compact way of mapping a Jones matrix onto its corresponding Mueller matrix. This relation can also be expressed in terms of the matrix outer product, from which one can form the so-called *Dirac matrices* from the Pauli matrices. See, e.g., [2]. The presence of both $\boldsymbol{J}$ and its conjugate $\boldsymbol{J}^\dagger$ means any overall phase in $\boldsymbol{J}$ is removed.

2.5c. Physicality of Mueller Matrices

What about the opposite problem? There is no guarantee that a Mueller matrix $\boldsymbol{M}$ will have a corresponding Jones matrix. Checking whether a Mueller matrix in question even has a corresponding Jones matrix is a preliminary check to be performed in this process. In a broader sense, there is no guarantee that an assembly of 4×4 numbers into a matrix can even constitute a physical Mueller matrix. This stands in contrast to Jones matrices, which may have any four complex entries while remaining physical (any 2×2 Jones matrix has a polar decomposition and can be thought of as a cascade of a retarder and diattenuator). How can we test whether 16 elements comprise a Mueller matrix and, given this, whether it has a corresponding Jones matrix?

These two questions are related: A 4×4 matrix can be deemed a physical Mueller matrix if there is no input polarization whose DoP is rendered unphysical, i.e., made to be larger than 1, by the transformation. Meanwhile, a Mueller matrix has a Jones matrix analog if it is non-depolarizing, i.e., if there is no incident Stokes vector that would be transformed to one with a *lower* DoP (a Jones matrix transformation may, however, increase DoP; a perfect polarizer, as an edge case, perfectly polarizes initially unpolarized light and all diattenuators increase the DoP of unpolarized light).

Many authors ([32–35], to name just a few) have considered this problem, which before long devolves into significant mathematical complexity. A particularly compact mathematical treatment was put forward by Cloude [36] and further elaborated by Gil [37]. We briefly summarize it here.

A 4×4 real-valued Mueller matrix $\boldsymbol{M}$—which may or may not be a physical Mueller matrix—can be associated with a 4×4 Hermitian matrix $\boldsymbol{\Sigma}$ given by

$$\boldsymbol{\Sigma} = \sum_{i=0}^{3} \sum_{j=0}^{3} m_{ij} \boldsymbol{\sigma}_i \otimes \boldsymbol{\sigma}_j, \tag{74}$$

where m_{ij} is the ij^{th} element of $\boldsymbol{M}$ and $\otimes$ is the *Kronecker* product between the Pauli matrices (a generalization of the outer product for vectors), yielding a 4×4 matrix. Note that when dealing with complex elements, the Kronecker product requires a complex conjugation of the second matrix. This transformation is reversible: given a matrix $\boldsymbol{\Sigma}$, the elements of $\boldsymbol{M}$ are given by

$$m_{ij} = \text{Tr}(\boldsymbol{\Sigma}(\boldsymbol{\sigma}_i \otimes \boldsymbol{\sigma}_j)). \tag{75}$$

Since $\boldsymbol{\Sigma}$ is a 4×4 Hermitian matrix, its four eigenvalues $\{\lambda_i\}$ are real, and its eigenvectors $\{\vec{V}_i\}$ are orthogonal by definition. This last fact means that $\boldsymbol{\Sigma}$ can be written as

$$\boldsymbol{\Sigma} = \sum_{i=0}^{3} \lambda_i \vec{V}_i \otimes \vec{V}_i, \tag{76}$$

where $\otimes$ here represents a vector outer product. It can be shown that the matrix $\boldsymbol{M}$ that generates the matrix $\boldsymbol{\Sigma}$ is a physical Mueller matrix if all eigenvalues $\{\lambda_i\}$ are positive—if even one is negative, the Mueller matrix is unphysical.

Each matrix term $\vec{V}_i \otimes \vec{V}_i$ in Eq. (76) corresponds to a $\boldsymbol{\Sigma}$ matrix itself, which can be converted back to a Mueller matrix $\boldsymbol{M}$ by Eq. (75). Each term itself yields a Mueller matrix in this way, which does have a corresponding Jones matrix. This matrix $\boldsymbol{J}$ can be found by, e.g., a polar decomposition of its $\boldsymbol{M}$, conversion of the diattenuation and retarder eigenvectors to Jones vectors, and construction of the corresponding Hermitian and unitary Jones matrices Eqs. (25) and (23) up to an arbitrary overall phase. This means that every Mueller matrix can be written as the sum of four Mueller matrices that correspond to Jones matrices. Even depolarizing Mueller matrices, then, can be considered as a superposition of up to four different non-depolarizing polarization transformations [38]. This also means that a Mueller matrix has a corresponding Jones matrix if and only if a single eigenvalue λ_i is nonzero.

2.5d. Matrix Exponential

Each of the Pauli matrices are both Hermitian and unitary, their defining property. When all elements of $\vec{\alpha}$ are strictly real, it can be seen by inspection of Eq. (62) that $\boldsymbol{J}$ must be Hermitian. It can also be seen by inspection that if all the coefficients of $\boldsymbol{J}$ are purely imaginary, $\boldsymbol{J}$ must be "skew-Hermitian", i.e., $\boldsymbol{J}^\dagger = -\boldsymbol{J}$. Since any Jones operator can be fully described by a complex-valued $\vec{\alpha}$, any operator can be thought of as being composed of a sum of a Hermitian operator (described by the real parts of the α_i) and a skew-Hermitian operator (described by the imaginary parts of the α_i).

Equation (62) is interesting because its coefficients can be linked to physical properties of an optical medium, which modifies light's polarization state and, when placed inside a matrix exponential, can generate the Jones matrix operator of a medium possessing those properties. This requires a generalization of the exponential function for 2×2 Jones matrix quantities.

For matrix-valued inputs $\boldsymbol{J}$, the exponential function $f(x) = e^x$ must be defined in terms of its Taylor series expansion as

$$e^J = \mathbb{I} + J + \frac{1}{2!}J^2 + \frac{1}{3!}J^3 + \frac{1}{4!}J^4 + \ldots = \mathbb{I} + \sum_{n=1}^{\infty} \frac{1}{n!}J^n. \tag{77}$$

One slightly counterintuitive result about the matrix exponential Eq. (77) is a lack of the commutivity that is usually taken for granted in the scalar case—namely,

$$e^A e^B \neq e^B e^A \neq e^{A+B}, \tag{78}$$

unless the matrices A and B themselves commute, i.e., $AB - BA = 0$. The identity matrix $\mathbb{I}$ commutes with all matrices. Then,

$$e^{\alpha_0 \mathbb{I} + J} = e^{\alpha_0} e^J \tag{79}$$

for any Jones matrix J. The physical meaning of including the identity matrix as a term in the matrix exponential is an overall loss (or gain), or a phase shift if α_0 is complex.

Having generalized the exponential function for matrix inputs, we derive a matrix analog of Euler's identity. We motivate this analogy with the scalar Euler's equation by first considering inputs that are skew-Hermitian, i.e., $J = iH = i(\vec{\alpha} \cdot \vec{\sigma})$, where H is a Hermitian Jones matrix and $\vec{\alpha}$ is real-valued. For reasons that will shortly become clear, we exponentiate the matrix $i(\vec{\alpha} \cdot \vec{\sigma})/2$ (reduced by a factor of 2):

$$e^{\frac{i(\vec{\alpha} \cdot \vec{\sigma})}{2}} = e^{i\frac{\alpha_0}{2}} e^{\frac{i(\vec{\alpha}' \cdot \vec{\sigma}')}{2}}. \tag{80}$$

Here, $\vec{\alpha}'$ and $\vec{\sigma}'$ are the last three elements of the $\vec{\alpha}$ and the Pauli vector $\vec{\sigma}$, respectively, and α_0 is the coefficient of $\sigma_0 = \mathbb{I}$. We have isolated the effect of the identity matrix, as in Eq. (79).

We expand the matrix exponential as

$$e^{\frac{i(\vec{\alpha}' \cdot \vec{\sigma}')}{2}} = \mathbb{I} + \sum_{n=1}^{\infty} \frac{1}{n!}\left(\frac{i(\vec{\alpha}' \cdot \vec{\sigma}')}{2}\right)^n. \tag{81}$$

In analogy with the scalar derivation of Euler's identity, Eq. (81) can be grouped into even and odd terms as

$$\left(\mathbb{I} + \frac{1}{2!}\left(\frac{i(\vec{\alpha} \cdot \vec{\sigma})}{2}\right)^2 + \frac{1}{4!}\left(\frac{i(\vec{\alpha} \cdot \vec{\sigma})}{2}\right)^4 + \ldots\right) + \left(\frac{1}{1!}\left(\frac{i(\vec{\alpha} \cdot \vec{\sigma})}{2}\right) + \frac{1}{3!}\left(\frac{i(\vec{\alpha} \cdot \vec{\sigma})}{2}\right)^3 + \ldots\right). \tag{82}$$

For the Pauli matrices in $\vec{\sigma}'$ (excluding σ_0), $\sigma_i \sigma_i = \mathbb{I}$ and $\sigma_i \sigma_j = -\sigma_i \sigma_j = i\sigma_k$, where the indices i, j, and k are any ascending, cyclic order from 1 to 3. Given this, it can be shown that even powers of $(i(\vec{\alpha}' \cdot \vec{\sigma}')/2)^n$ evaluate to a scaled version of the identity matrix,

$$\left(\frac{i(\vec{\alpha} \cdot \vec{\sigma}')}{2}\right)^n = (-1)^{\frac{n}{2}}\left(\frac{|\vec{\alpha}|}{2}\right)^n \mathbb{I}. \qquad \text{(for } n \text{ even)}, \tag{83}$$

while odd powers of $(i(\vec{\alpha} \cdot \vec{\sigma})/2)^n$, by extension of Eq. (83), evaluate to

$$\left(\frac{i(\vec{\alpha}' \cdot \vec{\sigma}')}{2}\right)^n = (-1)^{\frac{n-1}{2}}\left(\frac{|\vec{\alpha}'|}{2}\right)^{n-1}\frac{i(\vec{\alpha}' \cdot \vec{\sigma})}{2}. \qquad \text{(for } n \text{ odd)} \tag{84}$$

These identities take on simple forms thanks to the removal of the identity matrix in Eq. (80), i.e., dealing with $\vec{\sigma}'$ instead of the full Pauli vector $\vec{\sigma}$, simplifying the matrix arithmetic greatly. Then, the even grouping of terms in Eq. (82) reduces to

$$\left(1 - \frac{1}{2!}\left(\frac{|\vec{\alpha}'|}{2}\right)^2 + \frac{1}{4!}\left(\frac{|\vec{\alpha}'|}{2}\right)^4 - \frac{1}{6!}\left(\frac{|\vec{\alpha}'|}{2}\right)^6 + \dots\right)\mathbb{I} = \left(\cos\frac{|\vec{\alpha}'|}{2}\right)\mathbb{I}, \qquad \textbf{(85)}$$

and the grouping of odd terms in Eq. (82) can be shown to evaluate to

$$i\sin\frac{|\vec{\alpha}'|}{2}(\hat{\alpha}'\cdot\vec{\sigma}), \qquad \textbf{(86)}$$

where $\hat{\alpha}' = \vec{\alpha}'/|\vec{\alpha}'|$.

Combining Eqs. (85) and (86) with scalar exponential factored out in Eq. (80), we have

$$e^{\frac{i(\vec{\alpha}\cdot\vec{\sigma})}{2}} = e^{i\frac{\alpha_0}{2}}\left(\cos\frac{|\vec{\alpha}'|}{2}\mathbb{I} + i\sin\frac{|\vec{\alpha}'|}{2}(\hat{\alpha}'\cdot\vec{\sigma})\right). \qquad \textbf{(87)}$$

Equation (87) generalizes Euler's identity and describes a general *unitary* Jones matrix with a common phase of $\alpha_0/2$, a retardance of $|\vec{\alpha}'|$, and orthogonal eigen-polarizations with SOPs given by $\hat{\alpha}'$ and $-\hat{\alpha}'$. The description of a unitary operator in Eq. (87) is equivalent to the more functional description of a unitary operator of Eq. (23) cast in the bra–ket notation. The two descriptions can be linked through the relation $|\alpha'\rangle\langle\alpha'| = \frac{1}{2}(\mathbb{I} + \hat{\alpha}'\cdot\vec{\sigma}')$, an expression for the Jones matrix of an analyzer invoking the Pauli matrices and the Stokes vector, where $|\alpha'\rangle$ is the normalized Jones vector corresponding to the Stokes SOP $\hat{\alpha}'$. This relation can be derived from the form of a normalized Jones vector Eq. (6) and the definition of the Stokes vector Eq. (31).

Instead of the skew-Hermitian matrix $i(\vec{\alpha}\cdot\vec{\sigma})/2$ (with $\vec{\alpha}$ containing strictly real entries), we can also exponentiate $(\vec{\beta}\cdot\vec{\sigma})/2$ (where $\vec{\beta}$ also has purely real entries; this matrix is Hermitian). We again remove the identity matrix,

$$e^{\frac{(\vec{\beta}\cdot\vec{\sigma})}{2}} = e^{\frac{\beta_0}{2}}e^{\frac{(\vec{\beta}'\cdot\vec{\sigma}')}{2}}, \qquad \textbf{(88)}$$

where β_0 is again the weight on the identity matrix and $\vec{\beta}'$ and $\vec{\sigma}'$ represent the last three entries of $\vec{\beta}$ and $\vec{\sigma}$, respectively. By a completely analogous procedure, we can derive that

$$e^{\frac{(\vec{\beta}\cdot\vec{\sigma})}{2}} = e^{\frac{\beta_0}{2}}\left(\cosh\frac{|\vec{\beta}'|}{2}\mathbb{I} + \sinh\frac{|\vec{\beta}'|}{2}(\hat{\beta}'\cdot\vec{\sigma}')\right), \qquad \textbf{(89)}$$

which is a general form of a Hermitian Jones matrix, equivalent to the bra–ket form Eq. (25). Equation (89) describes a diattenuator with a common loss (or gain) of $\alpha_0/2$, an orthogonal eigenbasis of polarizations (which experience maximum and minimum transmittance) with SOPs given by $\hat{\beta}'$ and $-\hat{\beta}'$, and a diattenuation—the contrast in intensity between the maximum and minimum transmittance—given by $\mathcal{D} = \tanh\frac{|\vec{\beta}'|}{2}$.

Equations (87) and (89) show how skew-Hermitian and Hermitian matrices generate unitary and Hermitian polarization operations, respectively, through the matrix exponential function. By the polar decomposition of Subsection 2.3, any Jones matrix can be written as a product of a unitary and Hermitian Jones matrix. That is, for any J,

$$J = e^{\frac{i(\vec{\alpha}\cdot\vec{\sigma})}{2}}e^{\frac{(\vec{\beta}\cdot\vec{\sigma})}{2}} = UH \qquad \textbf{(90)}$$

(assuming a *right* polar decomposition). Specifying two, real-valued four-vectors $\vec{\alpha}$ and $\vec{\beta}$ is another way to fully constrain the eight degrees-of-freedom of the Jones matrix.

It should be noted that matrix exponentials and the Pauli matrices have made a relatively recent entrance into polarization optics. Credit is owed to Fano [39], Schmieder [40], and Whitney [41] for some of the earliest works identifying the role of these in the mathematical description of polarized light. For significantly expanded detail on these ideas, see [4] and [2].

2.6. Geometrical Interpretation of Polarization Transformations

2.6a. Retardance and Diattenuation Space

The polar decomposition (Subsection 2.3) means that any Jones matrix—any polarization device—can be viewed as a cascade of a diattenuator and a wave plate. These correspond to Hermitian and unitary Jones matrices, respectively. There are many mathematical descriptions of Hermitian and unitary operators, some of which we have considered here: In Subsection 2.3, we wrote general expressions for U and H in bra–ket notation, and in Subsection 2.5, we derived forms for these operators from the matrix exponential function. This latter approach (as encapsulated in Eqs. (87) and (89)) shows how the Jones matrix of a wave plate or diattenuator can be *generated* by the Stokes vector of its (orthogonal) eigenbasis, the strength of its polarizing effect (retardance or diattenuation), and an overall (phase or amplitude) scaling.

In Eqs. (87) and (89), the eigen-polarizations are dictated by the unit vectors $\hat{\beta}'$ and $\hat{\alpha}'$, respectively. These give the states of polarization of the eigenbasis, which allows us to construct a Poincaré sphere-like picture for representing these polarization *operators* (instead of merely polarization states). This is a representation we will find useful in Section 4 when we discuss the polarization transformations implemented by metasurfaces.

Diattenuator space. This is carried out separately for Hermitian and unitary operators. Recall that a general Hermitian operator can be written from Eq. (88) as $H = e^{\frac{\beta_0}{2}} e^{\frac{(\vec{\beta}' \cdot \vec{\sigma}')}{2}}$, fully defined by the common loss (or gain) β_0 and the vector $\vec{\beta}'$ (four parameters). Neglecting this polarization-independent β_0, the polarization-dependent amplitude transmission is governed by the magnitude $|\vec{\beta}'|$ and the unit vector $\hat{\beta}'$. $|\vec{\beta}'|$ is unbounded—it can range from 0 if there is no polarization selectivity to ∞ for a perfect polarizer. Recall from Eq. (26) that $\tanh(|\vec{\beta}'|)$ is known as the diattenuation. It is neatly bounded between 0 and 1.

We may then imagine a ball of unit radius that we call the *diattenuation sphere*. Each point within the sphere defines a diattenuator Jones matrix (up to an undefined common loss β_0, which is not a part of this picture). Each point within the sphere can be defined by the coordinates

$$\vec{j}_H = \tanh(|\vec{\beta}'|)\hat{\beta}'. \tag{91}$$

In other words, the Stokes vector of the diattenuation axis $\hat{\beta}'$ (the maximally transmitted polarization) defines the pointing direction, and the diattenuation magnitude $\tanh(|\vec{\beta}'|)$ defines its radial distance from the origin. All points on the surface of the sphere represent perfect polarizers, the origin represents zero diattenuation ($H \propto \mathbb{I}$), and all points in-between represent partial polarizers. The diattenuation sphere is shown in Fig. 6(b).

Retarder space. We may treat unitary matrices in much the same way. By Eq. (80), we have that a general unitary operator can be written as $U = e^{i\frac{\alpha_0}{2}} e^{\frac{i(\vec{\alpha}' \cdot \vec{\sigma}')}{2}}$. Here α_0

is an overall phase, and $\hat{\alpha}'$ and $|\vec{\alpha}|'$ are the retardance axis and retardance angle, respectively. Since retardance is an angular (circular) quantity, some care must be taken. Suppose the retardance can vary on the interval $(-\pi, \pi]$. There is an interplay between the retardance $|\vec{\alpha}|'$ and the polarization state $\hat{\alpha}'$, which is the wave plate's "fast-axis," so named because of its faster phase velocity and, thus, lower optical index and phase accumulation than $-\hat{\alpha}'$, the "slow-axis." The polarization $\hat{\alpha}'$ is *retarded* in phase by an angle of $|\vec{\alpha}'|$ relative to $-\hat{\alpha}'$, but this is equivalent to a situation in which the fast and slow axes are exchanged and the retardance is modified to $2\pi - |\vec{\alpha}'|$ to complete the unit circle.

With this in mind, we imagine a *retardance sphere* in which each point within a unit sphere defines a unitary operator up to an overall phase α_0. Each point within this sphere can be defined by the coordinates

$$\vec{j}_U = \sin\left(\frac{|\vec{\alpha}'|}{2}\right)\hat{\alpha}'. \tag{92}$$

A division by two ($|\vec{\alpha}'|/2$) is necessary to create a sphere of unit radius for $|\vec{\alpha}'| \in (-\pi, \pi]$. The direction from the origin defines the eigen-polarization of the wave plate's fast-axis, and its distance from the origin dictates its retardance. All wave plates of equal retardance lie on spherical shells. The surface of the sphere represents all half-wave plates ($\lambda/2$, or $|\vec{\alpha}'| = \pi$). All quarter-wave plates ($\lambda/4$) lie on a shell of radius $\sqrt{2}/2$. The center represents polarization-insensitive transformations (i.e., $U \propto \mathbb{I}$). The retardance sphere is shown in Fig. 6(a).

Of course, a general Jones matrix J is neither Hermitian nor unitary and is in general defined by eight parameters. This does not admit easy visualization; the best we can do is find its polar decomposition (given a certain order, right or left) and visualize each component in a separate space.

Figure 6
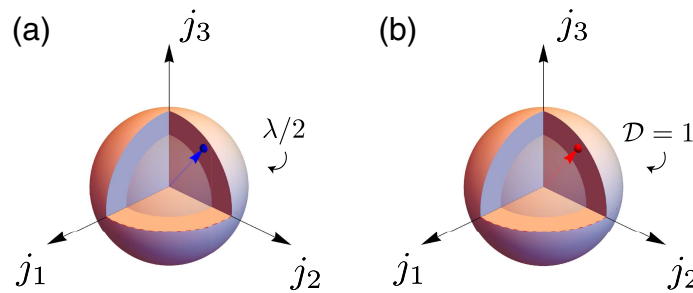
Retardance and diattenuation space. All unitary and Hermitian Jones matrices can be visualized as lying within a sphere that is referred to as (a) retardance and (b) diattenuation space, respectively. A point in the sphere corresponds to an operator. The line connecting the point to the origin gives the operator's eigen-polarizations (as the orthogonal Stokes vectors corresponding to that direction on the conventional Poincaré sphere), while its distance from the origin gives its retardance or diattenuation in accordance with Eqs. (92) and (91). For instance, in (a) the surface of the retardance sphere represents all wave plates with half-wave ($\lambda/2$) retardance, while in (b) the surface of the diattenuation sphere represents all perfect polarizers ($\mathcal{D} = 1$).

2.6b. Action of a Wave Plate on the Poincaré Sphere

While the use of a sphere to identify sets of polarization operators may seem very academic, even esoteric, it has immense use as an intuitive aid. As light propagates through a number of polarization elements, it is difficult to imagine how the polarization ellipse changes.

The action of a wave plate can—with the aid of the Poincaré sphere—be understood as a simple rotation. Recall that the Mueller matrix corresponding to a wave plate, a unitary Jones matrix, has a first row and first column equal to $(1 \quad 0 \quad 0 \quad 0)$ [Eq. (50)], a reflection of the fact that wave plates are lossless and cannot polarize unpolarized light. It can be shown that the lower 3×3 submatrix, however (the part that modifies the light's SOP and, thus, its polarization ellipse), takes the form of a rotation matrix [4,31].

Very simply, the action of a wave plate is to rotate (in a right-handed sense) the Stokes vector of incident light on the Poincaré sphere about its eigen-axis ($\hat{\alpha}'$) by an angle equal to its retardance ($|\vec{\alpha}'|$). Since the eigen-polarization of the wave plate lies along the axis $\pm\hat{\alpha}'$, it is unchanged by this rotation.

In this way, it is easy to see geometrically that a half-wave plate rotates the angle of linear polarization states—the π rotation about any axis in the equatorial plane returns a linear polarization back to the equatorial plane. Or it is easy to see why a quarter-wave plate oriented at 45° to a x polarization circularizes it—$\pi/2$ radians of rotation are exactly what is needed to bring it up to the sphere's pole. If incident polarization is not specified, the transformations enacted by a given wave plate as its retardance is varied are concentric circles around the axis $\pm\hat{\alpha}'$. Wave plates—unitary operators—enact rotations that preserve length (intensity) and inner product (angle) between Stokes vectors.

Manipulations that are unilluminating in the brute-force algebra of the Jones calculus become insightful when viewed this way. Some examples of polarization transformations by wave plates are shown in Fig. 7.

Figure 7
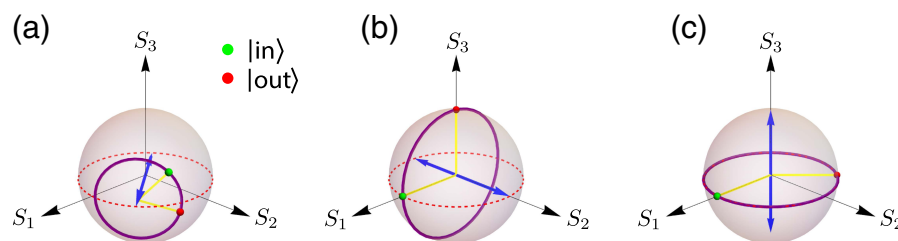
Action of a wave plate (unitary) operator visualized on the Poincaré sphere. (a) In general, a wave plate enacts a rotation of the Stokes state-of-polarization (SOP) on the Poincaré sphere. The input state $|in\rangle$ (whose SOP is represented by a green dot) processes about the eigen-polarization of the wave plate (whose Stokes vector is denoted by a blue arrow) by an angle equal to the retardance ($\pi/3$ shown here), yielding an output $|out\rangle$ (red dot). In general, output states from the unitary operator for any retardance, given $|in\rangle$ as an input, are constrained to lie along the purple circle. (b) This readily explains why x polarization is transformed into circular when passed through a wave plate with $\pi/2$ retardance oriented at 45° and (c) why a crystal with *optical activity* (phase retardance between circular polarizations) rotates the angle of linear polarization.

2.6c. Action of a Diattenuator on the Poincaré Sphere

Diattenuators, on the other hand, are lossy. A perfect polarizer, for instance, will convert all incident polarization states to its preferred pass-axis while reducing their intensity; the polarization orthogonal to the pass-axis is extinguished. In general, a diattenuator simultaneously scales the length (intensity) of an incident Stokes SOP $\hat{s}$ and changes its direction.

For a diattenuator with an eigen-axis given by $\pm\hat{\beta}'$ and a diattenuation $\mathcal{D} = \tanh(|\vec{\beta}'|)$, the transmitted intensity is

$$T = \frac{1}{1 + \mathcal{D}}(1 + \mathcal{D}(\hat{\beta}' \cdot \hat{s})), \tag{93}$$

which depends both on the diattenuation and the distance of the incident polarization and the diattenuator's pass polarization. This can be visualized by distorting the shape of the Poincaré sphere. The direction along $+\hat{\beta}'$ will remain of unit radius, but $-\hat{\beta}'$ will be brought closer to the origin (all the way to the origin, if $\mathcal{D} = 1$). T is constant in planes perpendicular to the $\pm\hat{\beta}'$ axis.

In the case of a perfect polarizer, any incident polarization exits as $\hat{\beta}'$. In general, we have [4,42]

$$\hat{t} = \frac{\sqrt{1 - \mathcal{D}^2}}{1 + \mathcal{D}(\hat{\beta}' \cdot \hat{s})}\hat{s} + \frac{\mathcal{D} + (1 - \sqrt{1 - \mathcal{D}^2})(\hat{\beta}' \cdot \hat{s})}{1 + \mathcal{D}(\hat{\beta}' \cdot \hat{s})}\hat{\beta}', \tag{94}$$

where $\hat{t}$ is the outgoing SOP. This is a complicated expression. It can be understood as a distortion of the Poincaré sphere along the diattenuator axis. Polarization states are "squeezed" to point closer to $+\hat{\beta}'$; the degree of this squeezing is governed by $\mathcal{D}$. This often represented by a wireframe in which all incident polarization states are represented by a wireframe that gives the original (undistorted) Poincaré sphere as mapped to new locations by the diattenuator. This is shown in Fig. 8.

2.7. Polarimetry

2.7a. Stokes Vector Polarimetry

The entirety of this section so far has been dedicated to the mathematical and physical description of light's polarization state. We have not addressed (directly, at least) how the polarization state of a beam can be measured. Such a measurement is known as *polarimetry*, and an instrument that carries it out is known as a *polarimeter*.

At low frequencies, the electric field vector can be observed directly. No optical oscilloscope exists, however, and all measurements of the electric field (and its phase) must be indirect, most commonly making use of square-law intensity detectors. Relative phase is an important concept in defining the Jones vector. Phase is measured in optics by interferometric means. In principle, for a perfectly polarized source, the Jones vector could be measured by projecting the beam onto its x- and y-polarized components, measuring their intensity, and deducing relative phase between the two in a Michelson interferometer, observing the shift in the fringes at zero path difference. Practically speaking, this is cumbersome, and absolute phase difference measurements are complicated by assuring this zero path delay condition, which requires subwavelength positioning precision. Moreover, this prescription does not work in the case of partially polarized light.

A more conventional technique involves projective measurements of the unknown Stokes vector onto other Stokes vectors using a diattenuator and measuring the resultant power. In fact, Stokes' prescription of the Stokes vector is an example of such a

scheme, involving six projective polarization state measurements as was first introduced in Eq. (31). Despite its more fundamental importance, the Stokes formalism, then, was built around the practical concerns of polarimetry.

Mathematical definition. Stokes' prescription, however, can be generalized further. Suppose a beam whose polarization state is to-be-measured has a Stokes vector given by $\vec{S}$. If this beam is passed through a diattenuator (a polarization optic that enacts polarization-sensitive intensity transmission) with a Mueller matrix $\boldsymbol{D}$, the resulting polarization state is given by

$$\vec{S}' = \boldsymbol{D}\vec{S}. \tag{95}$$

The observed intensity is given by the first element of $\vec{S}'$, S_0', but this in turn is governed by just the first row of $\boldsymbol{D}$. This first row is itself a Stokes vector, the so-called diattenuation vector [from Eq. (47)]. Then, we have

$$I = S_0' = \vec{D} \cdot \vec{S}. \tag{96}$$

Suppose this experiment is carried out N times while the diattenuation vector is made to vary (either by physically turning it, by modulating some electrically defined polarization optic, or by a variety of other methods). Then, the intensity resulting from the nth measurement is given by

$$I_n = \vec{D}_n \cdot \vec{S}. \tag{97}$$

All N measurements can be described once compactly in matrix notation as

---

Figure 8

$$\text{(a)} \quad \mathcal{D} = 0.5 \qquad \text{(b)} \quad \mathcal{D} = 0.95$$

Output power

Output polarization

Output power

Output polarization
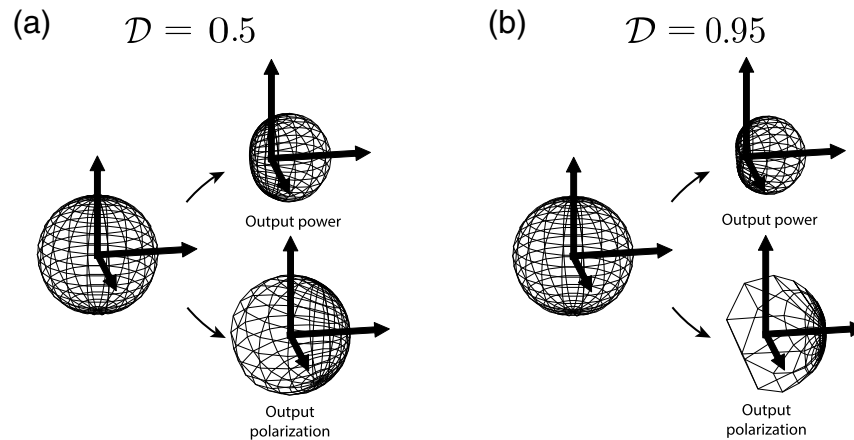
Action of a diattenuator visualized with the Poincaré sphere. The effect of a diattenuator (Hermitian) Jones matrix can be visualized by sampling the Poincaré sphere (the space of all possible input polarization states) with a wireframe mesh. A diattenuator in general modifies both the amplitude and polarization state of incoming light. These can be visualized separately by scaling the radius of the wireframe to represent output power as a function of input polarization [(in accordance with Eq. (93)] and by distorting the wireframe to represent output polarization [Eq. (94)]. This is done for a weak diattenuator [(a) $\mathcal{D} = 0.5$] and a strong one, approaching a perfect polarizer [(b) $\mathcal{D} = 0.95$], both for x-polarized light. In (b), the diattenuator's tendency to convert all incident polarizations to its preferred one is evident in the sparsity of the output wireframe.

$$
\begin{pmatrix} I_1 \\ I_2 \\ \vdots \\ I_N \end{pmatrix} = \begin{pmatrix} - & \vec{D}_1 & - \\ - & \vec{D}_2 & - \\ & \vdots & \\ - & \vec{D}_N & - \end{pmatrix} \begin{pmatrix} S_0 \\ S_1 \\ S_2 \\ S_3 \end{pmatrix},
\tag{98}
$$

or simply as

$$
\vec{I} = A\vec{S},
\tag{99}
$$

where $\vec{I}$ is a list of measured intensities and A is an $N \times 4$ matrix containing the four-element instrument vectors of each of the N diattenuators. A is often referred to as the *instrument matrix*—it is a mathematical description of the linear mapping between experimental observations (the entries of the intensity vector $\vec{I}$) and the incident Stokes vector $\vec{S}$.

If the instrument matrix is square (i.e., $N = 4$) and, notably, if all of its rows are linearly independent so that A is not singular, we can write

$$
\vec{S} = A^{-1}\vec{I}.
\tag{100}
$$

If the matrix A is known, and if the instrument performing the polarimetric measurement is *calibrated*, the incident Stokes vector $\vec{S}$ can be determined with a simple linear algebraic inversion. This directly shows that only four projective polarization state measurements are needed to constrain the four-element Stokes vector. Stokes' prescription, while intuitive, is not minimal.

As long as four, linearly independent analyzers form the rows of A, the Stokes vector can be determined. This will always be possible if the Stokes vectors of the analyzers, when plotted on the Poincaré sphere, subtend a three-dimensional (3D) volume when their tips are connected. This means that, for example, four linear polarizers at different orientations cannot form an invertible A, but the addition of one elliptical analyzer (pointing out of the equatorial plane of the sphere) makes the subtended volume nonzero and A non-singular. The volume subtended by the set of four analyzers is in some sense a measure of the fidelity of this inversion; four nearly identical, but slightly different, analyzers provide nearly the same information, subtend little volume, and yield an instrument matrix with $\det(A) \approx 0$. In the presence of any measurement noise, the Stokes vector itself is highly uncertain. The optimum scenario corresponds to when these four analyzers trace out the vertices of a regular tetrahedron on the Poincaré sphere, meaning the analyzers are maximally different from one another and the polarimetric measurement provides the maximum diversity of information (an observation first recorded by Azzam *et al*. [43]).

Measurement accuracy can be further enhanced if $N > 4$, as in Stokes' scheme, at the expense of needing to take more measurements. In that case, A is rectangular and cannot be inverted directly. Instead, we solve for $\vec{S}$ in the least squares sense (since it is overdetermined) by using the (left) pseudo-inverse:

$$
\vec{S} = ((A^T A)^{-1} A^T)\vec{I}.
\tag{101}
$$

In this case, the matrix condition number $\mathrm{cond}(A)$ quantifies the degree to which the polarimetric measurement is or is not invertible (low condition numbers are "well-conditioned"; high condition numbers—up to ∞—showcase "poor conditioning").

Applications of optical polarimetry. Polarimetry is of great interest in the study of polarization optics in general. Today polarimetry is used in a variety of scientific and technological applications, too numerous to name here. Some of these are highly technological in nature, such as in computer vision (where it is used for 3D surface-normal reconstruction [44–46]) and defense-related applications (where man-made objects may be discerned from the background based on the polarized nature of Fresnel reflection [47,48]). Much work on polarimetry has come from the remote sensing community, where the scattering of polarized light off of natural scenes may reveal interesting scientific information on its makeup. Polarimetry is a widespread technique in the radar community [49]. Optical polarimetry is currently used in atmospheric science where the scattering of linearly polarized light is observed from space, helping to constrain the particle size distribution of clouds and aerosols [50]. It is also widely used in astrophysical studies of the sun where Zeeman-splitting, observed with polarized light, sheds light on solar magnetic field distributions [51].

The applications of polarimetry would require a separate review article (and these already exist: see, e.g., [2,5,47,48]). So too would the technologies enabling it. The essence, however, is contained in Eq. (100). At least four projective measurements are needed to obtain the Stokes vector (or three, if only the linear contents S_0, S_1, and S_2 are needed as in many applications). Polarimeters differ in how these measurements are implemented. In a *division-of-time* polarimeter, measurements are taken with a single sensor as polarization-analyzing optics change. This commonly means mechanically rotating wave plates and polarizers, but some electrically modulated polarizers do exist (based on, e.g., LCs). This allows for a minimum of componentry, but the speed at which optics can be readjusted limits time resolution, and moving parts are often undesirable. In a *division-of-amplitude* polarimeter, the incoming beam is split among multiple paths (using, e.g., beam splitters, a grating, or other optics) that each implement different polarization analyzers. This allows for a snapshot measurement, at the detriment of compactness (more optics are required). In applications, the Stokes vector is often determined over a 2D photographic image. This is known as imaging polarimetry. A third technique exists in imaging polarimetry, in which the focal place of the imager itself has pixels patterned with polarization analyzers. This approach is compact and snapshot, but it suffers from the so-called "instantaneous field-of-view" issue in that adjacent pixels, being physically separated in space, do not look at exactly the same position in a scene.

We direct the reader to other resources for more thorough reviews of polarimetric applications and instrumentation [2,5,47,52].

2.7b. Mueller Matrix Polarimetry

In a variety of applications—especially those involving active illumination where the polarization of incident light can be controlled—it is of interest to not only determine the Stokes vector of a beam but to measure the polarization transfer characteristic of a sample as contained in its 16-element Mueller matrix M. The procedure of determining M is known as *Mueller matrix polarimetry*. We remark on it only briefly here (see [52] and [2] for more detail).

The Mueller matrix transforms an input Stokes vector $\vec{S}_{in}$ into an output $\vec{S}_{out}$:

$$\vec{S}_{out} = M\vec{S}_{in}. \tag{102}$$

In Mueller matrix polarimetry, a sample is probed with N input polarization states, and the polarization state emerging is measured by a Stokes vector polarimeter. This process can be expressed as

$$
\begin{pmatrix} -\vec{S}_{\text{out}}^{(1)}- \\ -\vec{S}_{\text{out}}^{(2)}- \\ \vdots \\ -\vec{S}_{\text{out}}^{(N)}- \end{pmatrix} = M \begin{pmatrix} -\vec{S}_{\text{in}}^{(1)}- \\ -\vec{S}_{\text{in}}^{(2)}- \\ \vdots \\ -\vec{S}_{\text{in}}^{(N)}- \end{pmatrix}, \tag{103}
$$

or more compactly as

$$
O = MI, \tag{104}
$$

where M is the Mueller matrix to-be-determined and O and I are $N \times 4$ matrices with output and input Stokes vectors, respectively, as their rows. Given suitably chosen input polarization states, I is invertible, and we can write

$$
M = OI^{-1} \tag{105}
$$

for $N = 4$ or

$$
M = O(I^T (II^T)^{-1}) \tag{106}
$$

if $N > 4$ and the system is overdetermined. In this case, we solve for M in the least squares sense, and Eq. (106) uses the (right) pseudo-inverse of I.

3. JONES MATRIX FOURIER OPTICS: PARAXIAL DIFFRACTION WITH POLARIZATION

In this section, we consider a simple mathematical framework by which polarization can be incorporated into the (paraxial) diffraction of electromagnetic waves. This same framework—which we refer to as *Jones matrix Fourier optics*—can, given a designer optical medium in which the polarization ellipse may vary controllably from point-to-point, be used as a mathematical and intuitive tool for designing useful optical elements.

We begin by summarizing Fourier optics as it is broadly understood in the context of diffraction and imaging systems.

3.1. Fourier Optics and the Plane Wave Expansion

Solution of the wave equation, Eq. (1), is greatly simplified by making two assumptions, in particular (1) that only a single polarization is of interest, so $\vec{E}(\vec{r}, t) = E(\vec{r}, t)\hat{d}$ along unit vector $\hat{d}$ and (2) that space and time dependence may be separated by assuming $E(\vec{r}, t) = U(\vec{r})e^{i\omega t}$. Given this assumption of a *monochromatic*, time-harmonic solution, we need only solve for the complex wave amplitude $U(\vec{r})$ at a single frequency ω. Substitution of this time-harmonic solution into the wave equation yields the Helmholtz equation,

$$
(\nabla^2 + k^2)U(\vec{r}) = 0, \tag{107}
$$

where $k = n\omega/c = 2\pi/\lambda$ is again the wave vector. It is readily verified that the plane wave $U(\vec{r}) = e^{i\vec{k}\cdot\vec{r}}$ is a solution of the Helmholtz equation. By linearity, so too are any and all superpositions of such plane waves.

This insight underlies the *angular spectrum* (or *plane wave expansion*) picture of diffraction. Suppose a monochromatic field is described by a (potentially complicated) $U(x, y, z = 0)$ in some plane $z = 0$ in space. Mathematically, $U(x, y, z = 0)$ can be described by its 2D Fourier transform,

$$A(k_x, k_y; z = 0) = \iint_{-\infty}^{+\infty} U(x, y, z = 0)e^{-i(k_x x + k_y y)}dxdy. \tag{108}$$

The function $A(k_x, k_y)$ weights sinusoidal functions in the plane $z = 0$ with k-vectors given by (k_x, k_y). In this way, we can imagine the field as a superposition of these as

$$U(x, y, z = 0) = \iint_{-\infty}^{+\infty} A(k_x, k_y)e^{i(k_x x + k_y y)}dk_x dk_y \tag{109}$$

This is simply an inverse Fourier transform. The use of a Fourier transform, at first just a mathematically justified choice, becomes physically interesting when paired with the realization that a field with an in-plane wave vector (k_x, k_y) is formed by a plane wave incident at off-normal incidence on the plane $z = 0$. At the chosen frequency ω (corresponding to a wavelength of $\lambda = 2\pi c/(\omega n)$), a plane wave has an in-plane wave vector (k_x, k_y) when

$$k_z = \sqrt{|k|^2 - (k_x^2 + k_y^2)} = \sqrt{\left(\frac{2\pi}{\lambda}\right)^2 - (k_x^2 + k_y^2)}. \tag{110}$$

The field $U(x, y, z = 0)$, then, can be formed by the interference of a continuum of plane waves incident at different angles, as governed by the Fourier transform $A(k_x, k_y; z = 0)$. The azimuthal angle of each plane wave is determined only by k_x and k_y, while its tilt relative to the normal is governed by the ratio $k_z/\sqrt{(k_x^2 + k_y^2)}$. Some of these plane waves have $(k_x^2 + k_y^2) > 2\pi/\lambda$, rendering k_z imaginary by Eq. (110); these "evanescent" plane waves are attenuated with increasing z.

If the field $U(x, y, z = 0)$ can be "thought of" as comprising these plane wave components, it *is* just a superposition of these plane wave components. By the linearity of the Helmholtz equation, each can be treated independently and propagates individually forward in space. We can immediately write that

$$A(k_x, k_y; z) = A(k_x, k_y; z = 0)e^{ik_z z}. \tag{111}$$

After advancing each plane wave component by the appropriate phase, we can synthesize the field in any plane z as

$$U(x, y, z) = \iint_{-\infty}^{+\infty} A(k_x, k_y; z = 0)e^{i(\sqrt{(2\pi/\lambda)^2 - (k_x^2 + k_y^2)})z}e^{i(k_x x + k_y y)}dk_x dk_y. \tag{112}$$

This is a highly intuitive way of understanding optical wave propagation in free space. Any signal can be broken into its plane wave components, and the phase of each can be suitably shifted with propagation in z. This is shown in Fig. 9(a).

Beyond simple propagation, the plane wave expansion picture aids in modeling the interaction of light with planar obstacles. We assume that an object lies in the plane $z = 0$, which modifies the field. In a simplistic way, we can relate the field just before the obstacle, U_-, to the field just after, U_+, with use of a transmission function,

$$U_+(x, y, z = 0) = U_-(x, y, z = 0)t(x, y). \tag{113}$$

This transmission function $t(x, y)$ is complex, encoding both amplitude scaling and phase shifts. Given knowledge of the field illuminating the obstacle, the field just

after can be calculated by Eq. (113) and propagated forward in space with Eq. (112). This understanding of an obstacle as being described by a transmission function $t(x, y)$—a sort of structured screen standing in as a proxy for what could potentially be a complex scattering problem—relies on several assumptions about the nature of the obstacle (see the discussion in Subsection 3.4), but is a notion that has nonetheless found widespread use in optics. Throughout this review, we will rely on this description to model the interaction of light with various engineered polarization-sensitive optical elements (Section 4).

Armed with the angular spectrum picture of wave propagation, we can make even more general statements about light propagation through optical systems. These, in general, may be composed of many optical elements, such as lenses, gratings, and even surfaces implementing spatially varying transfer functions like $t(x, y)$ (not to mention the empty spaces between them). We can describe any such system simply, so long as it is *linear*. Practically speaking, this means that the optical system's transfer characteristics cannot depend on the nature of the signal propagating through. In a more philosophical sense, a linear system cannot exhibit an "awareness" of the signal on which it operates.

Given a linear optical system (imaging or non-imaging), we can write that

$$U_2(x_2, y_2) = \iint_{-\infty}^{+\infty} h(x_2, y_2; x_1, y_1) U(x_1, y_1) \mathrm{d}x_1 \mathrm{d}x_2, \tag{114}$$

where $h(x_2, y_2; x_1, y_1)$ is an impulse response function, giving the electric field evoked in the output plane at (x_2, y_2) by a point disturbance at (x_1, y_1) in the input plane, with the form of h abstracting away all specifics of the optical system in question [Fig. 9(b)]. For imaging systems, Eq. (114) takes the particularly convenient form of a convolution integral [15].

The angular spectrum representation of optical fields and the transfer function abstraction of optical systems are important concepts of *Fourier optics* (Fig. 9). In Fourier optics, these methods are applied to space-dependent fields, but the same language and intuition are applicable to the time-dependent signals encountered in electronics. Fourier optics emerged from intense work in this area beginning in the 1920s, 1930s, and 1940s, benefitting greatly from the flurry of developments in radar

Figure 9
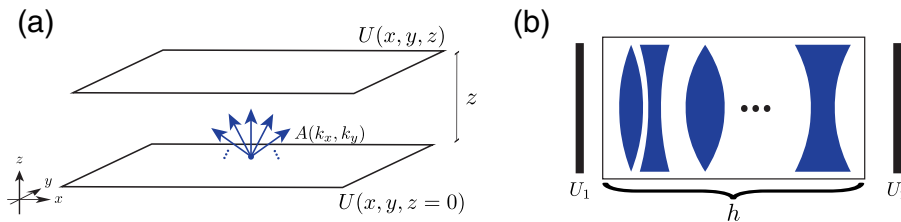
Two important concepts from Fourier optics. (a) A field $U(x, y)$ is composed of a spectrum of plane waves $A(k_x, k_y)$—its angular spectrum. Each plane wave in the set can be individually propagated forward in space. (b) Any linear optical system can be abstracted as a black box described by an impulse response function $h(x_2, y_2; x_1, y_1)$, where h describes the field evoked at (x_2, y_2) at the system's output in response to a point excitation (x_1, y_1) at the system's input. (Only lenses are shown here for illustration, as this formalism is often applied to imaging systems, but any configuration of linear elements, such as sections of free space, lenses, holograms, gratings, and mirrors, can be described in this manner.)

and RF electronics during the Second World War ([53] and [54] are two notable early references). Fourier optics was further solidified with the publication of J.W. Goodman's *Fourier Optics* [15] in 1968, written on the heels of the invention of the laser in 1960. The laser—with its ability to produce temporally and spatially coherent fields—hastened the widespread adoption of Fourier optics as a tool of research and a pillar of optics education.

3.2. Paraxial Interference of Plane Waves

3.2a. Two Polarized Plane Waves

Analytical treatment. Light is polarized and is inherently vectorial. Polarization, however, traditionally receives scant mention in Fourier optics. Goodman's text [15], for instance, makes mention of polarization only twice: once near the beginning when it is set aside in treating diffraction, and again in an appendix where polarization effects in LCs are introduced in relation to spatial light modulators (SLMs). Fourier optics is almost always spoken of with regard to scalar fields. Here, we will extend Fourier optics to apply to fields that have spatially varying polarization properties and to the optical elements that produce them.

The fact that any superposition of plane waves is a solution of the Helmholtz equation is the foundation of Fourier optics. This is true independent of the polarization state of the plane waves involved. We begin with the simplest problem: the interference of two plane waves with different polarization states.

For simplicity, this is done in one dimension. We define the global Cartesian coordinate system to be given by (x, y, z). Suppose there are two plane waves, $|E_1\rangle$ and $|E_2\rangle$ whose k vectors lie in the (x, z) plane. One plane wave points along the z axis with $\vec{k}_1 = k_0(0, 0, 1)$, and a second plane wave is tilted at an angle θ with $\vec{k}_2 = k_0(\sin\theta, 0, \cos\theta)$. These fields occupy all of space, but at some imaginary plane $z = 0$ we examine their interference. The electric field of the first plane wave lies in the $(x - y)$ plane, but the second plane wave has a tilted set of reference axes (x_2, y_2) in which its electric field lies. The Jones vectors of each plane wave can then be expressed as

$$|E_1(\vec{r})\rangle = \begin{pmatrix} E_1^x \\ E_1^y \end{pmatrix}, \tag{115}$$

$$|E_2(\vec{r})\rangle = \begin{pmatrix} E_2^{x_2} \\ E_2^{y_2} \end{pmatrix}. \tag{116}$$

This problem is shown schematically in Fig. 10. The total electric field in the global coordinate system is

$$\vec{E}(\vec{r}) = \begin{pmatrix} E_x \\ E_y \\ E_z \end{pmatrix} = |E_1\rangle e^{i(\vec{k}_1 \cdot \vec{r})} + |E_2\rangle e^{i(\vec{k}_2 \cdot \vec{r})} = \begin{pmatrix} E_1^x e^{i(\vec{k}_1 \cdot \vec{r})} + E_2^{x_2} e^{i(\vec{k}_2 \cdot \vec{r})} \cos\theta \\ E_1^y e^{i(\vec{k}_1 \cdot \vec{r})} + E_2^{y_2} e^{i(\vec{k}_2 \cdot \vec{r})} \\ E_1^x e^{i(\vec{k}_1 \cdot \vec{r})} + E_2^{x_2} e^{i(\vec{k}_2 \cdot \vec{r})} \sin\theta \end{pmatrix}. \tag{117}$$

Being 3D, this $\vec{E}$ is not a Jones vector, and in general it cannot be treated with any of the same mathematical machinery developed around plane wave polarization (e.g., the Stokes vector, Jones matrices, the Poincaré sphere). Crucially, we adopt a small angle limit, the *paraxial* limit, in which $\theta \sim 0$. In the paraxial limit, $\sin\theta \sim 0$ and $\cos\theta \sim 1$. Note that the former is a stronger small angle limit than is often used

in physics, in which $\sin \theta \sim \theta$. Here, we take only the zeroth-order term of the Taylor expansion. These small angle assumptions mean that the component of the field along the propagation direction z tends to 0, and the wave is again transverse (an approximation we grapple with in Subsection 3.4). The individual Jones vector coordinate systems of the two beams become identical and aligned with the global (x, y) axes.

We make a conscious decision, however, to not apply this small angle approximation to the k-vectors, which are still assumed to deviate by an angle θ. We can then write the overall field as

$$\vec{E}(\vec{r}) = \begin{pmatrix} E_1^x e^{i(\vec{k}_1 \cdot \vec{r})} + E_2^x e^{i(\vec{k}_2 \cdot \vec{r})} \\ E_1^y e^{i(\vec{k}_1 \cdot \vec{r})} + E_2^y e^{i(\vec{k}_2 \cdot \vec{r})} \\ 0 \end{pmatrix}. \tag{118}$$

In the plane $z = 0$, $\vec{r} = (x, y, 0)$, and we have

$$\vec{E}(\vec{r}) = \begin{pmatrix} E_1^x + E_2^x e^{i(k_0 \sin \theta)x} \\ E_1^y + E_2^y e^{i(k_0 \sin \theta)x} \\ 0 \end{pmatrix}. \tag{119}$$

The electric field is now transverse, and we can again use the Jones formalism to write

$$|E(x)\rangle = |E_1\rangle + |E_2\rangle e^{i(k_0 \sin \theta)x}. \tag{120}$$

In the plane, the resultant polarization state is the superposition of the two Jones vectors with a spatially varying phase shift. The polarization ellipse has a shape that varies in x, which repeats periodically after a grating period of $\Lambda = \lambda / \sin \theta$. In other words, the spatially varying linear phase shift in the plane $z = 0$ is mapped into a polarization interference pattern. If $\langle E_1 | E_2 \rangle = 0$, no intensity interference can occur, and only the polarization state changes. If $\langle E_1 | E_2 \rangle \neq 0$, interference can appear as both a change of polarization and a change of wave intensity. If $|E_1\rangle$ and $|E_2\rangle$ describe the same Jones vector, polarization is constant in x, and only intensity fringes appear.

As an aside, we mention that the superposition of two polarization states with variable phase can occur in other contexts in optics. For instance, if two frequencies with differing Jones vectors are combined, the frequency can be seen as a linear gradient of relative phase (going as $\Delta \omega t$) in time. In this way, a periodic, time-varying polarization ellipse appears, much like the patterns in this section appear separated in space. This was the basis of the discussion surrounding Fig. 5. The light in these gratings can

Figure 10

Geometry of an interference problem between two polarized plane waves.

also be seen to be unpolarized, if the ellipse is averaged over a distance that is large compared to the grating period.

Visualization with the Poincaré sphere. The Stokes formalism and Poincaré sphere provide useful geometric intuition here. It can be shown that the polarization state produced by the interference of two polarized plane waves as their relative phase varies from 0 to 2π traces out a circle on the Poincaré sphere. The nature of this circle depends on the two polarization states involved and their relative magnitude. For simplicity, suppose we are interested in the polarization ellipse produced by the interference

$$|E_{\text{tot}}\rangle (1-b)|E_1\rangle + b|E_2\rangle e^{i\phi}, \tag{121}$$

where we take both $|E_1\rangle$ and $|E_2\rangle$ to be normalized so that $b \in [0, 1]$ controls the relative magnitude of the two. We consider an example where $\langle E_1|E_2\rangle = 0$, and in particular $|E_1\rangle = |x\rangle$ and $|E_2\rangle = |y\rangle$. If $b = 1/2$ (equal magnitude), the resultant polarization sweeps a great circle located in the $s_1 = 0$ plane on the Poincaré sphere. For $\phi = 0$, $|45°\rangle$ linear polarization is produced, then $|R\rangle$ at $\phi = \pi/2$, and so on. If b is modified so that one polarization is stronger than the other, the circle remains centered on the s_1 axis but slides along it toward the Stokes vector corresponding to $|E_1\rangle$ or $|E_2\rangle$ (toward $|E_1\rangle$ for $b < 1/2$, toward $|E_2\rangle$ for $b > 1/2$). For $b = 0$ or $b = 1$, one polarization dominates, and the circle shrinks to a point. In this case of orthogonal polarizations, the amount of arc traversed along the circle is proportional to ϕ.

This is shown in Fig. 11 in which $|E_1\rangle = |x\rangle$ and $|E_2\rangle = |y\rangle$. Five cases are shown in Fig. 11, both as paths on the Poincaré sphere (left) and as periodic distributions of polarization ellipses seen in the plane $z = 0$ (right). These cases correspond to $b = \frac{1}{4}, \frac{1}{3}, \frac{1}{2}, \frac{3}{4}, \frac{4}{5}$, ordered from bottom to top. In the middle case ($b = \frac{1}{2}$), light goes from 45° linear to right-circularly polarized (RCP), then to 135° linear and left-circularly polarized (LCP), and back again: a great circle on the Poincaré sphere. Notably, because $\langle E_1|E_2\rangle = 0$, there is no amplitude modulation; interference only manifests as a modulation of the polarization ellipse's shape.

When $\langle E_1|E_2\rangle \neq 0$ (non-orthogonal states), however, this is not the case. As an example, we consider the interference of $|x\rangle$ linearly polarized light with a second linear polarization of equal magnitude that is not orthogonal (Fig. 12). In each case, ϕ is varied from 0 to 2π in discrete, evenly spaced steps, and the resulting polarization is visualized on the Poincaré sphere as the polarizations become more parallel from

Figure 11

Interference of $|x\rangle$ and $|y\rangle$ polarized light. Each circle on the Poincaré sphere denotes a different relative weight between $|x\rangle$ and $|y\rangle$ and corresponds by color to a row in the adjacent table, depicting how the interference between two slightly tilted plane waves appears as a periodic interference pattern of polarization state. One repeating period of this pattern is shown.

left to right. Once again, this traces out a great circle that bisects the line between the Stokes vectors of $|E_1\rangle$ and $|E_2\rangle$. However, the distance traversed along this great circle is no longer proportional to ϕ: points are sparser near the diametrically opposite end, increasingly so as the polarizations become parallel. This is a trade-off in interference "fringes" between the amplitude and polarization degrees-of-freedom of the light. When the polarizations are close to parallel, the polarization changes only slightly across the grating, but there is high intensity contrast—approaching perfect contrast (with $I \propto |\cos\phi|$) when the two states are parallel.

As a final note, we again emphasize that this view of plane wave interference relies crucially on a small angle approximation, essentially neglecting the longitudinal component E_z. This means that the distribution of polarization ellipses in the plane $z = 0$ shown throughout this section does not exactly satisfy Maxwell's equations. Nonetheless, we work in this regime throughout this work. We discuss this in Subsection 3.4.

3.2b. Multiple Polarized Plane Waves

Naturally, it is tempting to generalize this problem. Can we apply any of the intuition of the previous section to a case when many (>2) polarized plane waves interfere? If we adopt the same paraxial approximation wherein the Jones vectors of each plane wave can add as though their electric fields exist in the same transverse plane, albeit with differing transverse phase gradients, we can write

$$|E_{\text{tot}}(x)\rangle = \sum_{p=m}^{n} w_p |E_p\rangle e^{ip2\pi x}. \tag{122}$$

In Eq. (122), we assume a finite set of plane waves with indices between $p = m$ and $p = n$, as in Fig. 13. Distance has been normalized so that the grating repeats periodically on the range $x \in [0, 1)$. Each plane wave in the set has an amplitude weight w_p and a normalized Jones vector $|E_p\rangle$ and traverses p multiples of 2π of phase in a period.

We can attempt to apply the same visual intuition developed in the last section to this case; even with just three plane waves, this proves difficult. A casual investigation of this problem can yield a whole zoology of outcomes, with sometimes exotic paths

Figure 12
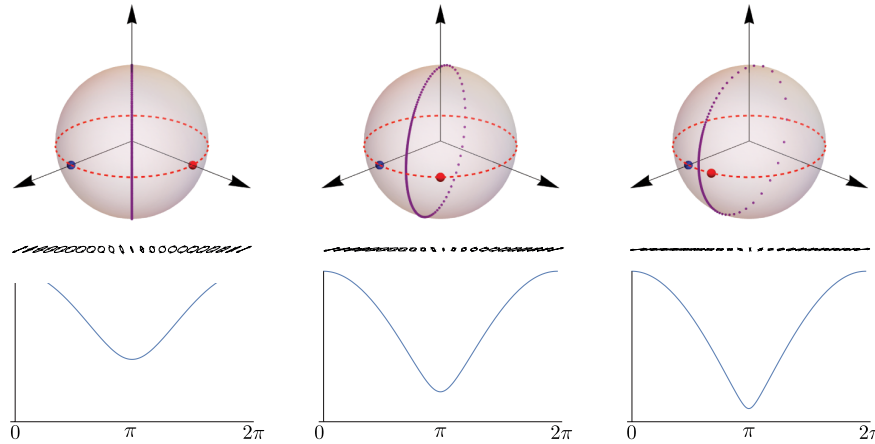
Interference of non-orthogonal polarization states, which induces amplitude modulation.

on the Poincaré sphere and complex variation in output intensity (some examples are shown in Fig. 14). As the number of orders involved increases, this problem becomes akin to Fourier analysis, which proves itself to be a more useful tool and language in describing these problems. In the next section, then, we adapt the language and formalism of Fourier optics to problems of polarized light.

3.3. Scalar, Vector, and Matrix Regimes

The incorporation of polarization into the formalism of Fourier optics lends itself to three related levels of abstraction. These are referenced throughout the review.

3.3a. Scalar

The plane wave decomposition is the fundamental concept of Fourier optics. Given a field $U(x, y)$ at a given plane, the plane wave spectrum $A(k_x, k_y)$, computed by Fourier transform [Eq. (108)], provides sufficient information to propagate $U(x, y)$ to any other plane in space. The field $U(x, y)$ is specified by amplitude and phase, two free parameters that can vary with space. We refer to this as the regime of *scalar* diffraction. At this level, polarization is not a part of the picture, set aside much as in conventional discussions of Fourier optics.

3.3b. Vector

Under the guise of the above paraxial approximation, we can also imagine a field $|U(x, y)\rangle$, which is a spatial distribution of Jones vectors. A Jones vector is composed of two complex fields, two orthogonal components of the polarization in any basis. It is described by four free parameters. These can be parameterized in several ways,

Figure 13
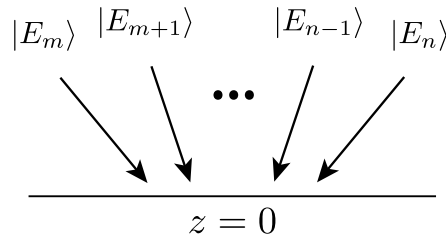
Interference of multiple polarized plane waves, equally spaced in angle, with indices lying between $p = m$ and n.

Figure 14
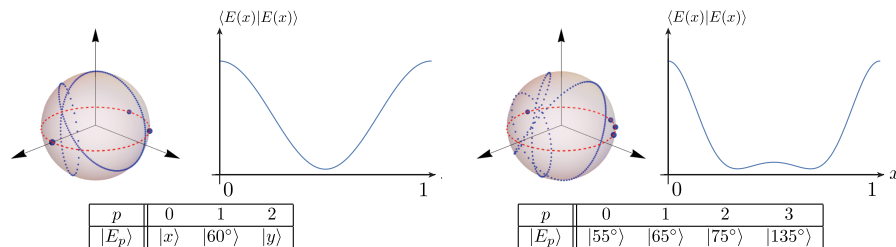
Complex polarization and intensity patterns over one grating period produced by three (left) or four (right) arbitrarily chosen, linearly polarized beams whose diffraction orders and angles of polarization are shown in a table for each case. The polarizations of the plane waves are labeled with blue dots on the Poincaré sphere. In each case, all plane waves have equal weight in the superposition. Each table denotes the polarization state of the assumed diffraction orders—here, $|\theta\rangle$ denotes linearly polarized light with an azimuth angle of θ.

for instance, as an overall phase, an overall amplitude, a phase difference between polarization components, and a relative amplitude between the two. Whatever the case, orthogonal polarizations do not interact and can be treated separately. If

$$|U(x, y)\rangle = \begin{pmatrix} U_1(x, y) \\ U_2(x, y) \end{pmatrix}, \tag{123}$$

then

$$A_1(k_x, k_y) = \iint_{-\infty}^{+\infty} U_1(x, y)e^{i(k_x x + k_y y)} \mathrm{d}x \mathrm{d}y \tag{124}$$

and

$$A_2(k_x, k_y) = \iint_{-\infty}^{+\infty} U_2(x, y)e^{i(k_x x + k_y y)} \mathrm{d}x \mathrm{d}y. \tag{125}$$

For convenience, we can express this as a single, vector-valued equation:

$$|A(k_x, k_y)\rangle = \begin{pmatrix} A_1(k_x, k_y) \\ A_2(k_x, k_y) \end{pmatrix} = \iint_{-\infty}^{+\infty} |U(x, y)\rangle e^{i(k_x x + k_y y)} \mathrm{d}x \mathrm{d}y. \tag{126}$$

In Eq. (126), we can imagine the Fourier transform as distributing over each element of the Jones vector $|U(x, y)\rangle$. The angular spectrum, now Jones vector-valued, describes the amplitude, weight, and polarization ellipse of the plane wave component propagating at an angle determined by its in-plane wave vector (k_x, k_y).

In computing $A(k_x, k_y)$, it is as though the arrows drawn in Figs. 10 and 13 have been reversed: Given a field, the plane waves propagating forward in space are determined. However, using an inverse Fourier transform, the field $|U(x, y)\rangle$ formed by a given plane wave spectrum $|A(k_x, k_y)\rangle$ can be determined. If $|A(k_x, k_y)\rangle$ is discrete and consists of diffraction orders with uniform spacing, the integral in Eq. (126) becomes a sum, and $|U(x, y)\rangle$ is periodic, a polarization grating, as in the previous section. If $|A(k_x, k_y)\rangle$ is instead continuous, $|U(x, y)\rangle$ has no periodicity, and a continuum of diffraction orders can be imagined to emerge. We refer to this picture linking $|U(x, y)\rangle$ with $|A(k_x, k_y)\rangle$ as the *vector* regime of diffraction.

3.3c. Matrix

Part of the power of Fourier optics is that it can deal adeptly with light's interaction with obstacles and—through the notion of an impulse response function—whole optical systems. In the scalar regime, that is because a field $U_-(x, y)$ just before an obstacle can be modified by an obstacle with a complex-valued transmission function $t(x, y)$, yielding $U_+(x, y) = U_-(x, y)t(x, y)$ just after. The transformation of polarization as described by the Jones vector has more degrees-of-freedom than a single complex number. When dealing with polarized light, the Jones matrix (which here we allow to vary spatially) is the analogous concept. A field of Jones vectors just before an obstacle $|U_-(x, y)\rangle$ will form $|U_+(x, y)\rangle$ just after as mediated by the Jones matrix function,

$$\boldsymbol{J}(x, y) = \begin{pmatrix} J_{11}(x, y) & J_{12}(x, y) \\ J_{21}(x, y) & J_{22}(x, y) \end{pmatrix}, \tag{127}$$

with

$$|U_+(x, y)\rangle = \boldsymbol{J}(x, y)|U_-(x, y)\rangle. \tag{128}$$

$\boldsymbol{J}(x, y)$ contains *four* spatially varying functions. The angular spectrum immediately after the obstacle is given by

$$|A_+(k_x, k_y)\rangle = \iint_{-\infty}^{+\infty} \boldsymbol{J}(x, y)|U_-(x, y)\rangle e^{i(k_x x + k_y y)} \mathrm{d}x\mathrm{d}y, \tag{129}$$

with the Fourier transform distributing over the two elements of the Jones vector, as before. Suppose that the incident field is a normally incident plane wave with a spatially uniform polarization state, amplitude, and phase. The analysis also applies to a plane wave incident at an angle, provided the Fourier transform is suitably shifted, or even to a non-plane-wave source if the convolution theorem is applied. This is a common situation in optics, with wide applicability. The output of a laser, for instance, can often be approximated in this way (even if its true profile is more Gaussian) if its beamwaist is large compared to the object or region of interest. Then, $|U_-(x, y)\rangle = |U_-\rangle$ with no space dependence. In that case, it can be removed from the integral in Eq. (129) as a constant,

$$|A_+(k_x, k_y)\rangle = \left(\iint_{-\infty}^{+\infty} \boldsymbol{J}(x, y) e^{i(k_x x + k_y y)} \mathrm{d}x\mathrm{d}y\right) |U_-\rangle. \tag{130}$$

It is notable that the quantity in parentheses in Eq. (130) is itself a Jones matrix, a kind of matrix-valued angular spectrum given by

$$\boldsymbol{A}(k_x, k_y) = \iint_{-\infty}^{+\infty} \boldsymbol{J}(x, y) e^{i(k_x x + k_y y)} \mathrm{d}x\mathrm{d}y = \begin{pmatrix} \mathcal{F}\{J_{11}(x, y)\} & \mathcal{F}\{J_{12}(x, y)\} \\ \mathcal{F}\{J_{21}(x, y)\} & \mathcal{F}\{J_{22}(x, y)\} \end{pmatrix}. \tag{131}$$

The matrix $\boldsymbol{A}(k_x, k_y)$ is a Jones matrix transformation that describes the *behavior* of the plane wave directed at an angle governed by the in-plane wave vector (k_x, k_y), obtained by distributing the Fourier transform over each of the four spatially varying entries of $\boldsymbol{J}(x, y)$. This is an important distinction. In this description, the Jones matrix angular spectrum $\boldsymbol{A}(k_x, k_y)$ is decoupled from any particular incident polarization, which may illuminate $\boldsymbol{J}(x, y)$; in a sense, this description is a bookkeeping technique that allows all possible incident polarization states $|U_-\rangle$ to be handled at once. At first, this is a strange perspective to adopt: Fourier analysis and diffraction are calculated on Jones matrices, which are not themselves electric fields. Rather, the Jones matrix is a stand-in for all possible electric fields that might illuminate the polarization-sensitive object.

Abstractly, a plane wave with in-plane wave vector (k_x, k_y) can be thought of as a polarization-sensitive *device* with a Jones matrix given by $\boldsymbol{A}(k_x, k_y)$. This device could be a wave plate, a diattenuator, or some combination of the two, as governed by the $\boldsymbol{A}(k_x, k_y)$'s matrix polar decomposition (Subsection 2.3). Moreover, if $\boldsymbol{J}(x, y)$ is periodic, these Jones matrix devices form a discrete set, carried by equally spaced diffraction orders.

Through this lens, a spatially varying polarization modifying obstacle $\boldsymbol{J}(x, y)$ can be viewed as enacting many polarization-sensitive devices in parallel, carried as Jones matrix weights on its diffraction orders. This perspective, along with the reciprocal nature of the Fourier transform, means that a device implementing many polarization transformations in one can be straightforwardly described. Taking a discrete case, assume there is a set of diffraction orders (a set $\{\ell\}$) onto which we wish to encode polarization devices with functions given by $\{\boldsymbol{J}_k\}$. Then, we can straightforwardly construct a periodic Jones matrix obstacle $\boldsymbol{J}(x, y)$, which will implement this desired behavior as

$$J(x, y) = \sum_{\vec{k} \in \{\ell\}} J_k e^{-i\vec{k}\cdot\vec{r}}. \tag{132}$$

Exactly how this mathematical description can be transformed to a real diffractive optical element is, however, not answered by Eq. (132) and is instead the subject of Section 4.

Broadly speaking, we refer to these notions, encapsulated by Eq. (131) linking a spatially varying Jones matrix with a Jones matrix angular spectrum, as the *Jones matrix* or simply *matrix* regime of diffraction.

This *Jones matrix Fourier optics* has appeared in other areas of optics, such as in the analysis of optical systems with polarization-dependent effects (both desired and undesired) [2], a history we briefly discuss in Subsection 3.5.

Note that the choice to use the Jones formalism here again makes use of the paraxial approximation. The choice to use the Jones formalism immediately neglects any longitudinal E_z component that may be present. This means that any spatially varying Jones matrix function must be "slowly varying" as compared to the wavelength to be physical (Subsection 3.4).

3.3d. Linking the Three Regimes
As a concluding note, we stress that these three regimes—scalar, vector, and matrix—are in fact intimately related, with the scalar and vector pictures as subcases of the matrix description. For simplicity of discussion, we assume a periodic $J(x, y)$ with a discrete spectrum $\{J_k\}$. If a plane wave with Jones vector $|j\rangle$ is normally incident on $J(x, y)$, a vector field $|j(x, y)\rangle = J(x, y)|j\rangle$ results with Fourier coefficients $|j_k\rangle = J_k|j\rangle$. If that vector field is then projected (analyzed) along a particular polarization $|\xi\rangle$, a scalar field $t(x, y) = \langle\xi|j(\vec{r})\rangle$ results with scalar Fourier coefficients $\tilde{a}_k = \langle\xi|j_k\rangle$. The vector description contains two independent scalar diffraction problems, while the matrix picture encodes two such vector problems, yielding the eight degrees-of-freedom of the Jones matrix. Simply stated, the Jones matrix picture can be seen as a container, a bookkeeping tool, albeit one that can yield additional insights. This hierarchy is illustrated in Fig. 15.

3.4. Paraxiality and Polarization
The concept of a Jones vector, as traditionally defined, only makes sense if a single transverse coordinate system is involved. Strictly speaking, we can only use the Jones calculus to keep track of the interference of plane waves having the same $\vec{k}$. Key to the idea of incorporating polarization into Fourier optics is the idea of multiple polarized plane waves interfering at different angles. To reconcile this, we said in Subsection 3.2a that we limit ourselves to *small angles* so that the transverse coordinate system in which the polarization of each plane wave component is defined roughly overlaps.

We begin by commenting the paraxial limit taken throughout this review is actually very similar in nature to a number of other approximations commonly made in diffractive optics as a whole, whether explicitly acknowledged or not. Chief among these is the very concept that an optical element can be described by an amplitude transmittance function. The assumption that the transfer through an optical element can be described by a simple multiplication of the incoming electric field by a scalar function assumes a certain locality to the interaction. This is equivalent to the notion that light at high angles cannot be involved, since it is light at steeper angles that would induce high k components that bring fast spatial variations into play. If the

field varies over short distances, the transfer of the optical element can no longer be local. These terms that are occasionally thrown around—a thin optical element, local interactions—are actually all one in the same, and all hint at an approximation that only plane waves propagating at small angular deviations from normal are involved.

In fact, the issue of polarization cannot be so easily dispensed of in Fourier optics (as it often is) without use of the paraxial approximation. The angular spectrum representation is an exact solution of Maxwell's equations. However, the superposition of more than one plane wave implies a field that is no longer transverse. So, unless this longitudinal component E_z is accounted for, a paraxial approximation (that it is small) is being tacitly made. This is the case in most Fourier optics arguments. So, the paraxial limit used throughout here in the form of Jones matrix Fourier optics is no more conspicuous than the approximations in the course of developing "normal" Fourier optics. We can, then, feel somewhat justified in its use, keeping in mind this limitation.

What is the alternative? Light's interaction with a periodic obstacle—including polarization—is fully described by the *rigorous coupled-wave analysis* (RCWA). RCWA is both a theoretical approach and, in its approximate form, a numerical technique for analyzing diffractive optical elements. RCWA considers a single normally incident plane wave on a periodic permittivity (and, thus, refractive index) modulation, i.e., a grating. It casts the boundary conditions from Maxwell's equations into a matrix equation whose solution dictates the weight and phase of all diffraction orders, one that can be solved numerically if the set of diffraction orders is truncated [55].

Cast as an analytically exact solution to Maxwell's equations, RCWA trudges into the E_z/non-paraxiality issue head-on and can be written for both transverse electric (TE) and transverse magnetic (TM) incident polarization. In fact, the polarization state and phase of each outgoing diffraction order can be computed. In this way, RCWA can ascribe a Jones matrix, a linear polarization transfer function, to each diffraction order, relative to the coordinate system defined by the $\vec{k}$ of each. The idea of specific k having an associated Jones matrix, then, is not fundamentally paraxial. However, the

Figure 15
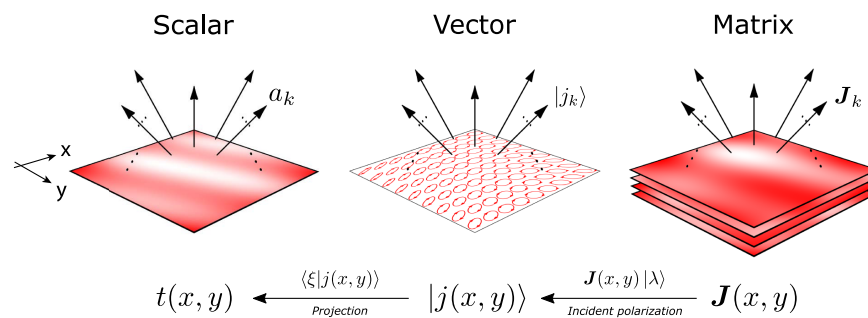
A hierarchical view of polarization-dependent paraxial diffraction. In the scalar regime (left), a periodic electric field distribution $t(x, y)$ produces discrete orders with scalar weights $\{a_k\}$. In the vector regime (middle), the full polarization state $|j(x, y)\rangle$ is allowed to vary periodically with space and produces diffraction orders with characteristic Jones vectors (polarizations) $\{|j_k\rangle\}$. Finally, in the matrix regime, the Jones matrix of the grating may vary with space as $\boldsymbol{J}(x, y)$—in this case, the Fourier coefficients $\{\boldsymbol{J}_k\}$ are themselves Jones matrix operators, encoding polarization-dependent behaviors. The vector field can be recovered from the matrix description if a particular polarization $|j\rangle$ is incident, and a scalar field from a vector one if analyzed along a particular polarization $|\xi\rangle$.

idea of a locally acting Jones matrix transfer function describing an optical element is. In their review [55], Gaylord and Moharam describe how RCWA can be seen as the top level of a hierarchy of a variety of approximations and heuristics, among them the amplitude transmittance model.

3.5. Origin of Jones Matrix Methods in Fourier Optics

Light's vectorial nature has been a consideration since the development of Maxwell's equations into what we know today as diffraction theory by Sommerfeld, Kirchoff, and others. Fourier optics is a formulation of diffraction theory in terms of impulse response and transfer functions, valid under certain approximations, that forms the basis of a particularly useful tool for optical design and intuition. Surprisingly, consideration of Fourier optics alongside the linear algebra of polarization, as we have presented here, is not widespread in the optics literature.

This work, however, is not the first to imagine combining the two. We remark briefly on past work of this nature here. Some of the earliest efforts in this direction were spurred by the analysis and design of imaging systems. By the 1950s, polarized light microscopy—that is, illuminating and analyzing samples in optical microscopy with linear polarizers—was a biological analysis tool of great interest. In a system containing a lens between crossed polarizers, a pattern of leakage with fourfold symmetry known as a "Maltese cross" is visible. This is an example of a polarization aberration, stemming ultimately from the mismatch between the cylindrical symmetry of lenses and the Cartesian symmetry of polarized light [2]. Inoué and Kubota observed and explained this, albeit without direct use of the Jones calculus, using Fourier optics concepts in the 1950s [56] (we thank Prof. Russell Chipman for making us aware of this work). This was later formalized by Urbańcyzk, who—in a series of papers in the 1980s—introduced more formally the idea of a Jones matrix impulse response function [57]. These ideas were further cemented by McGuire and Chipman who extended the methods to include a full study of polarization aberrations and polarization ray tracing in work that continues to this day [2,58–61].

In this line of work, spatially varying polarization effects are often implicitly treated as an undesired or unexpected outcome, to be characterized and mitigated. On the other hand, in the present work, we are concerned with optical elements where polarization-dependent effects can be quite deliberately and flexibly engineered. The idea of applying Jones matrix Fourier optics to the analysis of diffractive optics has appeared, to our knowledge, only once before, in the work of Moreno *et al.*, at first only theoretically [62] and later in a paper containing an experiment with an SLM [63]. Due to the limits imposed by working with only a single SLM, however, only fields with spatially varying polarization ellipses were synthesized (i.e., the vector regime above, not the most general matrix case). A number of other works have come quite close to the spirit of the approach here, however, and we will discuss a number of these in the next section.

4. SPATIALLY VARYING POLARIZATION OPTICS: PHYSICAL IMPLEMENTATIONS AND APPLICATIONS

We have said much of optical elements that modify the polarization of light spatially. In the last section, we described how these optical elements may be analyzed by extending Fourier optics to 2×2 Jones matrix quantities. With the help of the inverse Fourier transform, this formalism even dictates the design of these same optical elements by constraining the mathematical form of a spatially varying Jones matrix $J(x, y)$, as in Fig. 16.

Without a tangible connection to some physical implementation, however, all of this is only a mathematical exercise. How can an optical element be constructed that modifies the polarization of light in a desired way, point-by-point across an optical element? It is clear that this *physical layer*—in addition to all of the abstractions of Section 3—should occupy a position of crucial importance. After all, any constraints on what can be physically realized themselves place mathematical constraints on $J(x, y)$ and, ultimately, the achievability of a given far-field function $A(k_x, k_y)$ (Fig. 16).

A variety of optical devices have been proposed (and demonstrated), which enable spatial modulation of polarization at optical frequencies. This work spans many decades, with clusters of research occurring at different times in different communities of optics separated in time and space (in many cases, working without awareness of one another). This section seeks to catalog these past efforts. The sections below are dedicated to different diffractive optics technologies that manipulate light's polarization. The basic capabilities of each are elaborated, and selected past works in each area are discussed. In practice, research often evades neat categories. Some work fits under more than one category, and it is entirely possible that some contributions (even whole sub-fields of research) have been unwittingly omitted by this review. What follows is an attempt to approach this task as comprehensively and as clearly as possible while managing the trade-off between the two. A top-level summary of this effort is provided in Table 3.
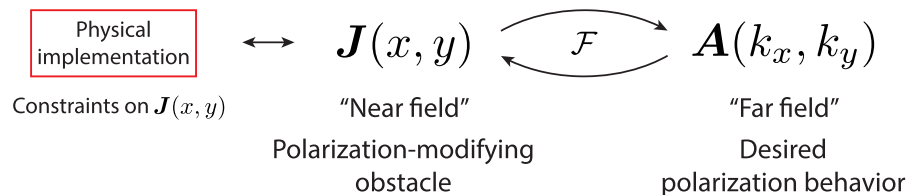
In the next section, we provide a scheme for classifying this work using the language of Sections 2 and 3, permitting comparison between different approaches and technologies.

4.1. Classifying Polarization-Sensitive Diffractive Optics Using the Poincaré Sphere

A scalar diffractive element is often characterized by a transmission function $\tilde{t}(x, y)$. Usually, $\tilde{t}$ cannot take on any complex value. What is achievable depends on its particular physical implementation. These restrictions distinguish one diffractive optic from another.

For instance—unless an element is capable of shuffling light between spatial locations (going against the limit of a thin optical element), without gain, $|\tilde{t}| \leq 1$, defining a unit disk in the complex plane. Within this disk, some diffractive platforms ("phase-only") can implement $\tilde{t}$ anywhere along the disk's edge; others ("amplitude-only") are constrained to remain along the real axis between 0 and +1. Still finer distinctions exist—some technologies may only implement a part of the full phase or amplitude range, or

Figure 16

$$\boxed{\text{Physical implementation}} \longleftrightarrow J(x, y) \overset{\mathcal{F}}{\longleftrightarrow} A(k_x, k_y)$$

Constraints on $J(x, y)$ "Near field"   "Far field"

Polarization-modifying   Desired
obstacle   polarization behavior

A spatially varying Jones matrix described by $J(x, y)$ and its corresponding Jones matrix plane wave spectrum $A(k_x, k_y)$ (related by Fourier transform $\mathcal{F}$) constitute a mathematical abstraction neglecting the fact that $J(x, y)$ must be somehow implemented. Different technologies for doing so place different constraints on $J(x, y)$, and the "near-field" produced just after the object, and the far-field behavior contained in $A(k_x, k_y)$. This physical layer is, thus, a key design consideration.

Table 3. Short-Form Comparison of Technologies Discussed in Section 4

Comparison of Technologies for Realizing Spatially Varying Polarization Transfer Functions

Name	Origin	Physical Basis	Fabrication Method	Spatial Resolution	Extent of Polarization Control (Table 4)	Discussed in ...
Polarization holograms	1970–1980	Weigert effect	Holographic recording	Optical diffraction limit of recording wavelength	Arbitrary linear retarder—Type F, possibly more general (material dependent)	Subsection 4.2
Elements directly etched into birefringent media	1990s	Bulk crystalline anisotropy	Multi-level lithography (e-beam) and etching	Several wavelengths, ~10 μm for visible	Arbitrary linear retarder with overall phase with discrete allowed retardance and phase values, no control over retardation axis—Type H	Subsection 4.3
Stress-engineered optical elements (SEOs)	~2007	Photoelastic effect	Heat and application of force	Deeply subwavelength (molecular effect)	Arbitrary linear retarder without overall phase—Type G, cannot be deterministically controlled from point-to-point	Subsection 4.4
Photoaligned liquid crystal elements	~1990	Molecular anisotropy guided by photoalignment (Weigert effect)	Holographic or direct-write with polarized light, spin-coating	Optical diffraction limit of photoalignment wavelength	Orientation with fixed overall retardance ("geometric phase")—Type E	Subsection 4.5b
Liquid crystal spatial light modulators (SLMs)	1970s	Molecular anisotropy	Rubbing and spin-coating	μm-scale	Tunable retardance, fixed phase, and orientation—Type I	Subsection 4.5d–4.5f
Metasurfaces	1990s–2010	Form birefringence	Lithography (generally e-beam) and etching	~10–20 nm	Arbitrary linear retarder (for pillar-based structures)—Type F	Subsection 4.7

some a mixture of the two. In others, this control may be discrete rather than continuous. Whatever the case, the geometry of the complex plane provides for simple comparison.

The Jones matrix has eight free parameters in contrast to $\tilde{t}$'s two. Nevertheless, the Poincaré sphere—rather than the 2D complex plane—provides a visual standard-of-comparison for polarization-sensitive diffractive optics: amplitude modulation is generalized as a Hermitian $\boldsymbol{J}$ while phase modulation is generalized as a unitary $\boldsymbol{J}$. An arbitrary Jones matrix is fully defined by where it lies in the space of Hermitian operators (diattenuation space, a three-vector; see Subsection 2.6a), where it lies in the space of unitary operators (retardance space, another three-vector; see Subsection 2.6a), and where its overall loss and overall phase, two scalars that themselves constitute a complex transmission function $\tilde{t}$, place it in a 2D complex plane. An arbitrary prescription of a polarization-sensitive diffractive element, then, can be represented as a region in diattenuation space, a region in retardance space, and a region on the complex plane. A "region" here could be a volume, a plane, a point, or a mixture thereof, where $\boldsymbol{J}(x, y)$ is free to reside at the discretion of the designer, given any physical constraints imposed by a given technology.

Several possibilities are shown in Table 4. Its first row shows an example of a rather arbitrary case in which the Hermitian component of $\boldsymbol{J}$ is constrained to lie in an oddly shaped volume in diattenuator space, its unitary component to a general surface, and overall phase/amplitude to a region in the complex plane. In general, these regions could be linked by a set of inequalities and could be quite complicated, although we note that any region can be rotated about the S_3 axis of the sphere by a physical rotation of the element in question. This representation also allows us to portray the fullest passive control possible. As shown in the second row, this would mean that a Jones matrix could fall anywhere in the full-ball volume of the diattenuation space, anywhere in the retardance sphere, and anywhere in or on the unit circle of the complex plane. At the other extreme, we can also represent elements with no polarization sensitivity whatsoever (second row, a "phase-only" diffractive optic where $\boldsymbol{H}$ and $\boldsymbol{U}$ both are $\mathbb{I}$).

The real technologies discussed throughout this section lie somewhere in-between. In each subsection that follows, and in the summary in Table 3, we describe a technology or area of research and classify its ability to spatially control polarization, matching each to its "Type" (the label in the leftmost column of Table 4). This hierarchy allows for high-level comparison between platforms.
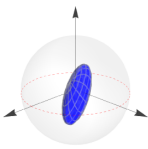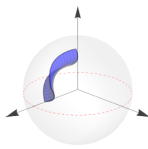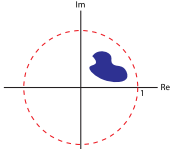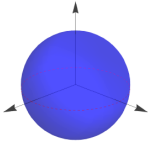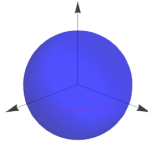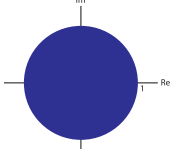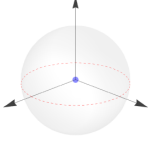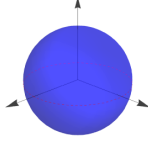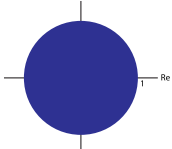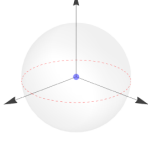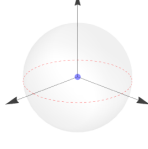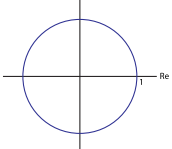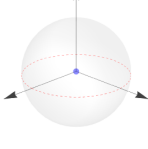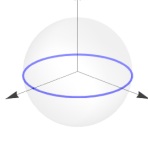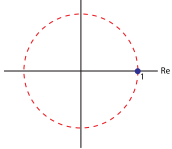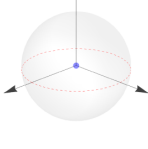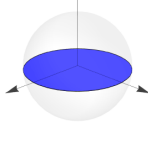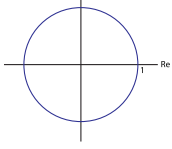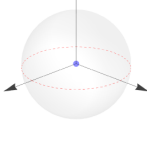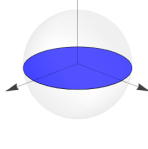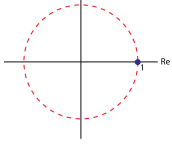
4.2. Polarization in Holography

4.2a. Early Commentaries

Some of the earliest work of this nature was born from holography. In the 1960s, the invention of the laser set forth a flurry of research in optical holography, posited earlier as a theoretical proposal in electron optics [64]. Holography—then as now—was largely imagined in a scalar sense. This oversight, however, did not entirely escape the notice of the optics community. Adolph Lohmann, the pioneer of the computer-generated hologram, wrote in 1965 that, while the word "holography" roughly translates as "total recording" from Greek, "a hologram is not really a total recording, since only one amplitude and one phase are recorded, which would be adequate if light were a scalar wave" [65]. Several works that followed offer early proposals of how the holographic recording and reconstruction process might be modified to yield an optical element—a hologram recorded in photographic film—creating fields upon reconstruction with polarization that could vary spatially [65–68].
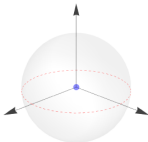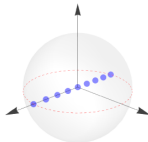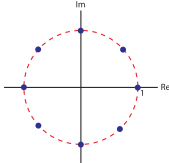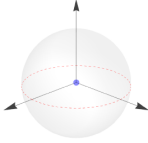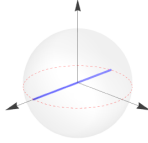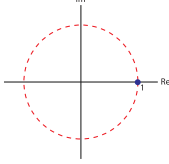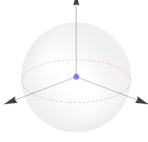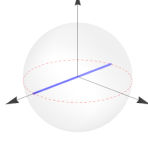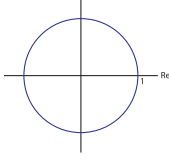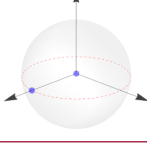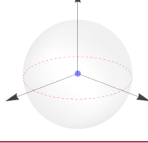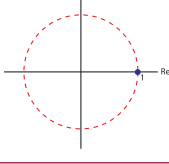
A key limitation of these schemes is the fact that typical photographic film, usually an emulsion of silver halide crystals, is neither sensitive to the polarization of light present during exposure nor is its transmission function sensitive to the polarization of illuminating light after development. This is what differentiates these earliest efforts with traditional holographic media from the technologies we detail throughout this section. Polarization was "recorded" in these schemes only inasmuch as controlled, polarized reference waves at different incident angles were present during both recording and reconstruction, a sort of angular multiplexing as is common in

Table 4.   Classes of Spatially Varying Polarization Optics as Defined by the *J* They Are Capable of Implementing*ᵃ*

Label	Description	Classes of Polarization Control Referenced Throughout Section 4		
		Diattenuator Space	Retarder Space	Overall Phase/Amplitude
A	An arbitrary case, for sake of example			
B	Complete control: any (passive) Jones matrix achievable at any point			
C	Full unitary control: any retarder Jones matrix with any retardance, overall phase, and fast-axis polarization achievable at any point			
D	Phase-only platform (no polarization sensitivity)			
E	Geometric phase only			
F	Any linear retarder with any retardance, and overall phase control			
G	Any linear wave plate; no phase control			

(Table continued)
(Table continued)

Classes of Polarization Control Referenced Throughout Section 4				
Label	Description	Diattenuator Space	Retarder Space	Overall Phase/Amplitude
H	Multi-level discrete control of overall phase and retardance; fixed retardance axis			
I	Continuously tunable retardance, no control over overall phase or retardance axis			
J	Continuously tunable retardance and overall phase with no control over retardation axis			
K	Polarization-selective, binary amplitude control (polarizer or no polarizer); no control over retardance, overall amplitude, or overall phase			

*J exists, in general, in an eight-dimensional parameter space. This is made intuitive by imagining it as a point in diattenuator space (describing its polarizer-like behavior), retarder space (describing its wave-plate-like behavior), and on the complex plane (representing its overall amplitude and phase).

holographic recording. Since the film itself was not polarization-sensitive, all polarizations would be affected by the transmission function for all polarization states, resulting in unwanted ghost images [65].

4.2b. Polarization Holograms

Materials do exist, however, in which optical anisotropy can itself be induced optically. These are known as *photoanisotropic* materials. The first recorded observation of photoanisotropy was by the German physicist Fritz Weigert in 1919 [69,70]. Weigert observed that a silver chloride film exposed to linear polarization induced linear dichroism. After exposure, the film attenuated light polarized orthogonal to the original illuminating light experienced higher transmission. Since then, a variety of photoanisotropic effects have been discovered in a variety of materials. These effects are not confined to linear dichroism; it is known that linear birefringence, and even circular dichroism and optical activity (circular birefringence), can also be induced by light of the correct polarization state. Which effect is induced and which is felt may vary with the illuminating wavelength (the "actinic light") and the probe wavelength. This diverse array of photoanisotropic effects are often dubbed simply the "Weigert effect," regardless of mechanism.

The Weigert effect may be observed in a variety of materials and films, including silver halides, alkali halides, organic dyes, and polymers with azobenzene side chains. The latter is perhaps the most popular choice. Numerous efforts are documented in the chemistry and optics literatures that seek to increase the strength and stability of photoanisotropy in these materials. The description we give here, however, is high level and does not delve into these details (see instead Chaps. 4 and 5 of [70]). We also note that the physical mechanism underlying the Weigert effect in these materials is itself a subject of scientific debate. Polarized light is thought to evoke a rearrangement at the molecular level. In azobenzenes, this is proposed to occur through rapid

cis-trans isomerization between two molecular conformations (twisting along the molecule's nitrogen double-bond), which induces random molecular reorientations that only cease upon alignment with the major axis of the polarization ellipse [71]. Being molecular in origin, the strength and orientation of photoanisotropy can vary on optically small size scales.

With the right chemistry, a photoanisotropic medium can retain memory of spatially varying polarization in the form of a spatially varying Jones matrix, even after the recording light is turned off. In the 1970s and 1980s, a community of researchers sought to use the Weigert effect to create "polarization holograms." The bulk of this research occurred in the former Soviet Union, and much of it is not documented in the English language. Sh. D. Kakichashvili, a physicist working in the Georgian SSR, is often cited as the pioneer of this area and was the first to propose polarization holography (in [72], and further summarized in [73,74] and his Russian-language textbook [75]). A recent book (2009) by Nikolova and Ramanujam [70] provides a modern, comprehensive account.

4.2c. Recording a Jones Matrix Mask

General principle. Here we provide a simple example of polarization holographic recording, paraphrasing and restructuring one given in Chap. 3 of [70]. In what follows, we assume that incident light, after some exposure time, induces only linear birefringence locally. This is true for some materials and wavelengths (such as in [76]), but as described above, photoanisotropy can manifest in other ways. Before exposure, we suppose the medium is isotropic with refractive index n_0, composed of randomly oriented molecules. When the medium is illuminated with linearly polarized light of intensity I, the long molecules will tend to rotate and align so that an anisotropy will be induced in the refractive index parallel and perpendicular to the polarization such that

$$\Delta n_\parallel = k_\parallel I$$

$$\Delta n_\perp = k_\perp I, \tag{133}$$

where $k_\parallel$ and $k_\perp$ are photoanisotropic properties that can be positive or negative [Fig. 17(a)]. Again, in the photoanisotropic effect treated here, linear birefringence is induced by linear polarization (i.e., for circularly polarized illumination, orthogonal linear polarization states would cancel the effect and induce no birefringence). Locally, the Jones matrix of the film

$$J = \begin{bmatrix} e^{ik(n_0 + \Delta n_\parallel)d} & 0 \\ 0 & e^{ik(n_0 + \Delta n_\perp)d} \end{bmatrix}, \tag{134}$$

where d is the film thickness and k is the free-space wavenumber. Since this is a power-dependent effect, we can operate in the Stokes formalism. A general elliptical polarization has a Stokes vector $\vec{S} = [\, S_0 \quad S_1 \quad S_2 \quad S_3 \,]^T$. $\vec{S}$, when fully polarized, represents a polarization ellipse tilted at some azimuth angle with some ellipticity. Only the components of the polarization linearly polarized along the ellipse's major and minor axes induce a change in refractive index. Defining $I_\parallel$ and $I_\perp$ to be the linearly polarized powers along the major and minor axes of the ellipse, respectively, we can write the intensities along the major and minor axes of the polarization ellipse as [Fig. 17(b)]

$$I_\parallel = \frac{S_0 + (S_1 + S_2)}{2}$$

$$I_\perp = \frac{S_0 - (S_1 + S_2)}{2}, \tag{135}$$

such that, by orthogonality,

$$\Delta n_\parallel = k_\parallel I_\parallel + k_\perp I_\perp,$$

$$\Delta n_\perp = k_\perp I_\parallel + k_\parallel I_\perp. \tag{136}$$

The retardance δ induced locally is given by $(n_\parallel - n_\perp)kd$, or

$$\delta = (k_\parallel - k_\perp)(I_\parallel - I_\perp)kd = (k_\parallel - k_\perp)(S_1 + S_2)kd = (k_\parallel - k_\perp)(s_1 + s_2)S_0kd. \tag{137}$$

In general, $\Delta n_\parallel$ and $\Delta n_\perp$ also induce a change in overall phase $\bar{\phi}$ given by $(n_\parallel + n_\perp)kd/2$, or

$$\bar{\phi} = \frac{(k_\parallel + k_\perp)(I_\parallel + I_\perp)kd}{2} = \frac{(k_\parallel + k_\perp)S_0kd}{2}, \tag{138}$$

where, as in Table 1, s_1 and s_2 are the first two components of the SOP. Figure 17(c) shows that both a retardance δ and an overall phase shift $\bar{\phi}$ are induced relative to the background n_0. Using the matrix exponential notation of Eq. (81), we can write (neglecting the constant overall phase n_0kd)

$$J = e^{i\bar{\phi}} e^{i\frac{\delta}{\sqrt{s_1^2 + s_2^2}}(s_1 \cdot \sigma_1 + s_2 \cdot \sigma_2)}. \tag{139}$$

Figure 17
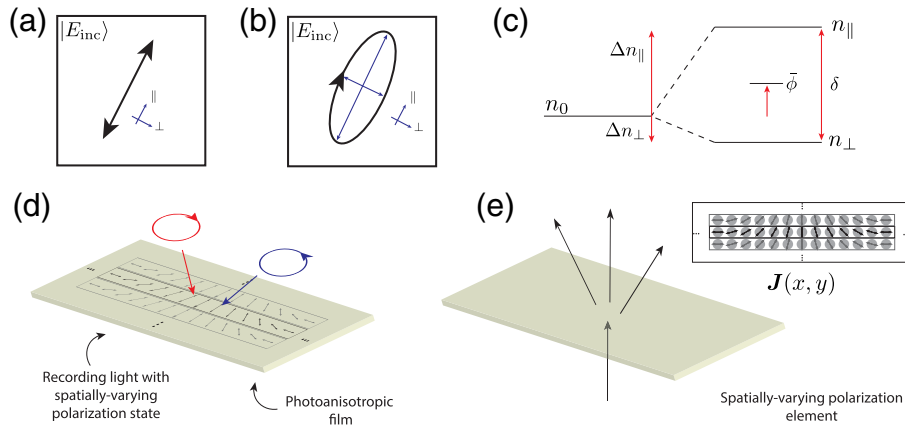
Polarization holographic recording. (a) In a photoanisotropic medium, linear polarization induces a local change in refractive index both parallel and perpendicular to its direction and proportional to its intensity. (b) In the general case of elliptically polarized light, a linear photoanisotropic medium feels only the linearly polarized components (denoted in blue), again inducing changes in refractive index in the parallel and perpendicular directions. (c) Full control over the magnitude of $\Delta n_\parallel$ and $\Delta n_\perp$ is sufficient to fully control retardance δ and overall phase shift $\bar{\phi}$. (d) A spatially varying polarization pattern will induce a spatially varying polarization transfer function in the photoanisotropic film. In this case, the interference of right- and left-circularly polarized light is shown. This particular case induces linear polarization of constant magnitude but periodically changing azimuth, which, in a linear photoanisotropic material, induces a spatially varying wave plate of constant retardance and periodic azimuth. This particular recording scenario, which produces an optic that will produce three diffraction orders regardless of illuminating polarization, has been used in practice in most work in polarization holography.

Equation (139) represents a linearly birefringent wave plate whose overall phase, retardance, and orientation are all independently tunable by varying $\vec{S}$ of the illuminating light. The orientation of the wave plate is fixed by the azimuth angle of the polarization ellipse, solely governed by s_1 and s_2 so that the normalized axis is $\frac{1}{\sqrt{s_1^2+s_2^2}}(s_1, s_2, 0)$. The overall phase can be tuned by adjusting the beam's intensity S_0, while the retardance can be tuned by changing the polarization's ellipticity, modifying the sum $s_1 + s_2$ by increasing or decreasing s_3. If a spatially varying polarization field $\vec{S}(x, y)$ can be created, $J(x, y)$ will result, representing an optic in which linear retardance, linear retardance axis, and overall phase can be controlled everywhere. This type of photoanisotropy falls under type F of Table 4.

Recording a polarization grating. An example makes this less abstract. As discussed in Subsection 3.2, interfering two plane waves at different angles with different polarization states is a simple way of creating a periodic, spatially varying polarization field. Suppose we (paraxially) interfere two plane waves of opposite circular polarization. The interference will trace the equator of the Poincaré sphere, always remaining linear, periodically repeating over a distance $\Lambda = \frac{\lambda}{\sin \theta}$, where θ is the angle between the beams' k-vectors. The Jones vector will be given by

$$|j(x, y)\rangle = \begin{bmatrix} \cos \frac{2\pi x}{\Lambda} \\ \sin \frac{2\pi x}{\Lambda} \end{bmatrix}, \tag{140}$$

or, in the Stokes formalism,

$$\vec{S}(x, y) = \begin{bmatrix} 1 & \cos^2 2\frac{2\pi x}{\Lambda} & \sin^2 2\frac{2\pi x}{\Lambda} & 0 \end{bmatrix}^T. \tag{141}$$

We have from Eqs. (137) and (138) that $\delta = (k_\parallel - k_\perp)kd$ and $\bar{\phi} = (k_\parallel + k_\perp)kd/2$—neither a function of space. The retardance axis on the other hand will rotate uniformly with space from 0 to 2π. In other words, if a photoanisotropic film is exposed to light with a spatially varying polarization given by Eq. (141), the Weigert effect will create a medium that acts as a spatially varying wave plate with uniform retardance and overall phase and a uniformly rotating fast-axis [Figs. 17(d) and 17(e)]. This is given by

$$J(x, y) \propto R\left(-\frac{2\pi x}{\Lambda}\right) \begin{bmatrix} e^{i\frac{\delta}{2}} & 0 \\ 0 & e^{-i\frac{\delta}{2}} \end{bmatrix} R\left(\frac{2\pi x}{\Lambda}\right), \tag{142}$$

where R is again a rotation matrix.

It can be shown that the matrix Fourier transform of this $J(x, y)$ has just three terms, so we can write

$$J(x, y) = \cos \frac{\delta}{2} \mathbb{I} + \left(\frac{i}{2} \sin \frac{\delta}{2} |L\rangle\langle R|\right) e^{+i\frac{2\pi}{\Lambda}x} + \left(\frac{i}{2} \sin \frac{\delta}{2} |R\rangle\langle L|\right) e^{-i\frac{2\pi}{\Lambda}x}. \tag{143}$$

The first term of Eq. (143) is a polarization-independent zero order, while the second and third terms are ± 1 orders that act as circular polarizers for opposite circular polarization states (while flipping their handedness at the output). The weight of the orders is governed by the induced retardance δ.

If we arrange, by choice of material, wavelength, recording beam intensity, and film thickness for $\delta = \pi$, the zero order vanishes, and all light is directed into the ± 1 orders. In scalar paraxial optics, it is impossible to losslessly diffract light into more than one diffraction order with a thin grating [77]. The polarization degree-of-freedom, however, relieves this constraint, a theme that has been remarked on by

several authors [78,79] (Subsection 4.6) but first by Kakichashvili in this context. Equation (142) also represents a *geometric phase grating* in which retardance and phase are held constant but angular orientation varies (type E of Table 4). Work by Kakichashvili *et al*. anticipated extensive later work on these gratings in the areas of metasurfaces and LCs (Subsections 4.5 and 4.7), some 30–40 years earlier.

4.2d. Applications of Polarization Holograms

The recording example of the last section—involving the interference of two orthogonal, circularly polarized plane waves—is just one specific use case out of an infinity of possibilities. In fact, its use is limiting, resulting in a less general sort of polarization control than could potentially be realized. Nevertheless, the fact that only three orders emerge and that the ±1 orders act as circular analyzers makes this particular recording scheme very intuitive. Research in polarization holography has tended to operate in this regime with two recording beams of opposite circular polarization.

Figure 18
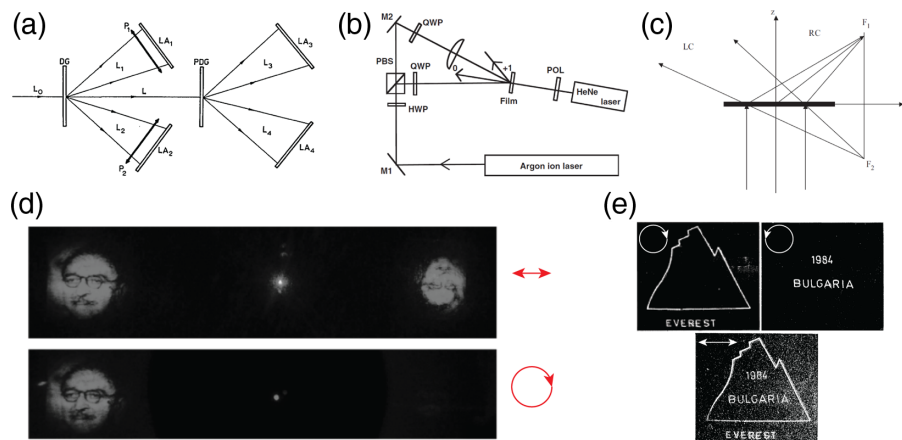
Applications of polarization holograms. (a) Spectropolarimetry with a polarization hologram. The full-Stokes vector of a beam can be measured over a band of wavelengths if linear detectors are placed on the diffraction orders of a polarization-insensitive grating and a circular polarization-splitting polarization hologram. Two polarizers on the left two diffraction orders suffice to determine S_1 and S_2. Reprinted with permission from [80]. Copyright 2000 Optical Society of America. (b) If one recording beam is passed through a lens, the period of the interference is spatially varying such that upon illumination (after recording), as in (c), the photoanisotropic film will function as an off-axis lens, focusing for one circular polarization and diverging for the other. (b) and (c) reprinted from Opt. Lasers Eng. **44**, Ramanujam *et al*., "Polarisation-sensitive optical elements in azobenzene polyesters and peptides," pp. 912–915, copyright 2006, with permission from Elsevier [81]. (d) If, in the recording scenario of (b), a transparency is placed (in this case an image of Denis Gabor), a holographic image will be recorded on the two inner diffraction orders. These are sensitive to opposite circular polarization states, and one is inverted with respect to the other, a characteristic of geometric-phase-only devices. Reproduced with permission of Cambridge University Press through PLSclear [70]). (e) This recording can be done twice, reversing the chiralities of the recording beams in-between transparencies. Then, each diffraction order can show two images depending on the sense of circular polarization incident, or both images simultaneously (for linearly polarized illumination). Reprinted with permission from [82]. Copyright 1985 Optical Society of America.

Applications of polarization-sensitive optical elements recorded into photoanisotropic materials can be sorted into two major application areas, with some examples shown in Fig. 18:

1. **Polarization-sensitive gratings for snapshot polarimetry:** The inner two orders of Eq. (143) act as circular polarizers. When the grating is illuminated with light of an unknown polarization state, if P_{+1} and P_{-1}—the power of these orders— are recorded, the Stokes parameters $S_0 = P_{+1} + P_{-1}$ and $S_3 = P_{+1} - P_{-1}$ can be immediately deduced. The remaining Stokes parameters S_1 and S_2 cannot be determined by these two grating orders alone. Several possible schemes exist to convert the grating into a full-Stokes polarimeter. Nikolova _et al._ proposed placing a polarizer on the zero-order channel to make it polarization-dependent, while tilting the grating at an angle to capture reflected light from the grating [83] which experiences a polarizer-like effect enacted by the Fresnel coefficients. In another scheme, a cascade of two gratings may be used-the first polarization insensitive and the second of the form of Eq. (134). The diffraction orders of the former are passed through polarizers prior to detection to enable determination of S_1 and S_2. This setup is shown in Fig. 18(a). Use of these gratings also splits colors (the more typical use of a grating in optics). Polarimetry may be performed over a continuous bandwidth if linear detectors are used, enabling spectropolarimetry [80,84].
   Nikolova and Todorov _et al._ were the first to propose the use of polarization-sensitive gratings in polarimetry, an application later explored with other technologies at different times (as we discuss throughout this section). These schemes [80,83,84], however, mandate optical loss, multiple gratings, or both in order to measure the full-Stokes vector. This stems directly from the simplification owed to recording only with orthogonal circularly polarized beams, which creates solely geometric phase optical elements without realizing the full freedom afforded by the platform.

2. **Polarization-sensitive optical elements:** So far the only polarization holograms we have treated are periodic diffraction gratings. However, our discussion can extend to _non_-periodic optical elements so long as they change at much lower spatial frequencies than the grating periodicity set by the angle between reference and object beams (a paraxial approximation). In this way, more general optical elements can be recorded into a polarization holographic material. If, for instance, a lens is placed before one beam during the recording process (and the NA of the lens is lower than the NA defined by the angle between the beams), a grating will be recorded with spatially varying period. This modified recording process is shown in Fig. 18(b). After recording, the element will act as a polarization-sensitive, off-axis lens. For RCP incident light, it will focus light in the direction of the +1 order; for incident LCP light, it will act as a diverging lens in the −1 order [as shown in Fig. 18(c)]. This type of lens has been demonstrated in azobenzene-containing polymers by Ramanujam _et al._ [81].
   More generally, if one recording beam passes through a transparency and then a Fourier transforming lens, upon later illumination, a holographic image of this transparency can be reconstructed in the far-field. This image is polarization-sensitive—the image will be formed on the +1 order and a point-inverted version thereof on the −1 order, a fundamental consequence of using the geometric phase alone. Each order moreover acts as a circular analyzer. Figure 18(d) shows a reconstructed far-field of an element encoding a transparency of D. Gabor. The image is formed on both orders upon illumination with linear polarization, but only on one with circular illumination [70]. Multiple holograms can be encoded if the recording process is carried out twice for two separate images, reversing

the polarizations of the two recording beams in-between (from $|R\rangle \to |L\rangle$ and $|L\rangle \to |R\rangle$). Figure 18(e) shows an example where one image appears on a single diffraction order, while another appears when the chirality of the illuminating light is reversed; both appear for linearly polarized illumination [82]. 3D holography is possible using similar schemes if scattered light from an object is used during recording.

Finally, we note that Fratz *et al.*, using a very similar azobenzene-containing polymer platform (recorded by direct laser writing), demonstrated polarization holograms for laser beam shaping [85] and computer-generated holographic imagery [86].

Numerous other applications have been proposed, including in optical data storage [87], optical information processing [88], and nonlinear optics [89].

4.2e. Discussion

Polarization holograms are—theoretically—among the most flexible technologies for spatially varying polarization optics reviewed here. In this section, we have focused on linear photoanisotropy, in which linear polarization induces linear birefringence. However, in some materials, photoanisotropy manifests as linear dichroism and even circular birefringence. The fact that several of these effects can occur at once in the same material means that polarization holograms can (potentially) access more general types of polarization control than other platforms. These effects, however, are not independent and constrain each other. For instance, linear birefringence and linear dichroism, when present together in a photoanisotropic material, will appear along the same axis and will be correlated in magnitude.

A drawback of polarization holography as presented here is its reliance on *recording*. The light-sensitive polarization effect is itself induced by light—possible designs are constrained by what distributions of intensity and polarization can be created in the first place. In that regard, it is unsurprising that most research in the field has centered on variants of two-beam interference, though direct laser writing is possible [81]. In contrast, other polarization technologies we discuss in this review, especially metasurfaces, enable rather arbitrary specification of the Jones matrix, even with discontinuities, from point-to-point, coming closer to the ideal of computer-generated holography. A second major drawback of the polarization holograms described here is materials and chemistry. Extensive research in polarization holography has centered on creating holographic media where the Weigert effect is stable over long time scales. These films have glass transition temperatures near ambient. This is responsible for photoanisotropy to begin with (so that molecules may rotate) but also means that photoanisotropic effects tend to fade. Azobenzene-containing polymers and polyesters, the most promising polarization holographic materials, are highly sensitive to ambient light and heat, which threaten to erase recorded patterns. A major advance in the field was the realization of holograms with stability over hours to days [76,82,90]. Polarization holograms with at least decade-long stability under proper storage conditions have been reported [81].

This field, which is not well-known in many corners of the optics community, may be an interesting area for future research. Other technologies discussed here can more ably create sophisticated spatially varying fields and, when combined with these photoanisotropic materials for recording, may yield new devices.

4.3. Elements Fabricated into Birefringent and Polarization Dichroic Substrates

The first polarization optics used in-built properties from crystal physics, namely birefringence and polarization dichroism, to manipulate polarization (Fig. 1). These

effects, however, are spatially homogeneous, inherent in the atomic lattice of the materials. It is natural to wonder whether a homogeneous polarization-sensitive crystal suitably patterned with modern lithography tools can surmount this.

General principles. This was a line of research pursued extensively in the 1990s by Y. Fainman *et al.*, summarized in Fig. 19. In these efforts, computer-generated holograms were obtained that implemented separate phase profiles for an orthogonal basis of linear polarizations (with this basis being constant across the optical element). Thus, the spatially varying Jones matrix implemented by these elements is given by

$$J(x, y) = \begin{bmatrix} e^{i\phi_x(x,y)} & 0 \\ 0 & e^{i\phi_y(x,y)} \end{bmatrix}, \tag{144}$$

where $\phi_x(x, y)$ and $\phi_y(x, y)$ are independent phase profiles imparted on orthogonal linear polarizations (labeled x and y for convenience). If an overall, polarization-independent phase $(\phi_x + \phi_y)/2$ is factored out from Eq. (144), it can be seen that Eq. (144) represents a wave plate with two independent degrees of freedom. Proper adjustment of ϕ_x and ϕ_y permits control of this overall phase as well as the wave plate's retardance $\phi_y - \phi_x$, though the wave plate's fast-axis remains fixed. For fabrication-related reasons we detail below, ϕ_x and ϕ_y must take on one of a set of a discrete values and are not continuously variable. Thus, the control implemented by these optical elements is of type H of Table 4.

Figure 19(a) shows the geometry of a single "pixel" of such an optical element. Two uniaxial (or biaxial) crystals are bonded together with a gap medium, which is isotropic. Before assembly, each uniform-birefringent substrate (often lithium niobate or calcite in these works) is patterned and etched to a given depth. Strictly speaking, only one of the substrates must be birefringent, a possibility the authors acknowledged [92], but both must be individually lithographically patterned. Control of the two depths d_1 and d_2 permits control of the two phases experienced by orthogonal linear polarization states [91] (labeled ϕ_o and ϕ_e in Fig. 19, in reference to ordinary and extraordinary waves). These depths, and consequently these phases, may vary across the optical element giving something in the end that resembles the schematic of Fig. 19, which may act as an independent phase hologram for orthogonal linear polarization states. With more traditional phase holograms, this function could only be achieved with a complicated configuration of many optical elements, first splitting the light on the basis of polarization, enacting the phase holograms, and recombining orthogonal polarization states with beam splitters [as in Fig. 19(c)]. One example of this presented by the authors was a lens element with a focal length of f for x-polarized light and $2f$ for y-polarized light. Then, when the incident polarization of coherent light illuminating an object was switched between x and y, either an image of the object or its Fourier transform were formed on a sensor plane [91,92]. Systems involving cascades of these birefringent holograms and switchable LC elements were also demonstrated for dynamic beam-routing [92,93].

Discussion. This line of work represents early efforts in this field, and Fainman *et al.* deserve credit for anticipating later research on polarization-switchable micro/nanofabricated optical elements. Since these elements are lithographically patterned, they allow arbitrary phase profiles and are of use in polarization-sensitive computer-generated holography. However, the approach of using birefringent media directly—which might at first seem to be the most natural approach—presents a number of drawbacks. For one, the approach relies on the birefringent substrate being experienced as a bulk medium at each pixel for the approach (using modulations in depth to encode modulations in phase) to work. Consequently, each pixel's lateral

extent must occupy at least several wavelengths, resulting in low sampling density and making zero-order-only diffraction challenging.

Additionally, the depth modulation required to achieve polarization-dependent phase mandates a complicated fabrication procedure. The technique of choice for micron-scale milling, reactive ion etching, is a top-down approach. Different depths can only be achieved sequentially using multiple steps of lithography (electron-beam lithography, in this case) and etching. This is known as multi-level diffractive optics [94]. Fabricating a structure with N discrete etch depths requires $\log_2 N$ discrete lithography/etch cycles. This approach with two birefringent substrates requires $4\log_2 N$ to achieve N discrete values of ϕ_x and ϕ_y, the phase profiles imparted on orthogonal polarizations [92]. Moreover, once fabricated, the two etched substrates must be carefully sandwiched and aligned to one another in a procedure that is, altogether, cumbersome {Fig. 19(e) and [92], with the authors presenting a later approach [95] that used one substrate with much deeper etching, avoiding this alignment}. Other authors [96,97] proposed additional improvements.

Figure 19
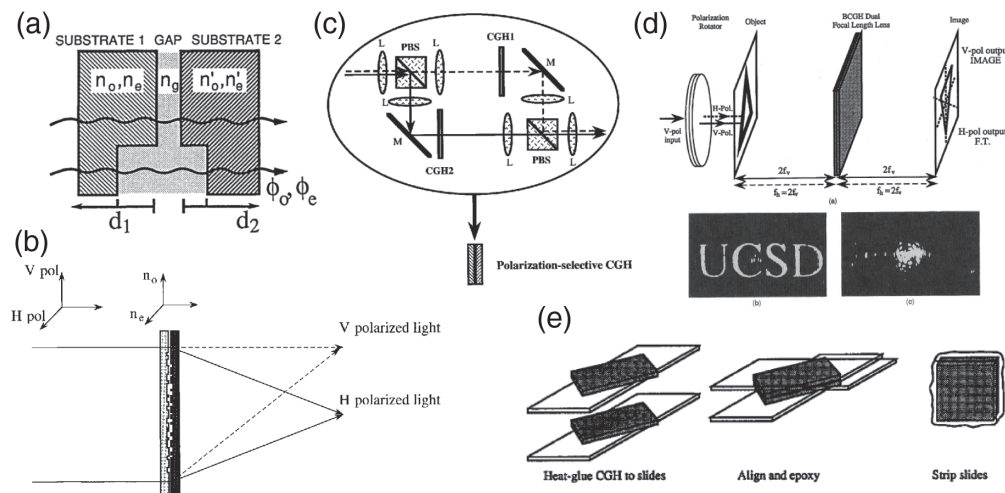
Computer-generated holograms etched directly into birefringent substrates. (a) Orthogonal linear polarizations can experience two arbitrarily specified phases upon propagation through two birefringent crystals sandwiched together with controllable etch depths. Reprinted with permission from [91]. Copyright 1993 Optical Society of America. (b) If these two etch depths can vary from point-to-point, two patterned birefringent substrates can form a computer-generated hologram that imparts two independent phase profiles on orthogonal linear polarization states. Reprinted with permission from [92]. Copyright 1995 Optical Society of America. (c) Such a hologram implements the function of two non-polarization-sensitive phase holograms placed in a setup in which polarization is split and recombined by polarizing beam splitters. Reprinted with permission from [93]. Copyright 1997 Optical Society of America. (d) In one application, the hologram can be designed to act as a lens with two different focal lengths depending on the polarization of incident light, either imaging a coherent target or producing its Fourier transform when input polarization is switched. (e) The two substrates must be patterned and etched separately in a multi-level fabrication process, then precisely aligned. Reprinted with permission from [92]. Copyright 1995 Optical Society of America.

The use of form birefringence, in which in-plane lateral dimensions are varied instead of depth, can be accomplished in a single lithographic step, surmounting the difficulties of using the natural birefringence of crystalline substrates. This is the approach used by more recent works (Subsection 4.7), and it appears that Fainman *et al*. also appreciated this [98–100]. We discuss this further in Subsection 4.7c.

Patterning dichroic materials. To conclude, we note that it is also possible to create polarization-sensitive computer-generated holograms by patterning a substrate that is dichroic, i.e., polarizer-like. This approach has received less attention, perhaps because polarizers are absorptive while birefringent media enable lossless phase-like holograms. Hossfeld *et al*. demonstrated that a polarizing sheet can be selectively "bleached" (i.e., ablated so that it no longer acts as a polarizer). This enables one polarization to pass while the orthogonal polarization experiences a binary amplitude hologram, passing where the polarizer was bleached and attenuated where it was not [101,102]. Nonetheless, these optical elements permit simple, planar fabrication with laser lithography. This class of control falls under type K of Table 4.

4.4. Stress-Engineered Optical Elements

The photoelastic effect. Mechanical stress—applied force over an area—can reorient materials at a molecular level and induce local changes in density. In transparent materials (e.g., glasses and plastics), these effects conspire to produce stress birefringence in which light experiences phase retardation. Stress at MPa scale usually induces a change in refractive index at the ~0.0001 level, a small change indeed, but one that can build up through the optically thick macroscopic scale of an optical element. This is known as the photoelastic effect and is well-known having been first described by David Brewster. Often, stress birefringence is regarded as a nuisance in optical systems, requiring careful accounting on the part of an optical designer [2]. It can be induced by a lens' mount or, in larger elements, even by gravity. Stress birefringence can also be "frozen in" during manufacturing, a concern especially relevant to the injection molded optics now common in consumer electronics. Less commonly, stress birefringence can be put to practical use. In a photoelastic modulator (PEM), a piezoelectric transducer resonantly excites a dielectric bar, allowing the device to act as a time-periodic wave plate (at the level of an entire beam). PEMs are used widely in precision polarimetric systems and a variety of scientific measurements.

Stress engineering. More relevant to this review, however, are "stress-engineered optics" (SEOs), in which stress birefringence is induced deliberately in a controlled way. Solid mechanics dictates the distribution of stress inside a material through the Poisson equation. Under given boundary conditions, the Poisson equation can be solved (using, for instance, finite element analysis) yielding the stress tensor σ across a material (which is 2×2 in the limit of a planar body with in-plane applied stress). The tensor σ can be diagonalized to give the principal stresses, which—through a material's stress-optic coefficients—dictate the retarder-like transmission function induced locally in the optic. The eigen-axes of σ dictate its angular orientation. In an SEO, stress birefringence is engineered through control of force boundary conditions. Several such schemes have been demonstrated. A glass round can be placed in a mount and stress birefringence induced by tightening set screws placed in desired locations. In another scheme, a glass round can be placed inside a metal ring that has undergone thermal expansion. As the ring cools, it compresses and stresses the glass optic. The ring itself can be structured to tailor the resulting stress distribution (see [103] for more details).

Applications. SEOs have been proposed for a number of applications, primarily by T. G. Brown *et al*. [104] in the 2000s and 2010s (see Fig. 20). A glass plate stressed in

three places (threefold symmetry) produces a spatially varying retarder near its center whose retardance scales with radius and whose angular orientation varies linearly with azimuth angle. Such an SEO may produce polarization vortices, i.e., radially and azimuthally polarized beams containing optical angular momentum [105]. Cast in different mathematical terms, the same SEO, when illuminated with circularly polarized light, can produce a "full Poincaré beam," an optical beam in which all polarization states are present [106,107], even partially polarized ones [108]. These Poincaré beams have spurred significant interest in the structured light community. When placed in a pupil plane of an imaging system, the SEO has a point-spread function (PSF) that is polarization-sensitive. This can yield optical systems producing different focal points for left- and right- circularly polarized light [109], and the PSF's image on a sensor can be used as a tool to ascertain the polarization state of incident light [110,111]—a polarimeter.

Polarimetry based on an SEO relies on imaging the whole PSF, rather than taking discrete point measurements as in other schemes. As a result, it can be used for imaging polarimetry only for spatially sparse sources wherein different parts of the source can form a PSF on an imaging sensor without overlapping with other parts of the source. The resolution of an SEO could be increased by shrinking the diameter of the PSF, at the expense of polarization accuracy. From a variational perspective, it has been shown that the simple SEO described above provides a nearly optimal balancing of the two [113].

Despite this limitation, SEO polarimetry has been demonstrated in several applications of sparse polarimetric imaging. One of these is multicore fibers [114] where an SEO can be used to determine the polarization of light in each of the many cores in a single shot. A second recent application of SEOs is a microscopy technique that permits the determination of the position, angular orientation, and wobble of fluorophore, even at the single molecule level, by coupling the SEO to a stochastic optical reconstruction microscopy (STORM) setup (a super-resolution technique) [112]. Being approximately an electric dipole, the fluorophore's orientation is intimately tied to its polarization; additionally, the variation of the PSF with defocus permits reconstruction of z position, while wobble manifests as depolarization. The SEO can be placed in the pupil plane of a high-NA microscope, as shown in Fig. 20(d). Analyzing the light for RCP/LCP is necessary to distinguish z position from orientation. An example of several single molecules whose positions, orientations, and wobbles have been reconstructed by this technique are shown in Fig. 20(e), at left (in this case, Alexa Fluor 488 molecules attached to a fiber of F-actin). The STORM image of one single molecule [Fig. 20(e), right top row] is shown with its closest theoretical reconstruction [Fig. 20(e), bottom row], which are reminiscent of the SEO PSFs in Fig. 20(c).

Discussion. In principle, polarization control attained by SEOs can span anywhere in the equator of retardance space—any wave plate with any retardance and angular orientation could be achieved somewhere within the aperture of an SEO (overall phase, however, cannot be spatially controlled). The polarization control they enact then falls under type G of Table 4. We note, however, that unlike many of the platforms here, this control cannot be arbitrarily defined from point-to-point. The spatially varying Jones matrix enacted by the SEO is governed by applied force. These applied forces can be customized creating potentially quite complex patterns [e.g., Fig. 20(b)] but can never be specified fully at-will. Stress birefringence, being molecular in nature, has no optically significant sampling limit (unlike other technologies discussed here, which are pixelated). The $J(x, y)$ realized by an SEO must be continuous and smoothly varying, lacking the freedom afforded by other spatially varying elements,

which could well contain sharp discontinuities. For this reason, an SEO is not capable of computer-generated holography in general.

Nevertheless, the origin of these fundamental limitations is also the strongest selling point of SEOs: their fabrication is simple, requiring only glass, heat, and simple applications of force.

Figure 20
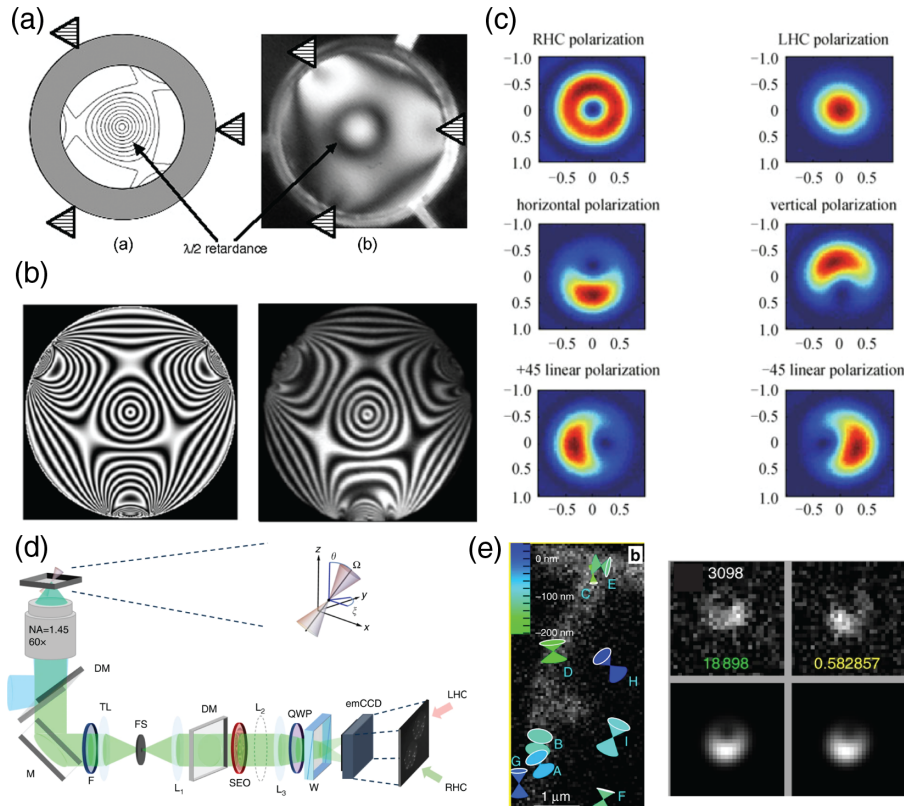
Stress-engineered optical elements (SEOs). (a) Example of SEO fabrication. A glass round is held in a mount, and stress is applied through three adjustable set screws, inducing stress birefringence visible in a broadband image viewed through crossed circular polarizers. Reprinted with permission from [105]. Copyright 2007 Optical Society of America. (b) Viewing through crossed circular polarizers with narrowband illumination highlights contours of equal retardance, showing how tailored stress birefringence induces complex patterns of spatially varying birefringence. Near the center of this SEO, the pattern displays azimuthal symmetry with retardance varying with radius and wave plate fast-axis with azimuthal angle. Reprinted by permission from Macmillan Publishers Ltd.: Brown and Beckley, Front. Optoelecton. **6**, 89–96 (2013) [104]. Copyright 2013. (c) When placed in the entrance pupil of an imaging system, an SEO modifies the system's point-spread function in a way that depends on incident polarization. This effect can be used to measure that incident polarization state. Reprinted by permission from Macmillan Publishers Ltd.: Brown and Beckley, Front. Optoelecton. **6**, 89–96 (2013) [104]. Copyright 2013. Reprinted with permission from [106]. Copyright 2013. (d) and (e) An application using SEO-enabled polarimetry to determine the orientation, position, and wobble of single molecule fluorophores, described in Subsection 4.4. Reprinted under a Creative Commons Attribution 4.0 International License [107].

4.5. Liquid Crystal Devices

4.5a. Introduction

Optical properties of LCs. LCs are a state of matter with properties lying between liquids and crystalline solids. Like a liquid, LCs can flow and exhibit viscosity. Like a crystal, LCs can exhibit long-range order and, as we discuss below, exhibit optical anisotropy. LCs are composed of long, rod-like organic molecules with lengths on the order of nanometers. The subject of a century of scientific inquiry, LCs are also the enabler of LC displays, today a multi-billion dollar industry. Much could be said here, ranging from the fundamental physics governing LCs' behavior to more technological considerations. In this review, however, we can scarcely begin to scratch the surface of this, a subject which deservedly forms the basis of many dedicated books (coming at the subject from both fundamental [115] and technological perspectives [116]).

A wide variety of organic compounds can be classified as LCs. In fact, the photore-fractive azobenzene-containing polymers of Subsection 4.2 can be considered LCs and could have been included here. In fact, as we will see below, similar materials are used in conjunction with other LCs to mediate *photoalignment*. The dedication of an independent section to polarization holograms above (Subsection 4.2), then, reflects a distinction that is primarily historical and contextual (a different literature at a different time) rather than fundamental in nature.

Here, LCs are of interest inasmuch as they are an important technology for polarization-dependent diffractive optics. A key property of LCs is their birefringence. LC molecules, being elongated cylinder-like rods, exhibit optical anisotropy. In a medium with aligned LC molecules, light polarized along the long axis of the LCs experiences a larger index (n_e, the extraordinary index) than light linearly polarized in the plane perpendicular to the molecules' long axis (n_0, the ordinary index). The specific values depend on the LC phase and molecular details, but Δn between the two is typically on the order of 0.2 but can be 0.4 or higher [116,117]. When ordered, LCs, thus, form a uniaxial medium.

Consider light propagating at an angle through a medium of LCs. In general, light in a uniaxial medium propagates in a superposition of two eigenmodes (ordinary and extraordinary rays). The index ellipsoid can be used as a geometrical aid to determine the refractive index experienced by each eigenmode [8,118] as a function of propagation angle. The index of the two linearly polarized eigenmodes is determined from (half) the length of the semi-major axes of the ellipse formed from the intersection of the index ellipsoid and a plane perpendicular to the light's $\vec{k}$ vector. If the light propagates parallel to the LCs' long axes, both eigenmodes will experience n_0 (the ellipse formed by the intersection is a circle). If light propagates perpendicular to the axes of the LCs, light can experience either n_0 or n_e, depending on its polarization state. In intermediate cases, one linear polarization will always experience n_0 while the other experiences an index n with $n_0 \leq n \leq n_e$, with $n(\theta) = n_e n_0 / \sqrt{n_e^2 \cos^2 \theta + n_0^2 \sin^2 \theta}$, with θ the angle between $\vec{k}$ and the extraordinary axes of the LCs [Fig. 21(a)].

LC cells. LCs, then, serve as a retarder whose retardance (per unit length) depends on the orientation of the LCs relative to incoming light. This, paired with two other crucial capabilities of LCs, forms the basis of most LC optical technology. These, which we describe only briefly here, are (1) *voltage-tunability*, wherein LCs placed in an electric field will, by virtue of an induced electric dipole, tend to align with that field, allowing the LCs to be rotated with application of an electrical bias and, (2) *anchoring*, wherein LCs can be fixed in a custom orientation near an appropriately patterned substrate.

These two effects make possible LC cells, two examples of which are sketched in Fig. 21(b) (we limit ourselves to nematic LCs—simply put, LCs that tend to align—the most common phase encountered in electro-optic technologies). A LC cell generally contains a medium of LCs sandwiched between two substrates, each with a polymer alignment layer that has been mechanically rubbed. This mechanical rubbing creates a boundary condition which, through van der Waals forces, coaxes the LC molecules near the alignment layer to orient along the rubbing direction. In equilibrium, LCs in the bulk tend to align with the boundary layers. However, if a voltage is applied (∼5 V, switching polarity at kHz rates), an induced dipole moment will cause LCs in the bulk to align with the applied electric field. In the case shown in the left half of Fig. 21(b), where the rubbing directions are parallel, this means the cell will act as a retarder with voltage-tunable retardance. When placed between crossed polarizers, this retardance effect can be converted into intensity modulation, the basis of LC displays. For practical reasons [namely, better field-of-view (FOV)], modern LC displays instead use a twisted nematic architecture [Fig. 21(b), right half], which

Figure 21
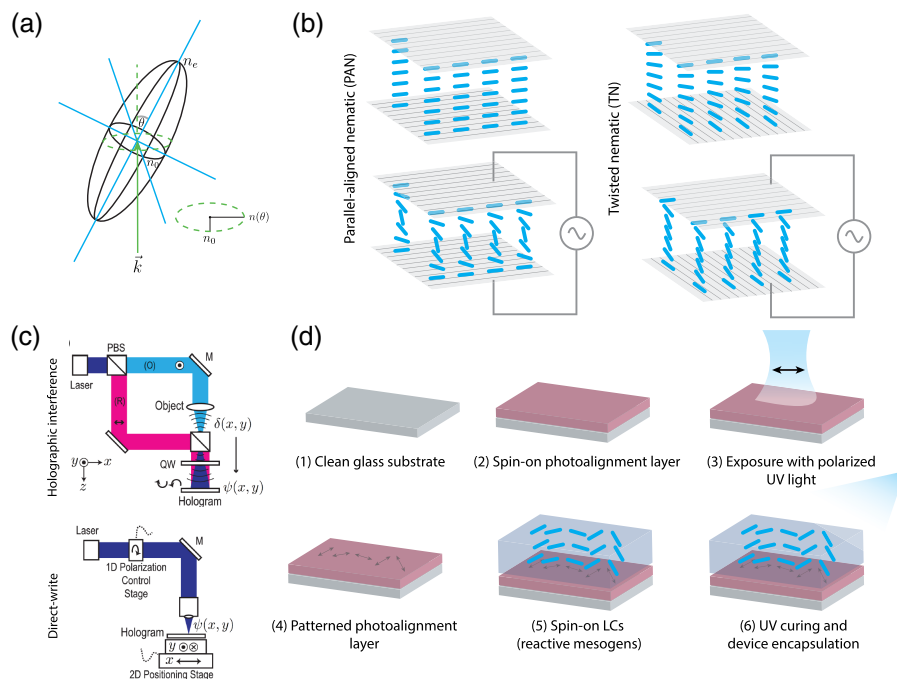
Liquid crystal (LC) devices. (a) A medium of ordered LCs is uniaxially birefringent due to the elongated nature of the LC molecules. At oblique incidence, one polarization eigenmode always experiences n_0, while the other experiences $n_0 \leq n \leq n_e$ depending on θ (and can be computed with aid of the index ellipsoid, pictured here). The retardance experienced varies with θ. (b) A layer of LCs can be sandwiched between substrates that have been mechanically rubbed. Van der Waals forces coax the LCs near the substrate to align with the rubbing directions. In a parallel aligned nematic crystal cell, the rubbing directions for both substrates are parallel so that the cell acts as a retarder. When a voltage is applied, LCs in the center of the cell rotate to align with the E-field, modifying the cell's retardance. In modern display applications, twisted nematic cells (placed between polarizers) are used instead. Here, lines on substrates denote rubbing directions for LC alignment (not polarizer directions). (c) Two techniques for patterning photoalignment materials with polarized light. Adapted from [119]. (d) A schematic of a typical fabrication procedure for photoaligned LC diffractive optics.

also exhibits a voltage-tunable polarization effect, albeit one that is not as simple as a pure modulation of retardance with applied bias [120].

This is as deep a survey of LC devices as we provide here, and in particular we do not delve into the exact physical mechanisms of these effects, including important issues such as the speed at which bias-tuning can occur and the trade-offs involved in using different LC types (twisted nematic, parallel aligned nematic, vertically aligned nematic, among many others) [116]. Instead, we next review how LC devices have enabled spatially varying polarization-sensitive diffractive elements. These fall into two different categories. In Subsection 4.5b, we describe LC devices enabled by substrate patterning, in particular a relatively new technique known as photoalignment. We describe polarization-dependent diffractive optics it has enabled, which have recently spawned several commercial products and new scientific applications. Then, in Subsection 4.5d, we describe diffractive devices where LCs are instead biased on an addressable grid, allowing for tunable, spatially varying polarization control. These are known as LC SLMs. We provide a top-level overview of the extent of polarization control possible with these LC SLMs (as in Subsection 4.1 and Table 4) and a review of past work.

4.5b. Photoaligned Liquid Crystal Polarization Diffractive Elements

LC displays were developed at RCA Corporation in the early 1960s and formally announced in 1968 [121–123]. In the decades since, the LC display industry has become ubiquitous and highly mature. From its inception, progress on displays has nurtured a parallel avenue of research in *non-display* optical applications [124] that capitalize on the unique optical characteristics of LCs. Using a variety of techniques over several decades, LCs have been used to realize gratings [125–128], tunable lenses [129–134], color filters [135,136] (often of the Lyot type), and even laser gain media (when doped with dyes) [137], among many others.

Our interests here center specifically on LC devices that explicitly use the anisotropy of LC devices to make designer polarization-sensitive diffractive optics, rather than simply using it as a means of phase accrual and doing away with the resultant polarization dependence by using a polarizer (the case in many LC optical devices). Fundamentally, a LC cell acts as a retarder, one whose retardance depends on the orientation of the LCs relative to the propagation direction and whose eigenbasis (fast-axis orientation) depends on their orientation in the plane perpendicular to that propagation direction. The former can be tuned with an applied bias, which when made to vary spatially provides one route to realize polarization-sensitive diffractive optics with LCs. Much effort has been dedicated this approach, the natural conclusion of which is an addressable array of electrodes placed on top of the LC cell, in which case the device is known as a LC SLM. These are the subject of Subsection 4.5d on SLMs {though we note here that other schemes for spatially dependent control short of a full array of electrodes have been investigated, particularly those based on resistive voltage divider networks that synthesize custom electrical potential gradients/functions (e.g., [132])}.

Photoalignment. The latter approach, varying the azimuth of the LCs' anisotropy axis, requires spatially varying control over the orientation of the LCs in the plane of the LC cell (perpendicular to the propagation axis). In principle this too could be voltage-controlled, but the fabrication of an array of electrodes perpendicular to a substrate is not compatible with top-down fabrication schemes. As a result, LC in-plane orientation must be controlled through substrate patterning, which, as described above, transfers to the LC molecules themselves through anchoring forces.

The most common method for this substrate patterning is mechanical rubbing, which is widely used in the LC display industry. For display needs, the required rubbing pattern is simple, requiring only one orientation over the entire substrate. However, the sophistication of patterns achievable by mechanical rubbing is limited. Patterns that are discontinuous, or those that change on short length scales, cannot be achieved in this way. These limitations constrain the types of optics achievable.

A breakthrough in this regard arrived around 1990, termed *photoalignment* (proposed by several groups around the world around the same time [138–141]). Photoalignment was originally developed in service of the LC display industry; for a different set of reasons (namely surface defects and charging), mechanical rubbing is not always ideal for display production, either. In photoalignment, a photoalignment layer— usually an azobenzene-containing polymer, much like the holographic materials of Subsection 4.2—is spun onto a glass substrate. In the presence of polarized UV illumination (laser or otherwise), the molecules of the photoalignment layer tend to align with the azimuth angle of the illuminating light's polarization ellipse through a rapid *cis-trans* photoisomerization process. Then, when a LC layer is spun atop this photoalignment layer, the LCs—by an electrostatic anchoring process—will tend to align with the photoalignment molecules. In this way, a LC layer can be fabricated whose in-plane orientation can be controlled by varying the linear polarization axis of light during the recording step with no mechanical contact necessary. Much has been written about photoalignment [142–144], but we point out that it is essentially similar to the polarization holography techniques discussed in Subsection 4.2 with the difference that a very thin polarization holographic material is used as an alignment layer for LCs, rather than as the optical medium itself. Figure 21(d) summarizes this, depicting a typical photoalignment-based process flow.

Polarization manipulation with photoaligned LC elements. Photoalignment permits arbitrary spatial variation of the LC axis, so long as the desired pattern can be generated as varying UV polarized light on the photoalignment layer. This can either be done in a holographic exposure using multiple tilted beams in a single shot [Fig. 21(c), top] or, for more arbitrary patterns, with a direct-write procedure using a focused laser, variable linear polarizer, and computer-controlled stage [Fig. 21(c), bottom]. This enables diffractive optics with spatially varying polarization transfer functions. In particular, it can realize an optic with a spatially varying Jones matrix of the form

$$J(x, y) = R(\theta(x, y)) \begin{bmatrix} e^{i\frac{\Delta}{2}} & 0 \\ 0 & e^{-i\frac{\Delta}{2}} \end{bmatrix} R(-\theta(x, y)), \qquad \textbf{(145)}$$

where R denotes a 2×2 rotation matrix, $\theta(x, y)$ is an arbitrary, spatially varying orientation function, and Δ is a retardance governed by the product of the thickness of the LC layer and the native birefringence of the LCs (Δ is potentially tunable on a whole-device layer by the application of a bias voltage to the cell). Generally, Δ is arranged to be π so that the optic consists of half-wave-plate-like elements of variable orientation. Usually, these optics are designed to work for circularly polarized incident light. In this case, the half-wave plates convert the handedness of the incident polarization state and apply a relative phase shift to the outgoing light equal to 2θ (where θ is measured against some arbitrary reference). The control exerted by these photoaligned LC elements can be classified as type E in Table 4, though the circle in the equator of the retarder space could vary in radius by controlling Δ; the LC layer acts as a linear retarder with fixed retardance but variable orientation.

Geometric phase gratings. The utility of photoalignment for producing diffractive optics was first appreciated by the technique's pioneers in the 1990s [145]. However,

a flurry of work on this subject appeared in the mid-to-late 2000s and continues to the present day. Early efforts beginning in $\sim 2004 - 2006$ concentrated on making _geometric phase gratings_. These are gratings that implement a linearly rotating fast-axis orientation. As a result, incident circularly polarized light experiences a linear geometric phase gradient and is deflected to the ± 1 order (depending on the handedness of the incident light) with theoretically unity efficiency. Interest in these was multifaceted: On the one hand, the requisite distribution of UV polarization needed to encode this pattern into a photoalignment material is simple to generate, being the result of two tilted circularly polarized plane waves. Additionally, the geometric phase, being a function of a physical orientation of the LC, is achromatic: as λ varies, the retardance Δ experienced will change too, but in a way that only decreases overall efficiency. Finally, as we will see in Subsections 4.6 and 4.7, these _polarization_ gratings attracted significant interest around the year 2000 for their ability to exhibit theoretically perfect diffraction efficiency from a thin diffractive element [78,146].

Geometric phase LC gratings were demonstrated at almost the same time by several different groups using photoalignment techniques [147–149], with very similar LC geometric phase gratings having been earlier demonstrated using microscale mechanical rubbing of a substrate with an atomic force microscope tip [150]. These were further developed by M. Escuti and others [151], including the important realization that two twisted layers of these photoaligned LCs with opposite twist could imbue these gratings with high efficiency ($>99\%$) over the entire visible spectrum [152–154]. Of course, the LC optical elements created by photoalignment need not be limited to periodic gratings. Direct-writing techniques (or, alternatively, the synthesis of complex vectorial wavefronts with SLMs) allow for the encoding of arbitrary geometric phase LC elements. In this way, lenses, axicons, and computer-generated holograms in general have been demonstrated [119,155]. These geometric phase holograms (GPHs) are also sometimes referred to as "cycloidal polarization holograms." An illustration of a LC geometric phase grating is given in Figs. 22(a) and 22(b).

Geometric phase optics beyond gratings. Photoaligned geometric phase LC optics has been proposed for a number of applications. First, LC geometric phase lenses have attracted interest as imaging optics, both as standalone components, as arrays of microlenses, and integrated with refractive lenses into compound systems [156]. Some success has been achieved at achieving high-NA (low f-number) LC lenses, down to $f/1.5$ [161]. LC geometric phase lenses are even commercially available from standard optics catalogs, as of this writing from Edmund Optics [157], as shown in Fig. 22(c). Due to their ease of fabrication, LC geometric phase lenses and gratings have recently attracted interest in the optical design of augmented and virtual reality ("AR/VR") systems [162–164]. At least one company (ImagineOptix, Inc. in North Carolina, USA) has been founded to commercialize LC geometric phase optics focused on the AR/VR application in particular, and, to name just one example, Facebook Reality Labs has recently demonstrated a compact virtual reality headset prototype based on LC polarization holographic elements [158] [Fig. 22(d)].

It is no surprise, perhaps, that these optics can be used for polarimetry. A geometric phase grating acts as a polarization beam splitter sensitive to circular polarization; as a result, measuring the intensity of its ± 1 diffraction orders directly yields S_0 and S_3 of impinging light. By combining several such gratings with additional polarization optics, a snapshot full-Stokes polarimeter can be constructed [165]. Cascades of several LC polarization gratings can be used for imaging polarimetry as well using a "channeled" approach in which the Stokes vectors are encoded as the modulation depth of white light fringes [48,159]. An example of a reconstructed image from

Figure 22
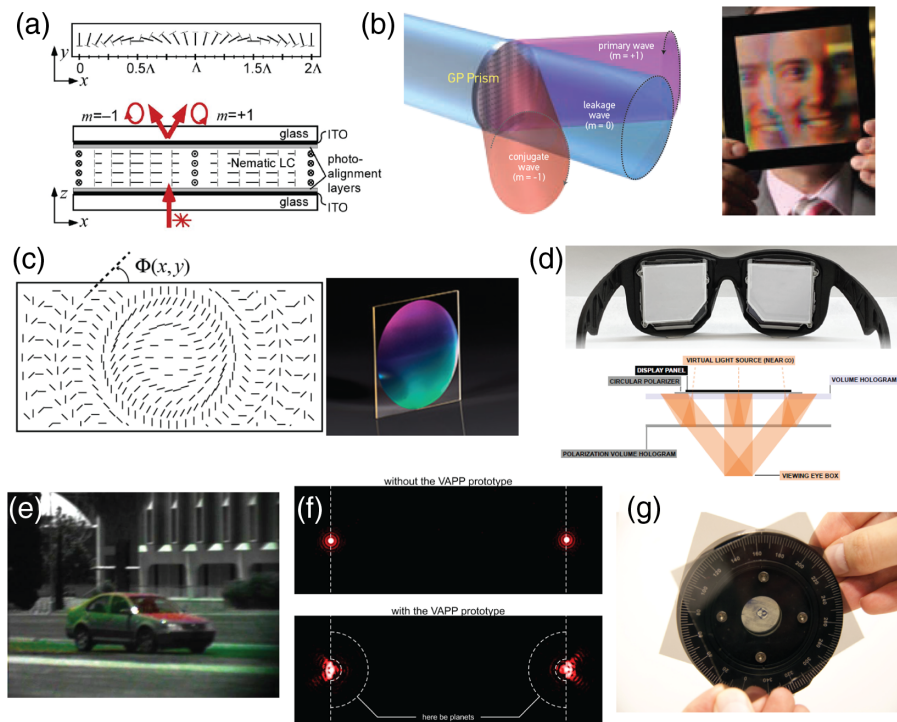
Optical devices and applications enabled by photoaligned LCs. (a) A geometric phase grating fabricated by illuminating a photoalignment layer with two tilted, circularly polarized beams that create a linearly polarized interference pattern of varying azimuth. LCs align with this patterned photoalignment layer to create a grating that (b) splits circularly polarized incident light into the ± 1 diffraction orders, with some leakage into the zero order if the cell's retardance deviates from π. These can be patterned uniformly over large areas, as shown by a grating fabricated by ImagineOptix, Inc. (a) Escuti and Jones, SID Symp. Dig. Tech. Pap. **37**, 1443–1446 (2006) [151]. Copyright Wiley-VCH Verlag GmbH & Co. KGaA. Reproduced with permission. (b) reprinted with permission from [156]. Copyright 2016 Optical Society of America. (c) The LCs can be patterned to realize a lens geometric phase profile. These components can be purchased off-the-shelf from Edmund Optics in ø1" format and $f = 45 - 100$ mm (example pictured at right). Reprinted with permission from Edmund Optics [157]. (d) Photoaligned holographic LC optics were recently used by Facebook Reality Labs in a virtual reality headset with a sunglasses-like formfactor. The prototype and optical design schematic are shown here (illumination source and screen electronics are located externally). Reprinted under a Creative Commons Attribution International 4.0 License [158]. (e) Systems incorporating several LC polarization gratings have been used for linear-only imaging polarimetry. The example here shows a white light image of a car taken through such a system where green and reddish colors are used to denote angle of linear polarization. Reprinted with permission from [159]. Copyright 2011 Optical Society of America. (f) LC geometric phase polarization holograms have been investigated for use in coronagraphic systems for exoplanet imaging applications. Here, they are referred to as vector apodizing phase plates ("vAPPs") and are advantageous for creating "cleared out" point-spread functions on both side of a host star where exoplanets can, potentially, be directly imaged. (g) Image of a fabricated vAPP between crossed polarizers. Reprinted with permission from Snik *et al.*, Proc. SPIE **8450** (2012) [160].

such a camera is shown in Fig. 22(e). In these polarimetric schemes, the limited control afforded by LC geometric phase optics mandates the use of multiple grating elements to determine light's full-Stokes vector, in contrast to what is possible with metasurface gratings, as we discuss in Subsection 4.7.

Photoaligned LC optics in coronagraphy. Finally, LC geometric phase elements have also attracted interest in the construction of new astrophysical instrumentation [166], in particular for exoplanet detection in systems known as coronagraphs. Coronagraphy, so named because it was originally intended for observations of the solar corona, describes a suite of related techniques for modifying the PSF of an imaging system (usually a telescope) to provide the contrast enhancement necessary to directly image a dim object in the vicinity of a much brighter one (such as an exoplanet orbiting a much brighter faraway star). Essentially, a coronagraph is an angular filter. A variety of techniques for coronagraphy using custom diffractive optical elements have been proposed [167]. These can be divided into focal plane and pupil plane-type instruments depending on where in the telescope system the designer optic is placed, with benefits and trade-offs to both classes. LC geometric phase optics has been proposed for both. In particular, they have been investigated for optical vortex coronagraphy (OVC), a focal plane technique that uses helical phase profiles [168] (we discuss this application in Subsection 4.5c). LC geometric phase optics has also been investigated for use in apodizing phase plate (APP) coronagraphs, a pupil plane technique. APP relies on the placement of a phase mask in a pupil (usually the entrance pupil) of a telescope that modifies the PSF of on-axis light (e.g., from a host star) to produce a one-sided dark region with high contrast that ideally allows light from a neighboring exoplanet to be directly imaged. The phase mask is not usually polarization-sensitive, but it can be implemented with a LC GPH (making it a vector APP, or vAPP) [160]. In this case, the light entering the telescope (which, practically speaking, is unpolarized) experiences two conjugated PSFs for each handedness of circular polarization. This coincidence, a result of the symmetry of the geometric phase, is useful in that it creates two PSFs with dark spots on *both* sides of the host star, enabling exoplanet detection over a wider area [shown in Fig. 22(f)]. The fact that the phase profile can be achromatized by using many layers of twisted LC elements is another advantage to this technology for APP coronagraphy. This and similar ideas have been investigated by Snik *et al*., both in the lab [160,169–171] and, more recently, in ground-based mid-infrared observatories, such as in the MagAO/Clio2 instrument at the Magellan/Clay telescope [172] and as part of the Keck OSIRIS imager [173].

Discussion and conclusion. To conclude, LC geometric phase optics enabled by photoalignment technology are a promising technology for polarization-sensitive diffractive optics that may enable a variety of applications. In contrast to other technologies discussed in this review, they can be fabricated over large areas (even on curved substrates) with relative ease using either holographic or direct-write techniques. This can be done even in small-scale facilities without the use of advanced technologies such as, e.g., vacuum systems and plasmas that might necessitate the use of specialized semiconductor foundries for scaling up. Multiple layers of patterned LCs are possible, and this capability allows for achromatization. These elements are known to exhibit very high efficiencies (in excess of 99% for gratings), and the ability to bias LC cells to tune overall retardance gives a post-fabrication knob to improve performance that does not exist for solid-state platforms such as, e.g., metasurfaces. Moreover, these technologies benefit from the widespread and highly mature LC display industry. The promise of LC geometric phase optics is evidenced by the number of researchers and firms investigating these today, and the technology has reached the point of ubiquity that completely custom patterned LC geometric phase

optics can be made-to-order from major optical vendors (e.g., Thorlabs, Inc. [174], which markets them as optical depolarizers and "patterned retarders"). These form the basis for at least two companies (known as ImagineOptix, mentioned above, and BEAM Co., based in Florida, USA). On a more creative note, these LC optics recently enabled a public art exhibition on the shed of the Amsterdam Centraal train station in the Netherlands [175].

A key disadvantage for LC geometric phase optics, at least from the perspective of this review, is the comparatively limited control over polarization they offer. With photoalignment-based fabrication, only the LCs' fast-axis orientation is tunable [Eq. (145)] while its retardance is a property of the LC thin film as a whole. That is, only one angular quantity of the full Jones matrix (out of eight total) can vary arbitrarily at the control of the designer. This stands in contrast to other technologies and techniques discussed throughout this section, which enable, mathematically speaking, more degrees-of-freedom (and can use geometric phase in tandem with propagation-based phase). The extent to which this matters depends on the application of interest; there are, however, cases in which other technology platforms can integrate polarization functions in a single device that would require multiple GPHs to realize (for the case of grating-based polarization analysis, see Subsection 4.7). A key disadvantage of LC GPHs more generally is, paradoxically, their polarization dependence; in applications that do not specifically use this polarization dependence and that require unpolarized illumination, this can mean wasting at least 50% of incoming light to a circular polarizer before the optical element.

4.5c. Vortex Beams and "q-Plates"

Here, we briefly discuss the application of LC devices to the generation of beams carrying optical orbital angular momentum (OAM). Optical OAM, while a highly related subject area, takes us somewhat far afield here. The reader is referred to one of numerous recent reviews [176–178]. Briefly, wavefronts carrying OAM are those with helical gradients of phase. These helical phase gradients can be analyzed in terms of wavefronts that are eigen-states for the angular momentum operator, which carry a phase dependence that goes as

$$e^{im\phi}, \tag{146}$$

with m being an arbitrary integer (the "topological charge") and ϕ being the usual azimuthal coordinate. Optics that produce this azimuthal phase dependence and that convert between different OAM states has attracted significant interest. These can be implemented in a variety of ways, including with purely refractive optical elements known as spiral phase plates.

Some implementations of Eq. (146) can be polarization-dependent. Of particular note are LC devices known as "q-plates." A q-plate is a LC device that implements the phase profile of Eq. (146) with a LC layer with half-wave (π) birefringence where the LCs' axes rotate. As a result, one circular polarization picks up a phase profile of $e^{im\phi}$. However, due to the symmetry of the geometric phase, the other circular polarization will acquire a phase profile of $e^{-im\phi}$. As a result, the OAM that results is coupled to the polarization handedness, or spin angular momentum, of the incident light. The q-plate, then, is often referred to as enacting "spin–orbit conversion."

Spin–orbit converting LC devices were brought to the fore by the work of Marucci *et al*. in 2006 [179] (though we note very similar earlier work, using mechanical LC alignment, by Stalder and Schadt a decade prior [180]) and have since provoked significant interest in the academic community for their application in both classical and quantum contexts (though we point out that Hasman *et al*. demonstrated spin–orbit conversion with geometric phase in a nanophotonic device several years earlier [181],

and metasurfaces, also a nanophotonic device, have since been shown to relieve the constraint of conjugate charges $\pm m$ [182], enabling "J-plates").

Unlike many of the devices of the previous section, q-plates can be realized using mechanically rubbed substrates (no need for photoalignment). Twisting two mechanically rubbed substrates relative to each other yields the correct LC orientation [179]. However, other authors have investigated creating these same structures using photoalignment techniques [183] for use in vortex coronagraphy [184,185], a focal plane coronagraphy technique discussed above. Here, however, LCs simply enable better, more precise vortex plates to be manufactured; their polarization-dependent nature does not play an explicit role or lend any advantage to the measurement technique (unlike in the case of the vAPP summarized above).

4.5d. Spatial Light Modulators

An SLM is a general term for any number of devices imparting spatially varying amplitude and/or phase transmission masks on incident light. Over decades of research and development, many technologies for SLMs have emerged utilizing a wide variety of physical effects. What these share is tunability, usually electrical (computer-controlled) in nature, but in some cases, especially in early implementations, SLMs can be controlled optically with a second light beam (optical addressing). SLMs are widely used today in applications ranging from beam and pulse shaping to quantum optics. A detailed discussion of SLM technologies and applications is beyond the scope of this review and has been treated extensively elsewhere (see, for instance, [15,186–190]). To provide just a few examples, SLMs have been implemented using magneto-optic effects, voltage-tunable absorption in multiple quantum wells, and with microelectromechanical systems (MEMS)-based deformable micro-mirror arrays.

Particularly relevant to our interests here, however, are SLMs based on LCs. In practice, too, today these are among the most common and widely available commercially, especially those integrated on silicon with CMOS drive electronics [liquid crystal on silicon (LCoS)] [117,191,192]. This is owed in large part to the similarity between LC SLMs and LC displays, and indeed, some authors often refer to such SLMs (especially in earlier work) as "liquid crystal TV displays," though there are of course important differences between devices sold as literal television screens and those intended for optical use.

LC SLMs are fundamentally a polarization-dependent technology. As described above, LCs can be rotated by application of an applied bias voltage. This effect enables, essentially, a retarder with an electrically variable retardance, which, when addressable over an array, forms an SLM. This effect can be either used as a pure-phase modulator (if the incident polarization is always linearly polarized along the bias-tunable axis) or as a pure-amplitude modulator (if the LC cell is placed between analyzers that may be crossed or parallel, depending on the exact implementation, as in LC displays). It is for these two purposes that LC SLMs are most often used.

Here, however, we are interested in the spatially varying polarization modulation enabled by these LC SLMs, or cascades thereof. In Subsection 4.5e, we take an abstract viewpoint, classifying the polarization control enabled by SLMs. This analysis, to the best of our knowledge, is new to this review. Then, in Subsection 4.5f, we briefly review past work and devices that use LC SLMs to implement polarization-sensitive diffractive optics.

4.5e. Polarization-Transformations with Systems of Multiple SLMs

Introduction. In this section, we consider the spatially varying polarization operations attainable with cascades of several SLMs, paired with bulk polarization optics. We classify the polarization control attainable for conceptual comparison with other technologies, such as those described throughout this section. To the best of our knowledge, this presentation is new to this review, though the configurations here are not unique and similar generalizations have recently been explored by other authors (e.g., [193], and others cited later in this section). Here, cascades of SLMs could be SLMs that are physically cascaded at optically close distances, SLMs successively imaged onto each other using $4f$ systems of lenses, or multiple passes through the same SLM, with different sections addressed with different phase masks. The ideas of this section are depicted in Fig. 23.

As described above, a single LC SLM pixel can be thought of as a tunable retarder, specified independently at each discrete point (x, y) across an array. Ignoring the overall, constant phase shift imparted upon the unmodulated polarization, a single SLM implements the spatially varying Jones matrix,

$$J(x, y) = \begin{bmatrix} e^{i\phi_x(x,y)} & 0 \\ 0 & 1 \end{bmatrix}, \tag{147}$$

where $\phi_x(x, y)$ is a phase shift on linear x-polarized light that can be arbitrary tuned across the array [Fig. 23(a)]. An SLM can be physically rotated by 90° or, alternatively, left unrotated but sandwiched between $\lambda/2$ plates oriented at $\pm45°$, to realize the same control over y-polarized light [Fig. 23(b)]. We denote this as $\phi_y(x, y)$. The case of a single SLM corresponds to type I of Table 4.

Two SLMs. A cascade of two such SLMs, one after the other (or, as noted above, encoded on separate sections of the same SLM with appropriate mirrors and polarization optics), can implement the spatially varying Jones matrix,

$$J(x, y) = \begin{bmatrix} e^{i\phi_x(x,y)} & 0 \\ 0 & e^{i\phi_y(x,y)} \end{bmatrix} = e^{i\frac{\phi_x+\phi_y}{2}} \begin{bmatrix} e^{i\frac{\phi_x(x,y)-\phi_y(x,y)}{2}} & 0 \\ 0 & e^{-i\frac{\phi_x(x,y)-\phi_y(x,y)}{2}} \end{bmatrix}. \tag{148}$$

Equation (148) describes a space-variant wave plate in which retardance $\delta = \phi_x - \phi_y$ and overall phase $\bar{\Phi} = (\phi_x + \phi_y)/2$ may be independently and arbitrarily specified. The addition of a second SLM, then, expands control to type J of Table 4. Two SLMs together act as a spatially varying wave plate whose overall phase and retardance are variable but whose retardance axis is fixed along x/y (s_1 axis).

Optical rotation with SLMs. It might at first seem that this is a fundamental limitation; after all, the pixels of the SLM cannot be individually rotated independently of one another. However, the ability to pair the SLM with bulk polarization optics relieves this constraint. Specifically, we consider an SLM sandwiched between two quarter-wave plates, turned at $\pm45°$ [Fig. 23(d)]. In this way, incoming light is effectively converted to the circular basis, retarded along one polarization by an angle that the SLM can control spatially, and converted back to its original basis. This system, viewed from the outside, acts as an optically active medium where the phase retardation between circular polarizations can vary arbitrarily from point-to-point; in practice, any polarization ellipse incident on the system will be rotated by the angle θ encoded by the SLM at each pixel, converting the phase shift θ to a physical rotation of the polarization ellipse.

Intuitively, this can be understood with the aid of the Poincaré sphere and the concepts of Subsection 2.6 [Fig. 23(e)]. One particular incident polarization is considered (light

linear polarized along x). A green path and arrow show the effective transformation

Figure 23
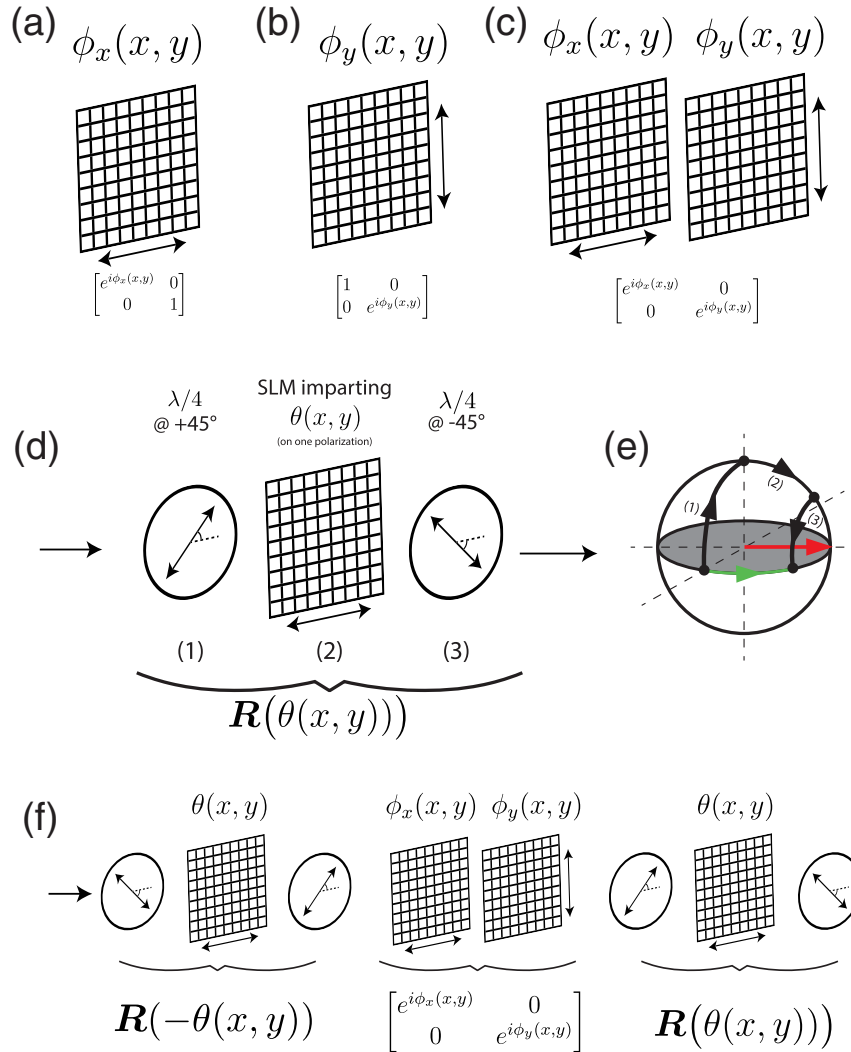
Implementation of spatially varying polarization control with configurations of spatial light modulators (SLMs). (a) A single LC SLM implements a phase profile $\phi(x, y)$ on one linear polarization and a constant phase (disregarded here) on the other, which can be addressed separately by (b) rotating the SLM, or equivalently, using half-wave plates. (c) Two orthogonally oriented SLMs can implement a retarder whose overall phase and retardance can be arbitrarily specified at each point in space. (d) A spatially varying rotation matrix can be realized by sandwiching such an SLM between two quarter-wave plates ($\lambda/4$) oriented at $\pm 45°$. (e) The operating principle of the system in (a) can be understood with the Poincaré sphere taking incident x-polarized light as an example. The cascade of a quarter-wave plate, SLM, and oppositely oriented quarter-wave plate takes the light on a path (in black) that, effectively, amounts to a rotation of the polarization state (in green). (f) Cascade of one rotation unit (as in (d)), two SLMs implementing the phase profiles $\phi_x(x, y)$ and $\phi_y(x, y)$, rotated 90° with respect to one another, and a final rotation unit to undo the first. Throughout this figure, it is assumed that the SLMs are located optically close to one another (or equivalently, imaged onto each other with systems of lenses) and perfectly aligned.

enacted by the system, i.e., a rotation in azimuth by a certain angle, a change in longi-tude on the Poincaré sphere. A black path, however, shows the three individual steps by which the system of Fig. 23(d) implements it. First, a quarter-wave plate oriented at 45° rotates the incident polarization 90° about the s_2 axis of the sphere. Then, the SLM, itself effectively a polarization retarder oriented along x, rotates the polariza-tion by an angle of θ about the s_1 axis of the sphere. Finally, the quarter-wave plate at $-45°$ rotates the polarization $-90°$ about the s_2 axis, back to the equatorial plane of the Poincaré sphere, having enacted an effective azimuth rotation by θ.

In other words, the configuration of Fig. 23(d) functions as a linear change of basis operation (where the angle of the change of basis can vary over the SLM array). As shown in Fig. 23(f), when paired with the configuration of Fig. 23(c), it enables a device that acts as a retarder whose retardance, overall phase shift, and fast-axis angu-lar orientation are all independently variable at each point. This works by first rotating the desired polarization basis into the x/y basis with $\boldsymbol{R}(-\theta)$, shifting its phase, and inverting the change of basis with $\boldsymbol{R}(\theta)$. In Fig. 23(f), this is shown implemented with four SLMs; however, practically speaking, the two change of basis transformations could be condensed into one system traversed in opposite directions. The combina-tion of SLMs depicted in Fig. 23(f) corresponds to type J in Table 4. As described in Subsection 4.7, this is the same level of polarization control that can be realized in a single plane with a dielectric pillar-based metasurface device, albeit without the tunability offered by SLMs.

The linear change of basis system of Fig. 23(d) can be extended to an arbitrary change of basis system with the addition of an SLM oriented along x preceding the system (though this choice is not unique). Then, in analogy with Fig. 23(f), a system could be constructed in which an arbitrary unitary Jones matrix could be constructed at each point, i.e., one in which overall phase, retardance, and the two parameters defining an arbitrary elliptical eigenbasis could be independently specified at each point (x, y) (implementing type C polarization control in Table 4, though this is not shown in the figure). Moreover, the concepts of this section could extend to configurations of SLMs realizing *Hermitian* spatially varying Jones matrices using polarization beam splitter cubes and *polarization-independent*, amplitude-only SLMs (i.e., not LC-based devices), combined with the change of basis configurations discussed here. Then, in theory, a configuration of SLMs could be assembled capable of realizing of fully arbitrary (passive) Jones matrices across an array (type B control).

In the next section, we review past work on SLM configurations that permit spatially varying polarization devices. By and large, most past work is more *ad hoc* and does not take as general a standpoint as we have motivated here, but can nonetheless be understood and classified in this context.

4.5f. Literature Review—Spatially Varying Polarization Elements with SLMs

Here we review some applications of LC SLMs, with some examples discussed here featured in Fig. 24. LC SLMs are widely used in a variety of applications, among them optical microscopy [194] (including super-resolution techniques such as STED microscopy), electrical beamsteering, digital holography, and beam shaping [186,190] (including in the generation of beams carrying optical OAM), and even as near-eye displays for AR/VR [195–198]. By and large, these efforts treat light as a scalar field, aiming to sculpt its phase or amplitude alone, and each would merit its own dedicated review article. Here, in contrast, we focus explicitly on past research efforts in which SLM-based systems have been used to implement diffractive optics with *designer polarization dependence*. Examples of this nature are considerably more limited, since most works treat the polarization-dependent nature of LC SLMs

as a route to achieve phase or amplitude modulation rather than for polarization manipulation itself.

Work of Davis and Moreno *et al*. Some of the most detailed work in this area, which best approximates the spirit of this review, has been performed by J. A. Davis, I. Moreno, *et al*. in a collection of related work from ~2001 to the present [193,200,201,203–209]. Broadly speaking, the work of Davis, Moreno *et al*. considers optical setups in which light is permitted to make multiple passes through an SLM and interceding polarization optics (wave plates). Much as in the discussion

Figure 24
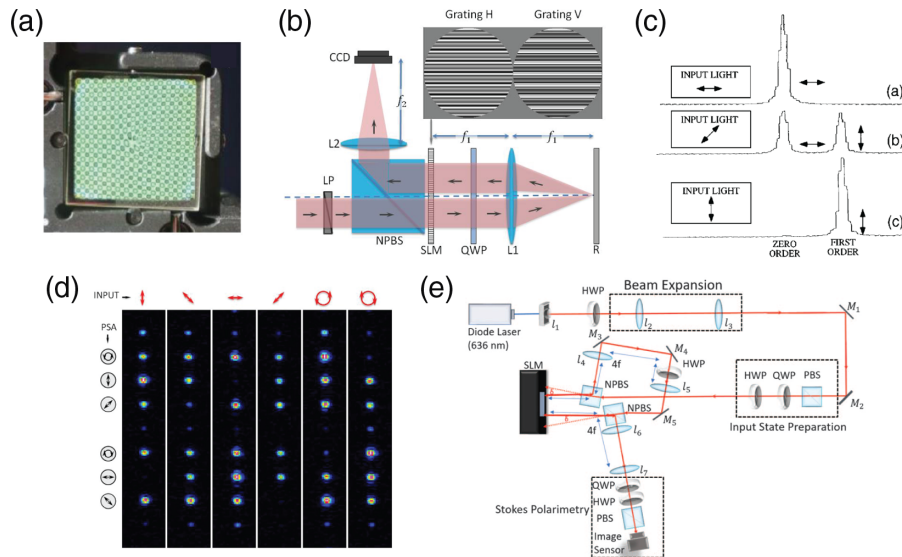
Spatially varying polarization transformation with liquid crystal SLMs. (a) Example of a polarization-dependent-phase mask encoded on a LC SLM, viewed between crossed polarizers. Reprinted with permission from [199]. Copyright 2019 Optical Society of America. (b) Typical setup for producing polarization-dependent diffractive optics with an SLM. Incident light passes through a section of the SLM and, by virtue of a reflective $4f$ system and quarter-wave plate, is imprinted with a second polarization-dependent phase profile encoded on the second half of the SLM. Taken together, this setup imparts arbitrary and independent phase profiles on the x- and y-polarized components of incoming light. Reprinted with permission from [200]. Copyright 2016 Optical Society of America. (c) A setup such as that in (b) can be used to create polarization-sensitive diffractive optics, such as gratings whose orders act as analyzers for particular polarization states, distributing light between orders according to the incident light's polarization state. Reprinted with permission from [201]. Copyright 2001 Optical Society of America. (d) This concept can be extended to generate gratings whose orders act as analyzers for arbitrarily specified states of polarization. The intensities of the different orders permit reconstruction of incident light's full-Stokes vector. Reprinted with permission from [200]. Copyright 2016 Optical Society of America. (e) Altogether very similar optical setups (here taken from [202], for sake of example) have been used to realize far-fields with arbitrary polarization state variation [functionally equivalent to (b), with two interactions with a LC SLM]. However, structuring the far-field polarization rather than polarization *transfer function* represents a subcase, rather than the most general capability of devices such as SLMs to serve as polarization-sensitive optical elements (Subsection 3.3). Reprinted with permission from [202]. Copyright 2018 Optical Society of America.

above, Davis *et al.* analyze the resulting diffraction patterns in terms of Jones matrix-weighted Fourier coefficients. We note here that a 2004 paper by Moreno is one of the only references before this work to cast Fourier optics in terms of Jones matrix quantities [62,63]. Moreover, the work of Davis and Moreno *et al.* is among the earliest examples of this type of SLM work in the literature so it constitutes an outsized role in our discussion here.

A setup characteristic of this type of work is shown in Fig. 24(b). While the precise implementation details can vary, generally speaking light is allowed to pass twice through a LC SLM with the plane of linear polarization rotated 90° between passes. In the example of Fig. 24(b), this is accomplished by directing light through half of an SLM, then through a quarter-wave plate at 45°, an off-axis lens, and the same configuration in reverse after a reflection from a mirror. The two quarter-wave plate passes rotate the initially *x*-polarized light by 90°, and the off-axis lens directs the light through both halves of the SLM while re-imaging the light. In this way, independent phase profiles can be addressed on orthogonal polarization states using the two halves of the SLM, as in Eq. (148) and Fig. 23(c).

The phase profiles imparted can be fully arbitrary, thus permitting many different applications. The earliest work of this nature by Davis *et al.* considered gratings—periodic phase profiles—the most fundamental choice. This work was partially motivated by the fact that polarization-dependent paraxial beam splitting gratings may have a higher efficiency than their scalar counterparts (see Subsection 4.6). In early work, Davis *et al.* showed the possibility for the diffraction orders of polarization-sensitive gratings to act as *analyzers* for pre-specified polarization states [Fig. 24(c)], allowing the distribution of light among the orders to vary with incident polarization state [201,204]. In later work, this was taken further to permit diffraction gratings with many orders analyzing for designer-specified polarization states [200,207]. Figure 24(d) shows the response of the far-field of such a grating constructed as in Fig. 24(b) with varying incident polarization state. The relative weights of the orders permit full-Stokes polarimetry (see Subsection 2.7). Davis and Moreno *et al.* used similar concepts to investigate many other areas that we do not describe in depth here. Among them were polarization-sensitive lenses [205,208], polarized vortex beam generators and analyzers [209], and computer-generated holograms in general [193].

Creation of vectorial fields. A variety of other work concerns the ability of multi-pass SLM configurations to generate fields whose polarization can vary arbitrarily over space for an input whose polarization state is known *a priori*. This possibility has been considered by many authors, both theoretically [210–212] and experimentally [202,203,206,213–215]. These share in common the notion that any given polarization state can be transformed to another by two retarder transformations with perpendicular retarder axes on the Poincaré sphere; these works—some quite recent—seem to have been carried out without awareness of the others. Similar ideas and setups can even be extended (using a cylindrical Bessel beam basis of modes) to control of the SOP along light's propagation direction (again given knowledge of the incident polarization state) [216–220]. This body of work, in which the spatial *polarization state distribution* rather than *transfer function* is controlled, does not represent the most fully general means of polarization control afforded by systems of LC SLMs, corresponding to the "vector" picture rather than the "matrix" one of which it is a subcase (Subsection 3.3).

Systems of SLMs provide the possibility to structure spatially varying polarization devices that can, in general, be quite arbitrary. The electrical, computer-addressed

tunability of SLMs is a compelling advantage. However, it is telling that all the examples cited here generally do not exceed two SLMs (or two SLM passes). This reflects the fact that these systems are cumbersome to use and align, requiring either optical proximity between SLMs or systems of lenses, mirrors, and/or prisms, resulting in a large system size. Metasurfaces, as we explore in Subsection 4.7, hold promise for enabling these possibilities with a single element, in a single plane.

4.6. Polarization Gratings

This section is different from others in this review in that it does not center around a technology. Rather, here we briefly summarize a body of papers that appeared around the new millennium (∼1999 − 2004) that considered, from a theoretical point-of-view, polarization gratings (and perhaps coined this term). Chronologically speaking, these works were not the first on the subject of polarization-dependent diffractive optics (or gratings in particular); see Subsection 4.2. However, they are significant from a historical perspective in that these increased the subject's visibility at a time when new technologies were emerging that enabled the ideas expressed to find experimental realization. The ideas expressed in these works spurred development in devices based on LCs (described in Subsection 4.5) and nanofabrication (metasurfaces, Subsection 4.7), through which their influence is still felt today.

Work of Gori (1999). The origin of this literature can be traced to a paper of F. Gori, published in 1999 [146]. Using the Jones calculus, Gori theoretically considers a transmissive, periodic optical element that behaves as a polarizer whose transmission axis rotates linearly between 0 and 180 degrees along one spatial direction. Gori shows that the structure has just three diffraction orders, 0 and ±1. The ±1 orders are circularly polarized (opposite handedness), irrespective of the polarization of the incident light, while their intensity depends on the projection of the incident polarization onto RCP and LCP. The zero order always matches the polarization of the input and has a constant intensity. Gori noted that such a grating, if implemented, could be used for Stokes polarimetry (given a second, rotatable polarizer). It is unclear whether Gori was aware of previous work on very similar polarization grating-type work using photoanisotropic materials (see Subsection 4.2; a related reference on four-wave mixing in these materials is cited [89], but Gori ultimately concludes that "the general subject of polarization gratings has not received much attention" [146]).

Gori's 1999 work stemmed from a line of investigation, involving Gori as well as others, on phase-only gratings, and phase-only diffractive optics more generally. Phase-only gratings (thin ones, treated in the paraxial limit, at least) can be shown to produce only one (in the case of a simple blazed grating) or an infinite number of diffraction orders [77]. This is an ultimately mathematical statement about the Fourier series of a function of constant modulus. A number of works, including by Gori, investigated how a phase-only grating can be optimally designed (from a variational standpoint) to direct as much light as possible into a limited, finite set of diffraction orders [221–225]. These gratings were, and still are, of interest for coherent beam-combination and division.

Work of Tervo & Turunen, *et al* **.** Inspired by Gori's work [146], Tervo and Turunen [78] *et al*. (here referred to as "T&T") made the connection between the two topics by recognizing that a polarization grating was not beholden to the same constraints as a scalar one. They showed, using the vector approach described in Subsection 3.3, that a periodically modulated retarder could indeed produce a finite number of diffraction orders with 100% efficiency. One special example considered is that of a geometric phase grating (though they did not use this term), wherein a half-wave plate is rotated periodically with space. T&T recognized that the extra degrees of freedom encoded

by polarization relieve the constraints of scalar optics. In further work, T&T introduced a method for generating the Jones vector distributions describing gratings with a (generally 2D) set of diffraction orders that numbers any power of two to a side [226]. This method is recursive, building from a base case of a two-order grating with orthogonally polarized beams. T&T also illustrated examples with non-power-of-two sets of diffraction orders [226] as well as cases where even with polarization considered perfect diffraction efficiency cannot be obtained [227]—though still, even now, no general method or mathematical proof has been demonstrated concerning when a polarization-dependent grating can exhibit perfect efficiency and when it cannot in a beam-division context.

Notably, T&T (and Gori, to a lesser extent) explicitly recognized that lithographically defined form-birefringent structures could be used to realize what was, in their work, only expressed theoretically. One strategy was proposed in [226]. Here, T&T proposed using an isotropic medium of variable thickness to impose a polarization-independent "bias" phase with the possibility to impart retardance with a form-birefringent grating of constant period but variable thickness. A proposed example implementation of a blazed grating with opposite blazing angles is shown in Fig. 25. In [226], an intention was declared to fabricate these, which would no doubt prove challenging due to the non-planar nature of the structure proposed. It seems that this research direction was not pursued (despite some later related works [228,229]). However, T&T presciently predicted that "rapid progress in microstructure fabrication technology" may soon render polarization gratings realizable [226]. The work of Gori and T&T was often cited as an influence in work on polarization diffractive technologies in the mid-to-late 2000s, such as in LC devices and nanophotonic gratings, later evolving into the wider field of metasurface optics.

4.6a. Mathematical Issue in Review of Cincotti (2003)

A brief review of work on polarization gratings, from the purely theoretical work of Gori and T&T to some experimental implementations, is provided in a 2003 review article by G. Cincotti [79]. In addition to a literature review, Cincotti provides a unified theory of polarization grating design based on many of the same concepts covered in Section 2 in this review, namely the Pauli matrices and the connection between the Jones and Stokes calculi.

Figure 25
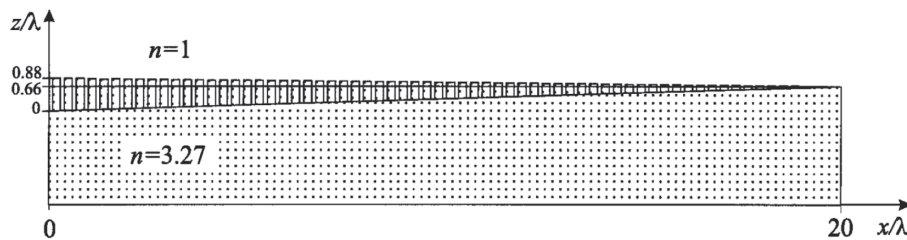
A proposed architecture for a lithographically defined polarization grating based on form birefringence capable of splitting x- and y-polarized light. A combination of a form-birefringent grating and an isotropic material was intended to impose the correct phases on orthogonal polarization states, with TiO_2 as a proposed dielectric. Given the difficulties associated with non-planar fabrication, this structure was seemingly never realized, but proposals such as these anticipated trends in micro- and nano-optics, especially metasurfaces (Subsection 4.7). Copyright 2000 from "Fourier array illuminators with 100% efficiency: analytical Jones-matrix construction" by Honkanen *et al*. Reproduced by permission of Taylor and Francis Group, LLC, a division of Informa plc [226].

However, we are concerned that the theoretical approach used in [79] may be mathematically incomplete, and a brief effort is made here to clarify this. Cincotti's approach is to break a spatially varying Jones matrix into a spatially varying part and a constant one. When a given polarization state is incident, the resulting Jones vector also has a spatially varying part and a constant part. Cincotti applies this approach separately for purely Hermitian and purely unitary cases, in view of the matrix polar decomposition (Section 3). In each case, it is found that the derivative of the spatially varying part of the Jones vector can be described with aid of a "polarization grating vector" $\vec{\Omega}$, which is unique to a given grating {e.g., Eqs. (18), (21), and (30) of [79]}.

A key conclusion made on this basis for both Hermitian and unitary gratings is that the Jones vectors of the grating's diffraction orders are solutions of an eigenvalue equation [Eq. (20)], which contains no dependence on the incident polarization state. Cincotti then concludes that the polarization state of diffraction orders from a polarization grating "do not depend on the polarization state of the incoming light and are fully characterized by the polarization grating vector." However, this conclusion is, in general, not correct. There are certainly cases in which the polarization of the orders of a polarization grating can depend on the incident polarization.

A very simple one that serves as a counter-example to this conclusion is a polarization-*independent* blazed grating, with a transfer function given by

$$J(x) = \begin{bmatrix} e^{ikx} & 0 \\ 0 & e^{ikx} \end{bmatrix}. \tag{149}$$

Equation (149) describes a grating with only one diffraction order whose polarization matches that of the incident light. Propagating a grating of the form of Eq. (149) through Eq. (20) of [79] gives an eigenvalue equation of with matrix of zeros, which gives complete freedom to the polarization state of the first diffraction order.

A perhaps deeper issue is that in the analysis of [79], a sum (Σ_n, over all diffraction orders) has been dropped in going from Eqs. (19) to (20). The specific examples treated in [79] all concern gratings with only two nonzero diffraction orders with orthogonal polarizations so that Eq. (20) still holds. However, in more general situations, particularly those implemented with metasurfaces or with multiple passes through LC SLMs, the polarization states of the diffraction orders will in general *not* be orthogonal, and Eq. (20) will not take the form of a simple eigenvalue problem.

A method that avoids these issues, regardless of the circumstance, is to simply compute the Fourier series of the spatially varying grating Jones matrix, the guiding principle of this review; the resulting Jones matrices of each diffraction order will reveal their polarization properties. A given order's polarization will only be independent of the incident light's polarization if its Hermitian (or polarizer-like) component has unity diattenuation.

4.7. Metasurface Optics

4.7a. Introduction

This section is dedicated to metasurfaces. A description and background of what precisely is meant by that term follows in the next section, but suffice it to say, metasurfaces have become an influential force in optics and photonics. Metasurfaces form the cornerstone of an academic and research community, not to mention increasing interest in potential applications in both science and technology. Thousands of papers have been published related to metasurfaces, metasurface design concepts, and related matters.

We begin this section, then, with a frank admission that, given this scale, we can only hope to begin to scratch the surface here. No review could possibly capture everything. The present review seeks to survey important concepts and work in metasurfaces *specifically* for spatially varying polarization control. This focus already pares down the greater metasurface field significantly, but even this area is extremely broad, and some scope must be defined. In this section, we aim to summarize developments in this area in terms of the level of polarization control exerted and the various design strategies used, classified by level of abstraction. A focus on these two aspects fits neatly with the classification scheme embodied in Subsection 4.1 and the scalar/vector/matrix hierarchy described in Section 3, and moreover it permits easy comparison with other non-metasurface technologies described previously.

However, a number of important works and topics will (necessarily and unfortunately) pass without mention along the way. Among these are fascinating topics such as exerting control over color and chromatic dispersion with metasurfaces, metasurfaces for nonlinear optics applications, and so-called "Huygens metasurfaces" based on Mie resonators and the Kerker conditions (see [230] for a recent review).

Fortunately, while this review may be somewhat unique in its exact focus, it is not unique in being a review article about metasurfaces. The reader is directed to several other review articles. The first is the review of Yu and Capasso [231] from 2014. Three more recent reviews that focus specifically on dielectric metasurfaces (now the main thrust of the metasurface community) are those by Genevet *et al.* (2017) [232], Kamali *et al.* (2018) [233], and Qiao *et al.* (2018) [234] (which takes more of a photonic crystal perspective). All of these devote some attention to polarization control. Several reviews treat holography with metasurfaces [235,236], and three recent reviews are even dedicated entirely to polarization optics with metasurfaces. Two of these, one by Hu *et al.* [237] and a second by Ding *et al.* [238], review spatially varying polarization control with dielectric metasurfaces. The third, by Intaravanne and Chen [239], discusses metasurface approaches for polarimetry. A review of Zheng *et al.* [240] also heavily focuses on polarization-dependent devices.

4.7b. What Is a Metasurface?

Working definition. A metasurface is an array of optical phase-shifting elements whose transverse spacing and dimensions are smaller than the wavelength of interest (*subwavelength features*). A distinguishing feature of a metasurface is that these elements achieve the desired phase-modulating effect with variations in transverse dimensions, rather than height. Metasurfaces—both the devices themselves and as a research field at-large—are often referred to as "flat optics."

Metamaterials. The definition just given will suit our purposes in this review. However, we note that the word metasurface—and the wide-ranging topics now categorized under that label—adeptly evades precise definition. "Metasurface" has found itself today used as a label for a surprisingly broad array of optics and RF research and applications, a body of work we can only review incompletely (at best) in this section. First, it is worth considering, briefly, metasurfaces and their origin. "Metasurface" evokes the word "metamaterial," an umbrella term for a research area that emerged in the early to mid-2000s. Research in metamaterials seeks to realize optical media with exotic properties not present in naturally occurring ones, among these negative refractive index ($n < 0$) and ϵ and μ values near 0. These properties were shown to have theoretical implications that, if realized, could upend a number of traditionally assumed limits of optics. Among these is the popular idea that a film of negative index material could focus and amplify evanescent waves, beating the traditional diffraction limit [241]. Metamaterials rely on the concept of a "meta-atom,"

a unit cell fashioned from a careful arrangement of traditional materials. In this way, light with a wavelength is larger than the size scale of the meta-atoms can be made to "feel" an effective medium that may have exotic constitutive properties.

The exact origins of the term metasurface, and metasurface research more generally, are somewhat unclear. One of its first mentions in archival literature dates from the abstract of a 2003 RF work [242], hearkening a version of metamaterials where, instead of a 3D bulk, meta-atoms are constrained to lie on a 2D surface. It did not appear again until 2007, but soon after it became a widely applied term in the RF and microwave literature.

Metasurface origins. Around the same time, it became increasingly clear that some of the initial promise of optical metamaterials—including the perfect lens—faced severe practical difficulties. The large metamaterials community, alongside researchers in the associated field of plasmonics (that is, the optics of metals hosting a plasma of free electrons [243]), was collectively eager to break new ground. An explosion of metasurface research in optics can be traced to a 2011 work by Yu *et al.* [244], showing that plasmonic (gold) antennas patterned with electron-beam lithography for operation at ∼8 μm wavelength could act as optical phased arrays, deflecting light in the manner of a blazed grating, made with a single lithographic step (in contrast to multi-level diffractive approaches, which require multiple steps of lithography). This work had its antecedents in efforts to collimate light from mid-infrared semiconductor lasers using gold antennas patterned directly on the laser's edge-emitting facet [245,246]. Before long, many promising applications of these metallic *metasurfaces* were proposed and demonstrated, among them vortex phase plates [231,244], diffraction gratings, computer-generated holograms, and lenses [247] (even a partial list of references would be impossible here). Metasurfaces implementing lens profiles have taken on a life of their own, and these *metalenses* form a significant area of study largely apart from the subject of this review.

Smaller wavelengths with dielectrics. As time went on, work that initially begin in the mid-infrared range (5–8 μm) gradually crept to shorter wavelengths. It became clear that metasurfaces based on metals—while appealing due to the extensive work conducted on similar structures under the guise of plasmonic metamaterials—were inherently lossy. Naturally, the community tended toward dielectric materials. This work began initially in the telecom and near-IR spectral regions where amorphous silicon is a high-index dielectric with low loss that is readily deposited as a thin film and patterned with reactive ion etching. This is true of other materials in the visible range, such as silicon nitride and titanium dioxide. Metasurfaces, including those for polarization applications, can take on any number of different forms, some of which are described in Subsection 4.7e; while the ideas presented here are general, this review tends to skew toward metasurfaces structured from dielectric materials.

Toward widespread application. Metasurfaces lean on a well-established base of knowledge and technological infrastructure from the semiconductor industry developed over decades. Their fabrication is both an advantage and a challenge: The subwavelength, sometimes asymmetric features of metasurfaces can pose a challenge to production at-scale, but at the same time their top-down fabrication mirrors that of integrated circuits and can borrow from the same methodology and facilities. As a result, metasurfaces have attracted significant industrial interest beyond their status as a subject of intense academic focus, promising applications from medical imaging to remote sensing and even consumer electronics [248,249].

It should be said, of course, that diffractive optics and holography have a long history, with metasurfaces being an especially promising new chapter. This too is true of

polarization-sensitive metasurfaces, as has been discussed throughout the preceding sections of this review. We note here that a number of important metasurface-like works for polarization control emerged before the post-2011 period, and these are described in Subsection 4.7d.

A (very) rough timeline of the discussion here, and the merger of ideas from various fields giving birth to metasurfaces is provided in Fig. 26. In what follows, we review work on metasurfaces that are polarization-sensitive, attempting to make sense of what has become a voluminous subject. As with other sections of this review, we categorize work on metasurfaces using the scalar/vector/matrix formalism embodied in Subsection 3.3. We conclude with a discussion of applications demonstrated with and enabled by polarization-sensitive metasurfaces.

4.7c. Form Birefringence

The individual structures comprising a metasurface can possess form birefringence. This is the fundamental reason why metasurfaces are an interesting medium for polarization optics.

Form birefringence is an effect that comes about when light interacts with a material that is structured anisotropically on a size scale comparable to or smaller than the optical wavelength. As a result of this anisotropy, interaction with the structures resembles that of a bulk anisotropic medium even if the materials involved are (in their bulk form) completely isotropic. Form birefringence specifically results when orthogonal polarization states experience different phase delays, but similar effects could yield form dichroism as well if differential losses are involved.

Any treatment of light's interaction with structured media requires solution of Maxwell's equations. Unfortunately, except in certain situations, these are analytically intractable, though a number of numerical schemes exist, among them the finite element method, finite differencing (in the time or frequency domains), and the RCWA. While quantifying form birefringence generally requires these, a number of different pictures can prove instructive in understanding its origins. We describe two of these here, one known as effective medium theory, and the other a more heuristic "waveguide"-like model common in metasurface works.

Effective medium theory picture. We first consider effective medium theory. We consider Fig. 27(a), which depicts a grating of period Λ structured from a bulk substrate of (isotropic) index n_3 in a background medium of index n_1; Fig. 27(a) is assumed to continue infinitely into and out of the page. The duty cycle of the grating is F with $F \in [0, 1]$. If the grating is subwavelength, that is, if $\lambda_0/(\max[n_1, n_3]\Lambda) < 1$ with λ_0 the free-space wavelength, only zeroth-order reflection and transmission will be experienced. Effective medium theory seeks to treat region 2 of Fig. 27 as

---

Figure 26
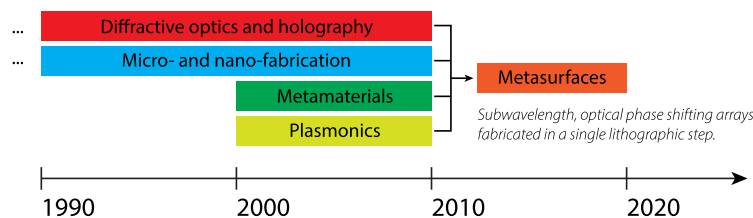
Metasurfaces emerged from research in a number of previously disparate fields of optics, as shown in this (very approximate) timeline.

a uniform thin-film slab with "effective" optical properties, so that the transmission through the structure can be treated using the Fresnel equations/transfer matrix formalism, so long as an "effective" index can be found for region 2.

This proceeds as follows [250]: First, consider light incident from above whose electric field is strictly along $\hat{y}$. We refer to this as the $\parallel$ direction as the light's polarization points along the grating ridges. The boundary conditions of Maxwell's equations stipulate that the electric field perpendicular to the material interface $\vec{E}_\parallel$ between n_3 and n_1 is constant across the boundary. This, however, implies that the displacement field $\vec{D}_\parallel$ will experience a discontinuity since $\vec{D}_\parallel = \epsilon_0 n^2 \vec{E}_\parallel$. Next, a quasi-static approximation is made, reasoning that since Λ is much smaller than the optical wavelength that the electric field $\vec{E}_\parallel$ must be relatively constant over the grating period. Averaged over the grating period, then, we have that $\vec{D}_\parallel = \epsilon_0 (n_3^2 F + n_1^2(1-F)) \vec{E}_\parallel = \epsilon_0 n_{\mathrm{eff},\parallel}^2 \vec{E}_\parallel$, so that

$$n_{\mathrm{eff},\parallel} = \sqrt{n_3^2 F + n_1^2(1-F)}. \tag{150}$$

If instead the incident light is polarized along $\hat{x}$, the $\perp$ direction, $\vec{D}_\perp$ is now the conserved quantity across material boundaries. Again we make a quasi-static approximation, given $\vec{E}_\perp = \frac{1}{\epsilon_0}(\frac{1}{n_1^2}F + \frac{1}{n_3^2}(1-F))\vec{D}_\perp$, so that

$$n_{\mathrm{eff},\perp} = \left(\frac{1}{n_1^2}F + \frac{1}{n_3^2}(1-F) \right)^{-\frac{1}{2}}. \tag{151}$$

In other words, due to the grating's anisotropy, orthogonal polarizations experience different refractive indices despite the isotropic nature of all materials involved. By a similar argument, an electric field polarized along z can be shown to also experience $n_{\mathrm{eff},\parallel}$ so that region 2 really does approximate a thickness of uniaxial crystal. Moreover, a more complete theory can be derived without a quasi-static approximation, of which Eqs. (150) and (151) are only first-order approximations [250,251].

Wavelength-scale structuring (in this example, through the duty cycle F) presents the possibility to tune this form birefringence. The grating vector can, moreover, be rotated to change the eigenbasis of this polarization transformation. Changing either or both of these on a spatially varying scale could yield a polarization-sensitive metasurface.

The waveguide picture. Another intuitive picture, one that is widely invoked in works on optical metasurfaces, is the notion of mode birefringence, i.e., appealing to the notion of a waveguide modes. Figure 27(b) depicts a schematic of a dielectric,

Figure 27

(a)   (b)
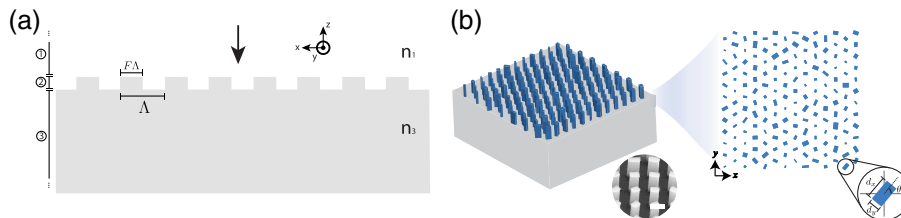
The origin of form birefringence.

pillar-based metasurface. This is an especially popular variety of a polarization-sensitive metasurface and will be described further in Subsection 4.7e; we introduce it here because it typifies this way of thinking. Each individual element, a pillar, of the metasurface of Fig. 27(b) possesses two perpendicular axes of mirror symmetry. These pillars are usually on the order of one wavelength in height with subwavelength transverse dimensions. Light's interaction with the pillar is said to be similar to light propagation in a 2D waveguide with anisotropic cross section. From the symmetry of the rectangular geometry, light linearly polarized along one axis or another will excite modes whose electric fields point along these directions as well. These modes experience different propagation constants, and accordingly different modal refractive indices, yielding form birefringence.

The effective medium and waveguide mode pictures presented here are a helpful aid to intuition and motivate form birefringence's origins. But these, along with most any other simple heuristic one could craft, are flawed in one way or another and can only be approximately right. The effective medium picture, for its part, assumes a quasi-static field and will fail especially as Λ approaches λ_0. On the other hand, a waveguide-like analogy is inaccurate for a host of reasons. For one, structures of finite (especially wavelength-scale) length are not waveguides in the traditional sense, and moreover it is not exactly accurate to say that the modes of a rectangular dielectric waveguide are orthogonally polarized. TE (with $E_z = 0$) and TM (with $H_z = 0$) modes exist. To a very good approximation, however, we can treat a rectangular waveguide as a superposition of two orthogonally oriented slab waveguide problems. In this limit, TE modes are orthogonally oriented and our picture remains. This is widely known as the Marcatili method [252].

The only foolproof solution is to apply rigorous simulation techniques that solve Maxwell's equations rather than applying any one simplified picture, and in fact, this is precisely how most works on metasurfaces approach the problem. Numerical tools are almost always used somewhere in the design loop and, in more contemporary methods (under the umbrella of "inverse design"), can control the entire design itself.

4.7d. Pre-"Metasurface" Works Exploiting Form Birefringence

It is important to mention here that a number of metasurface-like diffractive optics technologies were demonstrated prior to the emergence of the metasurface label itself. Many of these share key features with metasurfaces, including fabrication in a single lithographic step and subwavelength dimensions. We highlight here a collection of papers from 2001 [253] on contemporary research in subwavelength diffractive optics. Especially notable among these is a collection of papers by Lalanne *et al*. [254–256] (c. 1999) on subwavelength pillar-like TiO_2 phase shifters for operation at visible wavelengths. Like metasurfaces, these structures imparted phase using variations in lithographically patterned cross sections, as opposed to physical thickness variation and anticipated current trends in metasurface research. This work (along with most on subwavelength diffractive optics) did not explicitly seek to exert polarization control.

Form-birefringent diffractive optics. Several works from this time period are, however, notable for doing just that. Form birefringence, discussed in the last section, has long been an interest of the diffractive community. Early investigations in the 1970s and 1980s sought to exploit form birefringence for anti-reflective properties ([250,257–259], to name just a few examples; see [253]). Before long, the idea that form birefringence could form the basis of thin "holographic" wave plates emerged [260], from which the idea of an element with spatially varying form birefringence is a natural conclusion. If the period of a grating varies with space, so too will its form

birefringence. Throughout the late 1990s and early 2000s, this was explored by a variety of groups. Some of these, including Fainman *et al.*, had previously explored structures etched into bulk anisotropic substrates (as discussed in Subsection 4.3). The first such efforts focused on making binary gratings act as polarization beam splitters, allowing *x*- and *y*-polarized light to be directed to different orders. The earliest such effort is owed to Aoyama and Yamashita [261] in the visible region ($\lambda = 780$ nm), who used periodic form-birefringent structures at opposite orientations (albeit with low efficiency and polarization contrast). Later efforts by Fainman *et al.* [98] (associated with a theoretical work [99]) at 10.6 μm showed binary gratings that directed one polarization to the first order, while the other did not diffract at all. This type of work gradually became more sophisticated, moving from gratings to arbitrary computer-generated holograms. Zeitner *et al.* [262] showed that pixels containing metal gratings (exhibiting form dichroism, rather than birefringence) could be used to create polarization-selective holograms, while Mirotznik *et al.* [263] showed how, by appropriate modulation of the duty cycle of 2D form-birefringent gratings, a variety of phase levels ($\gg 2$) could be achieved for orthogonal linear polarization states. This latter work [263], realized by etching into silicon for operation at 10.6 μm, is notable for its use of library of diverse pre-simulated structures from which "best fit" geometries were selected. As we describe in Subsection 4.7g, this anticipated an approach that has become a fixture of polarization-sensitive metasurface design and may be the first example of its use. Figure 28(a) shows a graphical depiction of this best fit from a library approach for the two phases ϕ_x and ϕ_y, as well as a generated design [top right of Fig. 28(a)] and an SEM of a fabricated sample [bottom of Fig. 28(a)].

Work of Hasman *et al*. Of special note here, perhaps even beyond the above works, is a body of work owed to Erez Hasman and colleagues from around the year 2000. This formed the basis of a review article by Hasman *et al.* [267] published in 2005, which describes this in great detail and, not unlike this review, briefly describes other technologies for realizing polarization-dependent diffractive optics as well. In our summary here, we highlight selected works of Hasman *et al.* (but not to the extent of Hasman's own review [267], so the reader is referred there). Hasman *et al.* focused on the creation of polarization-sensitive subwavelength gratings, both metal and dielectric. All of these were designed to operate at $\lambda_0 = 10.6$ μm with GaAs as the substrate and dielectric material. Notably, throughout Hasman *et al.*'s work, the gratings act as spatially varying polarizers (for metal) or retarders (for dielectrics) whose orientations vary with *constant* duty cycle. For the case of spatially varying retarders, this means that these exhibit a constant retardance with variable fast-axis orientation. As a result, these exploit the geometric phase, in which the fast-axis orientation of a retarder (ideally with half-wave retardance) is used to impart a scalar phase profile on incident circularly polarized light; this falls under type E of Table 4. Throughout their work, Hasman *et al.* exploited this capability to create a variety of polarization-sensitive optical elements, only some of which we mention here. Figure 28(b) shows a typical example—a geometric phase grating. Here, the structure is designed to be continuously varying, which mandates a change of the grating period while the duty cycle is kept constant so that light feels the same retardance; this binary structure is designed using an analytical method based on a zero-curl condition of the grating vector [264,267,268]. Light of opposite circular polarization states feels phase gratings blazed in opposite directions and will diffract in the ± 1 orders. Figure 28(b) additionally shows an SEM typical of this work, showing ridges etched into a GaAs substrate. However, while having the ridges be continuous may be advantageous for smooth phase profiles, small grating units of differing orientation that are (discontinuously) stitched together are also possible. Geometric phase simply increases linearly with orientation, as shown in Fig. 28(c). This enables, among other applications, geometric

phase lenses [265] [see Fig. 28(d)] and computer-generated holographic imagery [269], each intended to function for circularly polarized illumination. Hasman *et al.* also showed how these types of geometric phase optics, when paired with a polarizer, can perform polarimetry (either on a whole beam or on light emerging from a sample) by imaging an interference pattern [267,270–272]. This works by application of Fourier analysis to the patterned formed by the interference of polarized grating orders after a polarizer [270]. Relative to other polarimetric techniques using diffractive optics discussed in this section, this has the disadvantage of requiring an

Figure 28
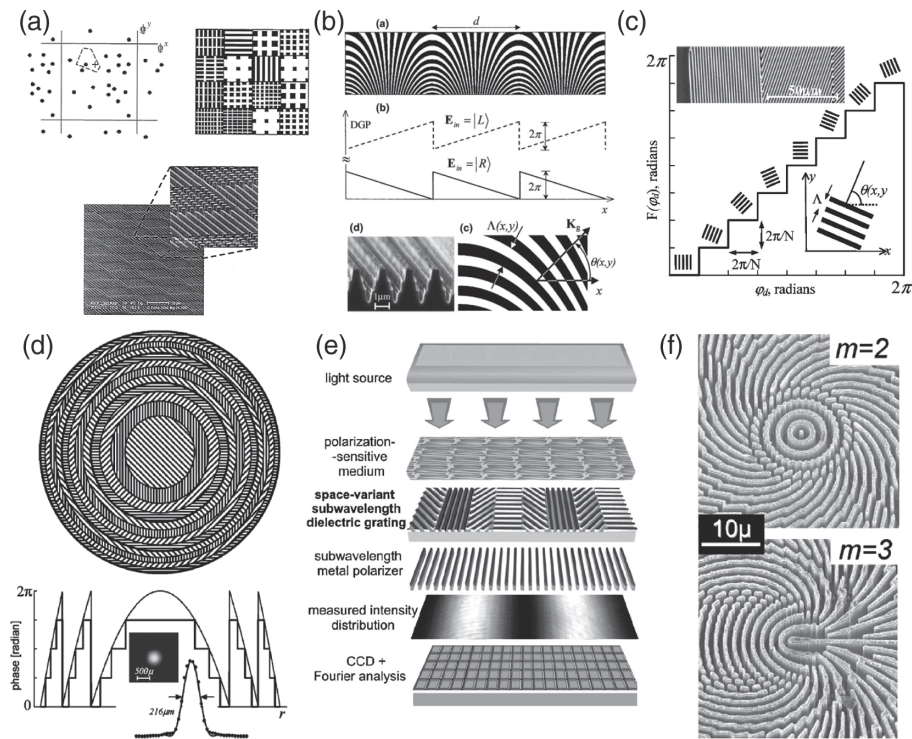
Pre-metasurface works approximating later work on metasurfaces. (a) Computer-generated hologram comprising pixels with differing form birefringence, etched into silicon. This work notably used a library-based approach to choose structures that best realize a desired pair (ϕ_x, ϕ_y). Reprinted with permission from [263]. Copyright 2004 Optical Society of America. (b) A periodic, geometric phase grating that directs $|R\rangle/|L\rangle$ to ±1 diffraction orders, including an SEM of the structure as realized in GaAs. Reprinted from Opt. Commun. **209**, Hasman *et al.*, "Polarization beam-splitters and optical switches based on space-variant computer-generated subwavelength quasi-periodic structures," pp. 45–54, copyright 2002 with permission from Elsevier [264]. (c) Discretely turning the grating imparts a geometric phase that varies linearly with orientation angle. (d) This can be used to, for instance, realize a geometric phase lens capable of focusing circularly polarized light. (c) and (d) Reprinted with permission from Hasman *et al.*, Appl. Phys. Lett. **82**, 328–330 (2003), AIP Publishing LLC. (e) A geometric phase grating paired with a polarizer and image sensor can be used as a detector of light's polarization state. Reprinted with permission from [266]. Copyright 2003 Optical Society of America. (f) Example of a device fabricated by Hasman *et al.* that is, qualitatively speaking, particularly reminiscent of later work on metasurface devices. Reprinted from Prog. Opt. **47**, Hasman *et al.*, "Space-variant polarization manipulation," 215–289, copyright 2005, with permission from Elsevier [267].

extended sensor to measure a beam's polarization state and in its use of an absorptive polarization element (the polarizer).

The work of Hasman *et al.*, despite targeting the long-wavelength infrared, deserves credit for anticipating later work on metasurface polarization optics we describe in the sections to come. Figure 28(f) depicts two GaAs devices reported by Hasman *et al.* from one of a handful of papers dedicated to creating vortex beam/structured-light-generating devices with these gratings (e.g., [181], an aspect we do not delve into here). This graphic is reproduced here to emphasize this qualitative similarity of appearance to later metasurface works. Roughly speaking, these differed from metasurface works that followed only in their insistence on using purely geometric phase effects (i.e., controlling the grating orientation); if these had also exerted control over fill factor/duty cycle, thus permitting control over propagation-type phase as well, these devices would have anticipated later work on metasurfaces almost completely.

4.7e. Some Typical Metasurface Architectures

It is worth remarking on a few typical geometries of the structures that make up polarization-sensitive metasurfaces. Each individual structure, separated from its neighbors by less than a wavelength (often on a lattice that is rectangular or hexagonal, but not necessarily so) is commonly referred to as the metasurface's "unit cell," or the "meta-atom" in the language of metamaterials. These unit cells are then stitched together to create a metasurface device, often with aid of a mathematical abstraction that idealizes the transmission (or reflection) properties of the structure (as described in Subsection 4.7g). To try to summarize every possible metasurface unit cell design would be an impossible task; instead, we focus on just three examples here.

Dielectric pillar-based metasurfaces. The first of these is the dielectric pillar, as depicted in Fig. 29(a). This consists of a structure of constant height across a metasurface device with a transverse cross section possessing two axes of mirror symmetry, most commonly a rectangle or an ellipse and less commonly a cross, annulus, or some other shape. These structures are usually of modest aspect ratio, around 5 or so. Accordingly, in view of a "waveguide"-like abstraction of its physical phase-shifting mechanism (as described in Subsection 4.7c), the polarization transfer function of the pillar can be abstracted as that of a retarder imparting independent phase shifts

Figure 29
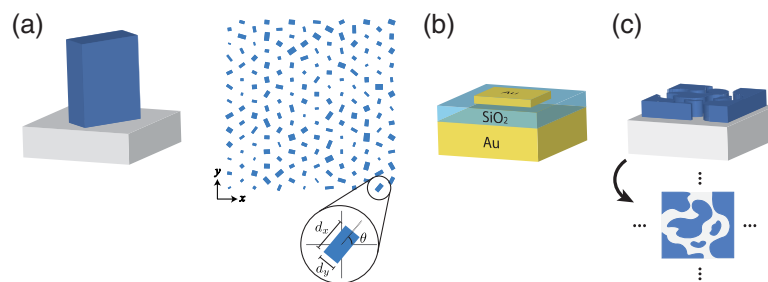
Some typical polarization-sensitive "unit cell" geometries used for metasurfaces. (a) Dielectric pillars with cross sections possessing two axes of mirror symmetry (e.g., rectangles, ellipses, or crosses). At each point on a metasurface composed of these, transverse dimensions can be adjusted to affect different phase shifts on light linearly polarized along the structures' symmetry axes, while the structures can be individually rotated. (b) Gap-plasmon resonator structures, with similarly variable transverse cross sections, for operation in reflection. (c) Freeform structures—the most general case in which all geometrical parameters can be regarded as variable and polarization effects arise as a result of potentially complex modal interference.

on a basis of linear polarization states polarized along these symmetry axes with an adjustable orientation. This is described by the Jones matrix,

$$J(x, y) = R(\theta(x, y)) \begin{bmatrix} e^{i\phi_x(x,y)} & 0 \\ 0 & e^{i\phi_y(x,y)} \end{bmatrix} R(-\theta(x, y)). \tag{152}$$

Equation (152) describes an optical element whose polarization control is classified as type F of Table 4. By varying the dimensions of a pillar, in consultation with a library of pre-simulated structures, any overall phase and retardance can be realized, ideally with equal (near unity) transmission for both eigen-polarizations; the structure can also be physically rotated. These pillar-based geometries are an extremely popular choice in contemporary metasurface work and have been for some time—at least some of their popularity is owed to the work of Arbabi *et al.* [273], which took great pains to thoroughly characterize their properties and create a more systematic description of their behavior. These structures are immensely flexible and can exhibit quite high efficiency when designed using high refractive index dielectric materials that permit a high degree of light confinement. Typically, these are fabricated on glass (often fused silica) substrates with the pillars made of a dielectric material whose choice is governed by the operating wavelength. Amorphous silicon is a natural choice for the near-IR [233] ($n \sim 3.5$), while titanium dioxide [274] ($n \sim 2.4$), silicon nitride [275] ($n \sim 2$), and even single crystal silicon [276] have been demonstrated for visible wavelengths (glass itself can even be used, permitted the structures can be of high aspect ratio to compensate for the low refractive index contrast of glass with air [277]). Recent metasurface research shows hafnia [278] (HfO$_2$, $n \sim 2.2$) to be a suitable dielectric for the near-UV, while the long-wavelength IR can be targeted by, e.g., GaAs as discussed in the last section. Depending on the materials involved, these structures can be fabricated with a single step of lithography (commonly electron-beam) and either a top-down etch or, in the case of TiO$_2$ and other dielectrics that permit conformal deposition, a more lift-off-like process [274,278]. Research using these types of pillar-based geometries will, admittedly, occupy most of our focus here.

Gap-plasmon resonators. A second, somewhat less popular choice is so-called gap-plasmon resonator structures [279], shown in Fig. 29(b). Metasurfaces composed of these elements operate in reflection, as the substrate of the device is essentially a mirror patterned with metallic structures (whose lateral dimensions can be adjusted) separated from the substrate by a dielectric layer. Commonly, the metal is gold, and the dielectric spacer is glass. These can be fabricated with relative ease using lithography (again usually e-beam) and metallic lift-off. The dielectric gap supports a resonance that combines elements of Fabry–Perot and plasmonic effects [280,281]; if this resonance is arranged to occur near the desired operating wavelength, the reflected phase sweeps the range 0 to 2π over a modest range of size parameters. In reflection, then, these structures ideally implement the same Jones matrix expressed in Eq. (152). The method of phase accrual is the greatest difference between gap-plasmon resonators (and structures like it) and the dielectric phase shifters of Fig. 29(a) and is also a potential downside: the necessity of operating near a resonance can make the task of achieving uniformly high transmission over the entire desired range of ϕ_x and ϕ_y challenging.

Freeform geometries. A final broad class of metasurface geometries, which we are obliged to mention here, is shown as "freeform" structures schematically depicted in Fig. 29(c). These are less a specific class of unit cell geometries than a natural conclusion of the mode of thinking used in metasurface design. As we describe in Subsection 4.7g, a specific class of unit cell is often selected, simulated in terms of a parameter sweep, and a metasurface designed based on some mathematical

abstraction of the physics at-play [Eq. (152) above is a perfect example], referencing the collection of simulated structures. However, this abstraction can be avoided entirely by techniques, dubbed inverse design or sometimes "topology optimization" (e.g., [282,283]), that treat the structure's *entire* geometry (dielectric, metal, or conceivably, even mixed materials) as freely varying, rather than just a few discrete dimensions. The result, while not immediately interpretable in any intuitive sense, can nonetheless realize a desired behavior and, if coupled with a rigorous solution to Maxwell's equations, circumvent any paraxial limit inherent in the use of the Jones calculus or other simple amplitude transmittance models. This, of course, comes at the cost of added simulation/computational burden.

In this review, we will not dwell much on these. But it should be kept in mind that almost any possible single-layer structure that we can think up to which an intuitive model can be ascribed is, in the end, a subcase of a more general, more complete approach dealing at the level of Maxwell's equations in which the entire structure itself is variable. However, as we discuss in the next section, any planar structure is nonetheless subject to certain symmetries that limit the extent of polarization control achievable.

4.7f. Linear Birefringence, Matrix Symmetry, and the Question of Multiple Layers
The structures discussed in the previous section share three key properties:

- **Unitarity**—the Jones matrix J describing the polarization transfer characteristic of the structure (ideally) does not attenuate any chosen orthogonal polarization basis, or does so equally for all polarizations, so that $J^\dagger J \propto \mathbb{I}$ everywhere.
- **Reciprocity**—light propagation through the structures obeys time-reversal symmetry.
- **Mirror symmetry**—Assuming the presence of a substrate has only a weak optical effect, any planar structures with vertical sidewalls, such as those comprising metasurfaces and described in the previous section, are symmetric about bisecting plane parallel to the $x - y$ plane.

Essential constraints imposed by the structures can be derived from these properties. We begin with reciprocity. We consider the Jones matrix transformation affected by traversing the structure at normal incidence from one of two sides: either bottom, through the substrate, or top, from air or other encapsulating medium as depicted in Fig. 30(a). These are described by the Jones matrix transformations J_{bottom} and J_{top}, each defined with reference to the right-handed coordinate systems xyz and $x'y'z'$, respectively.

We consider some polarization state with Jones vector $|j_{\text{bottom}}\rangle$ that is modified by the element to become $|j_{\text{top}}\rangle$ such that

$$|j_{\text{top}}\rangle = J_{\text{bottom}}|j_{\text{bottom}}\rangle. \tag{153}$$

Equation (153), which is written in the xyz coordinate system, is from the bottom's perspective. But it could just as well be written from the top's perspective in $x'y'z'$ coordinates. However, the polarization states $|j_{\text{top}}\rangle$ and $|j_{\text{top}}\rangle$ require modification. We suppose $|j_{\text{top}}\rangle = [\tilde{j}_{\text{top}}^{(1)} \ \tilde{j}_{\text{top}}^{(2)}]^T$ and $|\tilde{j}_{\text{bottom}}\rangle = [\tilde{j}_{\text{bottom}}^{(1)} \ \tilde{j}_{\text{bottom}}^{(2)}]^T$ (again here, a tilde $\sim$ denotes a complex number). Then, it is true that

$$|j'_{\text{bottom}}\rangle = \begin{bmatrix} \left(\tilde{j}_{\text{bottom}}^{(1)}\right)^* \\ \left(-\tilde{j}_{\text{bottom}}^{(2)}\right)^* \end{bmatrix} \text{ and } |\tilde{j}'_{\text{top}}\rangle = \begin{bmatrix} \left(\tilde{j}_{\text{top}}^{(1)}\right)^* \\ \left(-\tilde{j}_{\text{top}}^{(2)}\right)^* \end{bmatrix}. \tag{154}$$

The negation of the second element comes about from the reversal of y' relative to y, while the complex conjugation is a result of the change in the definition of handedness from the reversal of z' relative to z (this can also be stated as a reversal of the second and third Stokes components, s_2 and s_3). Given this, we can equally well write

$$|j'_{\text{bottom}}\rangle = \boldsymbol{J}_{\text{top}}|j'_{\text{top}}\rangle, \tag{155}$$

or, equivalently,

$$|j'_{\text{top}}\rangle = \boldsymbol{J}_{\text{top}}^{-1}|j'_{\text{bottom}}\rangle \Leftrightarrow |j'_{\text{top}}\rangle = \boldsymbol{J}_{\text{top}}^{\dagger}|j'_{\text{bottom}}\rangle, \tag{156}$$

which is true if $\boldsymbol{J}_{\text{top}}$ is unitary as presumed above. By complex conjugating the whole of Eq. (156), we find that

$$\begin{bmatrix} \tilde{j}_{\text{top}}^{(1)} \\ -\tilde{j}_{\text{top}}^{(2)} \end{bmatrix} = \boldsymbol{J}_{\text{top}}^{T} \begin{bmatrix} \tilde{j}_{\text{bottom}}^{(1)} \\ -\tilde{j}_{\text{bottom}}^{(2)} \end{bmatrix}. \tag{157}$$

Comparison of Eq. (157) to Eq. (153) shows that, if we assume

$$\boldsymbol{J}_{\text{bottom}} = \begin{bmatrix} \tilde{A} & \tilde{B} \\ \tilde{C} & \tilde{D} \end{bmatrix}, \tag{158}$$

then it must be true that

$$\boldsymbol{J}_{\text{top}} = \begin{bmatrix} \tilde{A} & -\tilde{C} \\ -\tilde{B} & \tilde{D} \end{bmatrix}, \tag{159}$$

with each written in its own coordinate system.

Next, we consider the mirror symmetry in the $x - y$ plane. The effect of symmetries on the Jones matrix transfer functions of optical systems, and metamaterial elements in particular, can be considered in a general context far beyond our discussion here [284]. In this specific example, the Jones matrix transformation should be preserved regardless of the direction the structure is traversed. In the way the problem has been constructed in Fig. 30(a), the coordinate systems xyz and $x'y'z'$ are, however, not mirror symmetric, being 180° rotated from one another. Mirror symmetry can, thus, be expressed as an equality of $\boldsymbol{J}_{\text{bottom}}$ and $\boldsymbol{J}_{\text{top}}$ under this rotation, expressed as follows:

Figure 30
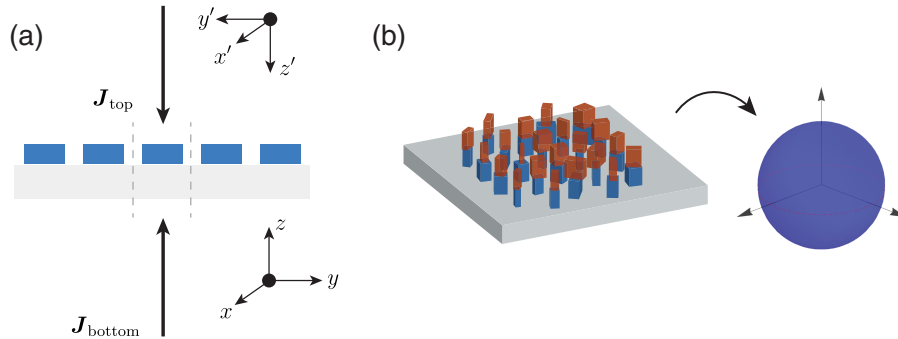
(a) Geometry forward and backward transmission through a planar metasurface device, used for a discussion in Subsection 4.7f. (b) Theoretically, a double-layer metasurface comprising, e.g., two layers of pillars whose dimensions and orientations can vary independently at each point of a metasurface is sufficient to realize any unitary Jones matrix, thus filling full retarder space as discussed in Subsection 2.6a.

$$J_{\text{top}} = M_{xy} J_{\text{bottom}} M_{xy}^{-1}, \qquad (160)$$

with

$$M_{xy} = \begin{bmatrix} 1 & 0 \\ 0 & -1 \end{bmatrix}. \qquad (161)$$

Again presuming J_{bottom} is of the form of Eq. (158), this implies that

$$J_{\text{top}} = \begin{bmatrix} \tilde{A} & -\tilde{B} \\ -\tilde{C} & \tilde{D} \end{bmatrix}. \qquad (162)$$

Comparing Eq. (162) with Eq. (159) above, one can immediately conclude that

$$J_{\text{top}}^{T} = J_{\text{top}}, \qquad (163)$$

with an identical conclusion for J_{bottom} obtained by repeating the above argument.

A single-layer metasurface must implement symmetric Jones matrix transformations. In other words, *the Jones matrix of a planar, metasurface-like structure is symmetric*. Paired with unitarity, this means that metasurface-like building blocks have *strictly orthogonal, linear eigen-polarizations*, i.e., they are achiral and strictly linearly birefringent. The assumptions underlying this result, however, break down at off-normal incidence. A fuller version of this argument is provided in the supplement to [285]. However, for our purposes (which are strictly paraxial), this statement is true. This statement is consistent with the Jones matrix abstraction Eq. (152) provided for the most common polarization-sensitive metasurface elements, dielectric pillars, but also applies more broadly to planar elements for which the above conditions hold (including freeform geometries).

A metasurface composed of such elements, then, must everywhere implement a symmetric Jones matrix. Below, we discuss how this restriction can in theory be surmounted by metasurfaces composed of two layers of such structures. But first, since the vast majority of work reviewed here will involve single-layer metasurfaces beholden to Eq. (163), it is worth considering what this matrix symmetry constraint means for the functions obtainable with metasurfaces, especially as regards the far-fields they can produce.

Far-field constraints imposed by unitarity. As described in Section 3, this is best understood with the aid of matrix Fourier optics. Suppose a metasurface described by $J(x, y)$ is illuminated with a normally incident plane wave. The matrix Fourier transform Eq. (131) gives the Jones matrix angular spectrum $A(k_x, k_y)$ governing the behavior of a specified direction with respect to the incident polarization state. It is helpful to recall that, mathematically speaking, a Fourier transform evaluated for a specific direction (k_x, k_y) is essentially an infinitesimal sum of Jones matrices weighted by exponentials (scalars). In the case of, e.g., a dielectric pillar-based metasurface, this integral actually truly does reduce to a sum over the discrete pillar locations. The far-field function of a metasurface, then, comes about as a result of weighted sums of unitary, symmetric Jones matrices. What constraints does this imply?

As a simple example, consider two unitary matrices U_1 and U_2 and their scalar-weighted sum $\Sigma = a U_1 + b U_2$. Is Σ also unitary? Consider that

$$\Sigma^{\dagger} \Sigma = (a U_1 + b U_2)^{\dagger} (a U_1 + b U_2) = (|a|^2 + |b|^2)\mathbb{I} + a^* b U_1^{\dagger} U_2 + b^* a U_1^{\dagger} U_2 \neq \mathbb{I}. \qquad (164)$$

A device comprising only unitary operators can, through the Fourier transform (itself realized through physical propagation away from the device), enact behavior that is _not necessarily unitary_ in specific directions. This enables considerable design freedom. The form of $A(k_x, k_y)$ for a specific direction can be controlled by tweaking $J(x, y)$ across a metasurface. That $J(x, y)$ is unitary for all (x, y) is a global statement of energy conservation, but when only specific directions of propagation (k_x, k_y) are considered, this energy conservation can be broken, and more general polarization functions can be enacted.

Far-field constraints imposed by matrix symmetry. What about the second constraint of linear birefringence, or matrix symmetry? We consider again two matrices S_1 and S_2 that are symmetric. Is a weighted sum of the two $\Sigma = a U_1 + b U_2$ also symmetric?

$$\Sigma^T = (a S_1 + b S_2)^T = a S_1^T + b S_2^T = a S_1 + b S_2, \tag{165}$$

so that $\Sigma^T = \Sigma$: the symmetry of Jones matrices is preserved under addition, true for a sum of any number of symmetric Jones matrices. Symmetry, if not unitarity, is a property that propagates to the far-field. If $J(x, y) = J^T(x, y)$ for all (x, y)—as is the case for single-layer dielectric metasurfaces—then $A(k_x, k_y) = A^T(k_x, k_y)$ for all (k_x, k_y). The far-field is everywhere governed by symmetric Jones matrices, too.

The requirement of Jones matrix symmetry is a statement of achirality, or an inability to distinguish between circular polarizations at a basic level. Somewhat counterintuitively, though, metasurfaces and other optical devices beholden to this constraint can still realize "chiral"-like effects in their far-field. This is best demonstrated by an example. Consider a polarizer that passes $|L\rangle$ and fully attenuates $|R\rangle$. This is given by $J = |L\rangle\langle L|$, a Hermitian matrix with $|R\rangle/|L\rangle$ as its eigenbasis, which—from our discussion above—is not symmetric and cannot be implemented in the far-field of a metasurface. Consider instead, however, $J = |R\rangle\langle L|$, which _is_ symmetric. This has the same intensity transfer characteristic as the desired polarizer (high for $|L\rangle$ and 0 for $|R\rangle$ input) and only differs with respect to the polarization coming out ($|R\rangle$ instead of $|L\rangle$, preserving matrix symmetry). This operation, chiral inasmuch as it distinguishes between chiralities, _can_ be implemented by a linearly birefringent metasurface, which itself has no chiral properties—in fact, this is the transfer characteristic of one diffraction order of a geometric phase grating.

Double-layer structures. As a final note, we discuss here how the constraint of symmetry/linear birefringence can be surmounted with a more complex metasurface unit cell geometry. The polarization properties of media composed of several layers of planar structures have been studied under the guise of metamaterials (e.g., [286]), but considerably less so when these are allowed to vary spatially forming a metasurface. Here we consider how a pillar-based dielectric metasurface can be augmented to enhance its polarization control beyond linear birefringence. This discussion is presented in significantly more depth in [287], which clarifies the precise mathematical "value added" of a second layer of pillars for polarization purposes, an idea that occasionally appears in the literature (e.g., [288]) usually without a general treatment.

The simplest, almost trivial, addition to a pillar-based dielectric metasurface would be to place the device between two bulk retarders whose retardances and eigenbases could be arbitrarily selected, but whose properties would be constant with space (e.g., placing the spatially varying metasurface between two slabs of uniaxial crystalline wave plates). It can be shown that the level of polarization control attainable by doing so corresponds to any unitary operator within an origin-centered ellipsoid in

retarder space. Any such ellipsoid can be obtained, given the correct choice of retarders before and after the metasurface (though, once these are specified, the ellipsoid is fixed). Any Jones matrix function $J(x, y)$ requiring control corresponding to such an ellipsoid in the retarder space can be realized with just a single-layer metasurface with suitable retarders on either side. To make this very abstract notion tangible, we consider the example of creating a geometric phase optic (a grating, lens, or otherwise) that operates on circular polarization while preserving its polarization state, an application for which double-layer metasurfaces have been proposed [289]. However, this can be achieved simply by placing an appropriately oriented half-wave plate after the metasurface, thus converting the handedness of outgoing circular polarization, without a need for two lithographically patterned layers.

It can be shown [287] that a double-layer metasurface affords the possibility to access the entirety of retarder space (the entire sphere, with arbitrary overall phase control). For this most general level of (unitary) control, two layers is sufficient, and in general $J(x, y)$ could be realized regardless of matrix symmetry. To our knowledge, however, this has not yet been shown experimentally with metasurfaces for polarization control.

4.7g. Implementing a Polarization-Sensitive Metasurface

Designing a polarization-dependent metasurface involves two distinct tasks: (1) determining the Jones matrix function $J(x, y)$ that will yield a desired behavior, and (2) designing the geometry of a dielectric metasurface that implements it. The former—methods of designing metasurfaces to achieve specific functions for particular applications—will be the subject of the next few sections. Here, however, we concern ourselves with the latter problem, which can be reduced to a procedure that, in many cases, follows a simple series of steps.

This starts with a given design $J(x, y)$. Ideally, $J(x, y)$ will already be unitary and symmetric for direct implementation with a metasurface described by a Jones matrix of the form of Eq. (152) (if not, several alternative strategies are discussed below). In that case, $J(x, y)$—which is usually defined on a discrete lattice of points, or sampled down to one—can be diagonalized to yield ϕ_x^d, ϕ_y^d (the desired eigen-phase shifts) and θ at each point.

This procedure presupposes that a library of metasurface elements has been pregenerated, comprising hundreds (or possibly thousands or more) of geometries with different shape parameters (d_x, d_y) that have been simulated using, e.g., finite-difference time-domain (FDTD) simulation or RCWA on a lattice with a specified spacing at a given design wavelength with *periodic boundary conditions* (the oft-debated use of periodic boundary conditions relates to the fact that all of this design presumes operation in the paraxial limit, in which interactions between neighboring elements are neglected). For each, the phase shifts ϕ_x and ϕ_y experienced by light linearly polarized along each symmetry axis of the pillar are determined from the simulation, along with t_x and t_y, the transmission efficiency of each through the pillar. The goal is to generate a library where any desired combination of (ϕ_x, ϕ_y) yields an element with high transmission efficiency, $t_x \sim 1$ and $t_y \sim 1$. A typical example of such a library is depicted in Fig. 31(a).

Then, at each lattice location on the metasurface, we compute the metric

$$\delta = |t_x e^{i\phi_x} - e^{i\phi_x^d}|^2 + |t_y e^{i\phi_y} - e^{i\phi_y^d}|^2, \tag{166}$$

where (ϕ_x^d, ϕ_y^d) are the desired phases to be imparted on light linearly polarized along the pillar's symmetry axes and (ϕ_x, ϕ_y) are the phases actually imparted by a

given element, along with their corresponding amplitude transmission values (t_x, t_y). We choose the simulated geometry from the library that minimizes δ. Minimizing δ is equivalent to minimizing the distance in the complex plane between the phasor representing what we want—the correct phase and unity transmission—and what the structure actually implements. This general scheme, including minimization of Eq. (166), was pioneered by Arbabi *et al.* [273], though—as discussed in Subsection 4.7d—it has a precedent in an earlier diffractive optics work of Mirotznik *et al.* [263].

This minimization is performed at each point on the metasurface, mapping $J(x, y)$ to a list of dimensions (d_x, d_y) and rotation angles θ. These form basis of a CAD (drawing) file to be fabricated.

4.7h. Realizing Hermitian Behavior (i.e., Amplitude Modulation)

As described above, the Jones matrix of conventional metasurface building blocks is constrained to be (1) symmetric and (2) unitary, in accordance with Eq. (152). The former constraint, that of matrix symmetry, fundamentally stems from the symmetries possessed by the structures themselves, as described above. The requirement of matrix symmetry can be relaxed by changing these symmetries, e.g., by utilizing two layers of pillar-like structures rather than one (again as described above).

But what about the former constraint, that of unitarity? To implement a structure that is not strictly unitary is to imply that the structure imparts loss (or gain, though here we focus only on passive structures)—that is, one which can have Hermitian behavior. This is reminiscent of a class of problems that emerges in scalar diffractive optics as well, generally termed "the phase problem," in which one wants to implement an

Figure 31
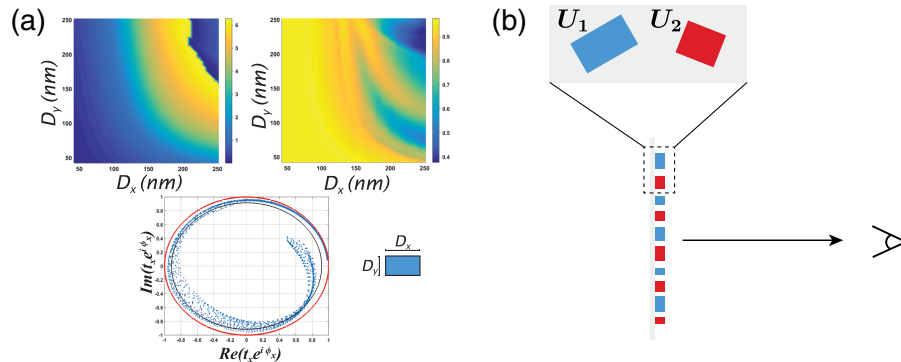
(a) Typical "library" of polarization-sensitive metasurface elements, often presented in this format in metasurface works. A polarization-sensitive structure, in this case a rectangular pillar with two orthogonal dimensions, is simulated using, e.g., FDTD or RCWA for a variety of different configuration of dimensions (D_x, D_y) at a given design wavelength (here 532 nm, with the pillars being made of TiO$_2$. Phase shift and transmission are shown for x-polarized light, with the plots for y being the same given an exchange of the plot axes. This is visualized on the complex plane, showing that geometries exist for phase shifts from 0 to 2π with relatively high transmission. Figures 1, 2, 3, and S3 reprinted with permission from Mueller *et al.*, Phys. Rev. Lett. **118**, 113901 (2017) [290]. Copyright 2017 by the American Physical Society. (b) Dual matrix holography for polarization-dependent amplitude control. As described in Subsection 4.7h, two unitary matrices when added together can realize Hermitian behavior in general, affecting polarization-dependent amplitude control when viewed from the zero-order perspective.

optical element with a phase-only diffractive optical element, which requires mixed amplitude and phase modulation. A suite of solutions has emerged in diffractive optics (e.g., with SLMs, conventional film-based holograms, or other platforms) by which complex functions can be realized with platforms that exert phase-only control. Some of these aim to implement a phase-only solution $e^{i\phi(x,y)}$, which is "closest" (in a variational calculus sense, relative to some distance metric in the space of functions) to the desired amplitude/phase profile (e.g., [291]). Iterative phase retrieval, often in the form of the Gerchberg–Saxton algorithm [292,293], also falls under this class of techniques (we will see below that it can apply to polarization-dependent problems, too).

Double-phase holography. A second class of techniques aims to implement amplitude modulation in a selected part of the far-field, while conserving energy overall. One such technique is known as "double-phase holography," conceived of in the 1970s [294] for use with conventional holograms and now widely used with other platforms, such as SLMs [295]. Double-phase holography stems from the realization that two phase-only quantities, $e^{i\phi_1}$ and $e^{i\phi_2}$, when coherently added, can realize a scalar quantity with *non*-unity amplitude. When viewed only from the zeroth diffraction order, the fields from two adjacent, displaced phase shifters can simply add together, effectively realizing amplitude modulation. However, light will diffract from the periodicity of "super-cell" comprising the two phase shifters so that this amplitude modulation is only realized on the zeroth order with higher diffraction orders (or reflected light, in the case that the periodicity is subwavelength and the two structures form a standalone meta-atom in their own right) acting as a "reservoir" to conserve overall energy conservation.

"Dual-matrix" holography. This concept has recently been generalized to metasurface polarization control; with aid of the SVD, it can be shown that two unitary matrices, when added together, can realize any matrix (which may have both unitary and Hermitian components in general) [296]. In the case of metasurface-like pillar elements, this means that a super-cell of two pillars, each of which implements unitary and symmetric Jones matrices, can be added together to realize any (passive) symmetric Jones matrix [296] [Fig. 31(b)]. A similar approach has been used to realize *scalar* amplitude control over orthogonal polarization states [297,298], a subcase of the "dual-matrix holography" approach described here and in [296]. In essence, this is a type of "spatial multiplexing," a popular approach in the metasurface field that always carries some trade-offs. This is discussed further in the next section.

4.7i. Scalar Regime

Starting with this section, we review past work on metasurface polarization optics. In this and the two sections that follow, this literature is cast in terms of the hierarchy of the scalar, vector, and matrix pictures described in Subsection 3.3 and Fig. 15.

We start here with the scalar picture, which by a large margin describes most past work on polarization-sensitive metasurfaces. Generally speaking, designs that fall under this scalar regime assume *a priori* that light incident on a metasurface of a given polarization state evokes a distribution of an electric field whose polarization ellipse is constant everywhere but whose amplitude and/or phase may vary across the metasurface device—Hence the name, since a spatially varying polarization-dependent problem, by way of assumption, is simplified into one involving only scalars.

In what follows, we provide a semi-chronological review of work in this scalar regime and how thinking about it—what it can do and how it is understood—has evolved over time.

The design strategy used in a wide swath of this work can be described as intuition-based. In this work, the metasurfaces are designed using scalar techniques that we term *propagation phase* and *geometric phase* designs. We describe each of these separately, and then we discuss how in a more general picture these can exist simultaneously.

Pure propagation phase designs. In propagation phase designs, arbitrary and independent phase (and/or amplitude) profiles are imparted on an arbitrarily selected basis of linear polarization states. In a pillar-based metasurface relying strictly on propagation phase, all pillars are aligned at the same angle (to address a chosen basis of linear polarization states with azimuth θ and $\theta + \pi/2$ with only the lateral dimensions of each pillar varying, shown schematically in Fig. 32(a). This is the sense in which using the propagation phase constitutes an intuitive design strategy—simply by looking at the metasurface, it is clear that the device imparts independent phase (or amplitude) profiles on orthogonal polarization states. A metasurface based on a propagation phase approach has a design (assuming phase-only control) of the form

$$\boldsymbol{J}(x, y) = \boldsymbol{R}(\theta) \begin{bmatrix} e^{i\phi_1(x,y)} & 0 \\ 0 & e^{\phi_2(x,y)} \end{bmatrix} \boldsymbol{R}(-\theta) = e^{i\phi_1(x,y)} |\theta\rangle\langle\theta| + e^{i\phi_2(x,y)} \left|\theta + \frac{\pi}{2}\right\rangle\left\langle\theta + \frac{\pi}{2}\right|,$$
(167)

which counts as control of type J with a fixed retardation axis that can lie anywhere in the equatorial plane. In other words, a propagation phase metasurface imparts independent phase profiles $\phi_1(x, y)$ and $\phi_2(x, y)$ on a fixed, pre-determined orthogonal basis of linear polarizations while preserving their polarization state upon transmission (or reflection).

Many examples of polarization-sensitive metasurfaces in the literature fall under this category. Generally speaking, any work that demonstrates a "polarization-switchable" device that can behave as two different optical elements (lenses, holograms, gratings, axicons, etc.) depending on whether x or y polarized light is incident (or any other set of orthogonal linear polarizations) will fall under this approach. As such, there are too many examples to name here. Instead, we try to identify examples most characteristic of what has been done.

A first possibility enabled by a propagation phase design is the ability to construct a device that acts as different blazed gratings for orthogonal linear polarization states, thus directing them to different directions. This has been proposed and demonstrated extensively [273,280,281,303–307], with one example shown in Fig. 32(b). Similarly, a propagation phase-only design can impart two separate lens phase profiles on x and y allowing incident light of each polarization to focus at a separate on- or off-axis focal point [273,308], as depicted in Fig. 32(c). Lastly, in the most general case, the phase profiles of two independent phase holograms can be imparted on orthogonal linear polarization states, yielding polarization-switchable far-field holographic images [273,299,309,310] [an example is shown in Fig. 32(d)]. Beyond these applications, polarization-switchable metasurfaces based on the propagation phase strategy are beginning to find their way into practical optical systems, such as phase contrast microscopes to name just one recent example [311].

Pure geometric phase designs. The second intuitive design strategy, one that captures a wide swath of work on polarization-sensitive metasurfaces, is the *geometric phase* approach. We have already encountered so-called "geometric" or "Pancharatnam–Berry" phases many times throughout this review, a concept that claims a significance in physics far beyond problems of polarized light [312–314]. The name geometric phase is indicative of the fact that phase is acquired by path-dependent effects, i.e., differences in the path by which polarization is transformed

rather than differences in actual, physical propagation length. In a geometric phase metasurface, the form this takes is a device composed of structures of identical shape whose orientations vary. Thus, a geometric-phase-only metasurface implements a design of the form

$$J(x, y) = R(\theta(x, y)) \begin{bmatrix} e^{i\frac{\Delta}{2}} & 0 \\ 0 & e^{-i\frac{\Delta}{2}} \end{bmatrix} R(-\theta(x, y)), \tag{168}$$

wherein light encounters a structure whose retardance Δ is fixed but whose orientation θ is variable (type E of Table 4). In the case that $\Delta = \pi$—half-wave retardance—it can be shown that one handedness of circularly polarized light experiences a phase profile given by $2\theta(x, y)$, while the other automatically experiences $-2\theta(x, y)$. It is in this sense that a geometric-phase-only strategy is said to be intuitive: The phase profile imparted by a geometric-phase-only metasurface is immediately apparent just by looking at the angular orientations of its individual elements. The typical appearance of a geometric-phase-only metasurface is sketched in Fig. 32(e).

Figure 32
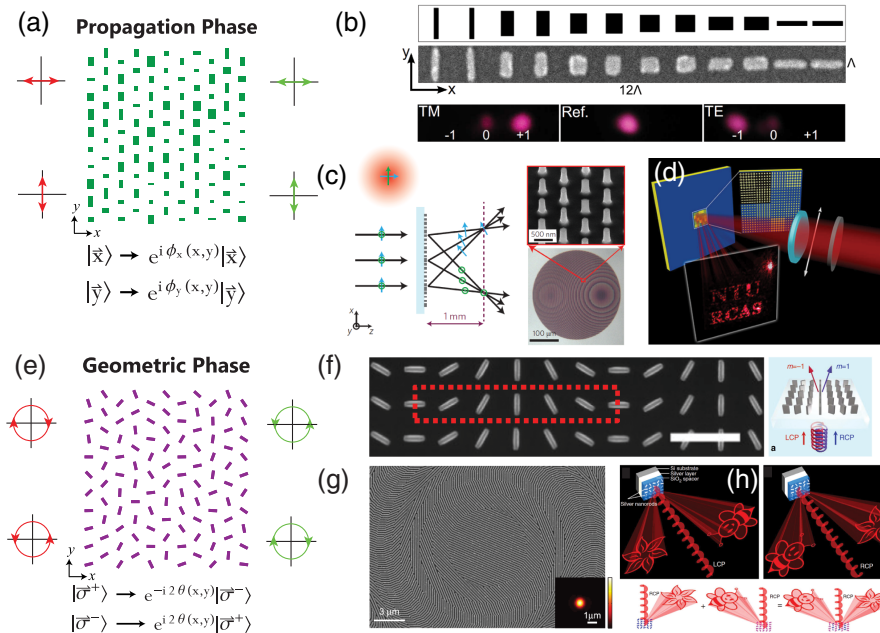
Examples of propagation (a)–(d) phase-only and (e)–(h) geometric-phase-only metasurface designs and applications. (a) Figures 1, 2, 3, and S3 reprinted with permission from Mueller *et al.*, Phys. Rev. Lett. **118**, 113901 (2017) [290]. Copyright 2017 by the American Physical Society. (b) Reprinted by permission from Macmillan Publishers Ltd.: Pors *et al.*, Sci. Rep. **3**, 2155 (2013) [280]. Copyright 2013. (c) Reprinted by permission from Macmillan Publishers Ltd.: Arbabi *et al.*, Nat. Nanotechnol. **10**, 937–943 (2015) [273]. Copyright 2015. (d) Reprinted with permission from Chen *et al.*, Nano Lett. **14**, 225–230 (2014) [299]. Copyright 2014 American Chemical Society. (e) Figures 1, 2, 3, and S3 reprinted with permission from Mueller *et al.*, Phys. Rev. Lett. **118**, 113901 (2017) [290]. Copyright 2017 by the American Physical Society. (f) Reprinted by permission from Macmillan Publishers Ltd.: Khorasaninejad and Crozier, Nat. Commun. **5**, 5386 (2014) [300]. Copyright 2014. (g) From Lin *et al.*, Science **345**, 298–302 (2014) [301]. Reprinted with permission from AAAS. (h) Reprinted under a Creative Commons License [302].

The geometric phase operates so simply on circularly polarized light by converting its handedness, in the manner of a half-wave plate. This mechanism of action confers a number of other advantages, too: If Δ deviates from the half-wave retardance condition, light exiting the device is elliptically polarized. But the exiting light can be expressed as a superposition of both handednesses of circular polarization, one converted and one unconverted. The converted part picks up the desired geometric phase profile, while the unconverted part contains no spatial phase modulation and is leaked into the zero order. For this reason, i.e., the design's forgiveness of imperfections in retardance perhaps stemming from fabrication errors or an off-design wavelength, the geometric-phase-only approach is popular for applications that, strictly speaking, do not even require its polarization sensitivity. In these cases, the need to use circularly polarized light can then be regarded as a 50% efficiency trade-off to be made (as in Subsection 4.5 as well). This is true of a number of works on metalenses [315,316].

The geometric-phase-only approach has been used to create a variety of circular polarization-switchable metasurface optics. In each case, it must be kept in mind that, while the designer can dictate a phase profile for one handedness, the geometric phase's symmetry automatically constrains it for the other. For instance, a blazed grating can be created deflecting one circular polarization to the +1 order, while the other must diffract to the −1 order [300,301,317]. An example of a geometric phase grating (fabricated with Si on glass) is shown in Fig. 32(f). The same principle can be used to implement a focusing lens profile for one circular polarization, while the opposite circular polarization will be constrained to experience a diverging lens phase profile [301,315,316]. When imaging natural light (which is generally *un*polarized), one circular polarization will create an unfocused background; if this is unacceptable, the lens must be preceded by a circular polarizer. An SEM of an example geometric phase metasurface lens is shown in Fig. 32(g). Finally, phase profiles of far-field holographic images can be encoded with the geometric phase, too. However, this comes with the caveat that the hologram evoked can only be controlled for one circular polarization state; for the other, symmetry dictates that a hologram point-inverted about the zero order will appear [302,318–323]. An example is shown in Fig. 32(h). Finally, to mention only one specific application area, we note that recent work has used geometric phase metasurfaces for atom trapping/cooling [324,325].

We also note here that a body of work has been published in the metasurface literature under the term "Malus metasurface"—see, e.g., [326]. These Malus metasurfaces are essentially geometric-phase-only devices as described here consisting of identical elements of variable rotation angle, with the device placed in-between polarization analyzers. Then, some measure of both amplitude and phase modulation can be achieved due to Malus' law.

Control of arbitrary orthogonal polarization states. As described above, the geometric-phase-only approach—for imparting a given phase profile on one of two circular polarizations—and the propagation phase approach—for imparting arbitrary phase profiles on any orthogonal set of linear polarization states—are intuitive in nature. The mathematical relations between phase profiles and structures are straightforward, and the devices themselves reflect this. In some ways, then, the Jones calculus is not really even required.

Much of the early work in polarization-sensitive metasurfaces (including the *earliest* work, described in Subsection 4.7d above) made use of one of these two simple approaches. However, even when limiting ourselves to a scalar picture, neither approach is fully general. Questions naturally arise that hint at this: Can the geometric phase approach be modified so that independent phase profiles can be imparted on

both circular polarizations, rather than being constrained to be the negates of each other? And what about elliptical polarization states in general?

It is indeed possible to design a pillar-based metasurface that imparts independent phase profiles (and/or amplitude profiles, using tricks such as those described in Subsection 4.7h [297,298]) on an arbitrary orthogonal basis of elliptical polarization states. A 2015 work by Arbabi *et al*. [273] first recognized this possibility and gave a theoretical sketch of how this could work in its supplement, shown with one specific example (described below). A later 2017 work by Mueller *et al*. [290] demonstrated this explicitly for arbitrary elliptical polarization states and explained that is enabled by a combination of geometric and propagation phase effects in a way that, unlike the two effects separately, is not readily intuited.

This proceeds as follows. We first choose an arbitrary, orthonormal polarization basis (linear, circular, or elliptical) given by $|j\rangle$ and $|j^\perp\rangle$. Our goal is at each point to find a Jones matrix such that

$$\boldsymbol{J}(x, y)|j\rangle = e^{i\phi(x,y)}|j'\rangle \quad \text{and} \quad \boldsymbol{J}(x, y)|j^\perp\rangle = e^{i\phi^\perp(x,y)}|j^{\perp,'}\rangle \qquad \textbf{(169)}$$

simultaneously. Here, $\phi(x, y)$ and $\phi^\perp(x, y)$ denote independent phase profiles imparted each incoming state, and $|j'\rangle$ and $|j^{\perp,'}\rangle$ denote the spatially uniform output polarization states evoked by the two chosen basis states. The requirement that $\boldsymbol{J}(x, y)$ be unitary mandates that $|j\rangle$ and $|j^\perp\rangle$ also form an orthonormal basis of polarization states. As described in [290], the symmetry of $\boldsymbol{J}(x, y)$ moreover requires that, for Eq. (169) to be have a solution, it must be true that

$$|j'\rangle = |(j)^*\rangle \quad \text{and} \quad |j^{\perp,'}\rangle = |(j^\perp)^*\rangle \qquad \textbf{(170)}$$

with $*$ again the complex conjugate. In other words, Eq. (170) mandates, that for arbitrary control over an arbitrary orthogonal basis of polarization states to be achievable, the output polarization states evoked must be of *reversed handedness* relative to the chosen basis states $|j\rangle$ and $|j^\perp\rangle$. This can be explained analytically but also with purely geometric arguments using the Poincaré sphere (see [290] and its supplement).

Given these constraints, once a basis $|j\rangle$ and $|j^\perp\rangle$ and corresponding phase profiles ϕ and $\phi^\perp(x, y)$ are selected, the Jones matrix of a metasurface realizing Eq. (169) can be straightforwardly written as [290]

$$\boldsymbol{J}(x, y) = \begin{bmatrix} | & | \\ e^{i\phi(x,y)}|(j)^*\rangle & e^{i\phi^\perp(x,y)}|(j^\perp)^*\rangle \\ | & | \end{bmatrix} \begin{bmatrix} | & | \\ |j\rangle & |j^\perp\rangle \\ | & | \end{bmatrix}^{-1}, \qquad \textbf{(171)}$$

where | denotes that a given ket forms the column of a matrix. It can be shown that this is equivalent to writing

$$\boldsymbol{J}(x, y) = e^{i\phi(x,y)}|(j)^*\rangle\langle j| + e^{i\phi^\perp(x,y)}|(j^\perp)^*\rangle\langle j^\perp|, \qquad \textbf{(172)}$$

which has a physical interpretation, showing that any incoming polarization state is projected into its components in the chosen orthonormal basis, with unique phase profiles applied to these components, and with each component exiting as a polarization with reversed handedness.

Once the Jones matrix is determined by Eq. (171) or (172), the physical parameters of each metasurface element ϕ_x, ϕ_y, and θ can be determined as described in Subsection 4.7g. The result is a structure where the link between the underlying function and the device's physical appearance is often not intuitive. In this most general

case, control over arbitrary orthogonal polarization states is achieved through a combination of the propagation and geometric phases in a single element, in a way that depends on the incident polarization state. We note that a theory exists to rigorously quantify the individual contributions of geometric and propagation phases for a given J and incident polarization state [327]. However, knowing the unique contributions of each is not necessary to design and work with these metasurfaces. In most metasurface works, then, the Jones matrix mathematics is, for better or worse, treated as a machinery that yields the correct result without taking great pains to interpret the mechanisms behind it. This is depicted in Fig. 33(a).

Applications of more general control. Applications demonstrated using this more general combined approach mirror those discussed before (gratings, lenses, holograms) albeit with certain constraints eliminated. As mentioned above, the possibility

Figure 33
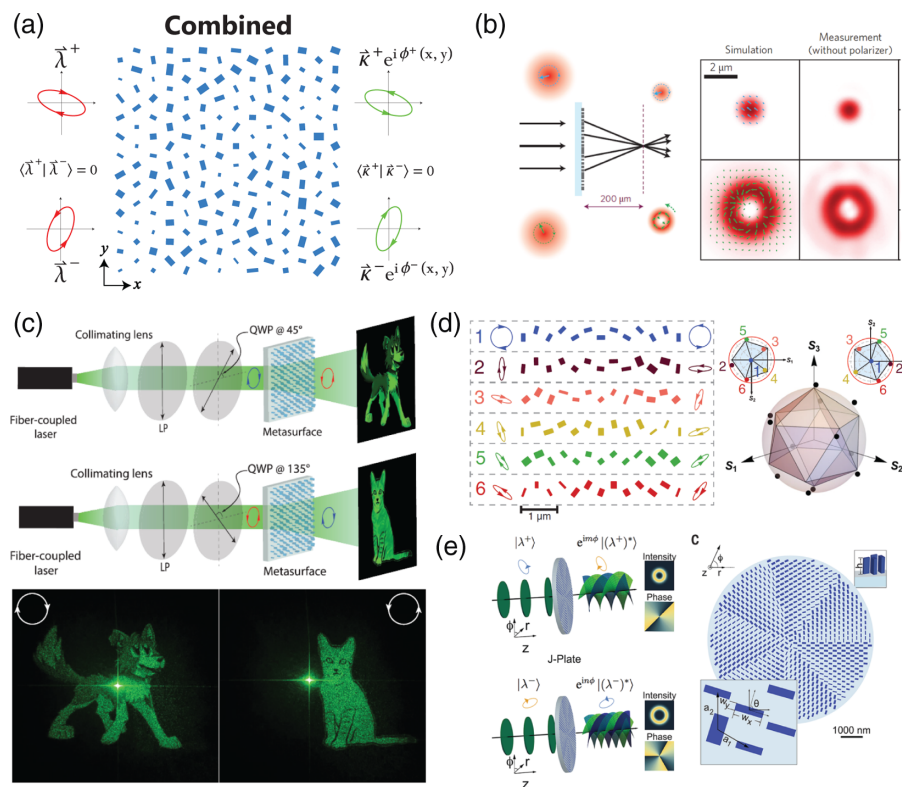
Combining geometric and propagation phases in a single metasurface. (a) Arbitrary phase (and/or amplitude) profiles can be imparted on an arbitrary basis of elliptical polarization states, so long as the output polarizations are of reversed handedness relative to the input. Figures 1, 2, 3, and S3 reprinted with permission from Mueller *et al.*, Phys. Rev. Lett. **118**, 113901 (2017) [290]. Copyright 2017 by the American Physical Society. (b) Conversion of $|R\rangle$ into a vortex beam while leaving $|L\rangle$ unchanged. Reprinted by permission from Macmillan Publishers Ltd.: Arbabi *et al.*, Nat. Nanotechnol. **10**, 937–943 (2015) [273]. Copyright 2015. (c) Circular polarization-switchable holograms. (d) Elliptical polarization beam splitting gratings. (c) and (d) Figures 1, 2, 3, and S3 reprinted with permission from Mueller *et al.*, Phys. Rev. Lett. **118**, 113901 (2017) [290]. Copyright 2017 by the American Physical Society. (e) Conceptual sketch of a "J-plate," an arbitrary spin–orbit converter. From Devlin *et al.*, Science **358**, 896–901 (2017) [182]. Reprinted with permission from AAAS.

of imposing arbitrary phase profiles on an arbitrary basis of polarization states was first recognized in [273]. However, most of the examples demonstrated therein used purely propagation or geometric phase designs with the exception of two devices {Fig. 5(b) and 5(c) of [273]}. These examples can be said to be the first polarization-sensitive metasurfaces employing a combination of propagation and geometric phases. However, in both cases, these are primarily geometric phase devices to which a polarization-independent propagation phase has been added. One of these, shown in Fig. 33(b), imparts a phase profile $e^{i2\phi}$ to $|R\rangle$ (a topological charge of 2) while imparting no azimuthal phase profile on $|L\rangle$. The working principle of the device as explained in [273] is that of a q-plate-like geometric phase device imparting $e^{\pm i\phi}$ on $|R\rangle/|L\rangle$ coupled with an overall, polarization-independent phase profile of $e^{i\phi}$. Still more is possible, however, by breaking this degeneracy and exploiting Eqs. (171) and (172) to the fullest. In [290], the possibility of creating an arbitrary hologram switchable on the basis of circular polarization was shown [Fig. 33(c)]. Mueller *et al.* [290], moreover, demonstrated experimentally the ability to address arbitrary orthogonal elliptical polarization states by creating blazed gratings to split these. Figure 33(c) shows grating periods of six different beam splitters and the elliptical polarization states they are designed to split, which are also shown on the Poincaré sphere at right. This combined approach can also be used to create circular polarization-switchable lenses where both chiralities can be focused at any desired locations, in contrast to geometric-phase-only lenses [328]. Finally, this combined approach can be used to surmount the limits of a geometric-phase-only approach in converting polarization states to OAM states of light. Recall that a q-plate (Subsection 4.5c) is constrained to impart equal and opposite topological charges on $|R\rangle/|L\rangle$. The generalized approach here, however, enables so-called "J-plates" in which any polarization basis (not only circular) can be mapped into any desired set of topological charges [182] [Fig. 33(d)], a possibility anticipated in part by [273].

Limitations of the scalar approach: To conclude, the scalar approach as described in this section is limited in that a particular basis is chosen *a priori* and the polarization state distribution created by the metasurface in response to each polarization in this basis is assumed to have a uniform polarization ellipse everywhere. The consequences of this are best illustrated by considering the polarization response of the far-field given by the Fourier transform of Eq. (172) as

$$A(k_x, k_y) = \mathcal{F}_{(k_x,k_y)}\{e^{i\phi^+(x,y)}\}|(\lambda^+)^*\rangle\langle\lambda^+| + \mathcal{F}_{(k_x,k_y)}\{e^{i\phi^-(x,y)}\}|(\lambda^-)^*\rangle\langle\lambda^-|. \quad \textbf{(173)}$$

The assumptions inherent in the scalar approach mean that any such metasurface will be limited to two unique far-field responses for two orthogonal polarization states that are fixed with the metasurface's design. Any other incident polarization state evokes a weighted superposition of the two. Thus, the device's polarization-dependent function is limited to a device whose function switches on the basis of just *two* chosen orthogonal polarization states. We will see that the matrix approach generalizes this considerably, allowing the device to create functions that "switch" on the basis of arbitrarily many polarization states across its far-field, as well as devices exhibiting behavior that is far more general than "polarization-switchability."

"Spatial multiplexing." Many works, conscious of the fact that the scalar approach limits the polarization-based multi-functionality of a metasurface to just two discrete behaviors for two polarization states (but perhaps unaware of the more general matrix picture) have attempted to enhance the polarization functionality of a metasurface through spatial multiplexing. Spatial multiplexing, sometimes also called "interlacing" or "shared aperture" (among other terms), involves designing two or more scalar regime metasurfaces separately to enact separate functions for separate

polarization bases. These are then interlaced in the same metasurface plane to allow a scalar regime metasurface to exhibit a multitude of polarization-dependent behaviors. However, this spatial multiplexing always has a trade-off. First, if the individual metasurfaces are interlaced closely together, this will create superperiodicities, which will support their own diffraction orders, creating unintended loss. If instead the metasurfaces are interlaced to occupy wholly separate regions, the design may well be several separate devices, and its function will entirely depend on where it is illuminated. Finally, interlacing always introduces switching based on sets of orthogonal polarization states. It can never introduce a dependence on one polarization without also adding dependence on its orthogonal counterpart. The matrix approach, on the other hand, can surmount this restriction, permitting addressing of sets of polarization states, which are in general non-orthogonal. Some less abstract, more practical consequences of spatial multiplexing for metasurface polarimetry are discussed in Subsection 4.7l below. A case-in-point of this discussion is embodied by the GPH of Fig. 32(h)—here, two metasurfaces have been interlaced to impart separate geometric phase profiles on $|R\rangle$ and $|L\rangle$. However, incident light "feels" both, so both images are produced in the far-field [302], with the images point-inverted through the origin when the incident chirality changes.

4.7j. Vector Regime

General description and examples. A key limiting assumption of the scalar design strategy above is that it assumes that an orthogonal basis of polarization states each creates a field that is everywhere uniform in polarization. This need not be the case—for a given incident plane wave polarization state $|j_{in}\rangle$, we can write

$$|j_{out}(x, y)\rangle = \boldsymbol{J}(x, y)|j_{in}\rangle, \tag{174}$$

itself corresponding to a far-field with a spatially variable polarization state given by

$$|a(k_x, k_y)\rangle = \mathcal{F}\{|j_{out}(x, y)\rangle\}, \tag{175}$$

with $\mathcal{F}$ distributing over both elements of the Jones vector. In designs classified under the *vector* approach, then, the ability of the metasurface to create a spatially varying distribution of polarization states for a given input $|j_{in}\rangle$ is explicitly acknowledged.

A wide body of past metasurface work falls under this category. These have a wide variety of motivations and goals but share the notion that a suitably designed metasurface can create a far-field with an arbitrary distribution of amplitude and/or polarization state, given an incident polarization state that is decided upon *a priori*. This engineered far-field can consist of just a few discrete diffraction orders (for a periodic metasurface) or it can be continuous (if the metasurface is aperiodic). It can be shown that, for a metasurface (where $\boldsymbol{J}(x, y)$ is linearly birefringent), Eq. (174) permits an arbitrarily selected input $|j_{in}\rangle$ to be mapped to a $|j_{out}(x, y)\rangle$ with an arbitrary phase and polarization ellipse (but whose amplitude matches that of $|j\rangle_{in}$ respecting unitarity). A near-field $|j_{out}(x, y)\rangle$ best creating a desired far-field polarization and amplitude distribution $|a(k_x, k_y)\rangle$ is often found using iterative phase retrieval or some other optimization scheme, and a metasurface is designed to produce $|j_{out}(x, y)\rangle$ for the chosen $|j_{in}\rangle$.

While the exact details and implementation can vary (some, for instance, apply spatially multiplexed designs) the description above generally applies to a wide body of past metasurface work; rather than explaining every possible variation, we cite these as a whole here [329–338]. We additionally show some examples of this far-field polarization control in Fig. 34.

Comparison to the more general matrix picture. In the scalar approach above, function is allowed to vary with incident polarization, but fixed *output* polarization state is assumed in the mathematical treatment, creating a scalar-valued problem. By contrast, in the vector approach, a fixed *input* polarization is assumed with output polarization allowed to vary, permitting mathematical analysis at the level of Jones vectors. This also means that if the incident polarization changes, so too will any carefully designed behavior of the device. The matrix approach, the subject of the next section, neither makes assumptions about the polarization state of the input nor output, permitting a top-level analysis at the level of the Jones matrix.

It is worth mentioning that several works classified above under this vector regime do anticipate this matrix approach, with Zhao *et al.* [331] perhaps coming closest. In [331], the metasurface is treated in terms of a Jones matrix, which the authors (much as in this work) explicitly acknowledge is limited to a unitary and symmetric form everywhere. However, generality is lost when the specific input polarization states are assumed (namely, $|x\rangle$, $|y\rangle$, $|45°\rangle$, $|135°\rangle$, $|R\rangle$, and $|L\rangle$) and the problem is treated primarily in terms of Jones vectors. A case in point is Eq. (4) of [331] in which the derived form of the Jones matrix at each pixel has only two free parameters (rather than the full three). Using a scheme that couples several Gerchberg–Saxton loops together (described in its supplement), the authors of [331] successfully demonstrate holograms that can address more than one orthogonal polarization basis at once (in the authors' words, "twelve polarization channels"), surmounting restrictions inherent in other past work. However, the *a priori* assumption of specific incident polarization states limits the scheme's generality. Instead, with the matrix approach, no such restriction exists, enabling effectively an infinite number of these channels.

Figure 34
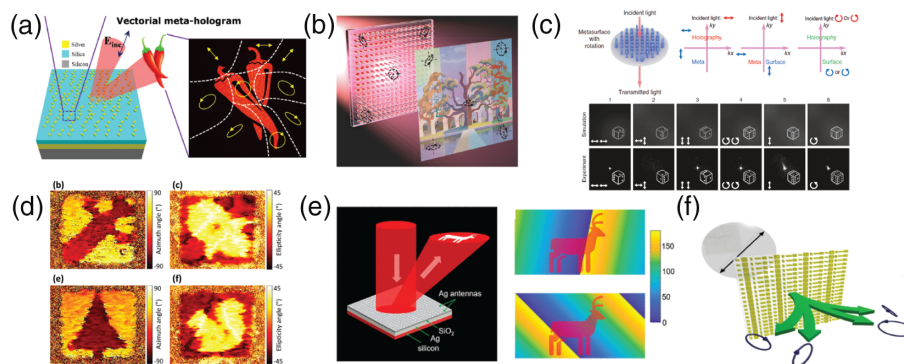
Summary examples of work using the vector approach to demonstrate metasurface devices producing far-fields or (discrete diffraction orders) whose polarization state and intensity distributions can be controlled through the metasurface's design. (a) Reprinted with permission from Deng *et al.*, Nano Lett. **18**, 2885–2892 (2018) [329]. Copyright 2018 American Chemical Society. (b) Reprinted with permission from Arbabi *et al.*, ACS Photonics **6**, 2712–2718 (2019) [330]. Copyright 2019 American Chemical Society. (c) Reprinted under a Creative Commons Attribution 4.0 International License from [331]. (d) Reprinted under a Creative Commons Attribution 4.0 International License from [332]. (e) Reprinted with permission from Wen *et al.*, Nano Lett. **21**, 1735–1741 (2021) [333]. Copyright 2021 American Chemical Society. (f) Reprinted with permission from [334]. Copyright 2018 Optical Society of America.

4.7k. Matrix Regime

In the most general picture, a polarization-sensitive metasurface can be designed operating consistently at the level of Jones matrices, with no assumptions made concerning the input or output polarization states. Only a few relatively recent works in the metasurface field can be classified at this level of generality. Below we review these and the new functions and optical components they enable. However, we first briefly discuss why pillar-based metasurfaces, in the larger scheme of this review, are perhaps the ideal polarization-sensitive diffractive optical element for description and design with this matrix generalization of Fourier optics.

Metasurfaces and Jones matrix Fourier optics. The Jones matrix approach for analyzing polarization-sensitive diffractive optics has been a common thread of this review. Primarily, it has been used here as an explanatory tool to help classify (alongside the matrix polar decomposition) different technologies and approaches from the literature over the years (as in Table 4). However, less commonly it has served as a design tool unto itself among all the different types of optical elements discussed so far.

It is worth considering why this is, and why metasurfaces are slightly different. Many optical elements discussed previously only had one or two degrees of freedom. Take, for instance, a LC SLM (Subsection 4.5d). Every pixel of an SLM has a common eigenbasis, so $J(x, y)$ (and, by extension, $A(k_x, k_y)$) can be expressed as a diagonal matrix in a common basis everywhere across the device, at all (x, y). There is little benefit to introducing a more complicated notion when these can just as easily be handled by considering only $|x\rangle$ and $|y\rangle$ polarizations separately. The same is true for the elements etched into birefringent substrates (Subsection 4.3), which have two degrees of freedom at each location—ϕ_x and ϕ_y—and can similarly be expressed in terms of diagonal matrices everywhere.

Geometric phase elements, such as those realized with LCs (Subsection 4.5b), are a slightly different story with the same conclusion. These are expressed as a spatially rotating half-wave plate, described by

$$J(x, y) = R(\theta(x, y)) \begin{bmatrix} i & 0 \\ 0 & -i \end{bmatrix} R(-\theta(x, y)). \tag{176}$$

Only one degree-of-freedom is available: control of $\theta(x, y)$, the elements' angular orientation. The matrix-valued Fourier transform of Eq. (176) is proportional to

$$\mathcal{F}\{e^{i2\theta(x,y)}\}|R\rangle\langle L| + \mathcal{F}\{e^{-i2\theta(x,y)}\}|L\rangle\langle R|. \tag{177}$$

Equation (177) tells us something we already knew about geometric-phase-only elements before going through the trouble of the matrix approach—a geometric phase element imposes one phase profile on the $|R\rangle$ component of incoming light and a conjugate one on $|L\rangle$, flipping the handedness of each in the process. The polarization dependence itself appears as a constant in Eq. (177) that cannot be changed with $\theta(x, y)$, the sole degree-of-freedom. In this case, the matrix approach still poses no real value, since in the end matrix Fourier transforms are simplified to scalar-valued ones weighted by constant Jones matrices.

Dielectric metasurfaces of the kind discussed in this review instead have three degrees of freedom at each location: two phases and one orientation angle, described by

$$J(x, y) = R(\theta(x, y)) \begin{bmatrix} e^{i\phi_x(x,y)} & 0 \\ 0 & e^{i\phi_y(x,y)} \end{bmatrix} R(-\theta(x, y)). \tag{178}$$

Equation ([178]) possesses enough complexity that nothing can be said about the nature of $\boldsymbol{A}(k_x, k_y) = \mathcal{F}\{\boldsymbol{J}(x, y)\}$ (it is not diagonalizable in a common basis across the device, nor do the matrices "pass through" the Fourier transform). Pillar-based dielectric metasurfaces are flexible enough that nothing is set in stone at the outset about $\boldsymbol{A}(k_x, k_y)$ (except that it must be symmetric, as described in Subsection [4.7f]). More complex polarization-dependent behavior can manifest that truly requires this matrix picture to understand and realize, and so metasurfaces (unlike several previous technologies reviewed here) stand to exploit it in a way that other technologies cannot.

Metasurface examples using the matrix approach. We discuss three examples of this here (since, to the best of our knowledge, only three metasurface examples have been reported using this most general strategy).

Metasurface-based polarization-dependent beam splitting gratings were discussed throughout Subsection [4.7i]. The examples shown there—whether based on propagation phase, geometric phase, or a combination of the two—are fundamentally subject to the constraint that only orthogonal polarization states can be "split." For instance, if x-polarized light is directed to one diffraction order of the grating, y-polarized light must be directed to another. While the polarization basis addressed is flexible using the combined approach, the fact that orders can only be created for orthogonal polarization states is not. In [339], an approach that uses the matrix picture of this review is adopted. A more general beam splitting grating is one in which a desired set of diffraction orders behaves as "analyzers" for a desired set of polarization states [Fig. [35](a)]. That is, each diffraction order can be described by a far-field Jones matrix given by $|(\lambda)^*\rangle\langle\lambda|$ whose intensity transfer characteristic matches that of a polarizer for an arbitrarily selected polarization $|j\rangle$ (outputting $|(\lambda)^*\rangle$ to preserve matrix symmetry). In [339], a metasurface grating was realized with four orders acting as analyzers for polarization states corresponding to the vertices of a tetrahedron inscribed in the Poincaré sphere [Fig. [35](b)]. Contrary to what could be accomplished using previous strategies, no member of this set of states is orthogonal to any of the others, and a single metasurface handles all of the beam splitting (with no need for, e.g., spatial multiplexing). This grating can function as a component for realizing full-Stokes polarimetry, so it is described below as well (Subsection [4.7l]).

A second work [340] takes these ideas to their natural conclusion, considering instead aperiodic metasurfaces (i.e., beyond gratings). In [340], a method is given based on the matrix polar decomposition to design metasurfaces whose far-fields exhibit continuous polarization dependence $\boldsymbol{A}(k_x, k_y)$ that can be engineered. Two classes of examples are considered: "polarizer-like" and "wave-plate-like." In the former, metasurfaces are demonstrated whose far-fields act as polarization analyzers, where the polarization analyzed can vary arbitrarily over the far-field [as sketched in Fig. [35](c)]. As a concrete example, this enables computer-generated holograms with arbitrary polarization-dependent intensity variation (subject to Malus' Law) with polarization state—far from the simple binary polarization-switchability mandated by the scalar approach. An example is shown in Fig. [35](d) of a hologram that projects different drawings of polarization ellipses to its far-field. The area comprising each drawing is actually an analyzer for the depicted polarization state, so the polarization state incident on the metasurface can simply be read out by inspection, making these holograms a sort-of "visual-polarimeter." In [340], a "wave-plate-like" example is also shown, in which it is demonstrated that the far-field can implement polarization transfer functions that are unitary. A hologram is designed in which light diffracts uniformly into a solid disk with the transfer function's retardance increasing from the center of the disk and its fast-axis orientation angle rotating around its perimeter (thus containing all possible linearly birefringent wave plate transformations, the equator

of retarder space, in the far-field). These possibilities—dubbed "Jones matrix holography" [340]—demonstrate new optical components enabled by metasurfaces and the use of this matrix approach specifically, and could find applications in correcting (or generating) custom polarization-dependent transfer functions for whole optical systems.

A third work [296] considers these notions along the optical axis (instead of in a far-field plane). The conventional Fourier integral is taken in [296] over k_z in cylindrical coordinates with Bessel functions [341] to enact control along the propagation direction [Fig. 35(e)]. This expansion can contain Jones matrix coefficients to describe polarization dependence, and the profile of an optical element implementing a desired polarization transfer function along the optical axis can be described with a Jones matrix and subsequently converted to a metasurface design. The resulting element implements this designer-specified polarization transfer function along the optical axis by carefully managing the distribution of light in sidelobes [296,341] [Fig. 35(f)]. In analogy to [340], an example is shown in Fig. 35(g) of a device that directs light along the optical axis as though a "virtual" linear polarizer were located there that rotates between 0° and 90° over some range along z. If the incident light is x-polarized, locations closer to the element are brighter and become dimmer along z in accordance with Malus' Law. The opposite is true of incident y-polarized light. Examples are also shown in [296] of wave-plate-like transformations. These devices may find application in, for instance, microscopy or particle manipulation.

4.7l. Polarimetry with Metasurfaces

The use of metasurfaces for polarimetry has recently garnered significant interest, with a large number of studies [323,334,339,342–351] and brief reviews [239,352] dedicated to the subject. Recall from Subsection 2.7 that polarimetry refers to the measurement of light's polarization state using a series of measurements in which the polarization of an unknown beam is projected onto a series of known polarization analyzers and the resulting intensity is measured. Measuring the full-Stokes vector $\vec{S} = [S_0, S_1, S_2, S_3]^T$—the most general description of a plane wave polarization state—requires at least four such measurements. The advantage of metasurfaces here lies in their ability to parallelize this process. Past works employ different methods of doing just that, at different wavelengths and using different metasurface material platforms.

Spatial multiplexing strategy. We have seen in previous sections that a metasurfaces can be designed to create gratings acting as "polarization beam splitters." For instance, a geometric phase grating divides an incoming plane wave into its $|R\rangle$ and $|L\rangle$ components. For a beam limited in size, these can be separated in space and measured independently. The sum of the two gives the overall intensity S_0 while their difference gives S_3, the chiral Stokes component. With a single metasurface polarization-switchable grating paired with two detectors, already two of the four Stokes components can be measured. By a similar arrangement, a grating splitting $|x\rangle/|y\rangle$ (or $|45°\rangle/|135°\rangle$) linearly polarized light could determine both S_0 and S_1 (or S_2) using a propagation-phase-only type design.

A logical conclusion, then, is that three such gratings (each designed using the scalar approach, Subsection 4.7i) should be used to determine $\vec{S}$ in full. A scheme such as this with *six* measurements ($|x\rangle/|y\rangle/|45°\rangle/|135°\rangle/|R\rangle/|L\rangle$) mirrors Stokes' own definition of the Stokes parameters. Consequently, a number of metasurface works have been demonstrated in which a metasurface is designed in which three gratings (one geometric phase grating for $|R\rangle/|L\rangle$ and two propagation phase-only designs for the others) are spatially multiplexed (interlaced) on a single substrate. Each grating is

designed to have a slightly different deflection angle (period) so that the beams do not overlap in the far-field and can be separately detected. A schematic of this idea and an example SEM of a metasurface device that implements it are shown in Figs. 36(a) and 36(b). The first metasurface example using this strategy was shown by Pors *et al.* [342], later replicated by other works [343,346,349]. Accurate laser beam polarimeters have been shown using this strategy, both at a single wavelength [342,343] and for broadband *spectro*polarimetry [346,349]. A similar device has even been applied to quantum optical correlation measurements of polarization entanglement [351].

As discussed in Subsection 4.7i, the spatial multiplexing approach, however, always carries some trade-off. The exact trade-off depends on how this is done: If the metasurfaces are interlaced [342,343,346] (a few periods of one grating, then a few periods of another, and so on), extraneous diffraction orders will be produced owing to the periodicity introduced by the interlacing [note the periodicity introduced along the y direction in Fig. 36(b)]. If the interlacing is carried out at very large periods so that the gratings are effectively in separate spatial locations [349], the extra diffraction orders disappear at the expense that the device becomes highly sensitive to alignment and beam-size, depending on which areas of which gratings are illuminated.

From a purely polarimetric point-of-view, this spatial multiplexing approach carries trade-offs as well. The minimum number of measurements necessary to determine $\vec{S}$ is *four*. The spatial multiplexing approach described here, however, requires six. This is in fact a fundamental limitation of the technique. In order for a system's 4×4 instrument matrix to be invertible (enabling a given set of polarization-sensitive measurements to serve as a full-Stokes polarimeter), it can be shown that the polarization states analyzed, when drawn as points on the Poincaré sphere, must form a shape enclosing *volume*. The larger this volume is, the higher fidelity the polarimeter so-constructed will be in terms of noise propagation from intensity measurements to $\vec{S}$ [25,353–355]. However, using a spatial multiplexing approach, no configuration of two gratings can be assembled so that this is the case. This is true whether two gratings of the three from the typical spatial multiplexing strategy are used [as in region (i) in Fig. 36(c), i] or for any set of two orthogonal polarization states in general [region (iii) in Fig. 36(c)], as could be realized by the combined propagation/geometric phase approach; either way, these can only ever form a plane of zero volume in the Poincaré sphere and cannot be used for a full-Stokes measurement. If all the diffraction orders are to be used, using the spatial multiplexing strategy described here mandates at least six measurements.

Full-Stokes polarimetry with a single grating. A different strategy described in the last section enables full-Stokes polarimetry with a single non-spatially multiplexed grating [339]. With awareness of the full Jones matrix approach, a grating can be designed whose inner four diffraction orders act as polarization analyzers for an arbitrary set of four polarization states. These can be arranged to correspond to a tetrahedron inscribed in the Poincaré sphere [e.g., iii in Fig. 36(c)], the optimum choice for a four-measurement full-Stokes polarimeter. This approach, too, carries its own trade-offs. The exact Jones matrix needed to losslessly perform this function is not in general unitary and symmetric everywhere, so a metasurface can only implement an optimized "best fit" version. This means that light must necessarily be leaked in part to extraneous diffraction orders, albeit in a way that potentially enacts less of an efficiency penalty than the spatial multiplexing approach (see [339] and its supplement for details).

Polarization imaging with metasurfaces. Polarimetry has been discussed here in terms of determining the Stokes vector of a single plane wave. However, the most promising applications of polarimetry require polarization imaging (often called

imaging polarimetry) in which the Stokes vector of light is determined over a photographic scene. Thus far, only two works have demonstrated full-Stokes polarization imaging with metasurface polarization optics [339,343].

Converting from a laser beam polarimeter to a polarization imager requires the merger of the metasurface with imaging optics, i.e., a camera. In addition to differences in metasurface design strategy (spatial multiplexing [343] versus the single grating approach described above [339]), these works also differ in their approaches to doing so. One approach is to design the metasurface as a focal plane element, as in [343]. The metasurface device of [343] combines interlaced polarization-sensitive gratings with a polarization-independent lens phase profile. The device is intended to serve as a polarization filter just above the sensor's pixels, much like the common division-of-focal-plane approach with pixelated polarizers but ideally without a 50% loss [343] associated with absorptive components. Groups of adjacent pixels are combined into one "super-pixel," which experiences different polarization analyzers, from which the Stokes parameters can be determined [Fig. 36(d)]. A second method taken by [339] entails placing the grating in the optical system's path, ideally in a pupil plane. Here, light from a faraway scene is collimated. Each ray over the camera's angular FOV is split into four rays, forming four completely separated images on the camera's sensor corresponding to different polarization channels. Provided the camera's FOV is limited, these can be registered to each other and analyzed pixel-wise to determine $\vec{S}$ over the scene [Fig. 36(f)]. Based on this approach, a portable metasurface polarization camera has been demonstrated, capable of outdoor and indoor full-Stokes polarization imagery (some examples of which are featured in Fig. 37).

Discussion and technical challenges. As described here, metasurface approaches have been widely demonstrated. It is worth briefly commenting on how these components compare to conventional polarization optics widely used in polarimetric applications in, for instance, atmospheric science [50] or astronomy [48,51,356,357]. One clear difference is that the polarization extinction ratio enacted by the diffraction orders of metasurface gratings is, at best, on the order of 10^2 (or a diattenuation of 0.99) [339], very modest compared to the best film (10^4) and the best prism-based (10^6) polarizers available. This is actually less of a problem than it may sound, so long as a metasurface device can be suitably calibrated—the accuracy of a polarimetric system is more strongly governed by the precision to which diattenuation is known than by its absolute value. Another technical challenge faced by metasurfaces is size—it is hard to manufacture a metasurface (especially using e-beam lithography) reliably over an area comparable to the aperture sizes of real optical systems (cm to meters), but this is a problem that is in theory (and, increasingly, in practice) solvable by stepper-based UV lithography and careful process control. Finally, the metasurface devices here are inherently chromatic, not only in the phase shifts their individual elements impart but also in the fact that they are by their very nature diffraction gratings whose orders will disperse in angle over a broad bandwidth. This is an effect that must be dealt with depending on a given end-application, or instead turned to the designer's advantage by using this dispersion to construct, e.g., a hyperspectral camera.

5. CONCLUSION AND OUTLOOK

In this review, we have discussed optical elements with spatially varying polarization properties. We have presented a conceptual framework for understanding these—Fourier optics coupled with the Jones calculus—and a mathematically oriented classification scheme—retarder and diattenuation space, based on the matrix polar decomposition—for comparing them. Through this lens, we have considered developments in this subject occurring over roughly the last half-century.

Any attempt to predict the future is by definition speculative, a task that without the benefit of hindsight is far more challenging than anything we have undertaken in this review so far. Consequently, this section will be short. Nevertheless, it is necessary to provide some comments and predictions regarding work still-to-come, albeit in terms that may be brief and perhaps even vague.

Throughout this work, different technologies have been categorized based on the *extent* of polarization control they can realize. This notion can be made rigorous by representing the eight degrees-of-freedom of the Jones matrix as three geometrical spaces (Subsection 4.1) and the type of polarization control that can be realized spatially across the device depicted as subspaces of these, which themselves affect the far-field polarization behavior possible. But as remarked in Subsection 4.7k, dealing at the level of abstraction afforded by the Jones matrix is not even truly necessary for most of the technologies discussed here, which only have one or two free parameters whose design can well be treated as a scalar-valued problem. Metasurfaces (and, technically speaking, polarization holographic films, Subsection 4.2) instead introduce three, creating a degree of complexity that necessitates and can benefit from a matrix approach. Three, however, is less than half of the eight available, and single-layer pillar-based metasurface-like elements only occupy a small fraction of possible polarization responses.

Flexible solutions for implementing the most arbitrary, most general local polarization responses could form an active area of research, including structures with custom-polarization-dependent loss (or gain), that is, full control over the Hermitian component of the Jones matrix. These may well come about through the use of inverse design techniques, rather than through a reliance on readily intuited structures as has been the course of this field so far. Moreover, it is possible that much may be gained through the combination of more than one of the different technologies described in this review.

The treatment of this review, and of work in the field up until now, has largely neglected a critical characteristic of polarized light: depolarization. That light is purely polarized has been a tacit assumption of most of the theory and previous work described throughout this review. Generalizations of past work to handle spatially varying, depolarizing optical elements is a potentially fruitful future area of investigation. This would require instead the use of Mueller matrix methods generalized to diffractive elements.

Finally, on a more practical note, there is hope that these polarization-sensitive diffractive optical elements will make their way into new types of optical systems that enable some new function beyond the components' intrinsic novelty itself (including scientific instruments such as novel telescopes and microscopes, polarimetric or otherwise, as well as systems for any number of potentially high-volume technological needs). One overarching constraint in this review, and of conventional polarization optics in general, is that of linearity with respect to incident polarization state (e.g., in the form of Malus' Law). It may be that in the future the optical elements described here can be paired with nonlinear and/or gain media whose underlying physics allow this to be surmounted, enabling new functions and designs.

FUNDING

ACKNOWLEDGMENTS

DISCLOSURES

The authors declare no conflicts of interest.

Data Availability.

No new data were generated or analyzed in the presented research.

REFERENCES

1. W. Shurcliff, *Polarized Light: Production and Use* (Harvard University, 1962).
2. R. A. Chipman, W.-S. T. Lam, and G. Young, *Polarized Light and Optical Systems* (CRC Press, 2019).
3. R. A. Chipman, "Polarimetry," in *OSA Handbook of Optics* (1995), Vol. **II**, pp. 22.1–22.35.
4. J. N. Damask, *Polarization Optics in Telecommunications* (Springer, 2005).
5. D. H. Goldstein, *Polarized Light*, 3rd ed. (CRC Press, 2010).
6. D. S. Kliger, J. W. Lewis, and C. E. Randall, *Polarized Light in Optics and Spectroscopy* (Academic, 1990).
7. M. Born and E. Wolf, *Principles of Optics* (Pergamon, 1999).
8. A. Yariv and P. Yeh, *Photonics: Optical Electronics in Modern Communications* (Oxford University, 2006).
9. C. Brosseau, "Chapter 3-Polarization and coherence optics: historical perspective, status, and future directions," in *Progress in Optics* (2010), Vol. **54**, pp. 149–208.
10. L. Kristjánsson, *Iceland Spar and its Influence on the Development of Science and Technology in the Period 1780–1930*, 4th ed. (University of Iceland, 2010).
11. G. Ropars, V. Lakshminarayanan, and A. L. Floch, "The sunstone and polarised skylight: ancient Viking navigational tools?" Contemp. Phys. **55**, 302–317 (2014).
12. R. Hegedüs, S. Åkesson, R. Wehner, and G. Horváth, "Could Vikings have navigated under foggy and cloudy conditions by skylight polarization? On the atmospheric optical prerequisites of polarimetric Viking navigation under foggy and cloudy skies," Proc. R. Soc. A **463**, 1081–1095 (2007).
13. B. Bernáth, M. Blahó, Á. Egri, A. Barta, G. Kriska, and G. Horváth, "Orientation with a Viking sun-compass, a shadow-stick, and two calcite sunstones under various weather conditions," Appl. Opt. **52**, 6185–6194 (2013).
14. C. Roslund and C. Beckman, "Disputing Viking navigation by polarized skylight," Appl. Opt. **33**, 4754–4755 (1994).
15. J. W. Goodman, *Introduction to Fourier Optics*, 3rd ed. (Roberts & Company, 2005).
16. R. C. Jones, "A new calculus for the treatment of optical systems I. Description and discussion of the calculus," J. Opt. Soc. Am. **31**, 488–493 (1941).
17. H. Hurwitz and R. C. Jones, "A new calculus for the treatment of optical systems II. Proof of three general equivalence theorems," J. Opt. Soc. Am. **31**, 493–499 (1941).
18. R. C. Jones, "A new calculus for the treatment of optical systems III. The Sohncke theory of optical activity," J. Opt. Soc. Am. **31**, 500–503 (1941).

19. R. C. Jones, "A new calculus for the treatment of optical systems. IV," J. Opt. Soc. Am. **32**, 486–493 (1942).
20. R. C. Jones, "A new calculus for the treatment of optical systems V. A more general formulation, and description of another calculus," J. Opt. Soc. Am. **37**, 107–110 (1947).
21. R. C. Jones, "A new calculus for the treatment of optical systems. VI. Experimental determination of the matrix," J. Opt. Soc. Am. **37**, 110–112 (1947).
22. R. C. Jones, "A new calculus for the treatment of optical systems. VII. Properties of the N-matrices," J. Opt. Soc. Am. **38**, 671–685 (1948).
23. R. C. Jones, "New calculus for the treatment of optical systems. VIII. Electromagnetic theory," J. Opt. Soc. Am. **46**, 126–131 (1956).

24. S.-Y. Lu and R. A. Chipman, "Homogeneous and inhomogeneous Jones matrices," J. Opt. Soc. Am. A **11**, 766–773 (1994).

25. J. S. Tyo, "Design of optimal polarimeters: maximization of signal-to-noise ratio and minimization of systematic error," Appl. Opt. **41**, 619–630 (2002).

26. S. Chandrasekhar, *Radiative Transfer* (Clarendon, 1950).

27. E. Wolf, *Introduction to the Theory of Coherence and Polarization of Light* (Cambridge University, 2007).

28. E. L. O'Neill, *Introduction to Statistical Optics* (Addison-Wesley, 1963).

29. J. W. Goodman, *Statistical Optics*, 2nd ed. (Wiley, 2015).

30. S.-Y. Lu and R. A. Chipman, "Interpretation of Mueller matrices based on polar decomposition," J. Opt. Soc. Am. A **13**, 1106–1113 (1996).

31. J. P. Gordon and H. Kogelnik, "PMD fundamentals: polarization mode dispersion in optical fibers," Proc. Natl. Acad. Sci. USA **97**, 4541–4550 (2000).

32. A. Aiello and J. P. Woerdman, "Linear algebra for Mueller calculus," arXiv:math-ph/0412061 (2004).

33. J. J. G. Perez and R. Ossikovski, *Polarized Light and the Mueller Matrix Approach* (CRC Press, 2016).

34. S. Savenkov, "Jones and Mueller matrices: structure, symmetry relations, and information content," in *Light Scattering Reviews 4*, A. A. Kokhanovsky, ed. (Springer, 2009), Chap. 3, pp. 71–119.

35. R. Barakat, "Conditions for the physical realizability of polarization matrices characterizing passive systems," J. Mod. Opt. **34**, 1535–1544 (1987).

36. S. R. Cloude, "Conditions for the physical realisability of matrix operators in polarimetry," Proc. SPIE **1166**, 177–187 (1990).

37. J. Gil, "Characteristic properties of Mueller matrices," J. Opt. Soc. Am. A **17**, 328–334 (2000).

38. J. J. Gil, I. S. José, and R. Ossikovski, "Serial–parallel decompositions of Mueller matrices," J. Opt. Soc. Am. A **30**, 32–50 (2013).

39. U. Fano, "A Stokes-parameter technique for the treatment of polarization in quantum mechanics," Phys. Rev. **93**, 121–123 (1954).

40. R. W. Schmieder, "Stokes-algebra formalism," J. Opt. Soc. Am. **59**, 297–302 (1969).

41. C. Whitney, "Pauli-algebraic operators in polarization optics," J. Opt. Soc. Am. **61**, 1207–1213 (1971).

42. N. Gisin, "Statistics of polarization dependent losses," Opt. Commun. **114**, 399–405 (1995).

43. R. Azzam, I. Elminyawi, and A. El-Saba, "General analysis and optimization of the four-detector photopolarimeter," J. Opt. Soc. Am. A **5**, 681–688 (1988).

44. L. B. Wolff and T. E. Boult, "Constraining object features using a polarization reflectance model," IEEE Trans. Pattern Anal. Mach. Intell. **13**, 635–657 (1991).

45. S. Rahmann and N. Canterakis, "Reconstruction of specular surfaces using polarization imaging," in *Proceedings of the 2001 IEEE Computer Society Conference on Computer Vision and Pattern Recognition* (2001), pp. 149–155.

46. A. Kadambi, V. Taamazyan, B. Shi, and R. Raskar, "Polarized 3D: high-quality depth sensing with polarization cues," in *Proceedings IEEE International Conference on Computer Vision* (2015), pp. 3370–3378.

47. J. S. Tyo, D. L. Goldstein, D. B. Chenault, and J. A. Shaw, "Review of passive imaging polarimetry for remote sensing applications," Appl. Opt. **45**, 5453–5469 (2006).

48. F. Snik, J. Craven-Jones, M. Escuti, S. Fineschi, D. Harrington, A. De Martino, D. Mawet, J. Riedi, and J. S. Tyo, "An overview of polarimetric sensing techniques and technology with applications to different research fields," Proc. SPIE **9099**, 90990B (2014).

49. S. R. Cloude, *Polarisation: Applications in Remote Sensing* (Oxford University, 2010).

50. O. Dubovik, Z. Li, and M. I. Mishchenko*et al.*et al., "Polarimetric remote sensing of atmospheric aerosols: instruments, methodologies, results, and perspectives," J. Quant. Spectrosc. Radiat. Transfer **224**, 474–511 (2019).

51. J. O. Stenflo, "Instrumentation for solar polarimetry," in *Solar Magnetic Fields: Polarized Radiation Diagnostics* (Springer Netherlands, 1994), pp. 312–350.

52. R. M. A. Azzam, "Stokes-vector and Mueller-matrix polarimetry," J. Opt. Soc. Am. A **33**, 1396–1408 (2016).

53. P. M. Duffieux, *L'integrale de Fourier et ses applications a l'Optique* (Societe Anonyme des Imprimeries Oberthur, 1946).

54. J. A. Ratcliffe, "Some aspects of diffraction theory and their application to the ionosphere," Rep. Prog. Phys. **19**, 188 –267 (1956).

55. T. K. Gaylord and M. G. Moharam, "Analysis and applications of optical diffraction by gratings," Proc. IEEE **73**, 894–937 (1985).

56. H. Kubota and S. Inoué, "Diffraction images in the polarizing microscope," J. Opt. Soc. Am. **49**, 191–198 (1959).

57. W. Urbańczyk, "Optical transfer function for imaging systems which change the state of light polarization," Opt. Acta **33**, 53–62 (1986).

58. J. P. McGuire and R. A. Chipman, "Diffraction image formation in optical systems withpolarization aberrations. I: Formulation and example," J. Opt. Soc. Am. A **7**, 1614–1626 (1990).

59. J. P. McGuire and R. A. Chipman, "Diffraction image formation in optical systems with polarization aberrations. II: Amplitude response matrices for rotationally symmetric systems," J. Opt. Soc. Am. A **8**, 833–840 (1991).

60. J. P. McGuire and R. A. Chipman, "Polarization aberrations. 1. Rotationally symmetric optical systems," Appl. Opt. **33**, 5080–5100 (1994).

61. J. P. McGuire and R. A. Chipman, "Polarization aberrations. 2. Tilted and decentered optical systems," Appl. Opt. **33**, 5101–5107 (1994).

62. I. Moreno, M. J. Yzuel, J. Campos, and A. Vargas, "Jones matrix treatment for polarization Fourier optics," J. Mod. Opt. **51**, 2031–2038 (2004).

63. I. Moreno, C. Iemmi, J. Campos, and M. J. Yzuel, "Jones matrix treatment for optical Fourier processors with structured polarization," Opt. Express **19**, 4583–4594 (2011).

64. D. Gabor, "A new microscopic principle," Nature **161**, 777–778 (1948).

65. A. W. Lohmann, "Reconstruction of vectorial wavefronts," Appl. Opt. **4**, 1667–1668 (1965).

66. O. Bryngdahl, "Polarizing holography," J. Opt. Soc. Am. **57**, 545–546 (1967).

67. M. E. Fourney, A. P. Waggoner, and K. V. Mate, "Recording polarization effects via holography," J. Opt. Soc. Am. **58**, 701–702 (1968).

68. O. Bryngdahl, "Polarization-grating moiré," J. Opt. Soc. Am. **62**, 839–848 (1972).

69. F. Weigert, "Über einen neuen effekt der strahlung in lichtempfindlichen schichten," Verh. Dtsch. Phys. Ges. **21**, 479–491 (1919).

70. L. Nikolova and P. Ramanujam, *Polarization Holography* (Cambridge University, 2009).

71. Z. V. Wardosanidze, "Holography based on the Weigert's Effect," in *Holograms: Recording Materials and Applications* (2011), Chap. 6, pp. 117–144.

72. S. D. Kakichashvili, "Method for phase polarization recording of holograms," Sov. J. Quantum Electron. **4**, 795–798 (1974).

73. S. D. Kakichashvili, "Polarization holography," Sov. Phys. Usp. **21**, 998 –999 (1978).

74. S. Kakichaahvili, "Methods and uses of polarization holography," Proc. SPIE **1731**, 148–157 (1992).

75. S. D. Kakichashvili, *Polyarizatsionnaya golografiya* (Nauka, 1989).

76. T. Todorov, L. Nikolova, and N. Tomova, "Polarization holography. 1: A new high-efficiency organic material with reversible photoinduced birefringence," Appl. Opt. **23**, 4309–4312 (1984).

77. F. Gori, "Diffractive optics: an introduction," in *Diffractive Optics and Optical Microsystems*, S. Martellucci and A. N. Chester, eds. (Springer US, 1997), pp. 3–22.

78. J. Tervo and J. Turunen, "Paraxial-domain diffractive elements with 100% efficiency based on polarization gratings," Opt. Lett. **25**, 785–786 (2000).

79. G. Cincotti, "Polarization gratings: design and applications," IEEE J. Quantum Electron. **39**, 1645–1652 (2003).

80. T. Todorov and L. Nikolova, "Spectrophotopolarimeter: fast simultaneous real-time measurement of light parameters," Opt. Lett. **17**, 358–359 (1992).

81. P. S. Ramanujam, C. Dam-Hansen, R. H. Berg, S. Hvilsted, and L. Nikolova, "Polarisation-sensitive optical elements in azobenzene polyesters and peptides," Opt. Lasers Eng. **44**, 912–925 (2006).

82. T. Todorov, L. Nikolova, K. Stoyanova, and N. Tomova, "Polarization holography. 3: Some applications of polarization holographic recording," Appl. Opt. **24**, 785–788 (1985).

83. L. Nikolova, T. Todorov, P. Sharlandjiev, and S. Stoyanov, "Polarimeter-photometer for quasi-monochromatic light," Proc. SPIE **1183**, 280–284 (1990).

84. T. Todorov, L. Nikolova, G. Stoilov, and B. Hristov, "Spectral stokesmeter. 1. Implementation of the device," Appl. Opt. **46**, 6662–6668 (2007).

85. M. Fratz, S. Sinzinger, and D. Giel, "Design and fabrication of polarization-holographic elements for laser beam shaping," Appl. Opt. **48**, 2669–2677 (2009).

86. M. Fratz, D. M. Giel, and P. Fischer, "Digital polarization holograms with defined magnitude and orientation of each pixel's birefringence," Opt. Lett. **34**, 1270–1272 (2009).

87. E. Loerincz, F. Ujhelyi, A. Sueto, G. Szarvas, P. Koppa, G. Erdei, S. Hvilsted, P. S. Ramanujam, and P. I. Richter, "Rewritable holographic memory card system," Proc. SPIE **4090**, 185–190 (2000).

88. T. Huang and K. H. Wagner, "Real-time joint transform correlation with photoanisotropic dye–polymer films," Appl. Opt. **33**, 7634–7645 (1994).

89. L. Nikolova, T. Todorov, N. Tomova, and V. Dragostinova, "Polarization-preserving wavefront reversal by four-wave mixing in photoanisotropic materials," Appl. Opt. **27**, 1598–1602 (1988).

90. T. Todorov, L. Nikolova, and N. Tomova, "Polarization holography. 2: Polarization holographic gratings in photoanisotropic materials with and without intrinsic birefringence," Appl. Opt. **23**, 4588–4591 (1984).

91. J. E. Ford, F. Xu, K. Urquhart, and Y. Fainman, "Polarization-selective computer-generated holograms," Opt. Lett. **18**, 456–458 (1993).

92. F. Xu, J. E. Ford, and Y. Fainman, "Polarization-selective computer-generated holograms: design, fabrication, and applications," Appl. Opt. **34**, 256–266 (1995).

93. A. V. Krishnamoorthy, F. Xu, J. E. Ford, and Y. Fainman, "Polarization-controlled multistage switch based on polarization-selective computer-generated holograms," Appl. Opt. **36**, 997–1010 (1997).

94. G. J. Swanson, "Binary optics technology: the theory and design of multi-level diffractive optical elements," Tech. Rep. (MIT Lincoln Laboratory, 1989).

95. F. Xu, R.-C. Tyan, Y. Fainman, and J. E. Ford, "Single-substrate birefringent computer-generated holograms," Opt. Lett. **21**, 516–518 (1996).

96. N. Nieuborg, C. Van de Poel, A. Kirk, H. Thienpont, and I. Veretennicoff, "Highly polarization selective diffractive optical elements for use in optical interconnection and routing systems," Proc. SPIE **2404**, 293–301 (1995).

97. N. Nieuborg, A. Kirk, B. Morlion, H. Thienpont, and I. Veretennicoff, "Polarization-selective diffractive optical elements with an index-matching gap material," Appl. Opt. **36**, 4681–4685 (1997).

98. F. Xu, R.-C. Tyan, P.-C. Sun, Y. Fainman, C.-C. Cheng, and A. Scherer, "Form-birefringent computer-generated holograms," Opt. Lett. **21**, 1513–1515 (1996).

99. I. Richter, P.-C. Sun, F. Xu, and Y. Fainman, "Design considerations of form birefringent microstructures," Appl. Opt. **34**, 2421–2429 (1995).

100. U. Levy, C.-H. Tsai, L. Pang, and Y. Fainman, "Engineering space-variant inhomogeneous media for polarization control," Opt. Lett. **29**, 1718–1720 (2004).

101. J. Hossfeld, D. Columbus, H. Sprave, T. Tschudi, and W. Dultz, "Polarizing computer-generated holograms," Opt. Eng. **32**, 1835–1838 (1993).

102. J. Hossfeld, T. T. Tschudi, and W. Dultz, "Polarization multiplexer/demultiplexer based on polarizing computer-generated holograms," Proc. SPIE **2043**, 132–136 (1994).

103. A. K. K. Spilman, "Stress-engineered optical elements," Ph.D. thesis (University of Rochester, 2008).

104. T. G. Brown and A. M. Beckley, "Stress engineering and the applications of inhomogeneously polarized optical fields," Front. Optoelectron. **6**, 89–96 (2013).

105. A. K. Spilman and T. G. Brown, "Stress birefringent, space-variant wave plates for vortex illumination," Appl. Opt. **46**, 61–66 (2007).

106. A. M. Beckley, T. G. Brown, and M. A. Alonso, "Full Poincare beams," Opt. Express **20**, 9357–9362 (2012).

107. A. M. Beckley, "Polarimetry and beam apodization using stress-engineered optical elements," Ph.D. thesis (University of Rochester, 2012).

108. A. M. Beckley, T. G. Brown, and M. A. Alonso, "Full Poincaré beams II: partial polarization," Opt. Express **20**, 9357–9362 (2012).

109. A. K. Spilman and T. G. Brown, "Stress-induced focal splitting," Opt. Express **15**, 8411–8421 (2007).

110. R. D. Ramkhalawon, T. G. Brown, and M. A. Alonso, "Imaging the polarization of a light field," Opt. Express **21**, 4106–4115 (2013).

111. B. G. Zimmerman and T. G. Brown, "Star test image-sampling polarimeter," Opt. Express **24**, 23154–23161 (2016).

112. V. Curcio, L. A. Alemán-Castañeda, T. G. Brown, S. Brasselet, and M. A. Alonso, "Birefringent Fourier filtering for single molecule coordinate and height super-resolution imaging with dithering and orientation," Nat. Commun. **11**, 1–13 (2020).

113. A. Vella and M. A. Alonso, "Optimal birefringence distributions for imaging polarimetry," Opt. Express **27**, 36799–36814 (2019).

114. S. Sivankutty, E. R. Andresen, G. Bouwmans, T. G. Brown, M. A. Alonso, and H. Rigneault, "Single-shot polarimetry imaging of multicore fiber," Opt. Lett. **41**, 2105–2108 (2016).

115. P. G. de Gennes and J. Prost, *The Physics of Liquid Crystals* (Oxford University, 1993).

116. D.-K. Yang and S.-T. Wu, *Fundamentals of Liquid Crystal Devices* (Wiley, 2014).

117. Z. Zhang, Z. You, and D. Chu, "Fundamentals of phase-only liquid crystal on silicon (LCOS) devices," Light Sci. Appl. **3**, e213 (2014).

118. B. E. Saleh and M. C. Teich, *Fundamentals of Photonics*, 2nd ed. (Wiley-Interscience, 2007).

119. J. Kim, Y. Li, M. N. Miskiewicz, C. Oh, M. W. Kudenov, and M. J. Escuti, "Fabrication of ideal geometric-phase holograms with arbitrary wavefronts," Optica **2**, 958–964 (2015).

120. R. Herke, M. H. Anderson, and T. Baur, "Liquid crystal in precision optical devices," Proc. SPIE **3800**, 45–51 (1999).

121. B. Gross, "How RCA lost the LCD," IEEE Spectrum **49**, 46–52 (2012).

122. J. C. Jones, "The fiftieth anniversary of the liquid crystal display," Liq. Cryst. Today **27**(3), 44–70 (2018).

123. R. Williams, "Electro-optical elements utilizing an organic nematic compound," U.S. patent 3,322,485 (May 30, 1967).

124. J. Beeckman, "Liquid-crystal photonic applications," Opt. Eng. **50**, 081202 (2011).

125. T. O. Carroll, "Liquid-crystal diffraction grating," J. Appl. Phys. **43**, 767–770 (1972).

126. R. A. Kashnow and J. E. Bigelow, "Diffraction from a liquid crystal phase grating," Appl. Opt. **12**, 2302–2304 (1973).

127. K. A. Suresh, Y. Sah, P. B. Sunil Kumar, and G. S. Ranganath, "Optical diffraction in chiral smectic-C liquid crystals," Phys. Rev. Lett. **72**, 2863–2866 (1994).

128. J. Chen, P. J. Bos, H. Vithana, and D. L. Johnson, "An electro-optically controlled liquid crystal diffraction grating," Appl. Phys. Lett. **67**, 2588–2590 (1995).

129. S. Sato, "Liquid-crystal lens-cells with variable focal length," Jpn. J. Appl. Phys. **18**, 1679–1684 (1979).

130. S. T. Kowel and D. S. Cleverly, "A liquid crystal adaptive lens," in *NASA Conference on Optical Information Processing for Aerospace Applications* (1981).

131. G. Williams, N. J. Powell, A. Purvis, and M. G. Clark, "Electrically controllable liquid crystal Fresnel lens," Proc. SPIE **1168**, 352–359 (1989).

132. N. A. Riza and M. C. DeJule, "Three-terminal adaptive nematic liquid-crystal lens device," Opt. Lett. **19**, 1013–1015 (1994).

133. K. Asatryan, V. Presnyakov, A. Tork, A. Zohrabyan, A. Bagramyan, and T. Galstian, "Optical lens with electrically variable focus using an optically hidden dielectric structure," Opt. Express **18**, 13981–13992 (2010).

134. J. F. Algorri, D. C. Zografopoulos, V. Urruchi, and J. M. Sánchez-Pena, "Recent advances in adaptive liquid crystal lenses," Crystals **9**, 1–20 (2019).

135. O. Aharon and I. Abdulhalim, "Tunable optical filter having a large dynamic range," Opt. Lett. **34**, 2114–2116 (2009).

136. J. Beeckman, D. P. Medialdea, T. Hui, K. Neyts, and X. Quintana, "Fast visible-near infrared switchable liquid crystal filter," Mol. Cryst. Liq. Cryst. **502**, 9–18 (2009).

137. A. D. Ford, S. M. Morris, and H. J. Coles, "Photonics and lasing in liquid crystals," Mater. Today **9**(7–8) 36–42 (2006).

138. K. Ichimura, Y. Suzuki, T. Seki, A. Hosoki, and K. Aoki, "Reversible change in alignment mode of nematic liquid crystals regulated photochemically by

command surfaces modified with an azobenzene monolayer," Langmuir **4**, 1214–1216 (1988).

139. W. M. Gibbons, P. J. Shannon, S.-T. Sun, and B. J. Swetlin, "Surface-mediated alignment of nematic liquid crystals with polarized laser light," Nature **351**, 49–50 (1991).

140. A. G. Dyadyusha, V. M. Kozenkov, T. Y. Marusiy, Y. A. Reznikov, V. Y. Reshetnyak, and A. I. Khizhnyak, "Light-induced planar alignment of nematic liquid-crystal by the anisotropic surface without mechanical texture," Ukr. Fiz. Zh. **36**, 1059–1062 (1991).

141. M. Schadt, K. Schmitt, V. Kozinkov, and V. Chigrinov, "Surface-induced parallel alignment of liquid crystals by linearly polymerized photopolymers," Jpn. J. Appl. Phys. **31**, 2155–2164 (1992).

142. K. Ichimura, "Photoalignment of liquid-crystal systems," Chem. Rev. **100**, 1847–1874 (2000).

143. V. G. Chigrinov, V. M. Kozenkov, and H.-S. Kwok, *Photoalignment of Liquid Crystalline Materials: Physics and Applications* (Wiley, 2008), Vol. **17**.

144. O. Yaroshchuk and Y. Reznikov, "Photoalignment of liquid crystals: basics and current trends," J. Mater. Chem. **22**, 286–300 (2012).

145. W. M. Gibbons and S. T. Sun, "Optically generated liquid crystal gratings," Appl. Phys. Lett. **65**, 2542–2544 (1994).

146. F. Gori, "Measuring Stokes parameters by means of a polarization grating," Opt. Lett. **24**, 584–586 (1999).

147. J. N. Eakin, Y. Xie, R. A. Pelcovits, M. D. Radcliffe, and G. P. Crawford, "Zero voltage Freedericksz transition in periodically aligned liquid crystals," Appl. Phys. Lett. **85**, 1671–1673 (2004).

148. G. P. Crawford, J. N. Eakin, M. D. Radcliffe, A. Callan-Jones, and R. A. Pelcovits, "Liquid-crystal diffraction gratings using polarization holography alignment techniques," J. Appl. Phys. **98**, 123102 (2005).

149. C. Provenzano, P. Pagliusi, and G. Cipparrone, "Highly efficient liquid crystal based diffraction grating induced by polarization holograms at the aligning surfaces," Appl. Phys. Lett. **89**, 121105 (2006).

150. B. Wen, R. G. Petschek, and C. Rosenblatt, "Nematic liquid-crystal polarization gratings by modification of surface alignment," Appl. Opt. **41**, 1246–1250 (2002).

151. M. J. Escuti and W. M. Jones, "39.4: Polarization-independent switching with high contrast from a liquid crystal polarization grating," SID Symp. Dig. Tech. Pap. **37**, 1443–1446 (2006).

152. C. Oh and M. J. Escuti, "Achromatic diffraction from polarization gratings with high efficiency," Opt. Lett. **33**, 2287–2289 (2008).

153. C. Oh and M. J. Escuti, "Achromatic polarization gratings as highly efficient thin-film polarizing beamsplitters for broadband light," Proc. SPIE **6682**, 668211 (2007).

154. C. Oh and M. J. Escuti, "Numerical analysis of polarization gratings using the finite-difference time-domain method," Phys. Rev. A **76**, 1–8 (2007).

155. M. N. Miskiewicz and M. J. Escuti, "Direct-writing of complex liquid crystal patterns," Opt. Express **22**, 12691–12706 (2014).

156. M. J. Escuti, J. Kim, and M. W. Kudenov, "Geometric-phase holograms," Opt. Photon. News **27**, 22–29 (2016).

157. "An introduction to polarization directed flat lenses," Edmund Optics, https://www.edmundoptics.com/globalassets/documents/polarization-directed-flat-lens-overview.pdf.

158. A. Maimone and J. Wang, "Holographic optics for thin and lightweight virtual reality," ACM Trans. Graph. **39**, 67 (2020).

159. M. W. Kudenov, M. J. Escuti, E. L. Dereniak, and K. Oka, "White-light channeled imaging polarimeter using broadband polarization gratings," Appl. Opt. **50**, 2283–2293 (2011).

160. F. Snik, G. Otten, M. Kenworthy, M. Miskiewicz, M. Escuti, C. Packham, and J. Codona, "The vector-APP: a broadband apodizing phase plate that yields complementary PSFs," Proc. SPIE **8450**, 84500M (2012).

161. K. J. Hornburg, J. Kim, and M. J. Escuti, "Experimental characterization of a F/1.5 geometric-phase lens with high-achromatic efficiency and low aberration," Proc. SPIE **10125**, 139–146 (2017).

162. Y.-H. Lee, G. Tan, T. Zhan, Y. Weng, G. Liu, F. Gou, F. Peng, N. V. Tabiryan, S. Gauza, and S.-T. Wu, "Recent progress in Pancharatnam–Berry phase optical elements and the applications for virtual/augmented realities," Opt. Data Process. Storage **3**, 79–88 (2017).

163. S. Lee, M. Wang, G. Li, L. Lu, Y. Sulai, C. Jang, and B. Silverstein, "Foveated near-eye display for mixed reality using liquid crystal photonics," Sci. Rep. **10**, 1–11 (2020).

164. L. Lu, T. Masood, and B. Silverstein, "Toward lighter, thinner AR/VR systems," Opt. Photon. News **32**(7), 42–47 (2021).

165. M. J. Escuti, C. Oh, C. Sánchez, C. Bastiaansen, and D. J. Broer, "Simplified spectropolarimetry using reactive mesogen polarization gratings," Proc. SPIE **6302**, 630207 (2006).

166. C. Packham, M. Escuti, J. Ginn, C. Oh, I. Quijano, and G. Boreman, "Polarization gratings: a novel polarimetric component for astronomical instruments," Publ. Astron. Soc. Pac. **122**, 1471–1482 (2010).

167. D. Mawet, L. Pueyo, and P. Lawson *et al.* et al., "Review of small-angle coronagraphic techniques in the wake of ground-based second-generation adaptive optics systems," Proc. SPIE **8442**, 844204 (2012).

168. G. Foo, D. Palacios, and G. A. Swartzlander, "Optical vortex coronagraph," Opt. Lett. **30**, 3308–3310 (2005).

169. G. P. P. L. Otten, F. Snik, M. A. Kenworthy, M. N. Miskiewicz, and M. J. Escuti, "Performance characterization of a broadband vector apodizing phase plate coronagraph," Opt. Express **22**, 30287–30314 (2014).

170. D. S. Doelman, F. Snik, N. Z. Warriner, and M. J. Escuti, "Patterned liquid-crystal optics for broadband coronagraphy and wavefront sensing," Proc. SPIE **10400**, 104000U (2017).

171. D. S. Doelman, F. Snik, and E. H. Por *et al.* et al., "Vector-apodizing phase plate coronagraph: design, current performance, and future development [Invited]," Appl. Opt. **60**, D52–D72 (2021).

172. G. P. P. L. Otten, F. Snik, M. A. Kenworthy, C. U. Keller, J. R. Males, K. M. Morzinski, L. M. Close, J. L. Codona, P. M. Hinz, K. J. Hornburg, L. L. Brickson, and M. J. Escuti, "On-sky performance analysis of the vector apodizing phase plate coronagraph on MagAO/Clio2," Astrophys. J. **834**, 1 –11 (2017).

173. D. S. Doelman, J. P. Wardenier, P. Tuthill, M. P. Fitzgerald, J. Lyke, S. Sallum, B. Norris, N. Z. Warriner, C. Keller, M. J. Escuti, and F. Snik, "First light of a holographic aperture mask: observation at the Keck OSIRIS Imager," Astron. Astrophys. **649**, A168 (2021).

174. Thorlabs Inc., "Patterned retarders ," https://www.thorlabs.com/newgrouppage9.cfm?objectgroup_id=8043.

175. F. Snik, M. Rodenhuis, M. J. Escuti, L. Brickson, K. Hornburg, J. Kim, C. Kievid, S. Groenhuijsen, and D. Roosegaarde, "Producing true-color rainbows with patterned multi-layer liquid-crystal polarization gratings," Opt. Mater. Express **9**, 1583–1589 (2019).

176. M. J. Padgett, "Orbital angular momentum 25 years on [Invited]," Opt. Express **25**, 11265–11274 (2017).

177. Y. Shen, X. Wang, Z. Xie, C. Min, X. Fu, Q. Liu, M. Gong, and X. Yuan, "Optical vortices 30 years on: OAM manipulation from topological charge to multiple singularities," Light Sci. Appl. **8**, 90 (2019).

178. A. Forbes, M. de Oliveira, and M. R. Dennis, "Structured light," Nat. Photonics **15**, 253–262 (2021).

179. L. Marrucci, C. Manzo, and D. Paparo, "Optical spin-to-orbital angular momentum conversion in inhomogeneous anisotropic media," Phys. Rev. Lett. **96**, 163905 (2006).

180. M. Stalder and M. Schadt, "Linearly polarized light with axial symmetry generated by liquid-crystal polarization converters," Opt. Lett. **21**, 1948–1950 (1996).

181. Z. Bomzon, G. Biener, V. Kleiner, and E. Hasman, "Radially and azimuthally polarized beams generated by space-variant dielectric subwavelength gratings," Opt. Lett. **27**, 285–287 (2002).

182. R. C. Devlin, A. Ambrosio, N. A. Rubin, J. P. B. Mueller, and F. Capasso, "Arbitrary spin-to-orbital angular momentum conversion of light," Science **358**, 896–901 (2017).

183. S. C. McEldowney, D. M. Shemo, R. A. Chipman, and P. K. Smith, "Creating vortex retarders using photoaligned liquid crystal polymers," Opt. Lett. **33**, 134–136 (2008).

184. D. Mawet, E. Serabyn, K. Liewer, C. Hanot, S. McEldowney, D. Shemo, and N. O'Brien, "Optical vectorial vortex coronagraphs using liquid crystal polymers: theory, manufacturing and laboratory demonstration," Opt. Express **17**, 1902–1918 (2009).

185. D. Mawet, E. Serabyn, K. Liewer, R. Burruss, J. Hickey, and D. Shemo, "The vector vortex coronagraph: laboratory results and first light at palomar observatory," Astrophys. J. **709**, 53–57 (2010).

186. A. Forbes, A. Dudley, and M. McLaren, "Creation and detection of optical modes with spatial light modulators," Adv. Opt. Photon. **8**, 200–227 (2016).

187. A. M. Weiner, "Femtosecond pulse shaping using spatial light modulators," Rev. Sci. Instrum. **71**, 1929–1960 (2000).

188. J. A. Neff, R. A. Athale, and S. H. Lee, "Two-dimensional spatial light modulators: a tutorial," Proc. IEEE **78**, 826–855 (1990).

189. U. Efron, *Spatial Light Modulator Technology: Materials, Devices, and Applications* (CRC Press, 1994), Vol. **47**.

190. C. Rosales-Guzmán and A. Forbes, *How to Shape Light with Spatial Light Modulators* (SPIE, 2017).

191. N. Savage, "Digital spatial light modulators," Nat. Photonics **3**, 170–172 (2009).

192. A. Jullien, "Spatial light modulators," Photoniques **101**, 59–64 (2020).

193. J. A. Davis, G. H. Evans, and I. Moreno, "Polarization-multiplexed diffractive optical elements with liquid-crystal displays," Appl. Opt. **44**, 4049–4052 (2005).

194. C. Maurer, A. Jesacher, S. Bernet, and M. Ritsch-Marte, "What spatial light modulators can do for optical microscopy," Laser Photon. Rev. **5**, 81–101 (2011).

195. A. Maimone, A. Georgiou, and J. S. Kollin, "Holographic near-eye displays for virtual and augmented reality," ACM Trans. Graph. **36**, 1–16 (2017).

196. A. Maimone, "Projector-combiner display with beam replication," U.S. patent 11,022,799 (June 1, 2021).

197. S. Choi, J. Kim, Y. Peng, and G. Wetzstein, "Optimizing image quality for holographic near-eye displays with Michelson holography," Optica **8**, 143–146 (2021).

198. C. Chang, K. Bang, G. Wetzstein, B. Lee, and L. Gao, "Toward the next-generation VR/AR optics: a review of holographic near-eye displays from a human-centric perspective," Optica **7**, 1563–1578 (2020).

199. D. Marco, M. M. Sánchez-López, A. Cofré, A. Vargas, and I. Moreno, "Optimal triplicator design applied to a geometric phase vortex grating," Opt. Express **27**, 14472–14486 (2021).

200. J. A. Davis, I. Moreno, M. M. Sánchez-López, K. Badham, J. Albero, and D. M. Cottrell, "Diffraction gratings generating orders with selective states of polarization," Opt. Express **24**, 907–917 (2016).

201. J. A. Davis, J. Adachi, C. R. Fernández-Pousa, and I. Moreno, "Polarization beam splitters using polarization diffraction gratings," Opt. Lett. **26**, 587–589 (2001).

202. M. T. Runyon, C. H. Nacke, A. Sit, M. Granados-Baez, L. Giner, and J. S. Lundeen, "Implementation of nearly arbitrary spatially varying polarization transformations: an in-principle lossless approach using spatial light modulators," Appl. Opt. **57**, 5769–5778 (2018).

203. J. A. Davis, D. E. McNamara, D. M. Cottrell, and T. Sonehara, "Two-dimensional polarization encoding with a phase-only liquid-crystal spatial light modulator," Appl. Opt. **39**, 1549–1554 (2000).

204. C. R. Fernández-Pousa, I. Moreno, J. A. Davis, and J. Adachi, "Polarizing diffraction-grating triplicators," Opt. Lett. **26**, 1651–1653 (2001).

205. J. A. Davis, G. H. Evans, K. Crabtree, and I. Moreno, "Programmable birefringent lenses with a liquid-crystal display," Appl. Opt. **43**, 6235–6241 (2004).

206. I. Moreno, J. A. Davis, T. M. Hernandez, D. M. Cottrell, and D. Sand, "Complete polarization control of light from a liquid crystal spatial light modulator," Opt. Express **20**, 364–376 (2012).

207. A. Cofré, A. Vargas, F. A. Torres-Ruiz, J. Campos, A. Lizana, M. M. Sánchez-López, and I. Moreno, "Quantitative performance of a polarization diffraction grating polarimeter encoded onto two liquid-crystal-on-silicon displays," Opt. Laser Technol. **96**, 219–226 (2017).

208. A. Cofré, A. Vargas, F. A. Torres-Ruiz, J. Campos, A. Lizana, M. M. Sánchez-López, and I. Moreno, "Dual polarization split lenses," Opt. Express **25**, 23773–23783 (2017).

209. I. Moreno, J. A. Davis, K. Badham, M. M. Sánchez-López, J. E. Holland, and D. M. Cottrell, "Vector beam polarization state spectrum analyzer," Sci. Rep. **7**, 1–10 (2017).

210. A. Sit, L. Giner, E. Karimi, and J. S. Lundeen, "General lossless spatial polarization transformations," J. Opt. **19**, 094003 (2017).

211. Q. Hu, Y. Dai, C. He, and M. J. Booth, "Arbitrary vectorial state conversion using liquid crystal spatial light modulators," Opt. Commun. **459**, 125028 (2020).

212. Q. Hu, C. He, and M. J. Booth, "Arbitrary complex retarders using a sequence of spatial light modulators as the basis for adaptive polarisation compensation," J. Opt. (UK) **23**, 065602 (2021).

213. X. Zheng, A. Lizana, A. Peinado, C. Ramirez, J. L. Martinez, A. Marquez, I. Moreno, and J. Campos, "Compact LCOS-SLM based polarization pattern beam generator," J. Lightwave Technol. **33**, 2047–2055 (2015).

214. J. Chen, L. Kong, and Q. Zhan, "Demonstration of a vectorial optical field generator with adaptive close loop control," Rev. Sci. Instrum. **88**, 125111 (2017).

215. J. A. Davis, I. Moreno, J. P. Sorger, M. M. Sánchez-López, and D. M. Cottrell, "Holographic projection system with programmable control of state of polarization, focus plane, and size of the reconstruction," Opt. Eng. **58**, 082403 (2018).

216. I. Moreno, J. A. Davis, M. M. Sánchez-López, K. Badham, and D. M. Cottrell, "Nondiffracting Bessel beams with polarization state that varies with propagation distance," Opt. Lett. **40**, 5451–5454 (2015).

217. S. Fu, S. Zhang, and C. Gao, "Bessel beams with spatial oscillating polarization," Sci. Rep. **6**, 1–7 (2016).

218. P. Li, Y. Zhang, S. Liu, H. Cheng, L. Han, D. Wu, and J. Zhao, "Generation and self-healing of vector Bessel-Gauss beams with variant state of polarizations upon propagation," Opt. Express **25**, 5821–5831 (2017).

219. R. P. Chen, Z. Chen, Y. Gao, J. Ding, and S. He, "Flexible manipulation of the polarization conversions in a structured vector field in free space," Laser Photon. Rev. **11**, 1700165 (2017).

220. M. Corato-Zanarella, A. H. Dorrah, M. Zamboni-Rached, and M. Mojahedi, "Arbitrary control of polarization and intensity profiles of diffraction-attenuation-resistant beams along the propagation direction," Phys. Rev. Appl. **9**, 24013 (2018).

221. F. Wyrowski, "Upper bound of the diffraction efficiency of diffractive phase elements," Opt. Lett. **16**, 1915–1917 (1991).

222. F. Gori, M. Santarsiero, S. Vicalvi, R. Borghi, G. Cincotti, E. Di Fabrizio, and M. Gentili, "Analytical derivation of the optimum triplicator," Opt. Commun. **157**, 13–16 (1998).

223. L. A. Romero and F. M. Dickey, "Theory of optimal beam splitting by phase gratings. I. One-dimensional gratings," J. Opt. Soc. Am. A **24**, 2280–2295 (2007).

224. L. A. Romero and F. M. Dickey, "Theory of optimal beam splitting by phase gratings. II. Square and hexagonal gratings," J. Opt. Soc. Am. A **24**, 2296–2312 (2007).

225. L. A. Romero and F. M. Dickey, *The Mathematical Theory of Laser Beam-Splitting Gratings* (Elsevier B.V., 2009), Vol. **54**.

226. M. Honkanen, V. Kettunen, J. Tervo, and J. Turunen, "Fourier array illuminators with 100% efficiency: analytical Jones-matrix construction," J. Mod. Opt. **47**, 2351–2359 (2000).

227. J. Tervo, V. Kettunen, M. Honkanen, and J. Turunen, "Design of space-variant diffractive polarization elements," J. Opt. Soc. Am. A **20**, 282–289 (2003).

228. H. Lajunen, J. Turunen, and J. Tervo, "Design of polarization gratings for broadband illumination," Opt. Express **13**, 3055–3067 (2005).

229. P. Birgit, N. Passilly, J. Pietarinen, P. Laakkonen, M. Kuittinen, and J. Tervo, "Low-cost fabrication of form-birefringent quarter-wave plates," Opt. Express **16**, 2939–2943 (2008).

230. M. Chen, M. Kim, A. M. Wong, and G. V. Eleftheriades, "Huygens' metasurfaces from microwaves to optics: a review," Nanophotonics **7**, 1207–1231 (2018).

231. N. Yu and F. Capasso, "Flat optics with designer metasurfaces," Nat. Mater. **13**, 139–150 (2014).

232. P. Genevet, F. Capasso, F. Aieta, M. Khorasaninejad, and R. Devlin, "Recent advances in planar optics: from plasmonic to dielectric metasurfaces," Optica **4**, 139–152 (2017).

233. S. M. Kamali, E. Arbabi, A. Arbabi, and A. Faraon, "A review of dielectric optical metasurfaces for wavefront control," Nanophotonics **7**, 1041–1068 (2018).

234. P. Qiao, W. Yang, and C. J. Chang-Hasnain, "Recent advances in high-contrast metastructures, metasurfaces, and photonic crystals," Adv. Opt. Photon. **10**, 180–245 (2018).

235. L. Huang, S. Zhang, and T. Zentgraf, "Metasurface holography: from fundamentals to applications," Nanophotonics **7**, 1169–1190 (2018).

236. Q. Jiang, G. Jin, and L. Cao, "When metasurface meets hologram: principle and advances," Adv. Opt. Photon. **11**, 518–576 (2019).

237. Y. Hu, X. Wang, X. Luo, X. Ou, L. Li, Y. Chen, P. Yang, S. Wang, and H. Duan, "All-dielectric metasurfaces for polarization manipulation: principles and emerging applications," Nanophotonics **9**, 3755–3780 (2020).

238. F. Ding, S. Tang, and S. I. Bozhevolnyi, "Recent advances in polarization-encoded optical metasurfaces," Adv. Photon. Res. **2**, 2000173 (2021).

239. Y. Intaravanne and X. Chen, "Recent advances in optical metasurfaces for polarization detection and engineered polarization profiles," Nanophotonics **9**, 1003–1014 (2020).

240. G. Zheng, Z. Li, and S. Yu, "Advances in exploiting the degrees of freedom in nanostructured metasurface design: from 1 to 3 to more," Nanophotonics **9**, 3699–3731 (2020).

241. J. B. Pendry, "Negative refraction makes a perfect lens," Phys. Rev. Lett. **85**, 3966–3969 (2000).

242. D. F. Sievenpiper, J. H. Schaffner, H. J. Song, R. Y. Loo, and G. Tangonan, "Two-dimensional beam steering using an electrically tunable impedance surface," IEEE Trans. Antennas Propag. **51**, 2713–2722 (2003).

243. S. A. Maier, *Plasmonics: Fundamentals and Applications* (Springer, 2007).

244. N. Yu, P. Genevet, M. A. Kats, F. Aieta, J. P. Tetienne, F. Capasso, and Z. Gaburro, "Light propagation with phase discontinuities: generalized laws of reflection and refraction," Science **334**, 333–337 (2011).

245. N. Yu, J. Fan, Q. J. Wang, C. Pflügl, L. Diehl, T. Edamura, M. Yamanishi, H. Kan, and F. Capasso, "Small-divergence semiconductor lasers by plasmonic collimation," Nat. Photonics **2**, 564–570 (2008).

246. N. Yu, R. Blanchard, J. Fan, F. Capasso, T. Edamura, M. Yamanishi, and H. Kan, "Small divergence edge-emitting semiconductor lasers with two-dimensional plasmonic collimators," Appl. Phys. Lett. **93**, 181101 (2008).

247. F. Aieta, P. Genevet, M. A. Kats, N. Yu, R. Blanchard, Z. Gaburro, and F. Capasso, "Aberration-free ultrathin flat lenses and axicons at telecom wavelengths based on plasmonic metasurfaces," Nano Lett. **12**, 4932–4936 (2012).

248. W. T. Chen and F. Capasso, "Will flat optics appear in everyday life anytime soon?" Appl. Phys. Lett. **118**, 100503 (2021).

249. J. Scheuer, "Optical metasurfaces are coming of age: short- and long-term opportunities for commercial applications," ACS Photon. **7**, 1323–1354 (2020).

250. D. L. Brundrett, E. N. Glytsis, and T. K. Gaylord, "Homogeneous layer models for high-spatial-frequency dielectric surface-relief gratings: conical diffraction and antireflection designs," Appl. Opt. **33**, 2695–2706 (1994).

251. S. M. Rytov, "Electromagnetic properties of a finely stratified medium," Sov. Phys. JETP **2**, 466–475 (1956).

252. E. A. J. Marcatili, "Dielectric rectangular waveguide and directional coupler for integrated optics," Bell Syst. Tech. J. **48**, 2071–2102 (1969).

253. J. N. Mait and D. W. Prather, *Selected Papers on Subwavelength Diffractive Optics* (SPIE, 2001).

254. P. Lalanne, S. Astilean, and P. Chavel, "Blazed binary subwavelength gratings with efficiencies larger chelette gratings than those of conventional échelette gratings," Opt. Lett. **23**, 1081–1083 (1998).

255. P. Lalanne, "Waveguiding in blazed-binary diffractive elements," J. Opt. Soc. Am. A **16**, 2517–2520 (1999).

256. P. Lalanne, S. Astilean, P. Chavel, E. Cambril, and H. Launois, "Design and fabrication of blazed binary diffractive elements with sampling periods smaller than the structural cutoff," J. Opt. Soc. Am. A **16**, 1143–1156 (1999).

257. P. Clapham and M. Hutley, "Reduction of lens reflexion by the 'moth eye' principle," Nature **244**, 281–282 (1973).

258. T. K. Gaylord, W. E. Baird, and M. G. Moharam, "Zero-reflectivity high spatial-frequency rectangular-groove dielectric surface-relief gratings," Appl. Opt. **25**, 4562–4567 (1986).

259. Y. Ono, Y. Kimura, Y. Ohta, and N. Nishida, "Antireflection effect in ultrahigh spatial-frequency holographic relief gratings," Appl. Opt. **26**, 1142–1146 (1987).

260. L. H. Cescato, E. Gluch, and N. Streibl, "Holographic quarterwave plates," Appl. Opt. **29**, 3286–3290 (1990).

261. S. Aoyama and T. Yamashita, "Grating beam splitting polarizer using multilayer resist method," Proc. SPIE **1545**, 241–250 (1991).

262. U. D. Zeitner, B. Schnabel, E. Kley, and F. Wyrowski, "Polarization multiplexing of diffractive elements with metal-stripe grating pixels," Appl. Opt. **38**, 2177–2181 (1999).

263. M. S. Mirotznik, D. M. Pustai, D. W. Prather, and J. N. Mait, "Design of two-dimensional polarization-selective diffractive optical elements with form-birefringent microstructures," Appl. Opt. **43**, 5947–5954 (2004).

264. E. Hasman, Z. Bomzon, A. Niv, G. Biener, and V. Kleiner, "Polarization beam-splitters and optical switches based on space-variant computer-generated subwavelength quasi-periodic structures," Opt. Commun. **209**, 45–54 (2002).

265. E. Hasman, V. Kleiner, G. Biener, and A. Niv, "Polarization dependent focusing lens by use of quantized Pancharatnam–Berry phase diffractive optics," Appl. Phys. Lett. **82**, 328–330 (2003).

266. E. Hasman, G. Biener, V. Kleiner, and A. Niv, "Polarization: spatial Fourier-transform polarimetry by use of space-variant subwavelength gratings," Opt. Photon. News **14**(12), 34 (2003).

267. E. Hasman, G. Biener, A. Niv, and V. Kleiner, "Space-variant polarization manipulation," in *Progress in Optics* (2005), Vol. **47**, pp. 215–289.

268. Z. Bomzon, G. Biener, V. Kleiner, and E. Hasman, "Space-variant Pancharatnam–Berry phase optical elements with computer-generated subwavelength gratings," Opt. Lett. **27**, 1141–1143 (2002).

269. G. Biener, A. Niv, V. Kleiner, and E. Hasman, "Geometrical phase image encryption obtained with space-variant subwavelength gratings," Opt. Lett. **30**, 1096–1098 (2005).

270. G. Biener, A. Niv, V. Kleiner, and E. Hasman, "Near-field Fourier transform polarimetry by use of a discrete space-variant subwavelength grating," J. Opt. Soc. Am. A **20**, 1940–1948 (2003).

271. Z. Bomzon, G. Biener, V. Kleiner, and E. Hasman, "Spatial Fourier-transform polarimetry using space-variant subwavelength metal-stripe polarizers," Opt. Lett. **26**, 1711–1713 (2001).

272. Z. Bomzon, G. Biener, V. Kleiner, and E. Hasman, "Real-time analysis of partially polarized light with a space-variant subwavelength dielectric grating," Opt. Lett. **27**, 188–190 (2002).

273. A. Arbabi, Y. Horie, M. Bagheri, and A. Faraon, "Dielectric metasurfaces for complete control of phase and polarization with subwavelength spatial resolution and high transmission," Nat. Nanotechnol. **10**, 937–943 (2015).

274. R. C. Devlin, M. Khorasaninejad, W.-T. Chen, J. Oh, and F. Capasso, "Broadband high-efficiency dielectric metasurfaces for the visible spectrum," Proc. Natl. Acad. Sci. USA **113**, 10473–10478 (2016).

275. S. Colburn, A. Zhan, E. Bayati, J. Whitehead, A. Ryou, L. Huang, and A. Majumdar, "Broadband transparent and CMOS-compatible flat optics with silicon nitride metasurfaces [Invited]," Opt. Mater. Express **8**, 2330–2344 (2018).

276. D. Sell, J. Yang, S. Doshay, K. Zhang, and J. A. Fan, "Visible light metasurfaces based on single-crystal silicon," ACS Photon. **3**, 1919–1925 (2016).

277. J.-S. Park, S. Zhang, A. She, W. T. Chen, P. Lin, K. M. A. Yousef, J.-X. Cheng, and F. Capasso, "All-glass, large metalens at visible wavelength using deep-ultraviolet projection lithography," Nano Lett. **19**, 8673–8682 (2019).

278. C. Zhang, S. Divitt, Q. Fan, W. Zhu, A. Agrawal, Y. Lu, T. Xu, and H. J. Lezec, "Low-loss metasurface optics down to the deep ultraviolet region," Light Sci. Appl. **9**, 1–10 (2020).

279. F. Ding, Y. Yang, R. A. Deshpande, and S. I. Bozhevolnyi, "A review of gap-surface plasmon metasurfaces: fundamentals and applications," Nanophotonics **7**, 1129–1156 (2018).

280. A. Pors, O. Albrektsen, I. P. Radko, and S. I. Bozhevolnyi, "Gap plasmon-based metasurfaces for total control of reflected light," Sci. Rep. **3**, 2155 (2013).

281. A. Pors and S. I. Bozhevolnyi, "Plasmonic metasurfaces for efficient phase control in reflection," Opt. Express **21**, 27438–27451 (2013).

282. J. S. Jensen and O. Sigmund, "Topology optimization for nano-photonics," Laser Photon. Rev. **5**, 308–321 (2011).

283. D. Sell, J. Yang, S. Doshay, R. Yang, and J. A. Fan, "Large-angle, multifunctional metagratings based on freeform multimode geometries," Nano Lett. **17**, 3752–3757 (2017).

284. C. Menzel, C. Rockstuhl, and F. Lederer, "Advanced Jones calculus for the classification of periodic metamaterials," Phys. Rev. A **82**, 053811 (2010).

285. Z. Shi, A. Y. Zhu, Z. Li, Y. W. Huang, Y. W. Huang, W. T. Chen, C. W. Qiu, and F. Capasso, "Continuous angle-tunable birefringence with freeform metasurfaces for arbitrary polarization conversion," Sci. Adv. **6**, eaba3367 (2020).

286. C. Menzel, C. Helgert, C. Rockstuhl, E. B. Kley, A. Tünnermann, T. Pertsch, and F. Lederer, "Asymmetric transmission of linearly polarized light at optical metamaterials," Phys. Rev. Lett. **104**, 253902 (2010).

287. Z. Shi, N. A. Rubin, J. S. Park, and F. Capasso, are preparing a manuscript to be called, "General spatial polarization transformation by single- and double-layer metasurfaces ," Phys. Rev. Lett., submitted for publication.

288. R. Lin and X. Li, "Multifocal metalens based on multilayer Pancharatnam–Berry phase elements architecture," Opt. Lett. **44**, 2819–2822 (2019).

289. B. Mirzapourbeinekalaye and A. Arbabi, "Implementation of lossless Jones matrices using bilayer birefringent metasurfaces," Proc. SPIE **10928**, 109281 (2019).

290. J. P. B. Mueller, N. A. Rubin, R. C. Devlin, B. Groever, and F. Capasso, "Metasurface polarization optics: independent phase control of arbitrary orthogonal states of polarization," Phys. Rev. Lett. **118**, 113901 (2017).

291. V. Arrizón, U. Ruiz, R. Carrada, and L. A. González, "Pixelated phase computer holograms for the accurate encoding of scalar complex fields," J. Opt. Soc. Am. A **24**, 3500–3507 (2007).

292. R. W. Gerchberg and W. O. Saxton, "A practical algorithm for the determination of phase from image and diffraction plane pictures," Optik **35**, 237–246 (1972).

293. J. R. Fienup, "Phase retrieval algorithms: a comparison," Appl. Opt. **21**, 2758–2769 (1982).

294. C. K. Hsueh and A. A. Sawchuk, "Computer-generated double-phase holograms," Appl. Opt. **17**, 3874–3883 (1978).

295. O. Mendoza-Yero, G. Mínguez-Vega, and J. Lancis, "Encoding complex fields by using a phase-only optical element," Opt. Lett. **39**, 1740–1743 (2014).

296. A. H. Dorrah, N. A. Rubin, A. Zaidi, M. Tamagnone, and F. Capasso, "Metasurface optics for on-demand polarization transformations along the optical path," Nat. Photonics **15**, 287–296 (2021).

297. Q. Fan, M. Liu, C. Zhang, W. Zhu, Y. Wang, P. Lin, F. Yan, L. Chen, H. J. Lezec, Y. Lu, A. Agrawal, and T. Xu, "Independent amplitude control of arbitrary orthogonal states of polarization via dielectric metasurfaces," Phys. Rev. Lett. **125**, 267402 (2020).

298. M. Liu, W. Zhu, P. Huo, L. Feng, M. Song, C. Zhang, L. Chen, H. J. Lezec, Y. Lu, A. Agrawal, and T. Xu, "Multifunctional metasurfaces enabled by simultaneous and independent control of phase and amplitude for orthogonal polarization states," Light Sci. Appl. **10**, 1–10 (2021).

299. W. T. Chen, K. Y. Yang, C. M. Wang, Y. W. Huang, G. Sun, I. D. Chiang, C. Y. Liao, W. L. Hsu, H. T. Lin, S. Sun, L. Zhou, A. Q. Liu, and D. P. Tsai, "High-efficiency broadband meta-hologram with polarization-controlled dual images," Nano Lett. **14**, 225–230 (2014).

300. M. Khorasaninejad and K. B. Crozier, "Silicon nanofin grating as a miniature chirality-distinguishing beam-splitter," Nat. Commun. **5**, 5386 (2014).

301. D. Lin, P. Fan, E. Hasman, and M. L. Brongersma, "Dielectric gradient metasurface optical elements," Science **345**, 298–302 (2014).

302. D. Wen, F. Yue, G. Li, G. Zheng, K. Chan, S. Chen, M. Chen, K. F. Li, P. W. Wong, K. W. Cheah, E. Y. Pun, S. Zhang, and X. Chen, "Helicity multiplexed broadband metasurface holograms," Nat. Commun. **6**, 8241 (2015).

303. M. Farmahini-Farahani and H. Mosallaei, "Birefringent reflectarray metasurface for beam engineering in infrared," Opt. Lett. **38**, 462–464 (2013).

304. M. I. Shalaev, J. Sun, A. Tsukernik, A. Pandey, K. Nikolskiy, and N. M. Litchinitser, "High-efficiency all-dielectric metasurfaces for ultracompact beam manipulation in transmission mode," Nano Lett. **15**, 6261–6266 (2015).

305. Z. Guo, L. Zhu, F. Shen, H. Zhou, and R. Gao, "Dielectric metasurface based high-efficiency polarization splitters," RSC Adv. **7**, 9872–9879 (2017).

306. Z. Guo, L. Zhu, K. Guo, F. Shen, and Z. Yin, "High-order dielectric metasurfaces for high-efficiency polarization beam splitters and optical vortex generators," Nano. Res. Lett. **12**, 2–9 (2017).

307. J. Li, C. Liu, T. Wu, Y. Liu, Y. Wang, Z. Yu, H. Ye, and L. Yu, "Efficient polarization beam splitter based on all-dielectric metasurface in visible region," Nano. Res. Lett. **14**, 34 (2019).

308. X. Zang, H. Ding, Y. Intaravanne, L. Chen, Y. Peng, J. Xie, Q. Ke, A. V. Balakin, A. P. Shkurinov, X. Chen, Y. Zhu, and S. Zhuang, "A multi-foci metalens with polarization-rotated focal points," Laser Photon. Rev. **13**, 1900182 (2019).

309. Y. Yang, W. Wang, P. Moitra, I. I. Kravchenko, D. P. Briggs, and J. Valentine, "Dielectric meta-reflectarray for broadband linear polarization conversion and optical vortex generation," Nano Lett. **14**, 1394–1399 (2014).

310. F. Cheng, L. Ding, L. Qiu, D. Nikolov, A. Bauer, J. P. Rolland, and A. N. Vamivakas, "Polarization-switchable holograms based on efficient, broadband multifunctional metasurfaces in the visible regime," Opt. Express **26**, 30678–30688 (2018).

311. H. Kwon, E. Arbabi, S. M. Kamali, M. S. Faraji-Dana, and A. Faraon, "Single-shot quantitative phase gradient microscopy using a system of multifunctional metasurfaces," Nat. Photonics **14**, 109–114 (2020).

312. S. Pancharatnam, "Generalized theory of interference and its applications," Proc. Indian Acad. Sci. **44**, 247–262 (1956).

313. M. Berry, "Quantal phase factors accompanying adiabatic changes," Proc. R. Soc. A **392**, 45–57 (1984).

314. M. Berry, "Anticipations of the geometric phase," Phys. Today **43**(12), 34–40 (1990).

315. M. Khorasaninejad, W. T. Chen, R. C. Devlin, J. Oh, A. Y. Zhu, and F. Capasso, "Metalenses at visible wavelengths: diffraction-limited focusing and subwavelength resolution imaging," Science **352**, 1190–1194 (2016).

316. M. Khorasaninejad and F. Capasso, "Metalenses: versatile multifunctional photonic components," Science **358**, 1 –8 (2017).

317. L. Huang, X. Chen, H. Mühlenbernd, G. Li, B. Bai, Q. Tan, G. Jin, T. Zentgraf, and S. Zhang, "Dispersionless phase discontinuities for controlling light propagation," Nano Lett. **12**, 5750–5755 (2012).

318. G. Zheng, H. Mühlenbernd, M. Kenney, G. Li, T. Zentgraf, and S. Zhang, "Metasurface holograms reaching 80% efficiency," Nat. Nanotechnol. **10**, 308–312 (2015).

319. M. Khorasaninejad, A. Ambrosio, P. Kanhaiya, and F. Capasso, "Broadband and chiral binary dielectric meta-holograms," Sci. Adv. **2**, e1501258 (2016).

320. E. Maguid, I. Yulevich, D. Veksler, V. Kleiner, M. L. Brongersma, and E. Hasman, "Photonic spin-controlled multifunctional shared-aperture antenna array," Science **352**, 1202–1206 (2016).

321. E. Maguid, I. Yulevich, M. Yannai, V. Kleiner, M. L. Brongersma, and E. Hasman, "Multifunctional interleaved geometric-phase dielectric metasurfaces," Light Sci. Appl. **6**, e17027 (2017).

322. B. Desiatov, N. Mazurski, Y. Fainman, and U. Levy, "Polarization selective beam shaping using nanoscale dielectric metasurfaces," Opt. Express **23**, 22611–22618 (2015).

323. X. Zhang, S. Yang, W. Yue, Q. Xu, C. Tian, X. Zhang, E. Plum, S. Zhang, J. Han, and W. Zhang, "Direct polarization measurement using a multiplexed Pancharatnam–Berry metahologram," Optica **6**, 1190–1198 (2019).

324. L. Zhu, X. Liu, B. Sain, M. Wang, C. Schlickriede, Y. Tang, J. Deng, K. Li, J. Yang, M. Holynski, S. Zhang, T. Zentgraf, K. Bongs, Y. H. Lien, and G. Li, "A dielectric metasurface optical chip for the generation of cold atoms," Sci. Adv. **6**, 4–9 (2020).

325. W. R. McGehee, W. Zhu, D. S. Barker, D. Westly, A. Yulaev, N. Klimov, A. Agrawal, S. Eckel, V. Aksyuk, and J. J. McClelland, "Magneto-optical trapping using planar optics," New J. Phys. **23**, 013021 (2021).

326. L. Deng, J. Deng, Z. Guan, J. Tao, Y. Chen, Y. Yang, D. Zhang, J. Tang, Z. Li, Z. Li, S. Yu, G. Zheng, H. Xu, C. W. Qiu, and S. Zhang, "Malus-metasurface-assisted polarization multiplexing," Light Sci. Appl. **9**, 1–9 (2020).

327. J. C. Gutiérrez-Vega, "Pancharatnam–Berry phase of optical systems," Opt. Lett. **36**, 1143–1145 (2011).

328. B. Groever, N. A. Rubin, J. P. B. Mueller, R. C. Devlin, and F. Capasso, "High-efficiency chiral meta-lens," Sci. Rep. **8**, 7240 (2018).

329. Z.-L. Deng, J. Deng, X. Zhuang, S. Wang, K. Li, Y. Wang, Y. Chi, X. Ye, J. Xu, G. P. Wang, R. Zhao, X. Wang, Y. Cao, X. Cheng, G. Li, and X. Li, "Diatomic metasurface for vectorial holography," Nano Lett. **18**, 2885–2892 (2018).

330. E. Arbabi, S. M. Kamali, A. Arbabi, and A. Faraon, "Vectorial holograms with a dielectric metasurface: ultimate polarization pattern generation," ACS Photon. **6**, 2712–2718 (2019).

331. R. Zhao, B. Sain, Q. Wei, C. Tang, X. Li, T. Weiss, L. Huang, Y. Wang, and T. Zentgraf, "Multichannel vectorial holographic display and encryption," Light Sci. Appl. **7**, 95 (2018).

332. Q. Song, A. Baroni, P. C. Wu, S. Chenot, V. Brandli, S. Vézian, B. Damilano, P. D. Mierry, S. Khadir, P. Ferrand, and P. Genevet, "Broadband decoupling of intensity and polarization with vectorial Fourier metasurfaces," Nat. Commun. **12**, 3631 (2021).

333. D. Wen, J. J. Cadusch, J. Meng, and K. B. Crozier, "Vectorial holograms with spatially continuous polarization distributions," Nano Lett. **21**, 1735–1741 (2021).

334. N. A. Rubin, A. Zaidi, M. Juhl, R. P. Li, J. P. B. Mueller, R. C. Devlin, K. Leósson, and F. Capasso, "Polarization state generation and measurement with a single metasurface," Opt. Express **26**, 21455–21478 (2018).

335. X. Zang, F. Dong, F. Yue, C. Zhang, L. Xu, Z. Song, M. Chen, P. Y. Chen, G. S. Buller, Y. Zhu, S. Zhuang, W. Chu, S. Zhang, and X. Chen, "Polarization encoded color image embedded in a dielectric metasurface," Adv. Mater. **30**, 1707499 (2018).

336. F. Ding, B. Chang, Q. Wei, L. Huang, X. Guan, and S. I. Bozhevolnyi, "Versatile polarization generation and manipulation using dielectric metasurfaces," Laser Photon. Rev. **14**, 2000116 (2020).

337. Q. Song, A. Baroni, R. Sawant, P. Ni, V. Brandli, S. Chenot, S. Vézian, B. Damilano, P. de Mierry, S. Khadir, P. Ferrand, and P. Genevet, "Ptychography retrieval of fully polarized holograms from geometric-phase metasurfaces," Nat. Commun. **11**, 2651 (2020).

338. Q. Song, S. Khadir, S. Vézian, B. Damilano, P. D. Mierry, S. Chenot, V. Brandli, R. Laberdesque, B. Wattellier, and P. Genevet, "Printing polarization and phase at the optical diffraction limit: near- and far-field optical encryption," Nanophotonics **10**, 697–704 (2021).

339. N. A. Rubin, G. D'Aversa, P. Chevalier, Z. Shi, W. T. Chen, and F. Capasso, "Matrix Fourier optics enables a compact full-Stokes polarization camera," Science **365**, eaax1839 (2019).

340. N. A. Rubin, A. Zaidi, A. H. Dorrah, Z. Shi, and F. Capasso, "Jones matrix holography with metasurfaces," Sci. Adv. **7**, eabg7488 (2021).

341. M. Zamboni-Rached, "Stationary optical wave fields with arbitrary longitudinal shape by superposing equal frequency Bessel beams: frozen waves," Opt. Express **12**, 4001–4006 (2004).

342. A. Pors, M. G. Nielsen, and S. I. Bozhevolnyi, "Plasmonic metagratings for simultaneous determination of Stokes parameters," Optica **2**, 716–723 (2015).

343. E. Arbabi, S. M. Kamali, A. Arbabi, and A. Faraon, "Full-Stokes imaging polarimetry using dielectric metasurfaces," ACS Photon. **5**, 3132–3140 (2018).

344. F. Afshinmanesh, J. S. White, W. Cai, and M. L. Brongersma, "Measurement of the polarization state of light using an integrated plasmonic polarimeter," Nanophotonics **1**, 125–129 (2012).

345. J. P. B. Mueller, K. Leosson, and F. Capasso, "Ultracompact metasurface in-line polarimeter," Optica **3**, 42–47 (2016).

346. W. T. Chen, P. Török, M. R. Foreman, C. Y. Liao, W.-Y. Tsai, P. R. Wu, and D. P. Tsai, "Integrated plasmonic metasurfaces for spectropolarimetry," Nanotechnology **27**, 224002 (2016).

347. M. Juhl, C. Mendoza, J. P. B. Mueller, F. Capasso, and K. Leosson, "Performance characteristics of 4-port in-plane and out-of-plane in-line metasurface polarimeters," Opt. Express **25**, 28697–28709 (2017).

348. S. Wei, Z. Yang, and M. Zhao, "Design of ultracompact polarimeters based on dielectric metasurfaces," Opt. Lett. **42**, 1580–1583 (2017).

349. F. Ding, A. Pors, Y. Chen, V. A. Zenin, and S. I. Bozhevolnyi, "Beam-size-invariant spectropolarimeters using gap-plasmon metasurfaces," ACS Photon. **4**, 943–949 (2017).

350. Z. Yang, Z. Wang, Y. Wang, X. Feng, M. Zhao, Z. Wan, L. Zhu, J. Liu, Y. Huang, J. Xia, and M. Wegener, "Generalized Hartmann-Shack array of dielectric metalens sub-arrays for polarimetric beam profiling," Nat. Commun. **9**, 1–7 (2018).

351. K. Wang, J. G. Titchener, S. S. Kruk, L. Xu, H.-P. Chung, M. Parry, I. I. Kravchenko, Y.-H. Chen, A. S. Solntsev, Y. S. Kivshar, D. N. Neshev, and A. A. Sukhorukov, "Quantum metasurface for multiphoton interference and state reconstruction," Science **361**, 1104–1108 (2018).

352. A. Martínez, "Polarimetry enabled by nanophotonics," Science **362**, 750–751 (2018).

353. R. M. A. Azzam, E. Masetti, I. M. Elminyawi, and F. G. Grosz, "Construction, calibration, and testing of a four-detector photopolarimeter," Rev. Sci. Instrum. **59**, 84–88 (1988).

354. D. S. Sabatke, M. R. Descour, E. L. Dereniak, W. C. Sweatt, S. A. Kemme, and G. S. Phipps, "Optimization of retardance for a complete Stokes polarimeter," Opt. Lett. **25**, 802–804 (2000).

355. M. R. Foreman, A. Favaro, and A. Aiello, "Optimal frames for polarization state reconstruction," Phys. Rev. Lett. **115**, 1–6 (2015).

356. F. Snik and C. U. Keller, *Astronomical Polarimetry: Polarized Views of Stars and Planets BT-Planets, Stars and Stellar Systems, Vol 2. of Astronomical Techniques, Software, and Data* (Springer Netherlands, 2013), pp. 175–221.

357. J. Hough, "Polarimetry: a powerful diagnostic tool in astronomy," Astron. Geophys. **47**, 3.31–3.35 (2006).

Noah A. Rubin is a researcher in Applied Physics at Harvard University. He received his Ph.D. in Applied Physics from Harvard University in 2020 studying metasurface polarization optics, supervised by Prof. Federico Capasso. Previously, he received a bachelor's degree in physics from the University of Pennsylvania in 2015. He is from Albany, New York, USA.

Zhujun Shi received her B.S. degree in physics from Tsinghua University in 2015 and her Ph.D. in physics from Harvard University in 2020. Her research focuses on designing novel nanophotonic devices for controlling free-space and on-chip light propagation. She has demonstrated nano-optical systems for bio-medical imaging, computational sensing, and novel display applications. Currently she is an optical research scientist at Reality Labs Research.

Federico Capasso is the Robert Wallace Professor of Applied Physics at Harvard University, which he joined in 2003 after a 27-year career at Bell Labs from postdoc to Physical Research VP. Highlights of his research are bandgap engineering of heterostructure materials and devices, including the invention of the quantum cascade laser, metasurface-based flat optics, N/MEMS based on the Casimir effect, and the measurement of a repulsive Casimir force. He is a member of the National Academy of Sciences, the National Academy of Engineering, and the American Academy of Arts and Sciences. His awards include the Ives Medal/Jarus Quinn Prize of Optica, the Balzan Prize for Applied Photonics, the King Faisal Prize, the American Physical Society Arthur Schawlow Prize, the Institute of Electrical and Electronics Engineers (IEEE) Edison Medal, the Franklin Medal, the Materials Research Society Medal, and the Enrico Fermi prize.

Figure 35
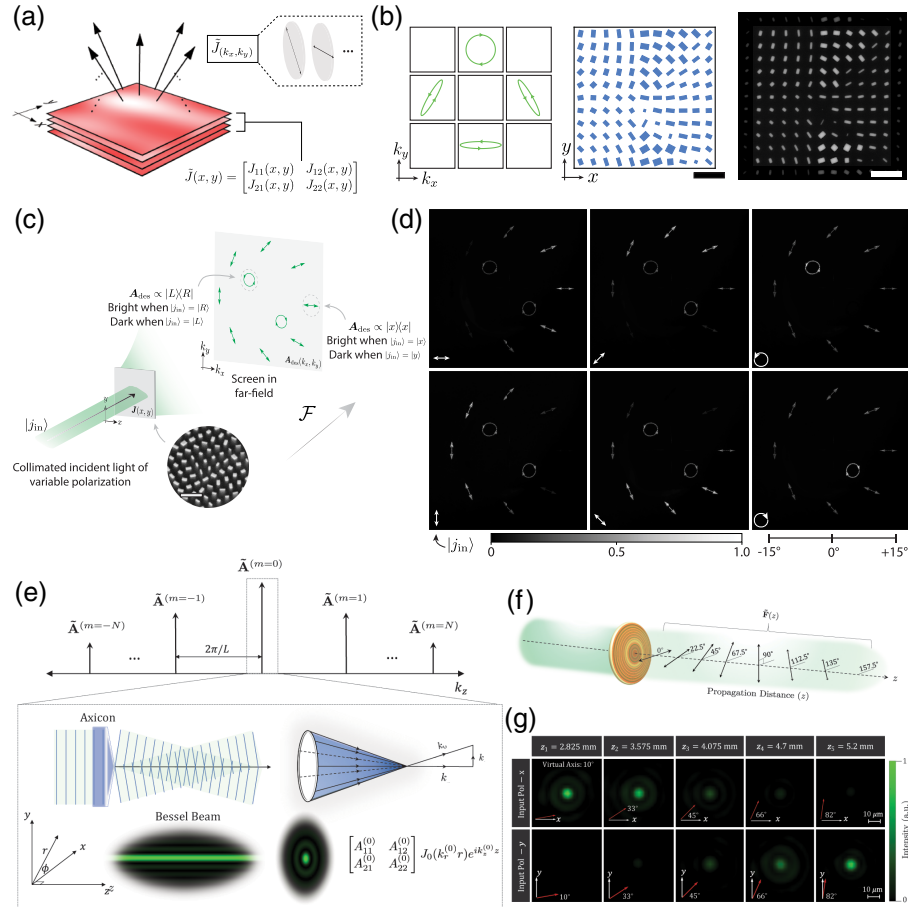
**Examples of metasurface devices designed with the full Jones matrix approach.**
(a) Metasurfaces can act as diffraction gratings whose orders may have specified
polarization sensitivity, emulating through diffraction functions that would ordinarily
require bulk birefringent and dichroic optics. (b) One example of these is a 2D peri-
odic grating (shown here made of TiO_2 pillars for use at visible wavelengths) whose
innermost four orders act as analyzers for the set of four non-orthogonal polariza-
tion states shown at left. This capability is enabled by the matrix approach described
here. (a) and (b) from Rubin *et al*., Science **365**, eaax1839 (2019) [339]. Reprinted
with permission from AAAS. (c) Similar ideas can be used to create aperiodic meta-
surfaces that realize Jones matrix holograms where each point in the far-field can
be ascribed its own designer Jones matrix transfer function. One example of this in
action is a hologram in which the hologram takes the form of a collection of polariza-
tion ellipses, where each polarization state drawn acts as an analyzer for its depicted
state. (d) This means that the hologram rearranges light on the basis of its polariza-
tion: Each drawing will be bright or dark depending on its state's projection onto the
incident light's polarization state so that the polarization of incident light can be read
out from the hologram by inspection. No external polarization analyzer is present. (c)
and (d) from Rubin *et al*., Sci. Adv. **7**, eabg7488 (2021) [340]. Reprinted with permis-
sion from AAAS. (e) Similar control can be exerted along the optical axis if a Jones
matrix-weighted expansion is carried out in k_z using Bessel beams of variable cone
angle as a basis. (f) This enables an optical element wherein a custom optical transfer
function is created at each point along the optical axis. (g) One example of this is
a device that acts as a linear polarizer that virtually "rotates" along the optical axis
from 0° to 90°, as shown by the amplitude profile in z for incident x- and y-polarized
light. Reprinted by permission from Macmillan Publishers Ltd.: Dorrah *et al*., Nat.
Photonics **15**, 287–296 (2021) [296]. Copyright 2021. All scale bars are 1 μm.

Figure 36
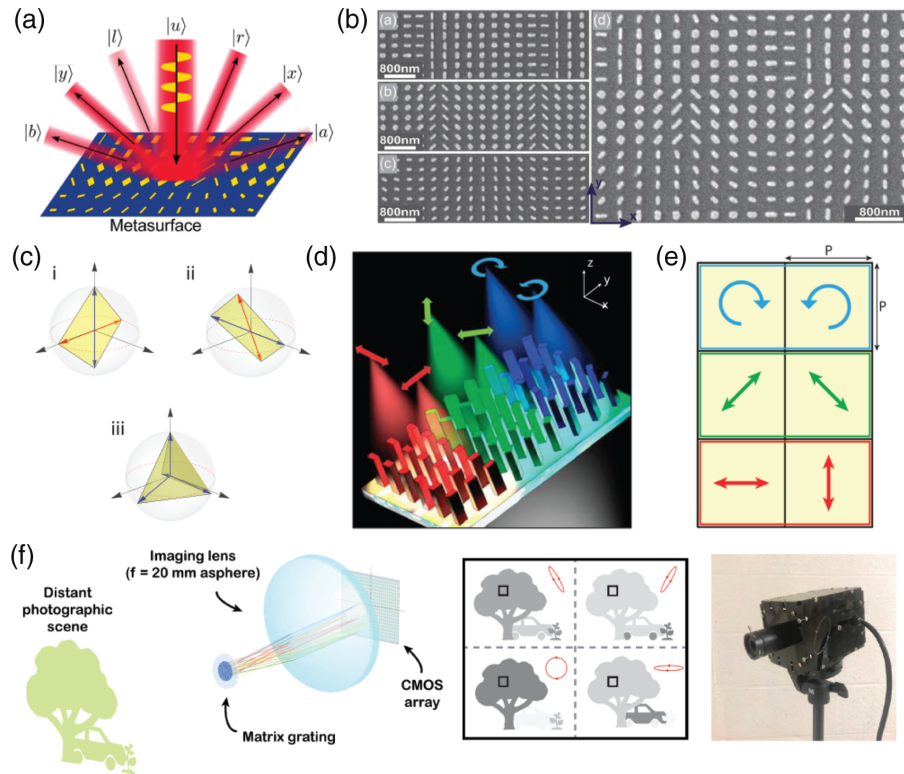
Polarization imaging using polarization-sensitive metasurfaces. (a) Schematic example of using a spatial multiplexing approach to create a grating that analyzes incoming polarization with respect to $|x\rangle$, $|y\rangle$, $|45°\rangle$, $|135°\rangle$, $|R\rangle$, and $|L\rangle$ simultaneously for independent measurement. (b) Example SEM of a grating interlaced to realize the function in (a). (a) and (b) reprinted with permission from [342]. Copyright 2015 Optical Society of America. (c) Shapes swept out by various sets of four polarization states. (i) and (ii) are not suitable for full-Stokes determination, while (iii), the tetrahedron, represents an optimum choice for full-Stokes polarimetry. (d) One approach to polarization imaging is to use the metasurface as a focal plane element, combining polarization-analyzing gratings (in this case using a spatially multiplexed approach) with focusing power to dedicate a superpixel (e) to the determination of $\vec{S}$. (d) and (e) reprinted with permission from Arbabi *et al*., ACS Photonics **5**, 3132–3140 (2018) [343]. Copyright 2018 American Chemical Society. (f) In a second approach to metasurface polarimetry, the grating is placed in collimated space, ideally in a pupil plane. Then, if the system's FOV is limited, several images each analyzed with respect to a particular polarization state are formed, which when registered permit determination of $\vec{S}$ over a scene. Using this approach, a compact metasurface-based polarization camera has been demonstrated. From Rubin *et al*., Science **365**, eaax1839 (2019) [339]. Reprinted with permission from AAAS.

Figure 37
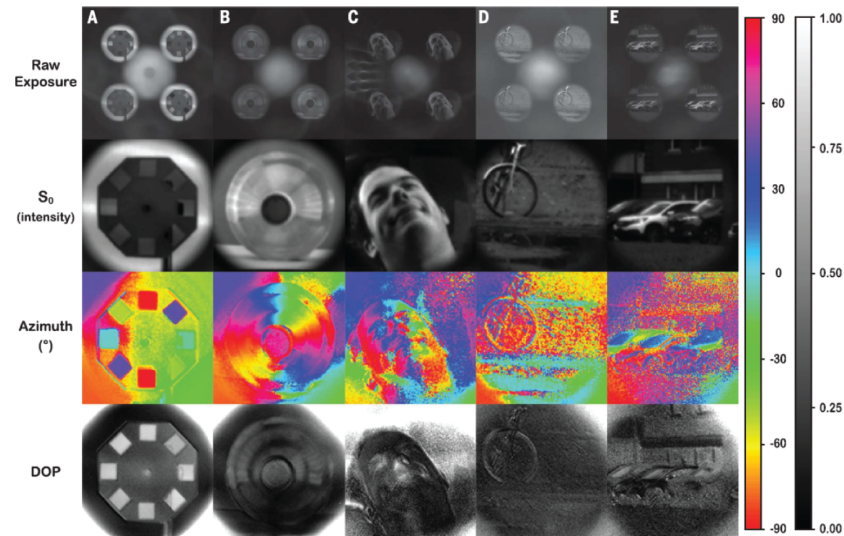
Examples of polarization imagery with a metasurface-based polarization camera. Real-world examples of polarization phenomena visualized through a metasurface polarization camera, described in full in [339]. The top row shows the raw sensor exposure in each case, displaying four quadrants corresponding to four polarization channels. When registered, a full-Stokes image can be computed from which the intensity (S_0), azimuth angle, and degree-of-polarization are derived. From Rubin *et al.*, Science **365**, eaax1839 (2019) [339]. Reprinted with permission from AAAS.